AN ABSTRACT OF THE DISSERTATION OF

Sam VanLaningham for the degree of Doctor of Philosophy in Oceanography presented on June 8, 2007.

Title: The Fluvial Response to Glacial-Interglacial Climate Change in the Pacific Northwest, USA

Abstract approved: _____

Robert A. Duncan Nicklas G. Pisias

This research focuses on the development of new techniques to explore terrestrial-ocean climate linkages along the Pacific Northwest-northeast Pacific Ocean margin. This is done by investigating river response to climate change and by unraveling this history preserved in continental margin sediments. A significant component of this work centers on developing a ^{40}Ar-^{39}Ar incremental heating method to fingerprint bulk fluvial sediment entering this region. Results show reproducible ages from individual rivers accounting for the majority of sediment delivered offshore. A ^{40}Ar-^{39}Ar detrital mixture model is developed to examine the fidelity of these results and shows that the bulk ages measured from river mouth sediments can be accurate indicators of the average age of feldspars eroded from a given catchment area.

The bulk sediment ages are combined with Nd isotopic analyses into a ternary mixing model to better understand the sources of terrigenous material delivered to offshore continental margin sites. Downcore Ar-Nd isotopic compositions can be described by three general river sediment sources proximal to the core site, the Umpqua, Rogue+Klamath, and Eel Rivers, from ~14 ka to Present. Results from the ternary model also suggest that differential contributions of

eroded material plays the primary role in provenance changes seen at the core site, rather than sediment transport changes due to ocean circulation.

This research culminates in a modeling effort to examine downcore provenance changes. We develop a model that balances basin-averaged ^{40}Ar-^{39}Ar ages (detrital mixtures) of the contributing fluvial basins and predicts the bulk sediment value at the core site. We find that the Upper Klamath Basin (which contained pluvial Lake Modoc during Marine Isotope Stage 2) is the most influential source area that can contribute to younger bulk sediment ^{40}Ar-^{39}Ar ages at the core site, relative to present day values. The Eel River is also shown to have a considerable influence on changes in margin sedimentation. Combinations of increases in the sediment fluxes out of these two basins can describe the ^{40}Ar-^{39}Ar provenance evolution observed at the core site over the 22-14 ka time period. Overall, this new ^{40}Ar-^{39}Ar isotopic technique, together with the Nd isotopic system and the use of detrital mixture modeling show tremendous promise as a multi-faceted strategy to assess erosion and provenance change through the continuous history preserved in fine-grained marine sedimentary records.

The Fluvial Response to Glacial-Interglacial Climate Change in the Pacific Northwest, USA

by
Sam VanLaningham

A DISSERTATION

submitted to

Oregon State University

in partial fulfillment of
the requirements for the
degree of

Doctor of Philosophy

Presented June 8, 2007
Commencement June 2008

Doctor of Philosophy dissertation of Sam VanLaningham presented on June 8, 2007.

APPROVED:

Co-Major Professor, representing Oceanography

Co-Major Professor, representing Oceanography

Dean of the College of Oceanic and Atmospheric Sciences

Dean of the Graduate School

I understand that my dissertation will become part of the permanent collection of Oregon State University libraries. My signature below authorizes release of my dissertation to any reader upon request.

Sam VanLaningham, Author

ACKNOWLEDGEMENTS

There is truly no way that I could have done this without the connection with, and help of others. First, I am very grateful that I had such great guidance from my committee. A large debt of gratitude goes to my co-advisor, Bob Duncan, for asking me if I would like to be involved with this project. At the time (~5 years ago) I was just finishing a M.S. in Geosciences at OSU and unsure of my future. I was not convinced that continuing my education was the right thing. I now know that I made the right decision and Bob's early enthusiasm towards me should take much of the credit. My other advisor, Nick Pisias, has been my "right-hand man" from early on in the project. Nick always gave me time to explain where I was at with my research and offered me an odd mix of mathematical and emotional support. He truly believed in my ideas throughout the progression of this research and always offered up excellent ideas of his own for my next course of action (which, near the end was simply "write your thesis, Sam"). Simple advice? Yes. Needed? Yes. Nick has intuitively known how to guide and motivate me from the start.

Dave Graham taught me how to be a geochemist and fostered the majority of my education in the subject. He refused to settle for anything but thoroughness in my work, which I would often fight, only to end up following his suggestions and learn that I was much better off and farther along for having done it. He also paid for lunch far too much. Steve Hostetler offered endless enthusiasm to ask the big questions related to the project, tolerated my relentless visits near the end and improved how I philosophically approach modeling. My graduate representative, Adam Kent also contributed to my growth academically. He gave a full effort to problems I ran into along the way and also asked some of the hardest questions during my orals, which improved my humility.

COAS is in part successful because of the research technicians that keep the instrumentation and facilities running smoothly. Mysti Weber guided me from the beginning on how to prepare samples. She has also been a great ear to bounce thoughts off of and she talked

golf. Andy Ungerer trained me on almost every mass spectrometer in COAS and guided me during the resurrection of the X-ray diffractometer. He taught me a variety of skills related to chemistry as well as data analysis. He also provided me with a screwdriver or hacksaw whenever I needed one. Bobbi Conard was exceptionally patient and supportive and taught me how to sample cores and digest samples. Bill Rugh helped me with a variety of technical problems and also improved the quality of basement life by playing his sax. John Huard grumpily and thoroughly taught me a tremendous amount in the Ar lab. He helped me troubleshoot a variety of problems and guided me through the analytical component of this research. He accepted nothing but analytical perfection. Tom Leach was very supportive, both comically and technically. He, Bruce and Chuck always talked shop about computers with me and helped with any networking or computer problem I had.

There is no way I could have enjoyed my time here as much if it weren't for Chris Russo. His unselfishness and acceptance of just about everything was refreshing and, I hope, contagious. He listened to problems about my research more than possibly my entire committee combined and offered incredible insights about my research. I wish I could have done the same for him but I am more selfish (and, hush-hush, way too bored with the mantle). Chris Romsos offered support as a friend during my time at COAS and also gave up a lot of technical tips with ArcGIS, web development, etc. I also thank Joel Johnson, who was my "type section" for graduate school and also a good friend.

Alan Mix has rigorously and critically investigated the logic behind my research and improved my ideas considerably. Gary Klinkhammer has always given me the time to talk marine sediments and diagenesis. Chris Goldfinger gave valuable insight into sedimentation on the Cascadia seafloor, while Joe Stoner taught me new skills on how to analyze and visualize downcore data. Beyond Corvallis, several scientists have lent support to me. Mitch Lyle, Steve Lund, Walter Dean and Charlotte Allen have offered data freely. I also thank family and friends for their support throughout this endeavor.

Just before beginning my PhD, I met my wife, Christie. She has supported me like no one ever has. I would not be as content with my life and work if not for her. I have been very lucky to have her unfailing encouragement and love. Now, it is my turn to give that in return to her and also give to others through education and service.

CONTRIBUTION OF AUTHORS

Chapters 2, 3 and 4 are the products of considerable collaboration with co-authors. My co-advisors Bob Duncan and Nick Pisias were instrumental in improving the concepts relayed in these works. Bob Duncan assisted with much of the ^{40}Ar-^{39}Ar technique development in the noble gas laboratory. He was also instrumental in guiding my writing and considerably improved how I convey more complex ideas on paper. Nick Pisias guided me to develop "big-picture" ideas into the quantitative models used in all three manuscripts. David Graham was instrumental in the third chapter, where he oversaw the development of Nd isotope chemistry in the COAS Keck Laboratory. He also helped with the ternary mixing models and improved the writing. For the final manuscript, Steve Hostetler brought a modeling perspective into the work and helped with both the details of the erosion model as well as ruminated on the larger climate controls in the northeast Pacific/Pacific Northwest region.

TABLE OF CONTENTS

TABLE OF CONTENTS (Continued)

Page

TABLE OF CONTENTS (Continued)

Page

LIST OF FIGURES

LIST OF FIGURES (Continued)

LIST OF TABLES

The Fluvial Response to Glacial-Interglacial Climate Change in the Pacific Northwest, USA

Chapter 1

Introduction

1.1 Foreword

There is evidence from the northeast Pacific Ocean to suggest that terrestrial and oceanic systems are tightly coupled on glacial-interglacial timescales. Pisias et al. (2001) have observed a strong correlation between pollen (an indicator of temperature and precipitation on land) and radiolaria (an indicator of sea-surface temperature). Specifically, changes in a linear combination of pollen assemblages heavily weighted by redwood (Sequoia) correspond temporally with a suite of radiolaria driven by an eastern boundary current (i.e., the California Current) assemblage. The relationship between these two climate proxies is shown in Figure 1.1. The hypothesis developed that when there is a strong California Current, as there is today, upwelling conditions are enhanced. This leads to more coastal fog and, in turn, to more redwood-dominated forests as seen presently in coastal southern Oregon and northern California (Figure 1.2A). These findings lead to a variety of questions related to climate and climate change in coastal regions. Do the climates of terrestrial and ocean environments oscillate as the result of the same forcing or are there climate response modes in one system that act independently of, or out-of-phase with, the other? Can the processes recording climate and climate change in the terrestrial realm be deconvolved from the history of this change archived in the ocean? Specifically, do pollen assemblages reflect terrestrial climate change directly or is their presence in marine sediments also dictated by transport pathways (ocean current systems) to the continental margin? Do transport pathways change on glacial-interglacial timescales (Figure 1.2C)?

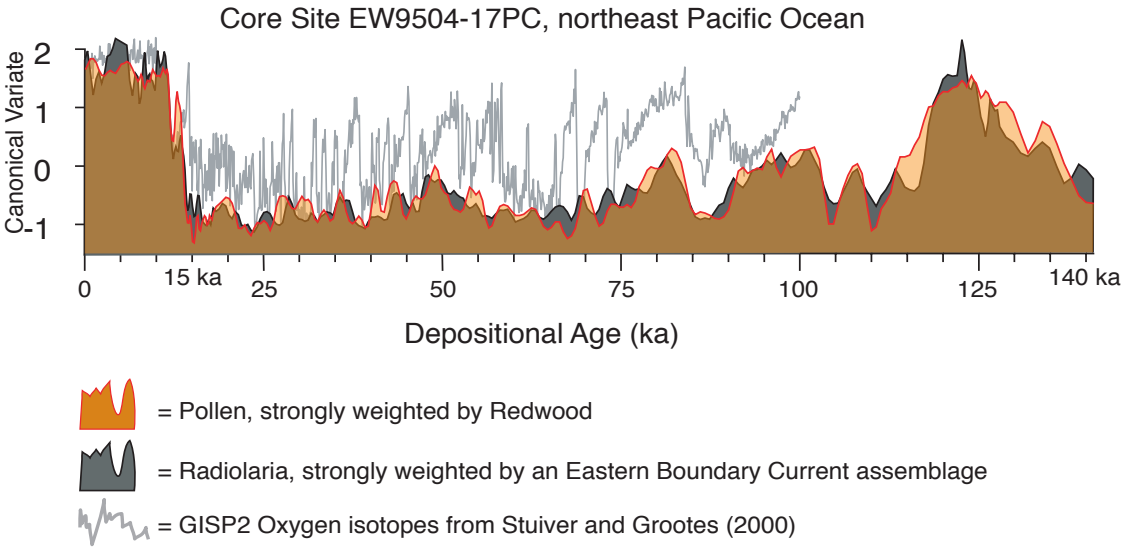

Figure 1.1 - Linear combination of pollen species (transparent orange with red outline) and radiolaria assemblages (dark gray with black outline) from Pisias et al. (2001). The strong coupling between terrestrial and ocean climate proxies suggest an in-phase climate linkage between the land and ocean systems. There is also a relationship between these northeast Pacific climate records and the arguably global oxygen isotope record from the GISP2 ice cores.

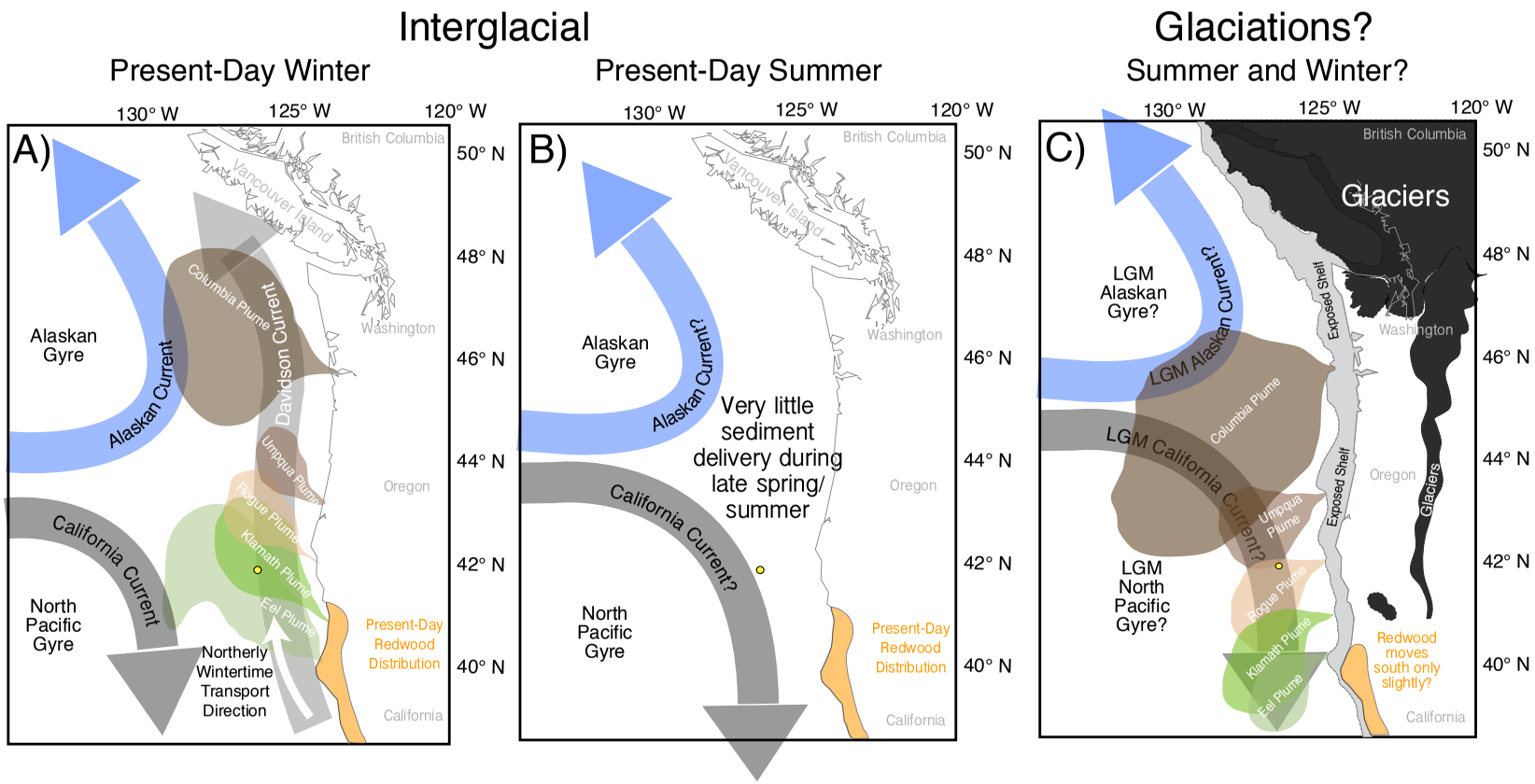

Figure 1.2 - Ocean currents and transport pathways in the northeast Pacific region. Core site EW9504-17PC is dentoed by the yellow circle in each frame. A) Sediment dispersal along the margin of northern California and Oregon occurs mostly in winter presently when the northerly-tracking Davidson Current is active (plumes are schematic). During summer months, when the California current is strong (B) and upwelling is favorable, little sediment is moved to the continental margin. But what if the dominant sediment transport direction changes. Figure 1.2C shows a hypothetical situation wherein the seasonality in ocean circulation is reduced and sediment transport direction is changed and follows the southward-flowing California Current? The carrier of pollen would change at the same time, compromising the relationship seen in pollen and radiolaria species. Examining the detrital sedimentology will illuminate whether ocean circulation changes in any significant way through time.

To address these questions, I have studied rivers and the material they transport, since they communicate a detailed history of earth surface processes to the deep ocean, where that history is preserved. My focus has been on the detrital minerals and rock fragments eroded from the continent, which are transported with pollen and other terrigenous material to the marine margin. The bedrock geology that is the source of this material does not change considerably over a glacial-interglacial cycle (excepting catastrophic geologic events such as volcanic eruptions or landslides). Thus, neither does the sediment fingerprint. So, even though climate dramatically alters the vegetative cover of the landscape and denudes the land surface, the detrital sediments remain faithful reflectors of their source rocks.

Yet, to unravel terrestrial-ocean climate linkages through provenance, techniques are needed that can take advantage of what is preserved in ocean sediments. A problem inherent to this is that deep-sea sediments are usually fine-grained and are often sample size-limited. Thus, methods that take advantage of the major strengths of marine sediment cores (the continuity of the record through time, for example) and overcome grain- and sample-size limitations are paramount to improving our understanding of climate-driven earth surface processes.

In this dissertation a methodology is developed that avoids or overcomes many of the common pitfalls in the marine realm such as diagenesis and other alteration effects, while at the same time extracts a robust signal from bulk sediment that is readily interpretable. This is done using the ^{40}Ar-^{39}Ar incremental heating technique. Instead of using it in the more traditional way whereby populations of single grains are analyzed (Heller et al., 1985; Copeland and Harrison, 1990; Hodges et al., 2005; Najman et al., 2005), it is employed to extract information from bulk sediments. This is not the first time this approach has been used (Hemming et al., 2002; Wong et al., 1995; Pettke et al., 2000). But this work does shed new light on the information contained in the bulk signal, with quantitative explorations into the meaning behind bulk sediment radiometric ages.

The main question addressed in the first manuscript (Chapter 2) is how reliable are the bulk sediment ^{40}Ar-^{39}Ar ages? It is shown here that they can be very reliable and from this finding explore, in quantitative terms, how accurately the bulk ages indicate the average age of

cooling/crystallization of the erodable source rocks within a given river basin. This develops a conceptual framework for interpreting the bulk sediment ^{40}Ar-^{39}Ar ages downcore.

To substantiate the value of the bulk sediment ^{40}Ar-^{39}Ar incremental heating technique and to improve its utility, it is combined with more traditional approaches such as bulk sediment Nd isotope methods and clay mineralogy, which have each shown their usefulness in provenance studies (Fagel et al., 2004; Liu et al., 2004; Walter et al., 2000; Lamy et al., 1998). The combined Ar-Nd isotopic approach is applied to examining provenance changes at core site EW9504-17PC, which lies in a sensitive transition zone between the North Pacific and Alaskan Gyres (Figure 1.2) to investigate the robustness of the pollen-radiolaria climate interpretations and unravel the response of coastal Pacific Northwest Rivers to climate change. This study is detailed in Chapter 3.

Chapter 4 offers a different approach to understanding climate-driven erosion. The study integrates regional climate model simulations of precipitation changes (e.g., Hostetler et al., 2006) and present-day sediment loads with the ^{40}Ar-^{39}Ar detrital mixture model over the Last Glacial Maximum and through the deglaciation to quantitatively address downcore changes in provenance observed at core site EW9504-17PC and investigate the changing erosional regime. The sensitivity of the erosion model is investigated, as is the amount of change needed in precipitation to arrive at the observed bulk sediment ^{40}Ar-^{39}Ar values. The larger climatic implications of the model findings are discussed. This dissertation concludes with a summary of major findings from all three manuscripts and also contemplates the future application of the approach developed here.

1.2 References

Copeland, P., Harrison, M., and Heizler, M. T., 1990, $^{40}Ar/^{39}Ar$ single-crystal dating of detrital muscovite and K-feldspar from Leg 116, southern Bengal Fan: Implications for uplift and erosion of the Himalayas, *in* Cochran, J. R., Stow, D. A. V., and et al., eds., Proceedings of the Ocean Drilling Program: Scientific Results: College Station, TX, Ocean Drilling Program, p. 93-114.

Dong, H., Hall, C. M., Peacor, D. R., and Halliday, A. N., 1995, Mechanisms of argon retention in clays revealed by laser ^{40}Ar-^{39}Ar dating: Science, v. 267, p. 355-359.

Fagel, N., Hillaire-Marcel, C., Humblet, M., Brasseur, R., Wieis, D., and Stevenson, R., 2004, Nd and Pb isotope signatures of the clay-size fraction of Labrador Sea sediments during the Holocene: Implications for the inception of the modern deep circulation pattern Paleoceangraphy, v. 19, p. doi:10.1029/2003PA000993.

Heller, P. L., Peterman, Z. E., O'Neil, J. R., and Shafiqullah, M., 1985, Isotopic provenance of sandstones from the Eocene Tyee Formation, Oregon Coast Range: GSA Bulletin, v. 96, p. 770-780.

Hemming, S. R., Hall, C. M., Biscaye, S. M., Higgins, S., Bond, G. C., McManus, J. F., Barber, D. C., Andrew, J. T., and Broecker, W. S., 2002, $^{40}Ar/^{39}Ar$ ages and $^{40}Ar^*$ concentrations of fine-grained sediment fractions from North Atlantic Heinrich layers: Chemical Geology, v. 182, p. 583-603.

Hodges, K. V., Ruhl, K. W., Wobus, C. W., and Pringle, M. S., 2005, $^{40}Ar/^{39}Ar$ thermochronology of detrital minerals, *in* Reiners, P. W., and Ehlers, T. A., eds., Low-Temperature Thermochronology: Techniques, Interpretations, and Applications: Reviews in mineraology and geochemistry.

Hostetler, S., Pisias, N., and Mix, A., 2006, Senstivity of the Last Glacial Maximum climate to uncertainties in the tropical and subtropical ocean temperatures: Quaternary Science Reviews, v. 25, p. 1168-1185.

Lamy, F., Hebbeln, D., and Wefer, G., 1998, Late Quaternary precessional cycles of terrigenous sediment input off the Norte Chico, Chile (27.5 °S) and palaeoclimatic implications: Palaeogeography, Palaeoclimatology, Palaeoecology, v. 141, p. 233-251.

Liu, Z., Colin, C., Trentesaux, A., Blamart, D., Bassinot, F., Siani, G., and Sicre, M.-A., 2004, Erosional history of the eastern Tibetan Plateau since 190 kyr ago; clay mineralogical and geochemical investigations from the southwestern South China Sea: Marine Geology, v. 209, no. 1-4, p. 1-18.

Najman, Y., Carter, A., Oliver, G., and Garzanti, E., 2005, Provenance of Eocene foreland basin sediments, Nepal; constraints to the timing and diachroneity of early Himalayan orogenesis: Geology Boulder, v. 33, no. 4, p. 309-312.

Pettke, T., Halliday, A. N., Hall, C. M., and Rea, D. K., 2000, Dust production and deposition in Asia and the north Pacific Ocean over the past 12 Myr: Earth and Planetary Science Letters, v. 178, p. 397-413.

Stuiver, M., and Grootes, P. M., 2000, GISP2 oxygen isotope ratios: Quaternary Research, v. 53, p. 277-284.

Walter, H. J., Hegner, E., Diekmann, B., Kuhn, G., and Rutgers van der loeff, M. M., 2000, Provenance and transport of terrigenous sediment in the South Atlantic Ocean and their relations to glacial and interglacial cycles: Nd and Sr isotopic evidence: Geochimica et Cosmochimica Acta, v. 64, no. 22, p. 3813-3827.

Chapter 2

Erosion by Rivers and Transport Pathways in the Ocean: A Provenance Tool using ^{40}Ar-^{39}Ar Incremental Heating on Fine-Grained Sediment

Sam VanLaningham, Robert A. Duncan and Nicklas G. Pisias

[1]College of Oceanic and Atmospheric Sciences
Oregon State University, Corvallis, Oregon 97331

VanLaningham, S., R.A. Duncan, N.G. Pisias, 2006, Erosion by Rivers and Transport Pathways in the Ocean: A Provenance Tool using ^{40}Ar-^{39}Ar Incremental Heating on Fine-Grained Sediment, Journal of Geophysical Research, vol. 111, doi:10.1029/2006JF000583.

2.1 Abstract

We use ^{40}Ar-^{39}Ar incremental heating to fingerprint bulk fluvial sediment entering the northeast Pacific Ocean, with the long-term intent of tracking sediment source and transport changes from the terrestrial system to the marine environment through time. We show reproducible age spectra from individual rivers accounting for the majority of sediment delivered to the Pacific margin. Two tests are performed to confirm the validity of the bulk sediment ^{40}Ar-^{39}Ar incremental heating measurements and to address why polymineralic sediment might yield concordant age steps. The first model tests, in light of bulk mineralogy and diffusion of Ar from silicates, whether measured K/Ca spectra (measured from ^{39}Ar and ^{37}Ar, respectively) are consistent with typical values for K- and Ca-bearing minerals. Calculations show that the bulk mineralogy is reflected in the outgassing K/Ca spectra and identify plagioclase as the dominant mineral contributing to the plateau-defining portion of the age spectra. A second model predicts bulk sediment ages from integrated bedrock cooling age-area estimates in order to examine whether bulk sediment plateau ages are representative of the average cooling age of rocks from a given river basin. Calculated and observed ages are notably similar in three river basins when topographic and lithologic effects are accounted for. Overall, this technique shows considerable promise, not only in tracking individual terrigenous sources in the marine realm but also for understanding processes such as erosion and sediment transport in terrestrial systems.

2.2 Introduction

Deep-sea sediments provide a particularly complete and integrated record of Earth's climate and tectonic systems. To fully appreciate information contained in the terrigenous fraction of marine sediments, that fraction derived from continental erosion, it is critical that we are able to identify the source regions and transport pathways of the sediment deposited at any given location. With this "provenance" information we can better delineate a variety of processes including the response of ocean circulation and continental landscapes to climate

change, as well as tectonic processes that modify the morphology of the landscape.

A variety of studies have illustrated the power of using terrigenous material to understand dynamics of Earth's climate system. For example, changes in oceanographic circulation over glacial-interglacial timescales have been discovered in many regions of the world through identification of terrigenous sources and their distribution in the sediment record (Fagel et al., 2002; Fagel et al., 1996; Jantschik and Huon, 1992; Walter et al., 2000). Patterns of sea-ice movement have been resolved by tracking entrained Fe-oxides from their original, terrestrial source (Darby, 2003). Spatially and temporally variable precipitation patterns in the coastal Chilean and Andean mountains have been better understood over the last 28,000 years through terrigenous Fe changes seen in offshore sediment cores (Lamy et al., 1999), while characterizing the provenance and pathways of ice bergs in the northeast Atlantic have been carried out by studies of ice-rafted and glacial debris using ^{40}Ar-^{39}Ar dating methods applied to detrital hornblendes and sediments (Hemming et al., 1998; Hemming et al., 2002). Identifying the cratonic sources of glacial till via large populations of single crystal ^{40}Ar-^{39}Ar total fusion ages has been a recent avenue for provenance study related to natural climate variations (Roy et al., 2005). Beyond the paleoclimate world, a variety of tectonic processes have also been unraveled through provenance studies of river sediments (Bernet et al., 2004; Carrapa et al., 2004; Clift et al., 2002; Clift et al., 2001; Garzanti et al., 1996; Garzanti et al., 2005; Reiners et al., 2005a; Spiegel et al., 2004; Wobus et al., 2003), while linking and deconvolving climatic and tectonic signals is at the forefront of studies of Earth surface processes today (Clift and Blusztajn, 2005; Kuhlemann et al., 2004).

The spatial resolution at which terrigenous sources can be identified is dependent on the diversity of the age, mineralogy and chemistry of rocks that are eroded and on the development of techniques that characterize those sources. Generally, provenance has been distinguished on the scale of geologic provinces (Fagel et al., 2002; Hemming et al., 1998; Lamy et al., 1998; 1999; Walter et al., 2000). There have been fewer studies that fingerprint specific fluvial sediment sources via isotopic methods (Clift et al., 2004; Clift et al., 2002) or mineralogic techniques (Garzanti et al., 2005). Since most rivers in a given region erode common rock types, it remains difficult to resolve provenance at the fluvial basin scale.

Fission-track studies (Brandon and Vance, 1992; Carter, 1999), U-Pb and (U-Th)/He dating of detrital zircons (Reiners et al., 2005a) and a variety of single-grain K-feldspar (Copeland et al., 1990) and mica analyses (Carrapa et al., 2004; Heller et al., 1992) have proven to be extremely powerful ways to resolve sediment source. However, the low abundances and very small particle sizes of minerals beyond the shelf-slope break make the applicability of these single-grain methods tenuous in the deeper marine realm. Yet, the deep sea is where the most continuous sediment records are preserved, since sea-level oscillations expose and erode the shelf. Moreover, terrigenous material makes up 77% of sediment in the world's oceans (Lisitzin, 1996), and yet detailed knowledge about the source of much of these sediments is lacking since so much of it is made up of very small particle sizes.

In this paper we investigate the resolution at which ^{40}Ar-^{39}Ar incremental heating methods can characterize provenance of bulk fluvial, silt-sized sediments (20-63 μm). Bulk sediment ages using the ^{40}Ar-^{39}Ar system were previously reported by Hemming et al. (2002). That work was part of a larger study that showed that the bulk sediment ages reflected terrestrial source, paving the way for this study. Hemming et al. (2002) did not explore the meaning of the age spectra, potential fluvial sources were not characterized and smaller size fractions were measured. Other ^{40}Ar-^{39}Ar incremental heating studies have been carried out on the clay-sized fraction of sediments, using a technique that overcomes problems related to Ar recoil and loss in fine-grained sediment (Dong et al., 1995). Although these methods can be invaluable in the marine setting (Pettke et al., 2000), we focus on the silt-sized fraction so as to better ensure that we capture reproducible ages related to source rock cooling, avoiding ages that could be a function of weathering or diagenesis (Dong et al., 1995).

We apply ^{40}Ar-^{39}Ar incremental heating methods to characterize fluvially borne terrigenous material at its last juncture before entering the ocean, with the expectation of applying it as a robust provenance tracer in marine sediments. In this paper we show that concordant middle to high temperature step ages derived from this method reflect the average cooling age of the rocks that are eroded from exposed source rocks, as others have inferred (Hemming et al., 2002; Pettke et al., 2000). Reproducible age spectra, including concordant step ages comprising a majority of the Ar release (termed plateaus) can be extracted from the

bulk sediment, in many cases. This work also suggests that it may be possible to accurately identify specific sediment sources that derive from the same geologic province(s), but drain varying proportions thereof. We use K/Ca information to address questions about why sediments produce age plateaus and what minerals are likely characterizing the gas at different temperatures. We finish with simple calculations that evaluate how well the measured bulk sediment ^{40}Ar-^{39}Ar plateau ages represent the average cooling age of minerals from contributing rock types in a given river basin and discuss this technique's promise and limitations.

2.3 Expectations for ^{40}Ar-^{39}Ar Incremental Heating Experiments on Multi-Phase Detrital Sediments

A ^{40}Ar-^{39}Ar total fusion (single step) age or K-Ar age documents the time at which a mineral, or whole rock cooled below a certain closure temperature (we use cooling age realizing that it is synonymous with crystallization age in volcanic rocks, but may be significantly younger in slowly cooled plutonic rocks). By using the incremental heating technique, valuable geologic information can be gained such as whether metamorphic, hydrothermal, or weathering events have affected the distribution of K and Ar in a mineral or whole rock sample. In essence, an incremental heating age spectrum (age vs. temperature or %gas released) can often reveal much of the thermal history of a mineral or whole rock. In this study we employ the incremental heating technique because of the information gained over a fusion age alone. For instance, since we extract gas from a fine-grained mixture of minerals from a variety of geologic provinces, the step heating information (both age and K/Ca) provides a way of determining the variety and relative contributions of minerals to the age patterns presented by the sediment samples. In the following section, we discuss the traditional features associated with ^{40}Ar-^{39}Ar age spectra so that there is a framework for understanding the methods and results from this study.

In an age spectrum derived from incremental heating of a single mineral, the main interpretable features are cooling age, Ar loss, inherited or excess Ar, and Ar recoil. Cooling

ages are often indicated by concordant step ages, forming a plateau (Figure 2.1A). Ar loss occurs from a variety of conditions such as reheating during metamorphic events, surface weathering, chemical alteration, and mechanical grinding (see summaries by Dalrymple and Lanphere, 1969; McDougall and Harrison, 1999). ^{40}Ar loss is evidenced by ever-increasing ages in the low temperature steps of the age spectrum (Figure 2.1B), presumably due to heating-activated diffusion from less retentive margins and fractures in crystals. Excess Ar, resulting from un-degassed mantle-derived ^{40}Ar at the time of crystallization or hydrothermally deposited, non-atmospheric ^{40}Ar, is often detectable in ^{40}Ar-^{39}Ar age spectra, usually by a saddle-shaped degassing pattern; i.e., older than actual crystallization ages at low and high temperature steps.

Ar recoil presents another problem. It results in ^{39}Ar and ^{37}Ar loss or relocation during irradiation, due to recoil of target atoms (K and Ca, respectively) during neutron capture (Faure, 1986; Turner and Cadogan, 1974). When ^{39}Ar is lost from crystal margins during irradiation in the reactor, the ^{40}Ar/^{39}Ar ratio at low temperature steps increases, and so does measured age. In fine-grained, multi-phase samples there is presumably also a net transfer of ^{39}Ar from K-rich to K-poor phases, making the K-rich components "too old" and the K-poor portions "too young" (Turner and Cadogan, 1974). Since K-rich phases outgas at low temperatures and K-poor phases outgas at high temperatures, Ar recoil can usually be recognized by an ever-decreasing step age with increasing temperature in the age spectrum (Figure 2.1C; McDougall and Harrison, 1999). Recoil can also transfer ^{37}Ar from Ca-rich to Ca-poor phases, resulting in under- or over-correction of ^{36}Ar interferences and a similar "inverse staircase" effect on the age of the spectrum. Combinations of Ar loss and recoil are also possible (Figure 2.1D).

In fluvial material, or the terrigenous fraction of marine sediments, it is expected that the age and K/Ca spectra will be different from analyses performed on a single mineral since the bulk sediments are multi-age and polymineralic. Age spectra may display variability in step ages and K/Ca throughout the heating schedule. This has been seen before in multi-phase samples, where irregular spectra have been obtained from old xenoliths carried in young basalt flows (Gillespie et al., 1982), meteorites showing bimodal trends in their K/Ca spectra due

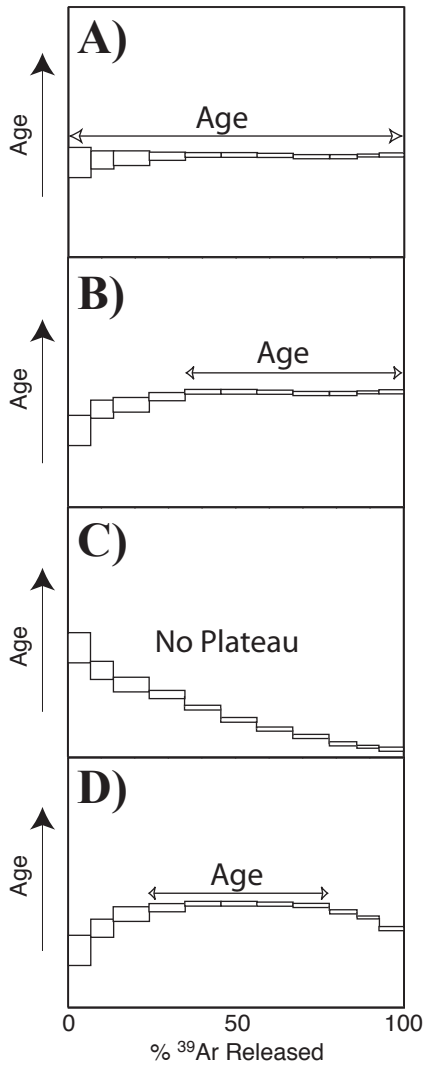

Figure 2.1 - Typical ^{40}Ar-^{39}Ar age spectra for single crystals and expected results in polymineralic, multi-age, fine-grained sediment mixtures. A) Single crystal degassing with homogeneous distribution of argon. In the case of a sediment mixture, a long plateau age like the one shown would require that all minerals degas synchronously or that all minerals are the same age, which are both unlikely. B) Argon loss in either single crystals or polymineralic sediment or, the presence of younger, low-temperature minerals. C) Argon recoil or younger high-temperature minerals (in sediments). D) Ar loss at low-temperatures and Ar recoil at high temperatures in single crystals or bulk sediment, or younger low-temperature and high-temperature minerals.

to the temperature-dependent degassing of plagioclase and pyroxene (Wang et al., 1980) and mixtures of detrital K-feldspar grains showing complex degassing patterns (Copeland and Harrison, 1990). Features like these might be observed in bulk sediment samples. However, previous studies show that concordant steps in polymineralic detritus might also be expected (Dong et al., 1995; Hemming et al., 2002; Pettke et al., 2000).

2.4 Study Area

Our ultimate goal is to develop methodologies to identify terrigenous sources for deep-sea sediment derived from the Pacific continental margin of northern California, Oregon and Washington. This is part of a larger project relating glacial-interglacial changes in down-core pollen and radiolaria assemblages (Pisias et al., 2001) to terrigenous sediment provenance as a means to distinguish continental vegetation changes from oceanic circulation changes, although the method has broader utility.

To characterize sediments entering this region of the Pacific Ocean for the purpose of tracing sources and transport pathways, we have obtained samples from the mouths of fourteen rivers in the Pacific Northwest (Figure 2.2). From San Francisco Bay to the Straits of Juan de Fuca, these rivers drain a diverse set of geologic provinces. In Washington, the rocks of the Olympic Mountains are comprised of a suite of sandstones, mudstones and volcanic lithologies that have Eocene to Miocene depositional ages (Brandon and Vance, 1992). The Quinalt River sample represents this region (QUI-1). In the southwestern coastal ranges of Washington and northwestern Oregon, rivers erode Eocene sedimentary and volcanic rocks (Walker and MacLeod, 1991). Samples were taken from Grays Harbor (GRA-1), Willapa Bay (WIL-2 and 4), and Tillamook Bay (TIL-1 and 2).

The Columbia River drains an immense area (Figure 2.2) and a large variety of rock types and geologic provinces with various cooling ages. Lithologies in the headwaters of the Columbia River (including the Kootenay and Okanogan River tributaries) in British Columbia are Mesozoic accreted terranes of sedimentary, volcanic and plutonic origins as well as many stocks that intruded into the accreted units (Ghosh, 1995; Monger et al.,

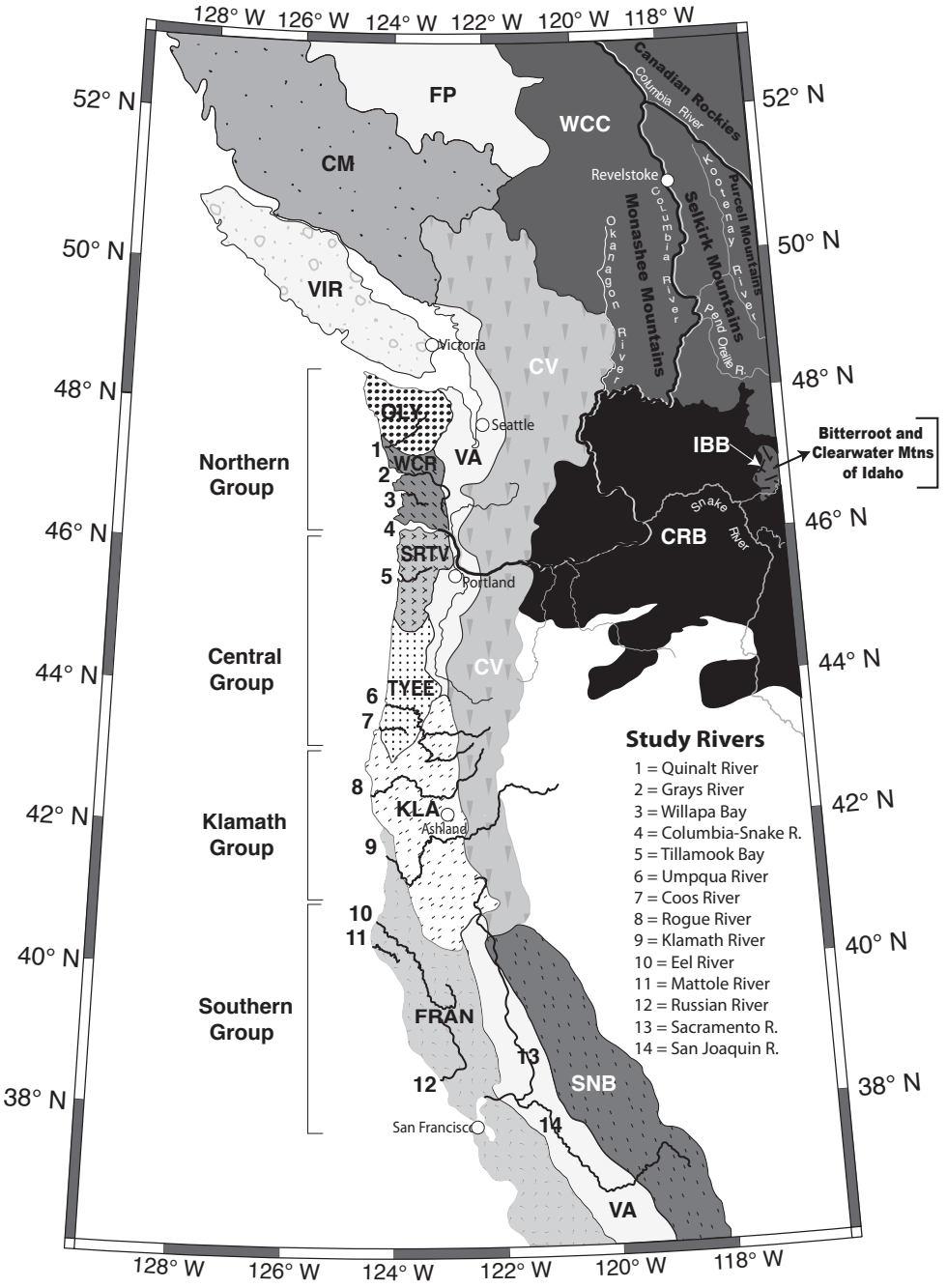

Figure 2.2 - Study rivers and bedrock geology of the western U.S. Major Columbia R. tributaries and British Columbia mtn. belts are shown for reference. The far eastern portion of the Columbia R. Basin is not shown for space considerations. OLY = Olympic Mountains; WCR = Washington Coast Ranges; SRTV = Siletz-Tillamook Volcanics; TYEE = Tyee Fm. Turbidites; KLA = Klamath Mtn. Accretionary Complex; FRAN = Franciscan Melange; VA = Valley Alluvium; SNB = Sierra Nevada Batholith; CV = Cascade Volcanics; CRB = Columbia River Basalts; WWC = Western Canadian Cordillera; IBB = Idaho-Bitterroot Batholith; VIR, CM and FP = Vancouver Island Ranges, Coast Mountains and Fraser Plateau (do not contribute to Col. R.). See text for an explanation of lithologies.

1982). The Snake River, a large tributary of the Columbia River, erodes mostly Cretaceous Idaho-Bitterroot Batholith granites in the high-relief regions and then flows across young Tertiary volcanic rocks in the Snake River Plain. The headwaters of the Pend Oreille-Clark Fork and Clearwater tributaries drain the 55-62 Ma granitic batholiths of the Bitterroot Mountains and meta-sedimentary rocks with Mesozoic to Paleozoic depositional ages from the Rocky Mountains of Montana. Over much of the Columbia Basin, the Columbia River and tributaries erode and flow through the vast area of Miocene Columbia River Basalts and the Tertiary to Recent arc volcanic rocks of the Cascade Mountains. Five samples were analyzed from the Columbia River (COL-1, 3, 5, 1341 and 1498).

Rivers along the central Oregon coast drain turbidite sequences and oceanic basalts with Eocene depositional ages (Coos River, COO-1A and 1C). The Umpqua River (UMP-1A, 1B, and 902) begins in Cenozoic basaltic and andesitic rocks of the central and southern Oregon Cascades and traverses the turbidites of the Oregon Coast Ranges en route to the Pacific Ocean. In southern Oregon and northern California, rocks of the Klamath Mountains are a Mesozoic accretionary complex composed of metasedimentary, meta-volcanic, granitic and gabbroic rocks and ophiolitic sequences eroded by the Rogue River (ROG-1A, 4, and 5) and the Klamath River (KLA-1, 2, 4 and 898). Both the Rogue and Klamath Rivers also have significant portions of their headwaters in the volcanic rocks in the southern Cascade Mountains.

The coastal range of northern and central California is dominated by the Franciscan Melange, a Cretaceous to lower Tertiary sequence of sandstones and mudstones, with large blocks (up to several kilometers in size) of serpentinite, blueschist, eclogite greenstone, chert and limestone (Blake and Jones, 1981; McLaughlin et al., 1994), although other less extensive volcanic lithologies are present in the region as well. The Eel (EEL-1A, 1B and 2), Mattole (MAT-1) and Russian Rivers (RUS-1 and 2) drain this region. The southernmost rivers (Sacramento and San Joaquin Rivers) drain the granitic rocks of the Mesozoic Sierra Nevada Mountains, Great Valley sediments and lesser contributions from the Klamath and Franciscan rocks. These rivers are represented by SAC-1 (Sacramento River), SAN-1 (San Joaquin River) and SCN-1 (sample from the confluence of the Sacramento and San Joaquin Rivers).

2.5 Sampling Methods

We sampled from riverbeds either by hand or using a PVC hand sampler in a skiff or by wading. To avoid tidally derived sediment, most samples were taken from riverbeds above the saltwater-freshwater interface. However, some samples were collected in estuaries because this is often where several sediment sources mix before being flushed into the open ocean during storm events. We wanted to capture the most representative samples that enter the ocean, but at the same time, avoid beach material transported into the estuary by tidal processes (Peterson et al., 1984). In the cases of Willapa Bay and especially Tillamook Bay, attempting to achieve these goals were unsuccessful since it was necessary to collect samples before the point where all main rivers and streams culminate.

Typically, several samples were collected from each river. Most samples were taken in shallow, lower energy environments where fine-grained material was deposited, such as the downstream side of point bars, sidebars and small embayments. When possible, samples were also taken in mainstream sections. Fine-grained samples were our target since the suspended load that is transported by ocean currents to continental margin sites is of a small particle size. We assume that the fine-grained material sampled here is representative of material that is transported to the ocean but falls out of suspension in the lower energy point bar, sidebar and embayed environments. All samples were collected during low flow conditions in the early summer of 2002, except COL-1341 and COL-1498, UMP-902 and KLA-898, which were collected in the mid 1970's (Oregon State University Marine Geologic Core Repository).

2.6 Analytical Procedures

The 20-63 μm size fraction was extracted from about 100-300 g of bulk material by sieving at 63 μm and then using the Stokes settling equation to remove the 0-20 μm fraction. The organic compounds were removed by initially adding 30 ml of 35% hydrogen peroxide to the samples. After eight hours of organic oxidation an additional 30 ml of the hydrogen peroxide was added and the samples were shaken for 72 hours. Two hydrogen peroxide steps

were needed because of the high organic content in the river sediments. Three washes in distilled water followed. Carbonate was removed by adding 200 ml of dilute acetic acid to each sample and then samples were shaken for 24 hours. The samples were then washed in distilled water three more times. All preparation steps were performed at room temperature.

Irradiation of ~50 mg of sample packaged with the FCT-3 monitor standard (age = 28.03±0.18 Ma; Renne et al., 1994) occurred for six hours in the core of the 1 MW reactor to induce the reaction ^{39}K (n, p) ^{39}Ar. The irradiated samples were analyzed using the MAP 215-50 mass spectrometer in the Ar geochronology laboratory at Oregon State University. Samples were loaded into a Cu sample holder, placed in a vacuum chamber and heated incrementally with a defocused 10W CO_2 laser programmed to traverse the sample during each heating step (for approximately five minutes). Samples were degassed with 13 to 15 temperature steps, from 200-300°C to fusion at around 1400°C. Laser temperature was calibrated to laser power with a pyrometer. For each laser-heating step, the extracted gas was exposed to Zr-Al getters for five minutes to remove active gases before measurement in the mass spectrometer. A five-minute pump out time was used between samples. Four blanks were run per sample in order to make corrections throughout sample analysis. Isotopic masses for ^{40}Ar, ^{39}Ar, ^{38}Ar, ^{37}Ar and ^{36}Ar were measured, with the latter three used to correct for interferences on ^{40}Ar and ^{39}Ar (McDougall and Harrison, 1999). The most important of these corrections is an atmospheric correction of ^{40}Ar via the $^{40}Ar/^{36}Ar$ ratio and reactor-induced ^{39}Ar and ^{36}Ar interferences from Ca that are corrected via ^{37}Ar.

The plateau and integrated (total fusion) ages were calculated from corrected $^{40}Ar/^{39}Ar$ ratios using ArArCalc (Koppers, 2002). A variety of corrections were made including those related to mass fractionation and short-lived radioactive decay, while error propagation was applied to every step-heating analysis and correction. Computations of the weighted age plateau and an estimate of its goodness of fit were determined as well. A plateau age, as defined for this study, is any age spectrum that has 50% or more of its total ^{39}Ar characterized by concordant steps (Koppers, 2002; McDougall and Harrison, 1999). A mean square of weighted deviations (MSWD) calculation was made for every plateau age to assess the goodness of fit. When this value is much greater than the expected value of one, it

suggests that errors on the weighted plateau are underestimated, while a value much less than one suggests that the weighted plateau error is likely to be overestimated (Koppers, 2002; McDougall and Harrison, 1999; Wendt and Carl, 1991).

Potassium - calcium ratios (K/Ca) were also calculated in ArArCalc from measured concentrations of ^{39}Ar derived from K and ^{37}Ar derived from Ca. This ratio was then multiplied by a constant of 0.43 (determined from a monitor standard with a known K/Ca ratio (Dalrymple et al., 1981; McDougall and Harrison, 1999) to arrive at the K/Ca values presented here. A subset of samples (16 of the 33) was analyzed for their K and Ca concentrations, using standard ICP-OES (inductively-coupled plasma-optical emission spectrometer) techniques following procedures by Walczak (2006). These were compared with K/Ca values determined from the step-heating Ar analyses and are discussed later in the paper.

The K/Ca values from the step-heating Ar data are also compared with published K/Ca ratios of the major K- and Ca-bearing minerals from the source rocks of geologic provinces in the study area (Deer et al., 1992; GEOROC database, http://georoc.mpch-mainz.gwdg.de/georoc/; Barnes, 1987; Barnes et al., 1986, 1992) to aid in our interpretation of the minerals contributing to the ^{40}Ar-^{39}Ar age spectra. These K/Ca values for different minerals are presented in Table 2.1. The minerals are presented in the general order that they most readily diffuse Ar gas as a function of temperature (Brady, 1995; Dalrymple et al., 1981; McDougall and Harrison, 1999).

Mineralogical identifications by X-ray diffraction (XRD) are presented from eleven Pacific Northwest fluvial samples to underscore our understanding of the gross features dictated by mineralogy in the age and K/Ca spectra. A Scintag Pad-V X-ray diffractometer was used from 5°-64° 2θ using Cu radiation. Samples were sprinkled through a sieve onto slides with double-sided tape and then "razor-tamped" following the procedures outlined by Zhang et al. (2003). This method provides a relatively simple way to attain randomly-oriented powders which are necessary to acquiring quantitative information about mineral abundances. The data were analyzed using MacDiff software (http://www.geologie.uni-frankfurt.de/Staff/Homepages/Petschick/RainerE.html). Relative mineral abundances were calculated on a quartz-free basis.

Mineral	K/Ca
Kaolinite	4.0
Vermiculite	0.03
Illite	15
Biotite	10 - 800
K-Feldspar	10 - 400
- Orthoclase	25 - 60
- Microcline	42
- Sanidine	55
CPX	0 - 0.04
OPX	0 - 0.02
Plagioclase	
- Albite	0.20 - 0.52
- Andesine	0.10 - 0.20
- Bytownite	0.01 - 0.10
- Anorthite	0.003 - 0.02
Amphibole	0.06 - 0.20

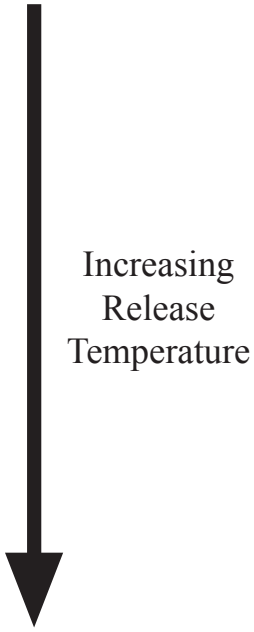

Table 2.1 - Common ranges of K/Ca values found in major K- and Ca-bearing minerals in their order of Ar release temperature (activation energy). Note: different potassium feldspar and plagioclase members do not necessarily release argon at different temperatures. K/Ca values from Deer et al., (1992), the GEOROC database (http://georoc.mpch-mainz.gwdg.de/georoc/), Barnes (1987), Barnes and others (1986; 1992). The order of release temperature is based on activation energies from a review paper by Brady (1995) and references therein, as well as Fechtig and Kalbitzer (1966).

2.7 Analytical Results

2.7.1 ^{40}Ar-^{39}Ar Age Spectra

A summary of results from the 33 ^{40}Ar-^{39}Ar incremental heating experiments is presented in Table 2.2. Bulk sediment plateau ages for Pacific Northwest river samples range from 76 Ma to 156 Ma. Twenty-two of the 33 samples produced multi-step, concordant ages in the mid- to high-temperature portions of their age spectra, accounting for at least 50% of the total gas released from the bulk polymineralic sediment. We term the weighted mean of these concordant step ages a plateau age, remembering that these step ages are the result of congruent degassing of several phases. Because of lower ages in the low temperature steps (likely from ^{40}Ar loss), the total fusion ages, obtained by summing all gas fractions and comparable to a conventional K-Ar age, are usually younger than the plateau ages, although most samples have a plateau age within 10% of the total fusion age.

The samples are organized into four geographic/lithologic groups (Figure 2.2): The Northern group (sediments from coastal Washington rivers and the Columbia River), the Central group (sediments from coastal Oregon rivers south of the Columbia River to ~43° N latitude), the Klamath group (sediments from the Rogue and Klamath Rivers eroding the Klamath Accretionary Complex), and the Southern group (northern and central Californian river sediments).

The plateau ages for the Washington coastal river sediments range from 121 to 125 Ma (Figure 2.3). The QUI-1 (Quinalt River) age spectrum does not develop a plateau. Step ages increase until a short, three-step maximum of 157 Ma. GRA-2, which was taken from the confluence of the Chehalis and Hoquiam Rivers in Grays Harbor, shows an initial ramp up in step ages followed by a five-step plateau (50% of the total gas) at 121 Ma and finishes with increasing step ages until fusion. For Willapa Bay, WIL-2 shows a continuous increase in age throughout the age spectrum while WIL-4 developed a six-step plateau containing 64% of the gas, at 125 Ma. Four out of five Columbia River samples display two fairly distinct plateaus in their age spectra (Figure 2.3). The lower temperature plateaus range from 103-113 Ma

	Sample Name	Latitude ° N	Longitude ° W	total fusion Ma	Plateau Age Ma	2-sigma error	#steps	% ^{39}Ar	MSWD	Plateau K/CA	Integrated K/Ca
Northern	QUI-1	47.35	124.29	103.8	156.6	2.5	3	19.8	1.5	0.14	0.33
	GRA-2	46.97	123.80	114.3	121.1	1.2	5	50.3	0.5	0.42	0.30
	WIL-2	46.72	123.93	112.3	No Plateau	NA	NA	NA	NA	NA	0.53
	WIL-4	46.72	123.93	115.4	124.8	2.2	6	64.3	14.0	0.36	0.26
	COL-1 LP	46.25	123.36	108.3	103.0	1.0	5	48.9	1.0	0.38	0.30
	COL-1 HP				113.3	1.4	3	26.0	0.4	0.28	
	COL-3 LP	46.25	123.49	111.7	108.9	1.3	4	48.9	0.8	0.32	0.25
	COL-3 HP				124.7	3.9	3	21.2	9.5	0.29	
	COL-5 LP	46.24	123.62	123.8	112.5	4.6	3	33.3	10.4	0.35	0.28
	COL-5 HP				138.1	1.5	4	33.8	0.6	0.38	
	COL-1341 LP	See	Below	125.7	106.1	1.4	7	27.6	1.4	0.69	0.54
	COL-1341 HP				133.8	1.3	6	47.9	1.8	0.48	
	COL-1498	See	Below	72.2	141.0	2.3	3	8.4	0.2	0.52	0.79
Central	TIL-1	45.48	123.90	102.6	110.5	1.2	8	73.6	3.0	0.26	0.41
	TIL-2	45.48	123.90	73.1	76.5	0.8	6	57.0	1.1	0.15	0.11
	UMP-902	See	Below	93.6	100.3	0.9	8	54.0	0.2	0.44	0.50
	UMP-1A	43.70	124.07	84.0	88.3	0.6	8	79.2	1.1	0.52	0.66
	UMP-1B	43.70	124.07	85.4	88.5	0.9	8	75.5	1.3	0.10	0.14
	COO-1A	43.38	124.18	92.5	99.9	0.5	3	41.2	0.8	0.47	0.33
	COO-1C	43.38	124.18	87.9	94.2	1.8	6	58.6	12.7	1.71	1.75
Klamath	ROG-900	See	Below	116.7	124.9	1.5	11	71.0	2.0	0.21	0.34
	ROG-1A	42.44	124.40	128.0	131.7	0.9	10	88.6	2.2	0.14	0.32
	ROG-4	42.44	124.38	117.9	127.2	2.0	9	79.8	1.7	0.12	0.17
	ROG-5	42.44	124.38	124.0	130.5	1.5	7	71.2	0.5	0.19	0.30
	KLA-898	See	Below	144.3	156.0	1.4	7	44.4	2.1	0.30	0.44
	KLA-1	41.52	124.00	126.9	No Plateau	NA	NA	NA	NA	NA	0.33
	KLA-2	41.52	124.02	137.2	148.1	1.6	6	51.6	2.1	0.14	0.25
	KLA-4	41.23	123.65	141.3	149.5	1.9	8	80.6	2.4	0.14	0.15
Southern	EEL-1A	40.64	124.28	124.6	131.7	0.8	5	65.5	1.6	0.90	0.95
	EEL-1B	40.64	124.28	123.3	126.6	1.5	8	84.3	2.1	0.69	1.07
	EEL-2	40.63	124.28	122.4	128.7	1.0	6	64.9	1.1	1.09	1.12
	MAT-1	40.31	124.28	67.3	77.9	1.8	5	46.2	3.4	0.69	0.66
	RUS-1	38.43	123.10	106.7	110.9	0.9	10	83.3	1.4	0.33	0.76
	RUS-2	38.43	123.10	108.5	116.3	1.2	6	68.1	1.1	0.27	0.19
	SCN-1	38.07	121.86	118.2	123.7	1.0	7	62.8	0.6	0.28	0.43
	SAC-1	38.06	121.79	121.7	125.6	1.5	5	67.7	2.6	0.47	0.56
	SAN-1	38.03	121.86	119.1	120.4	0.9	11	95.6	1.2	0.39	0.48

Table 2.2 - Summary of ^{40}Ar-^{39}Ar Incremental Heating Experiments for Pacific Northwest River Sediments. #steps = The number of steps that characterize the plateau; MSWD = Mean square of weighted deviations (Koppers, 2002). "LP" = low-temperature plateau and "HP" = high-temperature plateau. No precise location information is available for COL-1341, COL-1498, UMP-902, ROG-900 or KLA-898 (collected at the mouths of these rivers by J. Dymond and G.R. Heath).

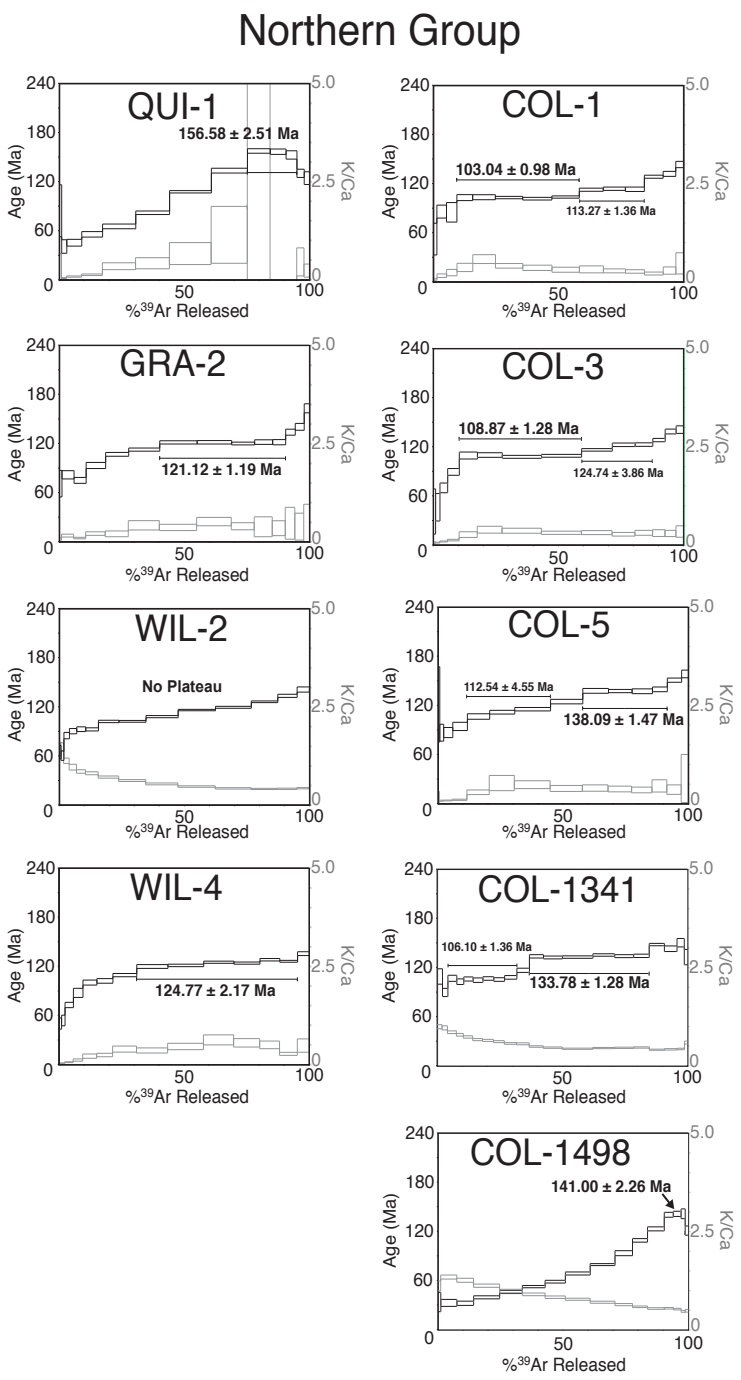

Figure 2.3 - ^{40}Ar-^{39}Ar incremental heating spectra and K/Ca spectra for river sediments from the Northern group (coastal Washington and Columbia watersheds) of the Pacific Northwest. Age spectra are black while the K/Ca spectra are green. Analytical uncertainties (2-sigma) related to age and K/Ca are depicted by the vertical scaling of each step-heating box.

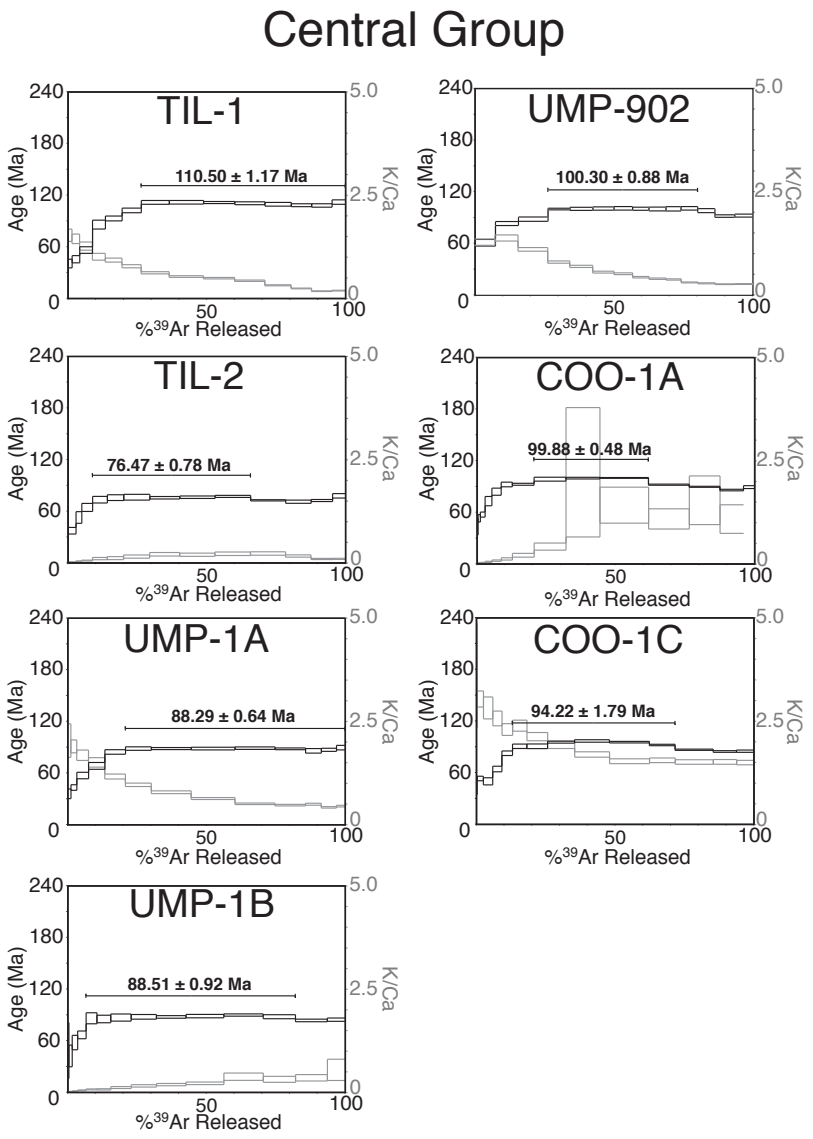

Figure 2.4 - ^{40}Ar-^{39}Ar incremental heating spectra and K/Ca spectra for river sediments from the Central group (coastal Oregon) of the Pacific Northwest. Age spectra are black while the K/Ca spectra are green. Analytical uncertainties (2-sigma) in age and K/Ca are depicted by the vertical scaling of each step-heating box.

while the higher temperature plateaus range between 113-138 Ma. These are the only samples from our study that show this dual plateau pattern. All samples in the northern group show evidence for minor Ar loss. We observe that most of these age spectra increase in age at the highest temperature steps, suggesting that no significant Ar recoil has occurred and that older, high-temperature minerals are present (amphiboles?).

River sediments from Oregon coastal rivers in the Central group are, as a whole, the youngest in the dataset (Figure 2.4). The age spectra for the seven samples show an initial increase in the step ages with temperature, followed by broad, multi-step plateaus that either continue to fusion or are followed by a slight decrease in step age, likely related to Ar recoil. The two samples from Tillamook Bay show good plateaus, but two markedly different ages (76.5 and 110.5 Ma). UMP-1A and 1B are identical in age (88.3 and 88.5 Ma, respectively), while UMP-902 (precise sampling location within the river is uncertain) is significantly older at 100 Ma. The Coos River sediment age spectra show similar patterns, with middle temperature plateaus (94-100 Ma) and decreasing step ages at higher temperatures, indicative of Ar recoil.

The Rogue River and Klamath River sediments (Klamath group) show consistent within-river results, but differ notably in between-river bulk sediment ages and degassing patterns (Figure 2.5), even though both rivers erode the same rocks in the Klamath Mountains. All four of the Rogue River samples produced good plateaus whose ages fall between 125-132 Ma. Their degassing patterns are very similar as well, with little evidence for recoil effects in the high temperature steps. Three of the four Klamath River samples show similar ages, between 148-156 Ma. The degassing pattern is somewhat different from the Rogue River samples, increasing in age over a greater temperature range initially, with a clear but narrower plateau. One sample (KLA-1) did not develop a plateau. It appears to contain a small proportion of some significantly older mineral that outgassed at high temperatures. Generally, the samples in the Klamath group show no consistent recoil patterns.

The Eel, Mattole, Russian, Sacramento and San Joaquin Rivers comprise the Southern group (Figure 2.6). The three samples from the Eel River are quite similar in age (127-132 Ma) and degassing pattern, with broad plateaus and decreasing step ages at the

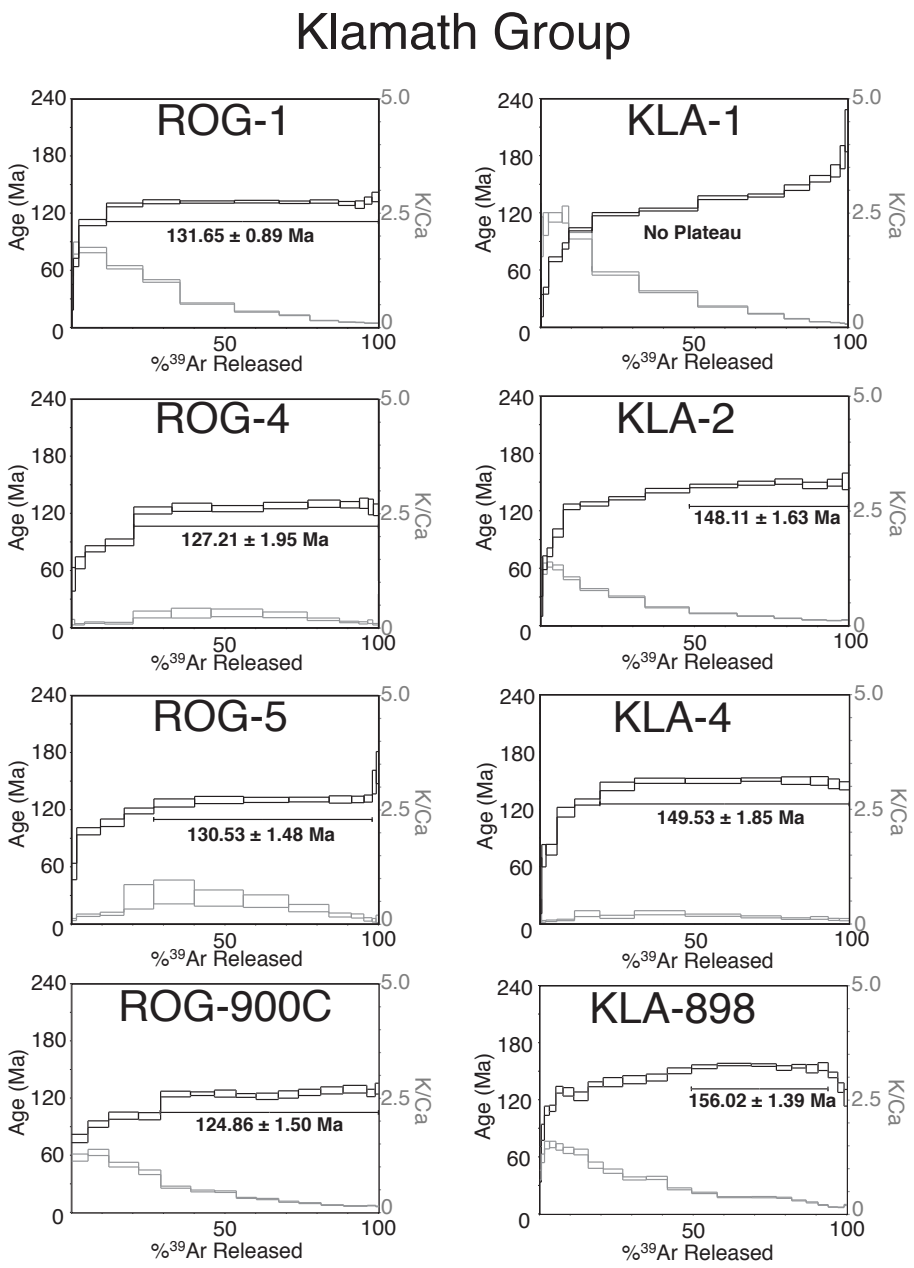

Figure 2.5 - ^{40}Ar-^{39}Ar incremental heating spectra and K/Ca spectra for river sediments from the Klamath group (southern Oregon and northern California) of the Pacific Northwest. Analytical uncertainties (2-sigma) in age and K/Ca are depicted by the vertical scaling of each step-heating box.

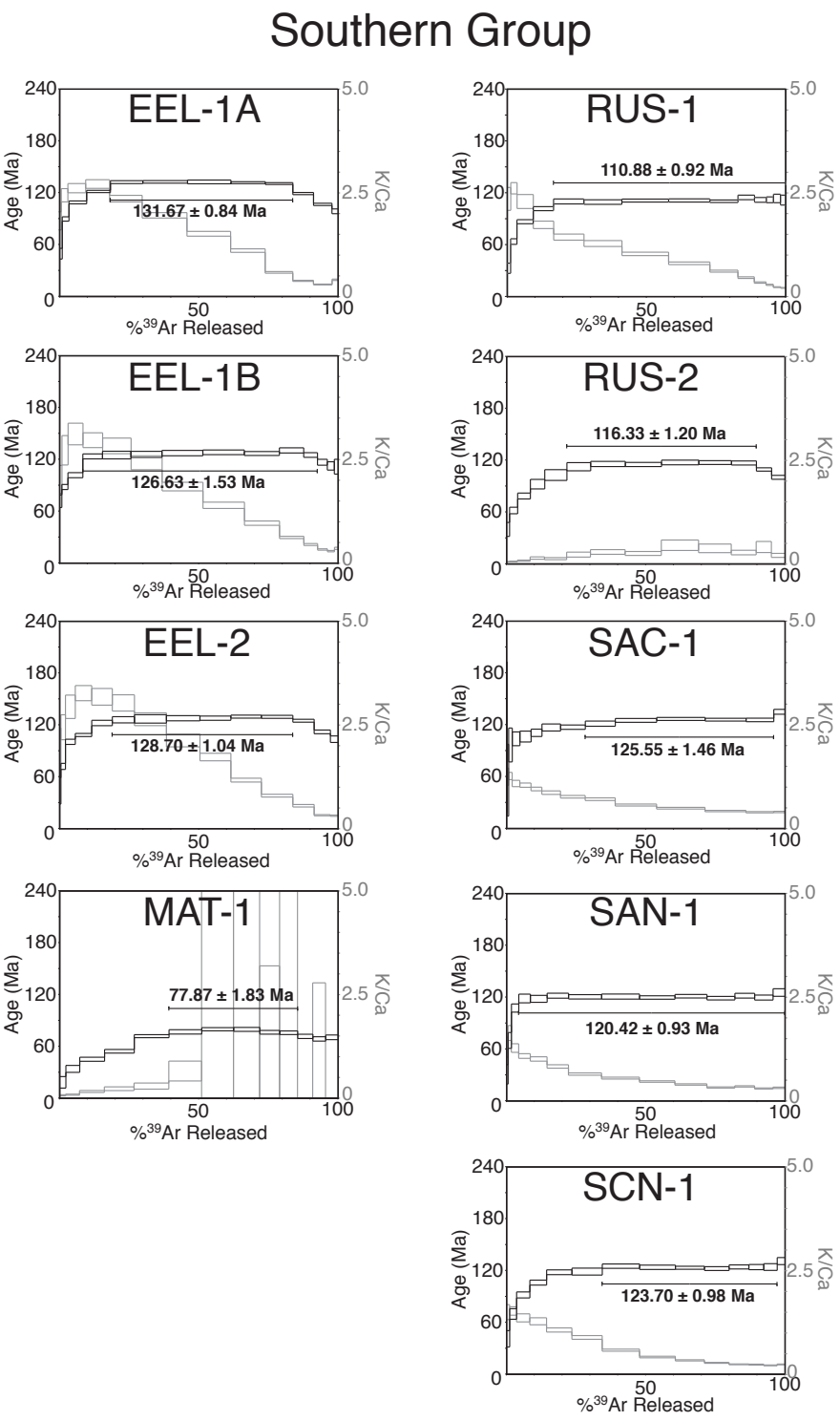

Figure 2.6 - ^{40}Ar-^{39}Ar incremental heating spectra and K/Ca spectra for river sediments from the Southern group (northern and central California). Age spectra are black while the K/Ca spectra are green. Analytical uncertainties (2-sigma) in age and K/Ca are depicted by the vertical scaling of each step-heating box.

highest temperatures. MAT-1 is one of the youngest samples in the dataset (78 Ma), with five concordant steps comprising just under 50% of the total gas released, and is much younger than the geographically adjacent Eel River samples. It drains a relatively small Miocene-Cretaceous sedimentary subunit of the Franciscan Melange Coastal Belt (McLaughlin et al., 1994) not shown in Figure 2.2. The spectra of the two Russian River samples produced good plateaus at 111 and 116 Ma. Although the ages differ somewhat, the Russian River samples share many of the features seen in the Eel River samples (Figure 2.6). Samples from both yield increasing step ages (30-60 Ma) for three to five steps then arrive at a plateau throughout the middle temperature steps and terminate with decreasing ages for the highest temperature steps. Both the Eel and Russian Rivers erode the Franciscan Melange, but a significant portion of the Russian River also erodes the Miocene-Pliocene Sonoma and Tolay volcanic rocks (Fox et al., 1985), which may explain the small age difference between the two rivers. The three southernmost samples from the Sacramento and San Joaquin Rivers have an average plateau age of 123 Ma. These samples display broad, continuous plateaus throughout the step-wise heating process, after only a short low-temperature set of steps affected by ^{40}Ar loss. Ar recoil appears to be important in the Eel, Mattole and Russian Rivers over the highest temperature steps, but not in the Sacramento-San Joaquin samples.

2.7.2 Mineralogy and K/Ca Spectra

XRD analyses performed on a subset of samples showed that, in order of relative abundance, the most abundant mineral is plagioclase (Table 2.3), followed by clinopyroxene, kaolinite, K-feldspar, vermiculite, hornblende (amphiboles), orthopyroxene and biotite (and other micas). Minerals releasing gas at the lowest temperatures are clays such as kaolinite and vermiculite. Their K/Ca ratios (Table 2.1; Deer et al., 1992) are low to moderate at 0.03-4.0. Although clays, strictly speaking, do not exist in the 20-63 μm fraction, they are present in our samples presumably by adhesion to larger grains. Biotite, muscovite, illite and other micas have high K/Ca values (K/Ca = 10-800, Deer et al., 1992; GEOROC database, http://georoc.mpch-mainz.gwdg.de/georoc/; Barnes, 1987; Barnes et al., 1986; 1992). The micas release

Sample	Latitude, °N	Plagioclase	CPX	Kaolinite	K-feldspar	Vermiculite	Hornblende AMPHIBOLE	OPX	Biotite MICA
QUI-1	47.4	61	15	7	8	3	1	3	2
COL-3	46.3	68	8	1	9	3	2	7	2
COL-5	46.2	67	13	1	10	1	2	4	1
TIL-4	45.5	45	27	1	9	15	0	4	0
UMP-1B	43.7	55	19	6	11	3	2	3	0
ROG-5	42.4	29	10	21	6	21	8	0	4
KLA-1	41.5	47	15	9	7	3	12	5	2
KLA-4	41.2	27	7	25	5	11	11	5	8
EEL-1A	40.6	43	8	15	8	13	2	6	5
RUS-2	38.4	47	14	10	9	7	4	5	5
SAN-1	38.0	62	16	5	10	1	2	3	2
AVERAGES		50	14	9	8	7	4	4	3
STANDARD DEVIATION		14	6	8	2	7	4	2	3
K/CA MODEL BEST FIT		60	8	4	10	7	4	2	6

Table 2.3 - The mineralogic abundances, in relative percent (calculated on a quartz-free basis), for major K- and Ca-bearing minerals as determined from X-ray diffraction (XRD) of 11 samples. The best-fit mineralogic abundances used later in the K/Ca degassing model are also shown. TIL-4 is the only sample analyzed by XRD from Tillamook Bay and was not characterized by ^{40}Ar-^{39}Ar methods. CPX = clinopyroxene; OPX = orthopyroxene, K-spar = potassium feldspar.

gas at moderate temperatures (Brady, 1995; Dalrymple et al., 1981; McDougall and Harrison, 1999), suggesting that the K/Ca ratios in bulk sediments during the low- to mid-temperature steps are likely to be influenced by these minerals, even though they are not overly abundant in the samples. Orthoclase, microcline and sanidine of the K-feldspar group degas at low (microcline and sanidine) to moderate (orthoclase) temperatures, with K/Ca ratios that are high (K/Ca = 10-400, Deer et al., 1992; GEOROC database, http://georoc.mpch-mainz.gwdg.de/georoc/; Barnes, 1987; Barnes et al., 1986; 1992). These minerals should produce obvious signatures in the K/Ca spectra, even if present in only low abundances. Pyroxenes degas at moderate to high temperatures and, although not a significant carrier of K, they have relatively high Ca concentrations (and correspondingly low K/Ca values between 0-0.04). Plagioclase and hornblende have low K/Ca ratios, ranging from 0-0.5 (Table 2.1). Although amphiboles are the most retentive (Brady, 1995; Dalrymple and Lanphere, 1969), they are found in only small amounts. Thus, plagioclase is the most likely mineral to be contributing to the age and K/Ca spectra at higher temperatures.

In the Northern group, K/Ca values show a variety of trends in the step-wise heating results. GRA-2, WIL-4, COL-1, 3 and 5 all share similar trends and low values of K/Ca ratios (Figure 2.3 and Table 2.2). After an initial rise during the low temperature heating steps, the K/Ca ratios become uniform at approximately 0.3-0.4, possibly indicative of either a high-K plagioclase or a mixture of a low- or moderate-K plagioclase with a higher-K mineral such as K-feldspar. There is no statistically significant difference in the K/Ca values over the two plateau intervals observed in the Columbia River age spectra.

Potassium-calcium trends in the Central group are also variable (Figure 2.4 and Table 2.2). The Tillamook Bay samples show different trends and average values, not surprising considering the age differences. Although the ages for UMP-1A and 1B are virtually identical, their respective K/Ca trends are quite different in the low temperature steps. UMP-1A begins at about K/Ca = 2.4 and decreases continually until the latter stages of the step-heating process, where K/Ca ratios trend towards a uniform value of about 0.5. UMP-1B, on the other hand, increases from very low K/Ca values to an average of about 0.1 that sustains until fusion. UMP-1A may have more high-K minerals degassing in the low temperature steps

(such as kaolinite and other clays and/or mica), explaining some of the contrast between the two samples. At high temperatures, the K/Ca values are indicative of plagioclase, amphibole and possibly, a small contribution from K-feldspar. The Coos River samples show markedly different K/Ca trends and values despite the fact that their age spectra are quite similar throughout the heating process. COO-1A begins with a very low K/Ca ratio and then steps upward to about 0.5, whereas COO-1C begins at K/Ca ~ 3 and decreases to about 1.7, high values relative to the rest of the dataset. The mineralogy comprising the Coos River bulk sediment plateaus must have greater abundances of high-K minerals (such as K-feldspar) than other samples or, conversely, low abundances of high-Ca minerals such as clinopyroxene.

The Klamath group, which is composed of the Rogue and Klamath Rivers, shows rather similar K/Ca trends. Five of the eight samples (ROG-1, ROG-900, KLA-1, 2, and 898) show a continuous decrease in K/Ca ratios during the heating process from K/Ca values of 1.5 (a possible mixture of kaolinite and vermiculite) down to values consistent with a plagioclase characterized by low- to moderate-K at around 0.1 (Figure 2.5). The other three Klamath group samples (ROG-4, 5 and KLA-4) show an initial small increase in K/Ca, followed by a short duration of successive steps releasing similar K/Ca values. The final termination is punctuated by small decreases in the K/Ca ratio. The notably low K/Ca values for all samples in the mid- to high-temperature steps suggest a mixture of plagioclase, hornblende and possibly pyroxene.

Trends of K/Ca for the Southern group are generally similar within each river basin. The Eel River samples display relatively high K/Ca (~2.5) during the low temperature steps, decreasing steadily to values around 0.3 (Figure 2.6), consistent with a mineralogy dominated by clays such as kaolinite, mica and possibly a low-temperature K-feldspar (microcline) at the lower temperatures and plagioclase during the middle to high temperatures. The Mattole River sample K/Ca ratios have large analytical uncertainties, suggesting that measurement error on ^{37}Ar (from Ca) was significant. The two Russian River samples have contrasting K/Ca trends. The RUS-1 K/Ca spectra, showing a pattern not unlike the Eel samples, has a high K/Ca contribution (K/Ca ~2.5) at the lower temperature steps, likely from kaolinite and mica while at higher temperatures the lower K/Ca values suggest a mixture of high- and

low-K minerals. The consistently low K/Ca values in RUS-2 (K/Ca = 0.2) suggest a K/Ca spectra dominated by plagioclase. All three of the Sacramento-San Joaquin samples display K/Ca patterns that decrease throughout much of the heating experiment. Toward the higher temperature steps, however, a plateau in the K/Ca ratio centered at 0.3 develops, consistent with plagioclase degassing, and possibly a small contribution of a high-K mineral such as K-feldspar.

In summary, the majority of samples for the entire dataset appear to have K/Ca values that are consistent with mostly plagioclase degassing during the middle to high temperature steps. This is also the temperature range that tends to develop ^{40}Ar-^{39}Ar age plateaus. However, the K/Ca ratios determined over age-plateau determining steps (K/Ca ~ 0.3) are a bit higher than measurements made on many plagioclases from the Columbia River Basalts, Cascades and Klamath Mountains (Barnes, 1987; Barnes et al., 1986; 1992, GEOROC database, http://georoc.mpch-mainz.gwdg.de/georoc/) suggesting that a higher-K mineral such as K-feldspar could also be releasing a small amount of Ar during the higher temperature steps.

2.8 Evaluating the K/Ca Spectra and Bulk Sediment Ages

2.8.1 K/Ca Degassing Spectra Reveal Bulk Mineralogy

To help support the connections we have proposed between K/Ca values and mineralogy, we have developed a forward model that predicts K/Ca spectra. The best-fitting values from the average abundances for each K- and Ca-bearing mineral (from XRD of 11 samples; Table 2.3) are used in conjunction with K and Ca concentrations (Table 2.4). The release of ^{39}Ar and ^{37}Ar (proxies for K and Ca, respectively, described in the analytical section) from each mineral with increasing temperature is assumed to follow a Gaussian distribution.

Each Gaussian degassing curve mean (temperature at which a given mineral reaches a diffusion maximum) and standard deviation (an estimate of the range over which a given mineral diffuses gas) are estimated from the available diffusion data for silicates (Brady,

	K, ppm Range	K/Ca Model Best Fit	Ca, ppm Range	K/Ca Model Best Fit
Plagioclase	2000-12,500	12,500	40,000-75,000	40,000
K-spar	100,000-150,000	150,000	600-2,000	600
Clinopyroxene	100-300	300	100,000-130,000	100,000
Orthopyroxene	100-300	300	10,000-20,000	10,000
Mica	60,000-80,000	80,000	100-1,000	100
Amphibole	5,000-10,000	10,000	60,000-90,000	60,000
Kaolinite	1,750	1,750	425	425
Vermiculite	200	200	12,000	12,000

Table 2.4 - Range of K and Ca concentrations determined from Deer et al. (1992), GEOROC database (http://georoc.mpch-mainz.gwdg.de/georoc/), Barnes (1987), and Barnes and others (1986, 1992).

1995; Fechtig and Kalbitzer, 1966; Harrison et al., 1985; Lovera et al., 1997; McDougall and Harrison, 1999) and correspond with the order of release temperatures presented in Table 2.1. These degassing patterns are presented in figures 2.7 and 2.8. Little is known about the precise release trends in minerals as a function of temperature (see McDougall and Harrison, 1999), so we use the relative relationships about diffusion among minerals expressed through values of activation energy and/or diffusion coefficients (Fechtig and Kalbitzer, 1966; Harrison et al., 1985; Lovera et al., 1997; McDougall and Harrison, 1999). The model provides a first-order view of how the various minerals in a polymineralic sample might combine to produce observed K/Ca spectra, acknowledging that the order that these minerals release their gas could be different from what we have chosen, especially with feldspars (McDougall and Harrison, 1999).

2.8.2 K/Ca Model Results

The results of the K/Ca degassing spectra model weighted by 1) the mineral abundances for eight minerals and 2) the amount of K and Ca released at each of seven temperature steps from 200 °C to 1400 °C are presented in Figure 2.9. The best-fitting model result is plotted along with the average and standard deviation of the measured K/Ca values for each temperature step from 24 samples that have not experienced appreciable ^{39}Ar loss. The modeled K/Ca values are generally in good agreement with the measured values considering the simplifications we have made for the diffusion of gases from these silicate minerals. These results suggest, that to a first-order, the K/Ca ratios at a given step are simply the average of contributions from the degassing minerals. Although this is intuitive, it is important to show that this simple calculation provides expected K/Ca similar to measured values from the bulk sediment ^{40}Ar-^{39}Ar incremental heating experiments. Moreover, we note that plagioclase, because of its high abundance in the samples and high temperature range of gas release, is the dominant mineral contributing to the age spectra at middle to high temperatures and therefore is the dominant mineral driving plateau development in these bulk sediment samples.

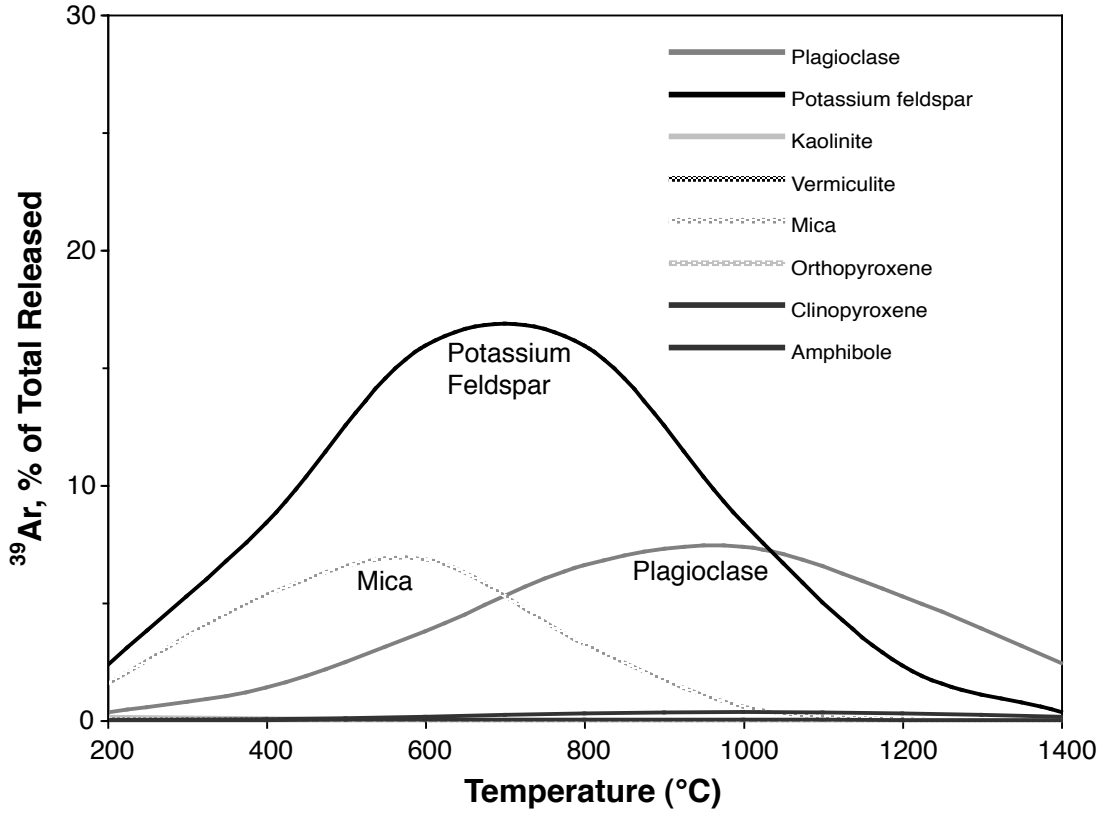

Figure 2.7 - Modeled ^{39}Ar (K) degassing patterns for selected minerals based on published K concentrations (see text and Table 2.4) and activation energies. Release expressed as % of total of all minerals degassing Ar. K concentrations based on best fit (Table 2.4). K-feldspar and mica dominate in the low to middle temperatures while plagioclase becomes important at high temperatures.

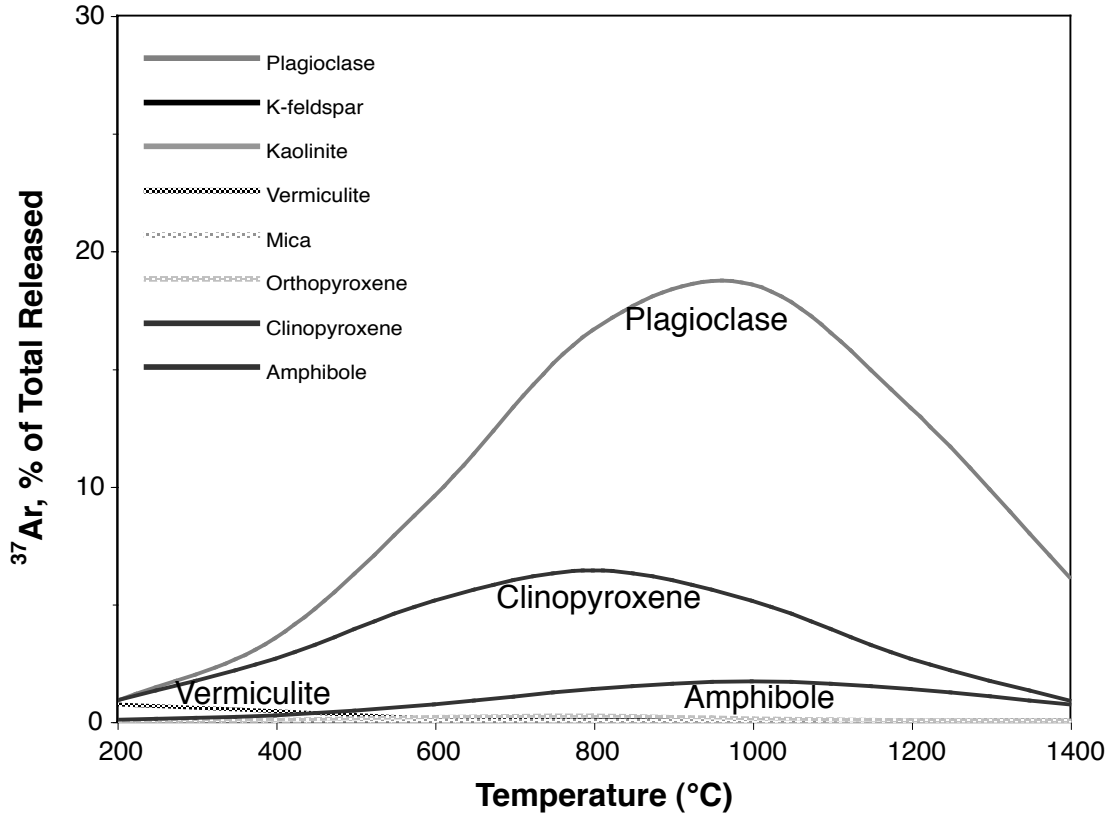

Figure 2.8 - Modeled ^{37}Ar (Ca) degassing patterns for selected minerals based on published Ca concentrations (see text and Table 2.4) and activation energies. Release expressed as % of total of all minerals degassing Ar. Ca concentrations based on best fit (Table 2.4). Plagioclase dominates almost the entire release pattern, while clinopyroxene, an insignificant contributor to the age spectra (low K), plays a significant role in the K/Ca spectra.

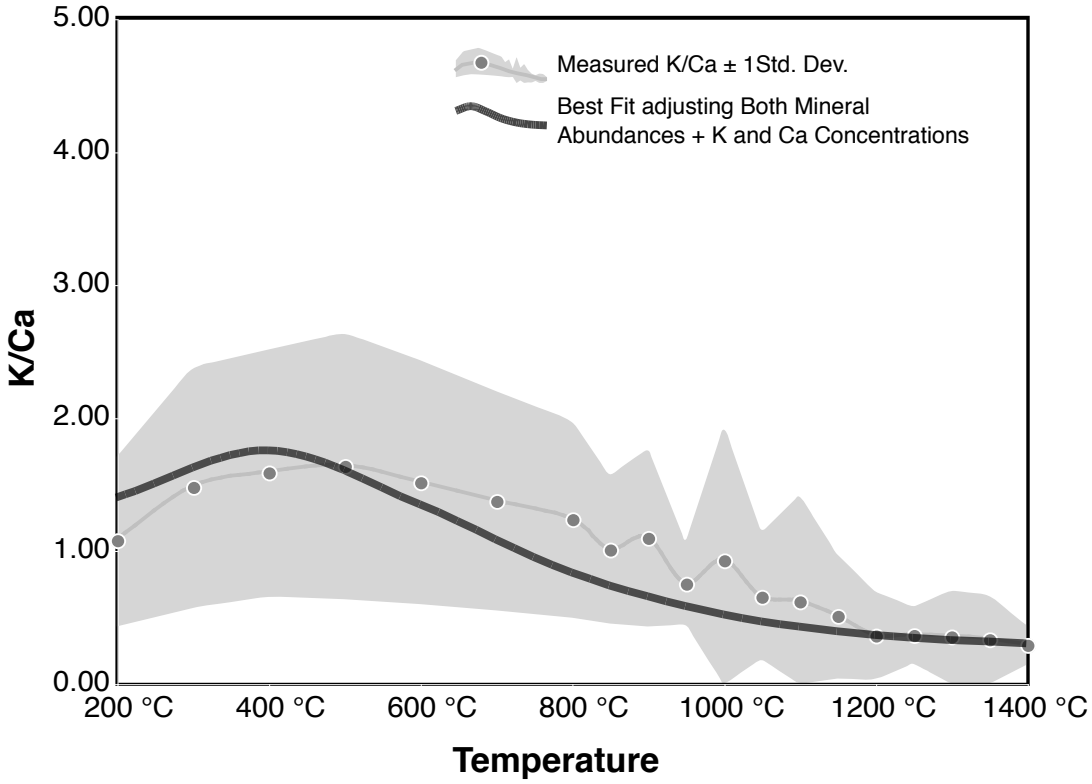

Figure 2.9 - K/Ca best fit model results (mineralogy, Table 2.3; K and Ca concentrations, Table 2.4) and observed average values for 24 samples (medium gray line, dark gray-filled, white-outlined circles) ± 1 standard deviation (light gray shading). The model result (dark gray line) generally shares a similar shape and magnitude of measured K/Ca trends. Y-axis same as K/Ca plots in figures 2.3 through 2.6.

2.8.3 Modeling the ^{40}Ar-^{39}Ar Ages of Detrital Mixtures

The observation of reproducible, well-defined plateau ages in the majority of our river samples is an important, yet surprising result considering that the sediment analyzed is a mixture of a variety of detrital minerals. The gas measured during any given temperature step is a mixture of all the contributions from K-bearing minerals releasing Ar at that temperature. To develop well-defined multi-step age plateaus, the ages of the suite of minerals degassing from one temperature to the next has to be, in total, the same. For this to occur either an unusually favorable mixture of minerals have to be present where only one or two minerals dominate the gas released during incremental heating, or conversely, all minerals are derived from the same-aged geologic province(s). From the previous discussion we conclude that, since degassing of plagioclase generally coincides with the development of age plateaus and plagioclase abundances are the highest of the major K-bearing minerals, plagioclase dominates the age-plateau results. To a lesser extent, K-feldspar could be a factor in some of the age plateaus since it can have an unpredictable degassing pattern over a broad temperature range (Brady, 1995; McDougall and Harrison, 1999) and has such high K-content.

We now take advantage of the finding that plagioclase and K-feldspar are the important minerals dictating release of Ar and develop a simple model to evaluate the meaning of the age spectra. The calculation takes into account mineral K-content, cooling age and the proportional area of each bedrock unit. We develop the model for the Umpqua, Rogue and Klamath River basins, given the availability of cooling age information and digital geologic maps, which makes calculations of the areas of individual mapped lithologies relatively easy and accurate. The conditions and assumptions are as follows.

Based on our age and K/Ca results, we assume that the plateau ages are dominated by K from plagioclase mostly and to a lesser extent, K-feldspar (in which the K concentration for this plagioclase – K-feldspar mixture is weighted by a 95% - 5% mixture since only a “tail” of K-feldspar is likely to be outgassing Ar at the higher, plateau-defining temperatures). Each of the mapped units is assigned K concentrations that are either based on plagioclase only (in the case of mafic or intermediate Cascade rocks as well as sediments derived from basaltic

or andesitic compositions) or a mixture of plagioclase and K-feldspar (in the case of granitic units and sediments derived from felsic protoliths). Plagioclase K concentrations differ in the model depending on whether the host rock is felsic (6000 ppm), intermediate (or andesitic; 4000 ppm), mafic (2000 ppm) or ultramafic (1000 ppm). Mixtures of these four values are also used when appropriate.

In the Umpqua River basin, the sedimentary Tyee Formation is divided into two groups derived from different protoliths (Ryu and Niem, 1999; Walker and MacLeod, 1991). One-half of the Tyee Formation is sourced from the paleo-Klamath Mountains, while the other half is derived from the Idaho Batholith. The Idaho Batholith-derived component is assigned an age of 67 Ma (Heller et al., 1985; Heller et al., 1992) and the Klamath Mountain component is assigned an age of 154 Ma, the average age for all of the Klamath Accretionary Complex plutonic rocks (Irwin and Wooden, 1999). This age is also assigned to meta-sedimentary terranes in the Klamath Mountains, where we assume an age equivalent to the age of the youngest plutons intruded into them (Wells et al., 2000). This is feasible since it is likely that most of the K-bearing minerals in these meta-sedimentary units were reset during contact and regional metamorphism. This allows us to calculate an average age of the Klamath-derived component of the Tyee Formation, which is estimated from the average age of 154 Ma for all plutons with radiometric ages available. For the Cascade arc-derived lithologies, the eleven most common mapped units exposed in the Umpqua River basin were simplified into three age/lithologic groups (Figure 2.10; Walker and Macleod, 1991). For the age of Cascade rocks in the Rogue and Klamath Rivers a weighted average of 21 Ma (calculated from the 11 units used in the Umpqua Basin) was used, recognizing that this number could realistically range from around 10-30 Ma.

The geologic map of Irwin and Wooden (1999) was used for extracting rock type and cooling age parameters in the Rogue and Klamath River basins. The areas of these units were calculated from digital geologic maps of the Klamath Mountains (Irwin, 1997). Most mapped units from Irwin and Wooden (1999) smaller than ~50 km^2 were not included in the analysis. Because of this, the summed rock-type areas of all units used in the model do not likely equal the true river basin areas of either the Rogue or Klamath Rivers. The total area not captured

Table 2.5 (next page) - Parameters used in the ^{40}Ar-^{39}Ar detrital mixture model. K concentrations are based on the simplification that (1) The plagioclase - K-feldspar contribution is 95% - 5% and (2) that the K concentration for plagioclase are 6,000 ppm, 4,000 ppm, 2,000 ppm and 1,000 ppm for granitic plagioclase, andesitic plagioclase, basaltic plagioclase and ultramafic plagioclase, respectively. Granitic rock units thus contribute the weighted average of 11,000 ppm K while sedimentary units that are derived from granitic units are given a more intermediate K concentration mixture of 6000 ppm. The "No Cascade Model" calculates a bulk sediment age by removing the CAS (Cascade) component from the Klamath river basin (see text). All major terranes were assigned ages of their youngest intrusion, since minerals are likely to have been reset unless metamorphic ages were were available in the literature; Wells et al. (2000), Walker and MacLeod (1991).

MAPPED UNITS, ROGUE AND KLAMATH BASINS from Irwin and Wooden (1999) Tus, Tub, Tu, Tbaa, Tt, Tsr, KJds, KJg, Js, Jv, Ju = see figure 10; CMTT = Condrey Mountain Terrane; WKT = Western Klamath Terrane; EHT = Eastern Hayfork Terrane; ash = Ashland Pluton; gb = Grayback pluton; gp = Grants Pass pluton; wr = White Rock pluton; w = Wimer pluton; MCT = May Creek Terrane; RST = Rattlesnake Terrane; chc = Chetco Complex; jo = Josephine Ophiolite; cs = Colebrook sediments; kjds = meta-sediments (Walker and Macleod, 1991); rs = redding subterrane; mm = Mule Mountain pluton, sb = Shasta Bally pluton; CMT = Central Metamorphic Terrane; HF = Hayfork terrane;; ww = Wildwood pluton; WKT = Western Klamath Terrane; wc = Wooley Creek; ep = English Peak Pluton; NFT = North Fork Terrane; rp = Russian Peak pluton; cc = Canyon Creek pluton; cp = Craggy Peak Pluton, sp = Sugar Piine pluton; pl = Porcupine Lake pluton; ccr = Castle Crags pluton; bk = Bonanza King pluton; cm = China Mountain pluton; cpg = CP gabbro; YT = Yreka terrane; FJT = Fort James terrane.

LITHOLOGIES: cai = calc-alkaline, felsic rocks; ande = andesitic; bas = basaltic; um = ultramafic rocks; mmv = mafic meta-volcanics; mv = meta-volcanics; mi = mafic intrusives; ss = sandstone; sh = shale; mud = mudstone; sl = slate; ms = meta-sediments; ims = interlayered metasediments.

KP = Klamath Protolith; IBP = Idaho Batholith Protolith; CAS = Cascade Volcanics; plag = plagioclase; kspar = potassium feldspar.

Ages for the Umpqua Basin from Wells et al. (2000), Duncan (1982) and Heller et al. (1985, 1992). Note that the Umpqua River drainage area shown here is larger than published values of 9,504 km^2 (Karlin, 1980) because of different calculation methods.

Ages for the Rogue and Klamath river basins from Walker and Macleod (1991) and Irwin and Wooden (1999).

UMPQUA RIVER BASIN total drainage area of ~11,800 km^2

unit	rock type	main minerals	K (ppm)	Area (km^2)	Age (Ma)		
Tt	ss,silt	---	---	4630	---		
- KP	ande	plag	4,000	2315	147		
- IBP	cai	plag, kspar	11,000	2315	67		
Tsr	bas	plag	2,000	405	57		
KJg	cai	plag, kspar	11,000	394	133		
KJds	ms	plag, kspar	6,000	1250	147		
Jv	mmv, ande	plag	4,000	297	147		
Js	ms	plag, kspar	6,000	556	147		
Ju/KJg	um and cai	plag, kspar	4,500	293	140		
CAS-Tus	ande	plag	4,000	1850	27		
CAS-Tub	bas	plag	2,000	1095	27	T_{kat}	^{40}Ar-^{39}Ar Age
CAS-Tu/Tbaa	bas-ande	plag	3,000	1030	9	90 Ma	92 Ma
				11800			

ROGUE RIVER BASIN total drainage area of ~13,400 km^2

			(ppm)	(km^2)	(Ma)		
CMTT	ms	plag, kspar	6,000	550	120		
WKT	um	plag	1,000	2330	139		
EHT	cai mv	plag, kspar	6,000	1447	148		
ash	cai	plag, kspar	11,000	360	136		
gb	cai	plag, kspar	11,000	97	153		
gp	cai	plag, kspar	11,000	148	139		
wr	cai	plag, kspar	11,000	740	156		
w	cai	plag, kspar	11,000	54	160		
MCT	mg	plag, kspar	6,000	360	156		
RCT	ims	plag	4,000	820	129		
chc	cai	plag, kspar	11,000	81	157		
jo	um	plag	1,000	887	161		
cs,kjds	ms	plag,kspar	6,000	2490	154	T_{kat}	^{40}Ar-^{39}Ar Age
CAS	bas-ande	plag	3,000	3036	21	128 Ma	129 Ma
				13400			

KLAMATH RIVER BASIN total drainage area of ~29,400 km^2

			(ppm)	(km^2)	(Ma)		
rs	ss, mmv,sh	plag, kspar	6,000	1918	125		
mm	cai	plag, kspar	11,000	87	400		
sb	cai	plag, kspar	11,000	320	136		
CMT	ms	plag, kspar	6,000	860	135		
HF, RST	ims,mud,um,cai	plag	4,000	7316	129		
ww	cai	plag, kspar	11,000	570	169		
WKT	sh, mud	plag	6,000	1800	135		
wc	cai	plag, kspar	11,000	350	162		
ep	cai	plag, kspar	11,000	130	162		
NFT	cai, mv	plag, kspar	6,000	1020	147	T_{kat}	^{40}Ar-^{39}Ar Age
rp	cai	plag, kspar	11,000	180	159	109 Ma	151 Ma
cc, cp, sp	cai	plag, kspar	11,000	254	136		
pl,ccr,bk,cm,cpg	mi	plag, kspar	6,000	324	421		
ts	um	plag	1,000	1200	136	No Cascade Model	
YT, FJT	ss, ism	plag	2,000	475	159	T_{kat}	^{40}Ar-^{39}Ar Age
CAS	bas, ande	plag	3,000	12596	21	147 Ma	151 Ma
				29400			

by this simplification is less than 10%.

Finally, this model assumes that erosion occurs evenly over all rock types and in all parts of the basin. Neither is true (Howard, 1998; Howard et al., 1994; Montgomery, 1994; Whipple et al., 1999; Whipple and Tucker, 1999), but at least in the cases provided by the Umpqua and Rogue Rivers, these factors could be negligible, as will be shown in the results. However, differential erosion and/or sediment transport and storage are needed to explain differences between the Klamath River model and ^{40}Ar-^{39}Ar plateau age results.

The equation that expresses the weighted average age based on the parameters of K-content, rock exposure area and cooling age (T_{kat}) of minerals in a given lithologic formation and ignoring differential erosion of rock types is then:

$$T_{kat} = \sum_{i=1}^{n} K_i a_i t_i \div \sum_{i=1}^{n} K_i a_i \qquad (1)$$

Where n is the number of rock types, K_i is the concentration of potassium in each rock type (in ppm), a_i is outcrop area of each rock type (in km^2), and t_i is the age of each rock type (in years). We adjusted the estimated ratio of Klamath-Idaho Batholith source contributions in the Tyee Formation to their reasonable upper and lower limits (70-30% Klamath-Idaho Batholith to 30-70% Klamath-Idaho Batholith ratios) to examine model sensitivity, wherein the modeled ages were seen to vary by ±7-10 Ma in the Umpqua River basin.

2.8.4 Results from the Bulk Sediment ^{40}Ar-^{39}Ar Detrital Mixture Model

The parameters and results for the model ages, T_{kat}, are presented in Table 2.5. For the Umpqua River, the modeled bulk sediment age is T_{kat} = 90 Ma (Figure 2.10, Table 2.5), virtually identical to the average bulk sediment ^{40}Ar-^{39}Ar plateau age measured on three Umpqua River samples and within error (92±7 Ma; Table 2.2). Even though the Rogue and Klamath Rivers erode both the Klamath Accretionary Complex and Cascade volcanics rocks, (Figure 2.2 and Figure 2.11) their model ages are quite different. The model result for

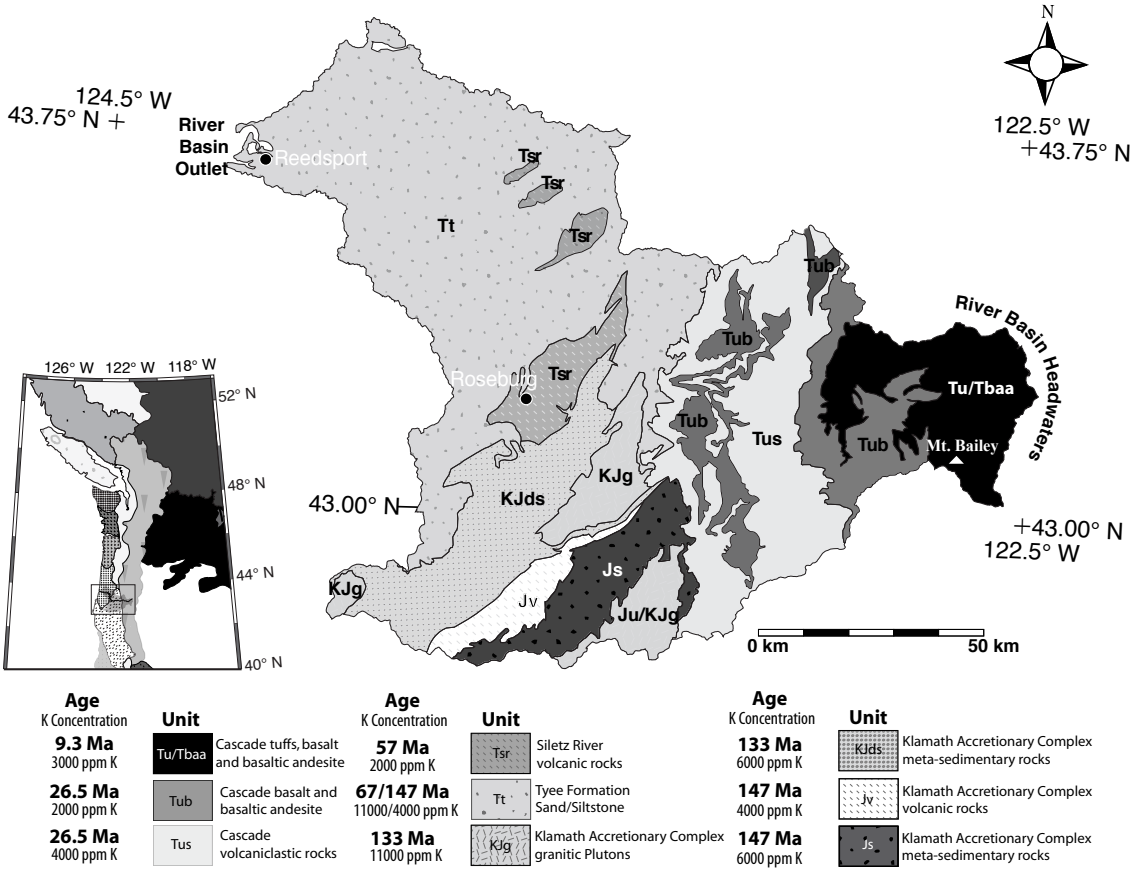

Figure 2.10 - Umpqua River basin and simplified geology. Bulk sediment age model parameters shown in legend (and Table 2.5) where "Age" is measured or estimated crystallization age of K-bearing minerals (plagioclase and K-feldspar) and "K concentration" denotes either K contents of plagioclase or a mixture of plagioclase and K-feldspar. Lithologic nomenclature after Walker and Macleod (1991). Geologic information from Heller and others (1985, 1992), Walker and MacLeod (1992), Irwin and Wooden (1999), Wells et al. (2000) and Barnes and others (1986, 1987, 1992)

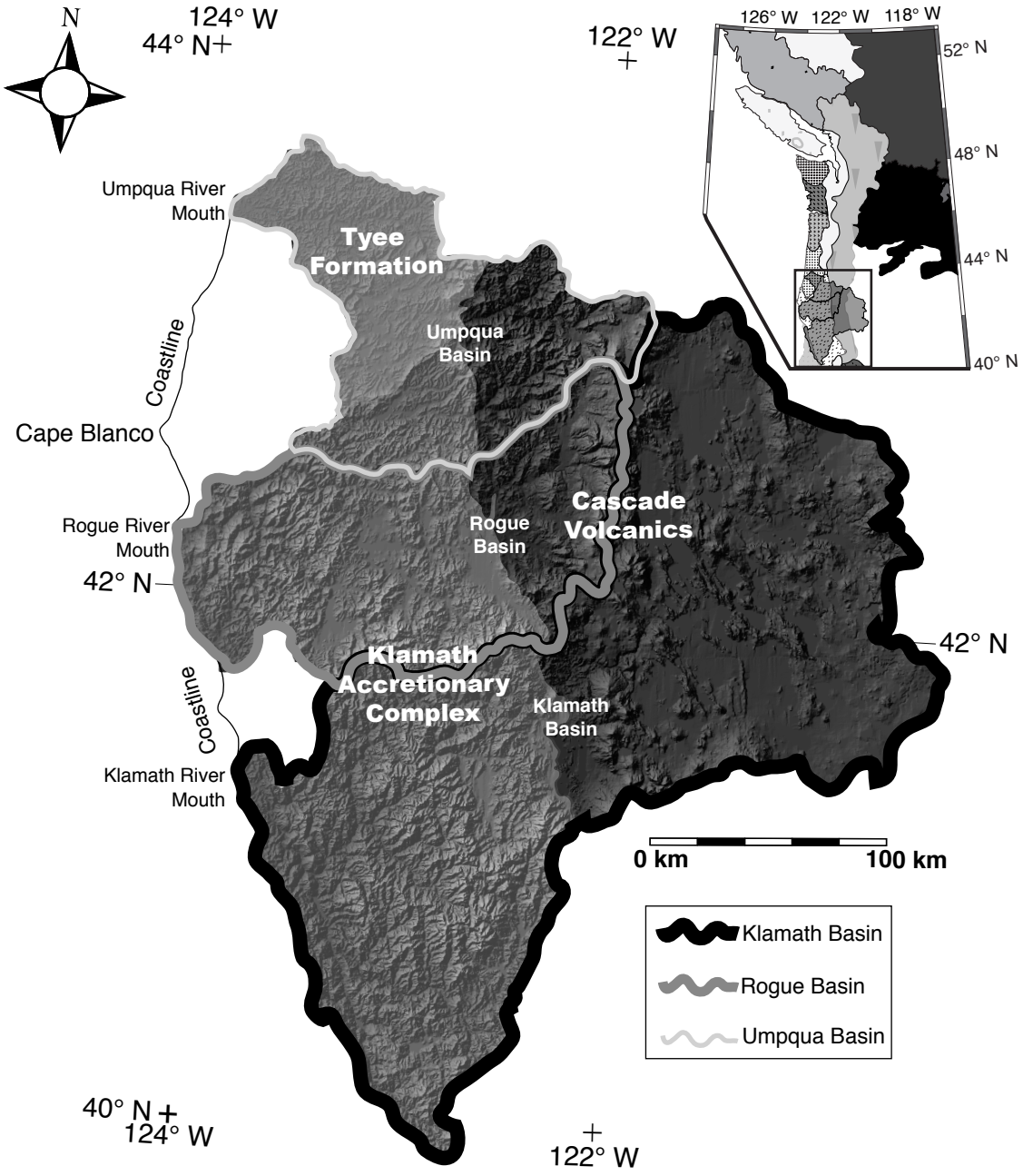

Figure 2.11-Shaded relief images of the Umpqua, Rogue and Klamath River basins. Transparent geologic provinces for the Tyee Formation (light gray), the Klamath Accretionary Complex (medium gray) and the Cascade volcanic arc (dark gray) are shown. Topography of the region is characterized by moderate relief in the Tyee Formation, high relief in the Klamath Accretionary Complex, moderate to high relief in the Cascades in the headwater regions of the Umpqua and Rogue rivers and notably low relief in the Upper Klamath basin.

the Rogue River is T_{kat} = 128 Ma while its average bulk sediment age from four samples is identical at 129 Ma. The Klamath River model result is T_{kat} = 109 Ma, markedly different than the bulk sediment average of 151 Ma.

The T_{kat} model does well in predicting the Umpqua River and Rogue River bulk sediment ages, suggesting that the bulk sediment plateau age results can be, to a first order, faithful indicators of the weighted average cooling age of source rocks in a given basin. However, the model does not do well in the Klamath River basin and requires further examination.

2.9 Discussion

The larger goal of this study is to characterize bulk fluvial sediment entering the northeast Pacific Ocean on a river basin scale in order to track sediment transport pathways to continental margin locations. We see distinct features in several of the large sediment contributors to the Pacific margin. Bulk sediments sampled from the mouth of the Columbia River present dual-plateau age spectra, although the age of each of the plateaus varies from sample to sample. The Klamath River, the third largest sediment producer in the Pacific Northwest also exhibits bulk sediment ages that are unique relative to other rivers in the Pacific Northwest, being the highest at 151 Ma. Rivers draining the Oregon Coast Ranges show distinct sediment plateau ages at around 88-100 Ma. Samples from the Eel River, which is presently the largest sediment producer on the Pacific margin, show age spectra that are very similar to those from the Rogue River, between 125 and 132 Ma.

We show that the K/Ca spectra (and therefore the age spectra) are dominated by plagioclase feldspar, and to a lesser extent K-feldspar. This greatly simplifies the interpretation of bulk sediment ^{40}Ar-^{39}Ar ages and we show that calculations based on a simple weighted average of source rocks and composition suggest that the bulk sediment ages are, to a first-order, faithful reflectors of provenance.

Our interpretations of incremental heating-derived age spectra distinguish provenance information from Ar loss, recoil or alteration. This technique is not likely compromised by

problems related to alteration and diagenesis since the step-heating procedure essentially degasses the sample from the outside inwards. For the most part, the outer portion of minerals is the part that will be susceptible to chemical exchange with fluids (e.g., river water and seawater) during the weathering and transport process. Thus, by incrementally heating sediment samples, we can evaluate (through the age spectra) the extent of alteration (or the effects of Ar loss and recoil) and thus, extract robust information about the source rocks from the unaltered inner portions of crystals.

2.9.1 Data-Model Mismatch in the Klamath Basin: Differential Erosion?

The extremely low bulk detrital mixture model age for the Klamath River (109 Ma vs. the average measured bulk sediment ^{40}Ar-^{39}Ar sediment age of 151 Ma) suggests that erosional processes in the Klamath basin may not be as simply interpreted as for the Umpqua or Rogue basins. One possibility is that marked differential erosion is occurring in the Klamath basin. A population of seventy-eight U-Pb ages (Allen et al., 2002) measured on zircons from sediment collected at the Klamath River mouth has an average age of 155 Ma, within error of the bulk sediment ^{40}Ar-^{39}Ar average of 151 Ma. Even though the closure temperatures are quite different for zircons and feldspars (see Reiners et al., 2005b), it is reasonable to compare the two ages since both the zircon U-Pb ages and ^{40}Ar-^{39}Ar ages of minerals in our bulk sediment samples are likely related to the Mesozoic emplacement of the Klamath plutons (therefore cooling ages of the two minerals should be similar to within a few million years). Of the zircon grains measured by Allen et al. (2002), none had a Cascade-like signature (0-30 Ma), suggesting that material in the Cascade portion of the Klamath River basin may not contribute significantly to the sediment load found at the mouth. Notably low relief is characteristic of the topography in the upper Klamath Basin (Figure 2.11) when compared to both the relief in the lower Klamath basin underlain by the Klamath Accretionary Complex as well as the portion of the Umpqua and Rogue basins eroding Cascades rocks. We hypothesize that the age difference between our T_{kat} age and the measured bulk sediment age is due to a negligible amount of sediment transported out of the low-relief upper Klamath basin

to the river mouth. In the extreme case where the upper Klamath basin is set to contribute no sediment to the bulk material collected at the mouth, our T_{kat} model age is 147 Ma, within error of the measured bulk sediment ^{40}Ar-^{39}Ar plateau age of 151 Ma (Table 2.5).

2.9.2 Bulk Sediment Ages in the Columbia River Sediment: Dominated by Interior Cordilleran Sources?

The dual-plateau spectra observed in four out of five Columbia River samples (Figure 2.3) suggest that two K-bearing mineral phases of different ages, and different degassing temperature ranges influence the total ^{39}Ar released. Approximately 45% of the Columbia River drainage area consists of Northwestern Cordillera (British Columbia, Montana Rockies and the Idaho Batholith). The Columbia River Basalts (CRBs) and lavas associated with the Snake River Plain (SRP) comprise another 45% of the total basin area. Thus, it is somewhat surprising that the ages presented here do not fall closer to an age in between the older, Cordilleran plutonic sources and the young Columbia River Basalt/Snake River Plain/Cascade sources. The majority of plutons comprising the Canadian portion of the upper Columbia Basin region (e.g., the Cretaceous Bayonne Magmatic Complex) are the 90-115 Ma Bayonne Suite and the 140-150 Ma Bigmouth Pluton in the Monashee, Selkirk and Purcell Mountains (Figure 2.2), although other Paleozoic and Early Tertiary intrusive bodies - which are less areally extensive - are present (Ghosh, 1995; Logan, 2002). An average age weighted by mapped rock exposure area for 46 K-Ar, ^{40}Ar-^{39}Ar or U-Pb dates of plutonic bodies in southeastern British Columbia (Logan, 2002) is 120 Ma, which is within error of the 122 Ma average calculated from the entire set of four low plateau and five high plateau ages for the Columbia River sediments (Table 2.2).

Nd isotopic analyses performed on suspended and bedload sediment from the Columbia River reflect interior, Cordilleran sources (as opposed to Cascade or Columbia River Basalt sources), supporting our ^{40}Ar-^{39}Ar bulk sediment age results. Two bedload samples have an average ε_{Nd} = -5.5 (Goldstein et al., 1984) and a suspended sediment sample has ε_{Nd} = -4.5 (Goldstein and Jacobsen, 1988). Since plagioclase is one of the major carriers

of the rare earth elements (out of the major rock-forming minerals) and all geologic provinces in this study have similar plagioclase abundances, it might be expected that the Nd isotopic values would reflect, to some extent, a mixture of all sources in the river basin. Yet, the river sediment Nd isotopic values do not reflect a mixture of Nd isotopic values from all Columbia River basin rock types (Figure 2.12), but values most closely resembling those of the British Columbia plutonic rocks from the Selkirk, Monashee and Purcell Mountains, which have an average ε_{Nd} = -7.5 (Ghosh, 1995), also suggesting that this region is the dominant source of sediment at the mouth of the Columbia River. It is possible, then, that the dual-plateau feature seen in the Columbia River sediment might be related to the two populations of granitic rocks mentioned above, found in the headwaters of the Columbia River basin, although this is speculative.

Another perplexing finding is that we do not see strong evidence for material derived from the high topographic-relief regions of the Idaho-Bitterroot Batholith (65-100 Ma) that are characterized by low $^{143}Nd/^{144}Nd$ (ε_{Nd} -10 to -20; Fleck, 1990; Mueller et al., 1995) nor Cascade arc rocks which have quite young ^{40}Ar-^{39}Ar ages (0-30 Ma, Walker and Macleod, 1991; Verplanck and Duncan, 1987) and have ε_{Nd} values of around 4.5 (GEOROC database, http://georoc.mpch-mainz.gwdg.de/georoc/). This is somewhat surprising considering that erosion rates are often greater in high relief regions (Ahnert, 1970; Burbank et al., 2003), or in regions experiencing high rates of rock uplift (Wobus et al., 2003) or precipitation (Reiners et al., 2003). Both regions comprise only about 8% each of the total area for the Columbia River catchment, which helps explain why the signatures of these geologic provinces are not seen in our analyses. However, considering how proximal the high-relief Cascades are to the mouth of the Columbia River and the fact that notable erosion is occurring there (Reiners et al., 2003) this explanation is not entirely satisfactory. Likewise, Reiners et al., (2005) saw little evidence for a Cascade signature from zircon analyses of Tertiary-age fluvial-derived sandstones in the Olympic Mountains, in spite of the fact that sediments comprising the units had to have been transported through the paleo-Cascades. This may indicate that the Cascades do not contribute a significant amount of sediment to the larger size fractions. Minerals from fine-grained

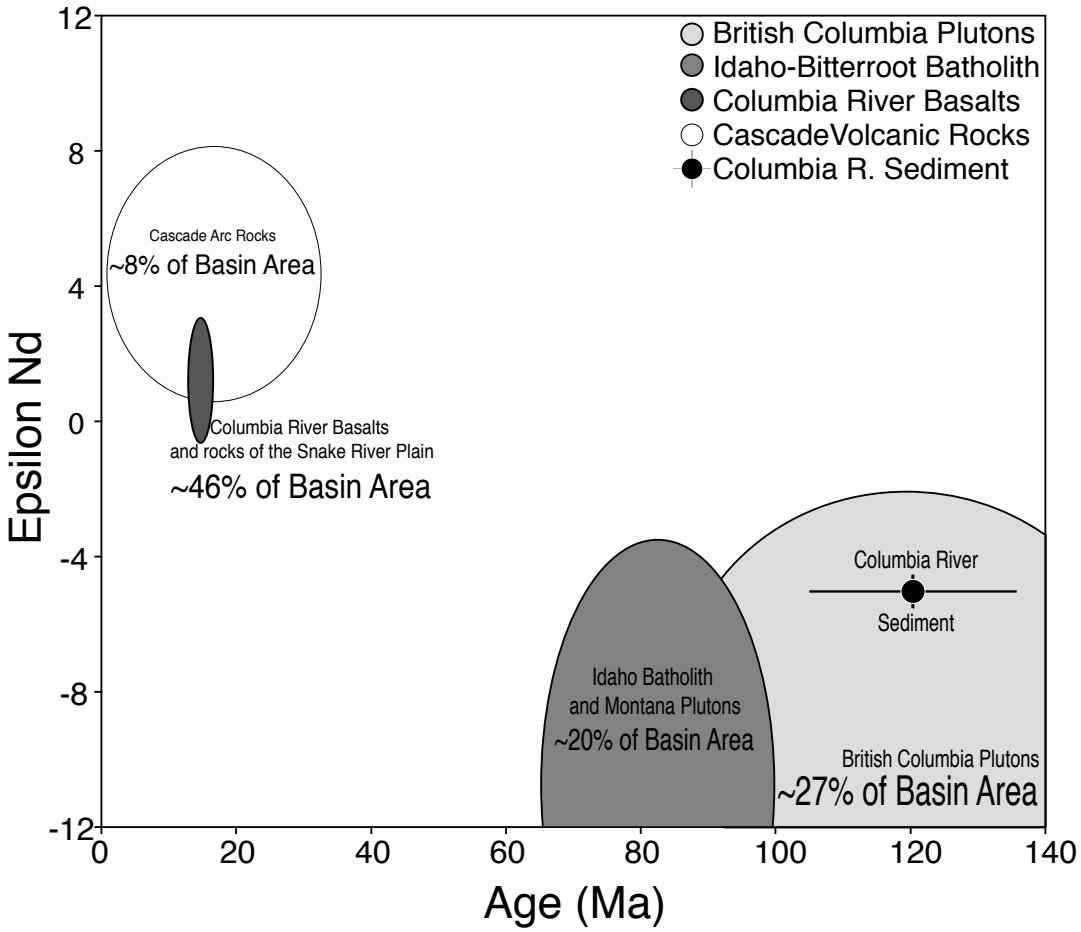

Figure 2.12 - Nd isotopes (epsilon Nd) versus cooling/crystallization age or, in the case of the Columbia River, bulk sediment ^{40}Ar-^{39}Ar plateau age. Data sources: Canadian Plutons from Ghosh (1995) and Logan (2002); Idaho Batholith data from Foster et al. (2001) and Fleck (1990); Columbia River Basalt and Cascade arc data from GEOROC (http://georoc.mpch-mainz.gwdg.de/georoc/); Columbia River Nd isotopic data and error from Goldstein et al. (1984) and Goldstein and Jacobsen (1988). As discussed in the text, the Columbia River sediment most closely resembles the intrusive rocks from British Columbia.

volcanic rocks may break down to smaller size fractions (< 20 μm) more easily/faster (relative to plutonic minerals) during erosion, producing a size fraction bias. It has been suggested that volcanic rocks break down by chemical weathering up to 50 times more quickly than granites (Drever and Clow, 1995). Thus, Cascade and other volcanic rocks in these catchments may be under-represented in silt-sized material and be more preferentially reflected through clays and the solute load. It has been shown that minerals related to granitic rocks like micas, K-feldspars and sodic to intermediate plagioclase are the longest lasting detrital minerals, while hornblende and calcic plagioclase have an order-of-magnitude shorter lifetime (Kowalewski and Rimstidt, 2003). These findings suggest that minerals comprising the sediment at the mouths of the Columbia, Rogue and Klamath Rivers, for example, could show bias to older, plutonic sources. An alternative explanation to these data is that high relief alone is not enough to dictate how much erosion is occurring in the different geologic provinces. Higher rates of rock uplift or precipitation may also be playing a role and this provides an area for future research.

2.9.3 Other Considerations

As noted earlier, loss of radiogenic ^{40}Ar and recoil of ^{39}Ar and ^{37}Ar can affect ^{40}Ar-^{39}Ar analyses. We see strong evidence for both. ^{40}Ar loss appears to be a consistent feature in almost all of the samples. The loss is generally confined to the lower temperature steps, where the less retentive minerals or the weathered margins of more retentive minerals are degassing. What is surprising is that ^{40}Ar loss is not much more pervasive, considering that most of the minerals in these sediments come from surface outcrops that are exposed to chemical weathering and have been mechanically broken down during transport. One possible explanation this is that the physical weathering process removes the less-retentive, altered and fractured outer edges, and leaves behind more pristine mineral crystals.

Ar recoil is most consistently observed in samples that drain the Tertiary Tyee Formation (Coos and Umpqua Rivers) and Mesozoic Franciscan Melange (the Eel, Mattole and Russian Rivers). Both of these sediment formations are comprised of mineral particles

that are sourced from Mesozoic protoliths, suggesting that recoil is common in material derived from old sedimentary rocks; possibly because of diagenetic factors compounded by exposure to more physical and chemical weathering (e.g., these minerals and rock fragments have been through the weathering process at least twice).

Some of the estuary samples did not provide ages that were reproducible. Since tides and longshore currents often bring material into the estuary it was important to avoid sampling near the mouth (Peterson et al., 1982). Yet, we now see that any sample taken further inland in an estuary with complex hydrography, away from tidally derived beach material, is not always representative of what enters the ocean, as evidenced by the wide range in ages from samples taken from the Tillamook and Willapa estuaries. However, this should only be true in cases where several major rivers feed into one estuary, and is dependent on the shape of the estuary and the distribution of erodable rock types in the contributing drainage area (Peterson et al., 1984). The bulk sediment ^{40}Ar-^{39}Ar ages from Willapa Bay (WIL-2 & 4) and Tillamook Bay (TIL-1 & 2) are unlikely to be fully homogenized (well-mixed) and therefore do not provide a reliable ^{40}Ar-^{39}Ar fingerprint.

The K/Ca spectra provide important insights into the composition of our bulk samples but generally do not provide much in the way of diagnostic provenance information since K/Ca values are seen to change through the step-heating process for different samples from the same river. The reasons for this are likely related to variable mineralogy, variable contributions of minerals to the plateau portion of the age spectra and ^{39}Ar loss in the reactor. When compared with ICP-OES K/Ca ratios, systematically lower Ar-derived integrated K/Ca values are observed in samples that have very low initial K/Ca values in their spectra (for example, COO-1A, Figure 2.4; ROG-5, Figure 2.5; RUS-2, Figure 2.6). The most plausible explanation for this difference is reactor-related loss of ^{39}Ar (i.e., K), which results in K/Ca measurements that are unexpectedly low and not truly representative of the mineralogy at the lower temperature steps. The K/Ca spectra acquired during the middle and high temperature steps, however, reflect real differences in mineralogy.

Finally, we acknowledge that other important factors dictating the flux and types of sediment delivered through the fluvial system, such as anomalous storms, mass wasting

events, fires, logging, agricultural practices and river diversion projects, are not considered here because of the difficulty in addressing these problems in the framework of longer-term, geological cycles and regional scales.

2.10 Conclusions and Implications

This paper highlights a new method that characterizes bulk sediment for provenance studies using the ^{40}Ar-^{39}Ar incremental heating technique. We analyzed the 20-63 μm size fraction of bulk river sediments from the mouths of 14 Pacific Northwest rivers for the purpose of identifying sources and examining the feasibility of using bulk sediment ^{40}Ar-^{39}Ar plateau ages and age spectra patterns to track the contributions of specific rivers to continental margin sedimentation. We examined the silt-sized material since this fraction contains mostly rock-forming minerals and yet it is small enough to be transported to most continental margin sediment sites via ocean currents. Significant findings are:

Reproducible age spectra provide robust "fingerprints" for many individual rivers in the Pacific Northwest, both by the shape of the age spectra and by the bulk sediment ^{40}Ar-^{39}Ar plateau ages. Major problems in this dataset appear to be related to sampling bias and not the technique itself (for instance, variability in age spectra seen in samples from large estuaries are related to non-homogenization of several river sources in a complex estuarine system).

A K/Ca degassing model is developed to test, in light of bulk mineralogy and diffusion of silicates, whether measured K/Ca spectra (determined from ^{39}Ar and ^{37}Ar) are reasonable indicators of contributing minerals, given typical K- and Ca-compositions. The model shows that the bulk mineralogy is reflected in the outgassing K/Ca spectra and that plagioclase is likely to be the dominant mineral producing the age plateaus, followed by K-feldspar.

A basin-scale "weighted average cooling age" model is also developed to test the consistency of our measured bulk sediment plateau ages with known source rock age and compositions. The simple model takes into account K-content (of plagioclase and K-feldspar), cooling age and areal extent of geologic units to predict bulk sediment plateau ages for the Umpqua, Rogue and Klamath river basins. The Umpqua basin model prediction is 90 Ma,

very similar to the average bulk sediment ^{40}Ar-^{39}Ar age (92 Ma). The model predicted 128 Ma for the Rogue River, virtually identical to the average bulk sediment age of 129 Ma calculated from four ^{40}Ar-^{39}Ar analyses. The modeled age for the Klamath River is 109 Ma, considerably younger than the average bulk sediment age of 151 Ma. However, if we include the effect of differential erosion occurring in the high-relief Klamath Mountains and low-relief Cascades and/or transport of this material to the mouth, a model age of 147 Ma is predicted.

Results from the Klamath and Rogue Rivers, which drain the same lithologic formations, show distinct ^{40}Ar-^{39}Ar bulk sediment plateau ages, highlighting the fact that this technique has the power to resolve sediment sources on a drainage basin scale. These results also suggest that in cases where "fingerprints" are the goal, this method shows promise to be as diagnostic as single-grain methods (e.g., ^{40}Ar-^{39}Ar age determinations on mica and K-feldspar, U-Pb age measurements on zircons, etc) often used in fluvial settings. For example, the Rogue and Klamath Rivers likely contain differing proportions of single grain populations in which a large number of analyses would be necessary to resolve differences statistically. However, these differing proportions of rock types contributing detrital minerals to the fluvial sediment can be resolved with very few measurements using incremental heating on bulk sediment. Future work involving the coupling of single-grain analyses with this bulk sediment ^{40}Ar-^{39}Ar incremental heating method will further refine the technique and will also expand its utility.

Based on Nd isotopic analyses (Goldstein and Jacobsen, 1988; Goldstein et al., 1984) in conjunction with our bulk sediment age results, we infer that the Columbia River sediment is dominated by detrital minerals from Canadian Cordilleran rocks. It is interesting that Cascade rocks seem to be "missing" in measurements made on the bedload sediment (both data presented here and that of Goldstein and others (1984; 1988)) of the Columbia River even though notable erosion occurs there (Reiners et al., 2003). This observation has been made before for much older fluvial-derived sediments in the Pacific Northwest (Reiners et al., 2005a) and may be related to a combination of grain size differences between plutonic and volcanic minerals and the rates at which these minerals break down. The information unraveled by the ^{40}Ar-^{39}Ar method presented here coupled with the few Nd isotopic analyses

from the Columbia River (Goldstein and Jacobsen, 1988; Goldstein et al., 1984) suggests that the two isotopic systems could prove to be a powerful combination in not only identifying provenance but also unraveling erosion dynamics on large fluvial basin scales.

Our results show promise for applying this technique to a variety of climatic and tectonic problems. These include delineating downcore provenance change on fluvial basin scales to unravel trends in oceanographic circulation and sediment fluxes through geologic time. Because the technique captures information about weathering and alteration, it may also be well suited to contrast physical vs. chemical weathering in terrigenous sediments. It could also be a valuable tool for understanding both spatial and temporal changes in basin hydrology related to natural climate and tectonic cycles over geologic timescales.

The inferences made by the "average cooling age" model suggest that there may also be a future for this technique in the realm of tectonic geomorphology and thermochronology at continental margin sites where single-grain analyses are not feasible. Although bulk sediment is inherently complex, the findings presented here show that quantitative information about provenance and erosion can be extracted from ^{40}Ar-^{39}Ar heating of polymineralic materials, and suggest that this method has broad application to documenting tectonic and climatic processes through the tracking of terrigenous material.

2.11 References

Ahnert, F., 1970, A comparison of theoretical slope models with slopes in the field: Zeitschrift Fur Geomorphologie Supplementband, v. 9, p. 88-101.

Allen, C. M., Barnes, C. G., and Campbell, I. H., 2002, U-Th-U ages from Klamath River detrital zircons using LA-ICP-MS: Geological Society of America-Abstracts with Programs, v. 34, no. 6, p. 434.

Barnes, C. G., 1987, Mineralogy of the Wooley Creek batholith, Slinkard pluton and related dikes, Klamath Mountains, northern California: American Mineralogist, v. 72, p. 879-901.

Barnes, C. G., Barnes, M. A., and Kistler, R. W., 1992, Petrology of the Caribou Mountain Pluton, Klamath Mountains, California: Journal of Petrology, v. 33, no. 1, p. 95-124.

Barnes, C. G., Rice, J. M., and Gribble, R. F., 1986, Tilted plutons in the Klamath Mountains

of California and Oregon: Journal of Geophysical Research, v. 91, no. B6, p. 6059-6071.

Bernet, M., Brandon, M. T., Garver, J. I., and Molitor, B., 2004, Fundamentals of detrital zircon fission-track analysis for provenance and exhumation studies with examples from the European Alps, in Bernet, M., and Spiegel, C., eds., Detrital Thermochronology - Provenance analysis, exhumation and landscape evolution of mountain belts: Boulder, Colorado, Geological Society of America Special Paper 378, p. 25-36.

Blake, M. C., and Jones, D. L., 1981, The Franciscan melange in northern California: A reinterpretation, in W.G., E., ed., The geotectonic evolution of California: Englewood Cliffs, NJ, Prentice Hall, p. 306-328.

Brady, J. B., 1995, Diffusion data for silicate minerals, glasses and liquids, in Ahrens, T. J., ed., A handbook of physical constants: Mineral physics and crystallography (Vol.2): Washington D.C., American Geophysical Union, p. 269-290.

Brandon, M. T., and Vance, J. A., 1992, Tectonic evolution of the Cenozoic Olympic subduction complex, Washington state, as deduced from fission track ages for detrital zircons: American Journal of Science, v. v. 292, p. p. 565-636.

Burbank, D. W., Blythe, A. E., Putkonen, J., Pratt-Sitaula, B., Gabet, E., Oskin, M., Barros, A. P., and Ojha, T. P., 2003, Decoupling of erosion and precipitation in the Himalayas: Nature, v. 426, no. 11 December 2003, p. 652-655.

Carrapa, B., Wijbrams, J., and Bertolli, G., 2004, Detecting provenance variations and cooling patterns within the western Alpine orogen through $^{40}Ar/^{39}Ar$ geochronology on detrital sediments: The Tertiary Piedmont Basin, northwest Italy, in Bernet, M., and Spiegel, C., eds., Detrital Thermochronology - Provenance analysis, exhumation, and landscape evolution of mountain belts: Boulder, Colorado, The Geological Society of America, p. 67-103.

Carter, A., 1999, Present status and future avenues of source region discrimination and characterization using fission track analyses: Sedimentary Geology, v. 124, p. 31-45.

Clift, P. D., and Blusztajn, J., 2005, Reorganization of the western Himalaya river system after five million years ago: Nature, v. 438, no. doi:10.1038, p. 1001-1003.

Clift, P. D., Campbell, I. H., Zhang, X., Carter, A., Hodges, K. V. K., A.A., and Allen, C. M., 2004, Thermochronology of the modern Indus River bedload: New insight into the controls on the marine stratigraphic record: Tectonics, v. 23, no. 5.

Clift, P. D., Lee, J. I., Hildebrand, P., Shimizu, N., Layne, G. D., Blum, J. D., Garzanti, E., and Khan, A. A., 2002, Nd and Pb isotope variability in the Indus River system: Implications for crustal heterogeneity in the Western Himalaya: Earth and Planetary Science Letters, v. 200, p. 91-106.

Clift, P. D., Shimizu, N., Layne, G. D., and Blusztajn, J., 2001, Tracing patterns of erosion and drainage in the Paleogene Himalaya through ion probe Pb isotope analysis of detrital K-feldspars in the Indus Molasse, India: Earth and Planetary Science Letters, v. 188, no. 3-4, p. 475-491.

Copeland, P., Harrison, M., and Heizler, M. T., 1990, $^{40}Ar/^{39}Ar$ single-crystal dating of detrital muscovite and K-feldspar from Leg 116, southern Bengal Fan: Implications for uplift and erosion of the Himalayas, in Cochran, J. R., Stow, D. A. V., and et al., eds., Proceedings of the Ocean Drilling Program: Scientific Results: College Station, TX, Ocean Drilling Program, p. 93-114.

Dalrymple, G. B., Alexander, E. C., Jr., Lanphere, M. A., and Kraker, G. P., 1981, Irradiation of samples for $^{40}Ar/^{39}Ar$ dating using the Geological Survey TRIGA reactor: U. S. Geological Survey Professional Paper.

Dalrymple, G. B., and Lanphere, M. A., 1969, Potassium-argon dating: Principles, techniques and applications to geochronology: San Francisco, W.H. Freeman and Co., 258 p.

Darby, D. A., 2003, Sources of sediment found in sea ice from the western Arctic Ocean, new insights into processes of entrainment and drift patterns: Journal of Geophysical Research, v. 108, no. C8, p. 3257.

Deer, W. A., Howie, R. A., and Zussman, J., 1992, An introduction to rock-forming minerals: New York, John Wiley and Sons, Inc, 696 p.

Dong, H., Hall, C. M., Peacor, D. R., and Halliday, A. N., 1995, Mechanisms of argon retention in clays revealed by laser ^{40}Ar-^{39}Ar dating: Science, v. 267, p. 355-359.

Drever, J. I., and Clow, D. W., 1995, Weathering rates in catchments, in White, A. F., and Brantley, S. L., eds., Chemical weathering rates in silicate minerals: Washington, D.C., Mineralogical Society of America, p. 463-481.

Fagel, N., Innocent, C., Gariepy, C., and Hillaire-Marcel, C., 2002, Sources of Labrador Sea sediments since the last glacial maximum inferred from Nd-Pb isotopes: Geochimica et Cosmochimica Acta, v. 66, no. 14, p. 2569-2581.

Fagel, N., Innocent, C., Stevenson, R., Gariepy, C., and Hillaire-Marcel, C., 1996, A high resolution Nd and Pb isotopic study of Labrador Sea clays at the 2/1 transition; implications for sedimentary supplies and deep circulation changes: Enriched: AGU 1996 fall meeting Eos, Transactions, American Geophysical Union, v. 77, no. 46, p. 324.

Faure, G., 1986, Principles of isotope geology: New York, John Wiley and Sons, 589 p.

Fechtig, H., and Kalbitzer, S., 1966, The diffusion of argon in potassium-bearing solids, in Schaeffer, O. E., and Zahringer, J., eds., Potassium Argon Dating: Berlin-Heidelberg, Springer-Verlag, p. 68-107.

Fleck, R. J., 1990, Neodymium, strontium and trace-element evidence of crustal anatexis and magma mixing in the Idaho Batholith, in Anderson, J. L., ed., The nature and origin of Cordilleran magmatism: Boulder, CO, The Geological Society of America, p. 359-374.

Garzanti, E., Critelli, S., and Ingersoll, R. V., 1996, Paleogeographic and paleotectonic evolution of the Himalayan Range as reflected by detrital modes of Tertiary sandstones and modern sands (Indus transect, India and Pakistan): Geological Society of America Bulletin, v. 108, no. 6, p. 631-642.

Garzanti, E., Vezzoli, G., Andò, S., Paparella, P., and Clift, P. D., 2005, Petrology and mineralogy of Indus River sands : a key to interpret erosion history of the Western Himalayan Syntaxis: Earth and Planetary Science Letters, v. 229, p. 287–302.

Ghosh, D., 1995, Nd-Sr isotopic constraints on the interactions of the intermontane Superterrane with the western edge of North America in the southern Canadian Cordillera: Can. Jour. Earth Sci., v. 32, p. 1740-1758.

Gillespie, A. R., Huneke, J. C., and Wasserburg, G. J., 1982, An assessment of ^{40}Ar-^{39}Ar dating of incompletely degassed xenoliths: Journal of Geophysical Research, v. 87, no. B11, p. 9247-9257.

Goldstein, S. L., and Jacobsen, S. B., 1988, Nd and Sr isotopic systematics of river water suspended material: Implications for crustal evolution: Earth and Planetary Science Letters, v. 87, p. 249-265.

Goldstein, S. L., O'Nions, R. K., and Hamilton, P. J., 1984, A Sm-Nd isotopic study of atmospheric dusts and particulates from major river systems: Earth and Planetary Science Letters, v. 70, p. 221-236.

Harrison, T. M., Duncan, I., and McDougall, I., 1985, Diffusion of ^{40}Ar in biotite: Temperature, pressure and compositional effects: Geochimica et Cosmochimica Acta, v. 49, p. 2461-2468.

Heller, P. L., Peterman, Z. E., O'Neil, J. R., and Shafiqullah, M., 1985, Isotopic provenance of sandstones from the Eocene Tyee Formation, Oregon Coast Range: GSA Bulletin, v. 96, p. 770-780.

Heller, P. L., Renne, P. R., and O'Neil, J. R., 1992, River mixing rate, residence time, and subsidence rates from isotopic indicators: Eocene snadstones from the U.S. Pacific Northwest: Geology, v. 20, p. 1095-1098.

Hemming, S. R., Broecker, W. S., Sharp, W. D., Bond, G. C., Gwiazda, R. H., McManus, J. F., Klas, M., and Hajdas, I., 1998, Provenance of Heinrich layers in core V28-82, northeastern Atlantic: ^{40}Ar/^{39}Ar ages of ice-rafted hornblende, Pb isotopes in feldpar grains, and Nd-Sr-Pb isotopes in the fine sediment fraction: Earth and Planetary Science Letters, v. 164, p. 317-333.

Hemming, S. R., Hall, C. M., Biscaye, S. M., Higgins, S., Bond, G. C., McManus, J. F., Barber, D. C., Andrew, J. T., and Broecker, W. S., 2002, $^{40}Ar/^{39}Ar$ ages and $^{40}Ar^{*}$ concentrations of fine-grained sediment fractions from North Atlantic Heinrich layers: Chemical Geology, v. 182, p. 583-603.

Howard, A. D., 1994, A detachment-limited model of drainage basin evolution: Water Resources research, v. 30, p. 2261-2285.

-, 1998, Long profile development of bedrock channels: Interaction of weathering, mass wasting, bed erosion and sediment transport, in Tinkler, K. J., and Wohl, E. E., eds., Rivers over rock: Fluvial processes in bedrock channels: Washington, American Geophysical Union, p. 323.

Irwin, W. P., 1997, Preliminary map of selected post-Nevadan geologic features of the Klamath Mountains and adjacent areas, California and Oregon: U.S. Geological Survey Open-File Report, v. 97-465, p. 29p.

Irwin, W. P., and Wooden, J. L., 1999, Plutons and accretionary episodes of the Klamath mountains, California and Oregon.

Jantschik, R., and Huon, S., 1992, Detritial silicates in northeast Atlantic deep-sea sediments during the Late Quaternary: Mineralogical and K-Ar isotopic data: Eclogae geol. Helv., v. 85, no. 1, p. 195-212.

Koppers, A. P., 2002, ArArCalc - software for $^{40}Ar/^{39}Ar$ age calculations: Computers & Geosciences, v. 28, p. 605-619.

Kowalewski, M., and Rimstidt, J. D., 2003, Average lifetime and age spectra of detrital grains: Toward a unifying theory of sedimentary particles: Journal of Geology, v. 111, p. 427-439.

Kuhlemann, J., Frisch, W., Dunkl, I., Kazmer, M., and Schmiedl, 2004, Miocene siliciclastic deposits of Naxos Island: Geodynamic and environmental implications for the evolution of the southern Aegean Sea (Greece), in Bernet, M., and Spiegel, C., eds., Detrital Thermochronology - Provenance analysis, exhumation, and landscape evolution of mountain belts: Boulder, Colorado, The Geological Society of America, p. 51-65.

Lamy, F., Hebbeln, D., and Wefer, G., 1998, Late Quaternary precessional cycles of terrigenous sediment input off the Norte Chico (27.5°S) and paleoclimatic implications: Paleogeography, Paleoclimate, Paleoecology, v. 141, p. 233-251.

-, 1999, High resolution marine record of climatic change in mid-latitude Chile during the last 28 ka based on terrigenous sediment parameters: Quaternary Research, v. 51, p. 83-93.

Lisitzin, A. P., 1996, Oceanic sedimentation: Lithology and geochemistry: Washington D.C., American Geophysical Union, 399 p.

Logan, J. M., 2002, Intrusion related mineral occurrences of the Cretaceous Bayonne Magmatic Belt, southeast British Columbia.

Lovera, O. M., Grove, M., Harrison, T. M., and Mahon, K. I., 1997, Systematic analysis of K-feldspar $^{40}Ar/^{39}Ar$ step heating results: I. Significance of activation energy determinations: Geochimica et Cosmochimica Acta, v. 61, no. 15, p. 3171-3192.

McDougall, I., and Harrison, T. M., 1999, Geochronology and thermochronology by the $^{40}Ar/^{39}Ar$ method: New York, Oxford University Press, 269 p.

McLaughlin, R. J., Sliter, W. V., Fredriksen, N. O., Harbert, W. P., and McCulloch, D. S., 1994, Plate motions recorded in tectonostratigraphic terranes of the Franciscan Complex and evolution of the Mendocino Triple Junction, Northwestern California.

Monger, J. W., Price, R. A., and Templeman-Kluit, D. J., 1982, Tectonic accretion and the origin of the two major metamorphic and plutonic belts in the Canadian Cordillera: Geology, v. 10, p. 70-75.

Montgomery, D. R., and Dietrich, W. E., 1994, A physically-based model for the topographic control on shallow landsliding: Water Resources Research, v. 30, p. 1153-1171.

Mueller, P. A., Shuster, R. D., D'Arcy, K. A., Heatherington, A. L., Nutman, A. P., and Williams, I. S., 1995, Source of the northeastern Idaho Batholith: Isotopic evidence for a Paleoproterozoic terrane in the northwestern U.S.: Journal of Geology, v. 103, p. 63-72.

Peterson, C., Scheidegger, K. F., and Komar, P., 1982, Sand-dispersal patterns in an active-margin estuary of the northwestern United States as indicated by sand composition, texture and bedforms: Marine Geology, v. 50, no. 1-2, p. 77-96.

Peterson, C., Scheidegger, K. F., P, K., and Niem, W., 1984, Sediment composition and hydrography in six high-gradient estuaries of the northwestern United States: Jour. Sed. Petrology, v. 54, no. 1, p. 86-97.

Pettke, T., Halliday, A. N., Hall, C. M., and Rea, D. K., 2000, Dust production and deposition in Asia and the north Pacific Ocean over the past 12 Myr: Earth and Planetary Science Letters, v. 178, p. 397-413.

Pisias, N. G., Mix, A. C., and Heusser, L., 2001, Millennial scale climate variability of the northeast Pacific Ocean and northwest North America based on radiolaria and pollen: Quaternary Science Reviews, v. 20, p. 1561-1576.

Reiners, P. W., Campbell, I. H., Nicolescu, S., Allen, C. M., Hourigan, J. K., Garver, J. I., Mattinson, J. M., and Cowan, D. S., 2005a, (U-Th)/(He-Pb) Double Dating Of Detrital Zircons: American Journal of Science, v. 305, p. 259-311.

Reiners, P. W., Ehlers, T. A., Mitchell, S. G., and Montgomery, D. W., 2003, Coupled spatial variations in precipitation and long-term erosion rates across the Washington

Cascades: Nature, v. 426, p. 645-647.

Reiners, P. W., Ehlers, T. A., and Zeitler, P. K., 2005b, Past, present, and future of thermochronology, in Reiners, P. W., and Ehlers, T. A., eds., Low-Temperature Thermochronology: Techniques, Interpretations, and Applications, p. 1-18.

Renne, P. R., Deino, A. L., Walter, R. C., Turrin, B. D., Swisher, C. C., Becker, T. A., Curtis, G. H., Sharp, W. D., and Jaouni, A.-R., 1994, Intercalibration of astronomical and radioisotopic time: Geology, v. 22, p. 783-786.

Roy, M., Clark, P. U., Duncan, R. A., and Hemming, S. R., 2005, Constraints on a long-lived Keewatin ice dome from $^{40}Ar/^{39}Ar$ dating of mineral grains from midcontinent glacial deposits.

Ryu, I., and Niem, A. R., 1999, Sandstone diagenesis, reservoir potential and sequence stratigraphy of the Eocene Tyee Basin, Oregon: Journal of Sedimentary Research, v. 69, no. 2, p. 384-393.

Spiegel, C., Siebel, W., Kuhlemann, J., and Frisch, W., 2004, Toward a comprehensive provenance analysis: A multi-method approach and its implications for the evolution of the Central Alps, in Bernet, M., and Spiegel, C., eds., Detrital Thermochronology - Provenance analysis, exhumation, and landscape evolution of mountain belts: Boulder, Colorado, The Geological Society of America, p. 37-50.

Turner, G., and Cadogan, P. H., 1974, Possible effects of ^{39}Ar recoil in ^{40}Ar-^{39}Ar dating: Geochimica et Cosmochimica Acta, v. 5, no. 2, p. 1601-1615.

Verplanck, E. P., and Duncan, R. A., 1987, Temporal variations in plate convergence and eruption rates in the Western Cascades, Oregon: Tectonics, v. 6, p. 197-209.

Walczak, P. W., 2006, Submarine plateau volcanism and Cretaceous Ocean Anoxic Event 1a : geochemical evidence from Aptian sedimentary sections: Oregon State University, 172 p.

Walker, G. W., and MacLeod, N. S., 1991, Geologic Map of Oregon: U.S. Geological Survey, scale 1:500,000.

Walter, H. J., Hegner, E., Diekmann, B., Kuhn, G., and Rutgers van der loeff, M. M., 2000, Provenance and transport of terrigenous sediment in the South Atlantic Ocean and their relations to glacial and interglacial cycles: Nd and Sr isotopic evidence: Geochimica et Cosmochimica Acta, v. 64, no. 22, p. 3813-3827.

Wang, S., McDougall, I., Tetley, N., and Harrison, T. M., 1980, $^{40}Ar/^{39}Ar$ age and thermal history of the Kirin Chondrite: Earth and Planetary Science Letters, v. 49, p. 117-131.

Wells, R. E., Jayko, A. S., Niem, A. R., Black, G., Wiley, T., Baldwin, E., Molenaar, K. M., Wheeler, K. L., DuRoss, C. B., and Givler, R. W., 2000, Geologic map and database of the Roseburg 30 X 60 quadrangle, Douglas and Coos counties, Oregon.

Wendt, I., and Carl, C., 1991, The statistical distribution of the mean standard weighted deviation: Chemical Geology (Isot. Geosci. Sect.), v. 86, p. 275-285.

Whipple, K. X., Kirby, E., and Brocklehurst, S. H., 1999, Geomorphic limits to climate-induced increases in topographic relief: Nature, v. 401, p. 39-43.

Whipple, K. X., and Tucker, G. E., 1999, Dynamics of the stream-power river incision model: Implications for height limits of mountain ranges, landscape response timescales, and research needs: Journal of Geophysical Research, v. 104, p. 17661-17674.

Wobus, C. W., Whipple, K. X., Kirby, E., Snyder, N. P., Johnson, J., Spyropolou, K., Crosby, B. T., and Sheehan, D., 2006, Tectonics from topography: Procedures, promise and pitfalls, in Willett, S. D., Hovius, N., Brandon, M. T., and Fisher, D., eds., Tectonics, Climate and Landscape Evolution: Geological Society of America Special Paper 398: Boulder, CO, Geological Society of America, p. 55-74.

Wobus, C. W., Hodges, K. V., and Whipple, K. X., 2003, Has focused denudation sustained active thrusting at the Himalayan topographic front?: Geology, v. 31, no. 10, p. 861-864.

Zhang, G., Germaine, J. T., Martin, R. T., and Whittle, A. J., 2003, A simple sample-mounting method for random powder X-ray diffraction: Clays and Clay Minerals, v. 51, no. 2, p. 218-225.

Chapter 3

Tracking fluvial response to climate change in the Pacific Northwest: A combined provenance approach using Ar and Nd isotopic systems on fine-grained sediments

Sam VanLaningham, Robert A. Duncan, Nicklas G. Pisias, David W. Graham

College of Oceanic and Atmospheric Sciences
Oregon State University, Corvallis Oregon 97331

To be submitted to Earth and Planetary Science Letters
Or
Quaternary Science Reviews

3.1 Abstract

We use traditional provenance techniques (Nd isotopes and clay mineralogy) in conjunction with recently developed bulk sediment ^{40}Ar-^{39}Ar radiometric methods on both river and continental margin sediments to determine whether the terrestrial source changes through time. We utilize these tools on Pacific Northwest river material and sediment from piston coring site EW9504-17PC (2671 m water depth) offshore southern Oregon. The ultimate goal is to provide insight about the coupling of land surface processes and ocean circulation related to climate change. Nd isotopic analyses on river silts show a range of around ten ε_{Nd} units, highlighting promise for the technique in the northeast Pacific Ocean as a provenance tracer. The Columbia River, north of the core site, has ε_{Nd} = -7.6. The Coos River, eroding the Tyee Formation has a value of ε_{Nd} = -10.8, while rivers more proximal to the core site have increasingly more radiogenic values from north to south of ε_{Nd} = -5.0 (Umpqua River), ε_{Nd} = -1.3 (Rogue River), ε_{Nd} = -0.6 (Klamath River) and ε_{Nd} = -3.0 (Eel River). Downcore ranges in ε_{Nd} at the core site show subtle changes between ε_{Nd} = -0.9 to -2.5. The bulk sediment ^{40}Ar-^{39}Ar plateau ages show more notable downcore variation across the interval spanning the last glacial interval, ranging from 113.5 Ma to 124.0 Ma.

We combine the Nd isotopic analyses with bulk sediment ^{40}Ar-^{39}Ar plateau ages into a ternary mixing model to better understand the sources of terrigenous material. Downcore Ar-Nd isotopic mixtures can be described by three general sources proximal to the core site (the Umpqua, Rogue+Klamath and Eel Rivers) from ~14 ka to Present. However, samples from 22 ka to 25 ka are not adequately described by the present-day rivers and require another source. Our favored explanation is an enhanced contribution from the interior Cascade volcanic arc (of which the Umpqua, Rogue and Klamath each have their headwaters) during this time. The Cascades were glaciated and contained pluvial Lake Modoc throughout Marine Isotope Stage 2 and thus, suggests that 25 to 22 ka (just before the Last Glacial Maximum), the sediments arriving at the core site were characterized by an increase in Cascades-derived material relative to today. From 22-14 ka, however, the influence of Cascades sediment at the core site was overprinted by contemporaneous glaciation and sediment production in the

Klamath Mountains and possibly the Eel River region as well. Thus, differential contributions of eroded material plays the primary role in provenance changes seen at the core site, rather than sediment transport changes due to ocean circulation. By 14 ka the source of sediment to the core site appears similar to today, although a more subtle change in provenance around 10 ka suggests an influx of sediment related to regional aggradation of Oregon Coast Range rivers. When the pollen record of spruce at EW9504-17PC is recast with the added information from provenance changes, it suggests that the spruce pollen abundances are an integrated signal of both precipitation and temperature related to vegetation succession as well as a function of erosional flux changes related to glaciation and precipitation. Overall, the combined Ar-Nd isotopic technique distinguishes sources of sediment to the western North American margin and suggests that fine-grained silicate detritus can be resolved into components of the fluvial basins and/or geologic provinces from which they are eroded.

3.2 Introduction and Motivation

Marine sedimentary records at continental margins capture the integrated signal of oceanic, atmospheric and terrestrial processes (e.g., Pisias et al., 2001; Lamy et al., 2001; Clift, 2006). Rivers communicate the terrestrial component of change through the erosion, entrainment, and delivery of material to the continental margin (e.g., Clift and Blusztajn, 2005). Since changes over climatic timescales ($<10^5$ years) on the continental surface are mostly in response to atmospheric processes, combining marine and terrestrial studies at ocean margin core sites casts a wide spotlight on the entire climate system. A blessing and curse in the deep marine realm is that it preserves a thorough and continuous history of earth surface processes unaffected by transgressions and regressions of the ocean. Yet, with that comes the fact that material transported beyond the continental shelf and slope to the deep ocean is usually fine-grained and difficult to characterize. Thus, a need remains for studies that can extract the important source information captured in fine-grained silicates.

This paper focuses on new isotopic approaches to characterize silt-sized river-borne, terrigenous sediment and documents the source of terrestrial material to the northeast Pacific

margin offshore Oregon over the last glacial-interglacial period. We focus on the silt-sized component since it captures the rock-forming minerals and yet is small enough to be transported long distances.

The study region along western North America (Figure 3.1) shows evidence for a tight coupling between terrestrial-ocean-atmospheric systems and lies in a transition zone between the North Pacific and Alaskan Gyres. Radiolaria abundances (that are typified by an eastern boundary current species) and pollen assemblages (that are dominated by redwood) co-vary on glacial-interglacial timescales (Pisias et al., 2001). A hypothesis is that, when there is a strong eastern boundary current due to strong wind-stress curl along the margin there is increased coastal fog due to upwelling of cold, deeper waters, inevitably leading to conditions favorable to redwood growth. However, what if this apparent coupling between terrestrial and ocean systems recorded in marine sediments is due to ocean circulation changes, a reasonable possibility considering the relationship between ocean circulation and climate? One way to test this is by examining if the carrier of the pollen (terrigenous sediment) changes contemporaneously with the pollen assemblages on appreciable temporal and/or spatial scales.

In this paper, we combine Nd isotopic analyses with a newly established ^{40}Ar-^{39}Ar incremental heating technique (VanLaningham et al., 2006) applied to fine-grained sedimentary material to determine the terrestrial sources of sediment arriving at the core site. The new Nd isotopic data provide additional means to precisely characterize the river-borne sediment in this region. We address how sediment composition changes over the last 25,000 years and evaluate to what extent the pollen record preserved at the core site is a record of terrestrial climate change as opposed to changing transport pathways of this pollen (and sediment) from ocean circulation or other surface process mechanisms. We demonstrate that sediment provenance has indeed changed at the core site, but only from proximal sources and thus, was not driven by circulation changes. The change was mostly due to differential erosion in river basins that result in transport of material from different parts of the onshore landscape that are affected by climate differently (and thus contain different flora). We then discuss our findings in terms of the continental Pacific Northwest-northeast Pacific oceanic climate system and provide insights about terrestrial-ocean climate linkages.

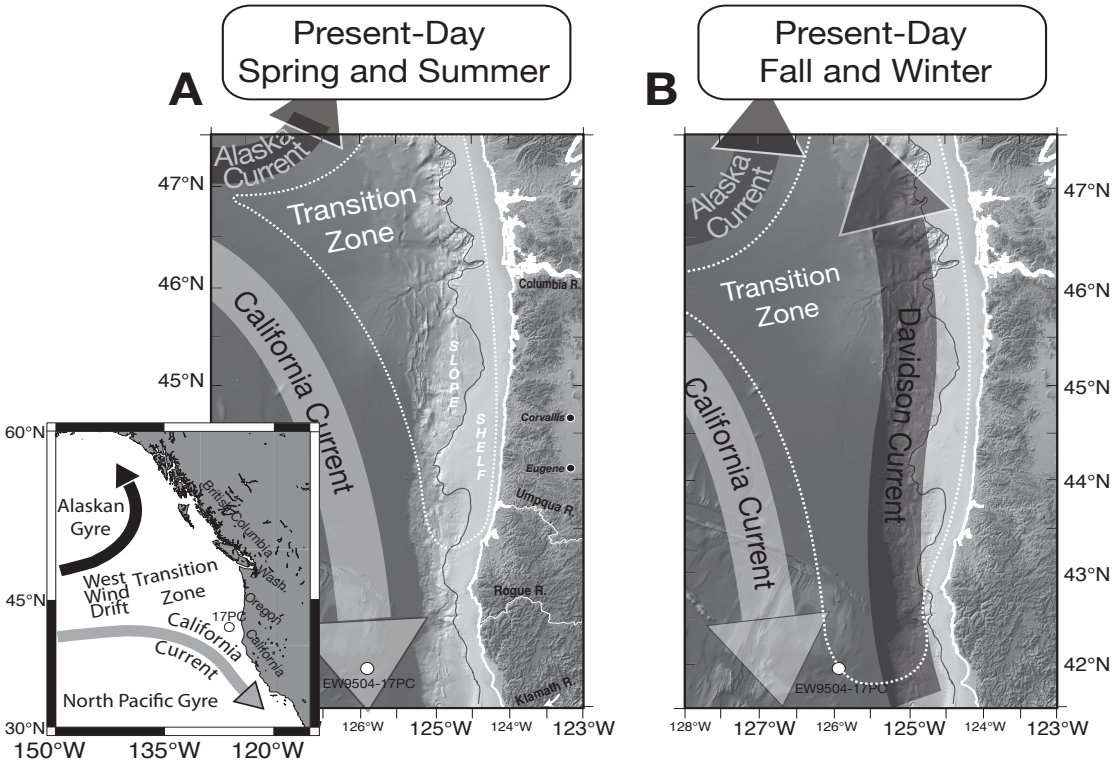

Figure 3.1 - Present-day upper ocean currents in the northeast Pacific Ocean. Piston core site EW9504-17PC (synonymous with "17PC") is shown as a white circle with black outline. A) Spring and summer conditions. The California Current and northerly winds have a strong influence on surface flow from the coast out to the deep ocean. Upwelling related to these conditions persists from the beginning of spring to early fall. B) Fall and winter conditions. Shelf and slope regions along the margin of western North America become affected by the northward-flowing countercurrent of the California Current (i.e., the Davidson Current) during the winter months. The California Current is displaced offshore (Hickey et al., 2003) making way for the Davidson Current.

3.3 Study Area

This study examines a sediment core from the northeast Pacific Ocean and the fluvial sources to those sediments. Piston coring site EW9504-17PC (42.24° N, 125.89° W) is located about 120 km west of the Oregon-California border at a water depth of 2671 m (Figure 3.1). The core was collected on a local bathymetric high on the east flank of Gorda Rise to avoid turbidites and to capture a continuous record of hemipelagic sedimentation. All potential river-borne sediment sources to the core site were examined. We sampled 14 major rivers from as far north as the Olympic Peninsula, Washington to as far south as San Francisco Bay, California to determine fine-grained sediment compositions.

3.3.1 Ocean Circulation and Climate

Ocean circulation in the northeast Pacific Ocean is today dominated by the California Current system. It shows strong seasonality driven by changes in the locations and intensities of the North Pacific and Alaskan Gyres, which reflect wind stress conditions over the Pacific (Figure 3.1). The major components of ocean circulation are the California Current, the Davidson Current and the California Undercurrent, although smaller-scale flow exists (Hickey, 1979; Werner and Hickey, 1983; Hickey and Royer, 2001; Hickey and Banas, 2003). In the spring and summer, the California Current flows south along the west coast as a ~1000 km wide swath from the surface to 500 m depth (Hickey and Banas, 2003). The narrow (10-40 km) California Undercurrent flows northward beneath the surface along the continental slope during this time.

In fall and winter, coastal circulation changes considerably. Surface flow along the margin switches to northward from Point Conception, California past Oregon and Washington (Hickey and Banas, 2003) and is known as the Davidson Current. It spreads ~100 km wide across the distal continental shelf and slope. Inner and mid-shelf circulation generally follows trends of the California and Davidson Current, whereby flow is southward during spring and summer and northward in fall and winter (Strub, 1987). The southward-flowing California

Current drives upwelling along the margin of the Pacific Northwest today during spring and summer, although its strength and duration increase from north to south. Upwelling offshore Oregon occurs from about March to September, while it generally shuts down during fall and winter (Strub, 1987).

Sedimentation along the margin follows shelf and slope circulation. Surface sampling of sediments characterized by their clay mineralogy (Karlin, 1980) indicates that sedimentation offshore northern California, Oregon and Washington occurs dominantly in winter and is northward, when the Davidson Current is active and when the coastal region experiences extensive precipitation (Figure 3.2, Karlin surface maps). There is some input of sediment related to spring runoff from alpine, interior regions in the Columbia, Umpqua, Rogue and Klamath River basins. However, clay mineralogy data suggest that presently only the Columbia River has a north to south sediment delivery during the spring, when circulation offshore Washington and Oregon transitions to southward surface flow (Figure 3.2) and also because the large Columbia freshwater plume disturbs circulation (Hickey and Banas, 2003).

3.3.2 Onshore Climate Setting

Present-day climate over the onshore Pacific Northwest consists of temperate coastal, alpine and steppe provinces north of southern Oregon/northern California. In California the climate is much more moderate and Mediterranean-like and influenced by the Great Basin high-pressure system. Annual precipitation in Washington coastal areas is approximately 230-250 cm/yr while the Olympic Mountains accrue as much as 650 cm/yr (http://www.ncgc.nrcs.usda.gov/). In western Oregon, 200-230 cm/yr of precipitation occurs along the coast, between 250-400 cm/yr occurs just inland in the coastal mountains to the east (the Oregon Coast Ranges and Klamath Mountains) while farther inland, the Willamette Valley receives around 125 cm each year.

Whereas the coastal regions of Washington and Oregon show substantial west-east orographic gradients in precipitation, coastal California and the coastal mountains south of the Klamath Mountain region show very little orographic control on precipitation patterns,

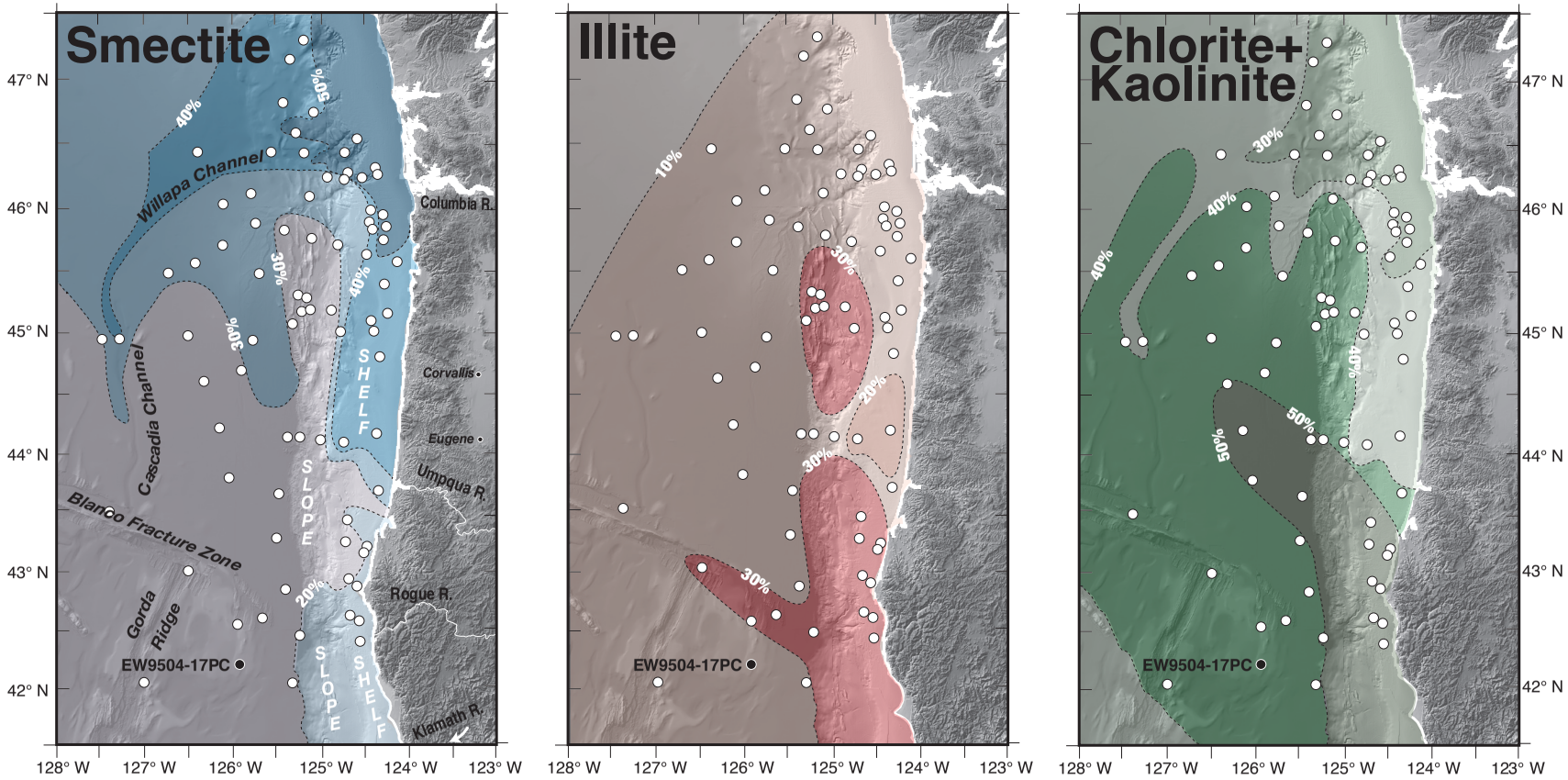

Figure 3.2 - Relative abundances of clay minerals smectite (montmorillonite), illite and chlorite+kaolinite for surface sediments in the northeast Pacific Ocean from Karlin (1980). Piston core site EW9504-17PC shown as black circle with white outline. Seventy-seven core top samples (white circles) were analyzed. Percent abundances were calculated according to Biscaye (1965). These data suggest that present-day sediment transport is dominantly from the south. Elevation and bathymetry from Haugerud (1999, U.S. Geological Survey Open-file Report 99-369). Clay distribution map redrafted from Karlin (1980).

although a notable latitudinal gradient is observed. Annual rainfall decreases from about 175 cm around Eureka, CA (~41° N) to around 100-150 cm in the San Francisco Bay area (38° N).

Farther inland, the Cascade Mountains receive a diminished amount of rainfall relative to the coastal mountains (about 150-250 cm/yr), with higher values generally in the north and at higher elevations. The Cascade Mountains create a considerable rain shadow effect and precipitation reduces considerably over the Columbia Plateau and high desert of eastern Oregon (25-50 cm/yr). The headwaters of the Columbia River in the Rocky Mountains of British Columbia and Montana experience about 150 cm/yr while lower topography in these regions amass around 50-60 cm/yr. Precipitation rates in the Snake River region, the southern arm of the Columbia River, are around 25-40 cm/yr in the lower plains and 75-125 cm/yr in the surrounding mountains (http://www.ncgc.nrcs.usda.gov/).

3.3.3 Present-day river discharge and sediment loads

River discharge and sediment loads from the Pacific Northwest vary widely (Karlin, 1980; Sherwood et al., 1990; Wolf et al., 1999; Wheatcroft et al., 2005) and are presented in Table 3.1. At 216 km^3/yr, the Columbia River releases over 20 times more freshwater to the northeast Pacific Ocean than the second largest contributor (Rogue River, 10.1 km^3/yr) in the region and about 75% of the total freshwater output from all of the major Pacific Northwest rivers combined. In terms of total sediment loads, however, the Eel River delivers the most sediment presently at about $18x10^9$ kg of sediment per year, whereas estimates for the Columbia River suggest that it contributes only about $5x10^9$ kg now (Table 3.1). Notably however, dams may have reduced the Columbia River sediment load by at least 50% (Sherwood et al., 1990) and possibly as great as 75% (Vorosmarty et al., 2003; Wolf et al., 1999; Syvitski et al., 2005), which would place its pre-dam sediment load in the range of 10-$20x10^9$ kg/yr, comparable to the present-day Eel River. There has been a less severe reduction in clay- and silt-sized sediments (~33%; Sherwood et al., 1990), which are the size fractions we have analyzed. The Klamath (and Trinity River tributary), Rogue, Mad and Umpqua Rivers are the other major sediment sources to the margin and straddle the core site.

Table 3.1 - River statistics. N is the number of days used in the rating curve determination. Sediment yields from basins with letter subscripts were estimated based on the measured yields from adjacent basins, $_{a}$Umpqua, $_{c}$Smith, $_{d}$Eel, $_{e}$Russian. The Rogue $_{(b)}$ is a composite of the Klamath and Smith (refer to Wheatcroft and Sommerfield, 2005 for details).

River	Basin size (km^2)	Avg. discharge (km^3/yr)	Avg. annual load ($\times 10^9$ kg)	Sed. yield ($\times 10^3$ kg/km^2/yr)	Refs.	Period of record	N
Quinalt	684	2.6	0.1	125*	(1)		
Grays Harbor	5,776	8.1	0.7	114.5+	(1)		
Willapa Bay	1,046	1.9	0.1	125*+	(1)		
Columbia	661,211	216					
-Present-Day			5.0	7.6	(3)	1964-1969	
-Pre-Dams			20.0	30.2	(4), (5)		
Tillamook Bay	1,400	2.7	0.2	125*+	(1)		
Siletz	523	1.4	0.1	125*+	(1)		
Yaquina	665	1.0	0.1	128.8	(1)		
Alsea	865	1.5	0.1	75	(2)	1939–P	188
Siuslaw	1,523	1.8	0.1	62	(2)	1967–1994	826
Umpqua	9,534	6.7	1.4	147	(2)	1905–P	139
$Coos_a$	*1,567*	*2.7*	*0.2*	*150*	(2)		
$Coquille_a$	*1,960*	*2.2*	*0.3*	*150*	(2)		
$Rogue_b$	*13,394*	*10.1*	*2.3*	*170*	(2)		
$Chetco_c$	*702*	*2.3*	*0.2*	*250*	(2)		
Smith	1,590	3.3	0.4	252	(2)	1931–P	264
Klamath	21,950	7.3	3.3	150	(2)	1927–P	1696
Trinity(Klamath Trib.)	7,390	4.7	6.8	920	(2)	1931–P	1876
	29,340	12.0	10.1	344			
Redwood Creek	720	0.9	1.3	1805	(2)	1953–P	2034
Mad	1,256	1.3	2.6	2070	(2)	1950–P	1495
Eel	8,063	6.6	18.0	2232	(2)	1913–P	1817
$Mattole_d$	*635*	*1.1*	*1.3*	*2000*	(2)		
$Navarro_e$	*785*	*0.5*	*0.2*	*300*	(2)		
$Gualala_e$	*901*	*0.4*	*0.3*	*300*	(2)		
Russian	3,452	2.4	1.1	318	(2)	1939–P	1510
		302					

Sediment yields (a drainage area-normalized measure of sediment flux) are extremely high in the central and northern California coastal rivers such as the Eel, Mad, Mattole, Trinity Rivers and Redwood Creek. This is mostly related to the combined effects of erodable Franciscan Melange rocks (McLaughlin et al., 1994) and their degree of shearing related to high deformation rates relative to the rest of the Pacific Northwest margin due to tectonism along the San Andreas fault and surrounding structures in the Mendocino Triple Junction (Merritts and Vincent, 1989; Snyder et al., 2000).

3.3.4 Geology of source terranes

Western North America is comprised of a diverse set of geologic provinces that contribute to sediments accumulating in the northeast Pacific Ocean (Figure 3.3). Sediment sources to the margin in Washington are mostly from the rocks of the Olympic Mountains, Washington Coast Ranges and Columbia River. The Olympic Mountains are comprised of a suite of sandstones, mudstones and volcanic lithologies that have Eocene to Miocene depositional ages (Brandon and Vance, 1992). In the southwestern coastal ranges of Washington and northwestern Oregon, source material is made of Eocene sedimentary and volcanic rocks (Walker and MacLeod, 1991). The Columbia River drains an immense area of western North America and a large variety of rock types and geologic provinces. Lithologies in the headwaters of the Columbia River (including the Kootenay and Okanogan River tributaries) in British Columbia are Mesozoic accreted terranes of sedimentary, volcanic and plutonic origins as well as many stocks that intruded into the accreted units (Ghosh, 1995; Monger et al., 1982). The Snake River, a large tributary of the Columbia River, erodes mostly Cretaceous Idaho-Bitterroot Batholith granites in the high-relief regions and then flows across young Tertiary volcanic rocks in the Snake River Plain. The headwaters of the Pend Oreille-Clark Fork and Clearwater tributaries drain the 55-62 Ma granitic batholiths of the Bitterroot Mountains and meta-sedimentary rocks with Mesozoic to Paleozoic depositional ages from the Rocky Mountains of Montana. Over much of the Columbia Basin, the Columbia River and tributaries erode and flow through the vast area of Miocene Columbia River Basalts (~50%

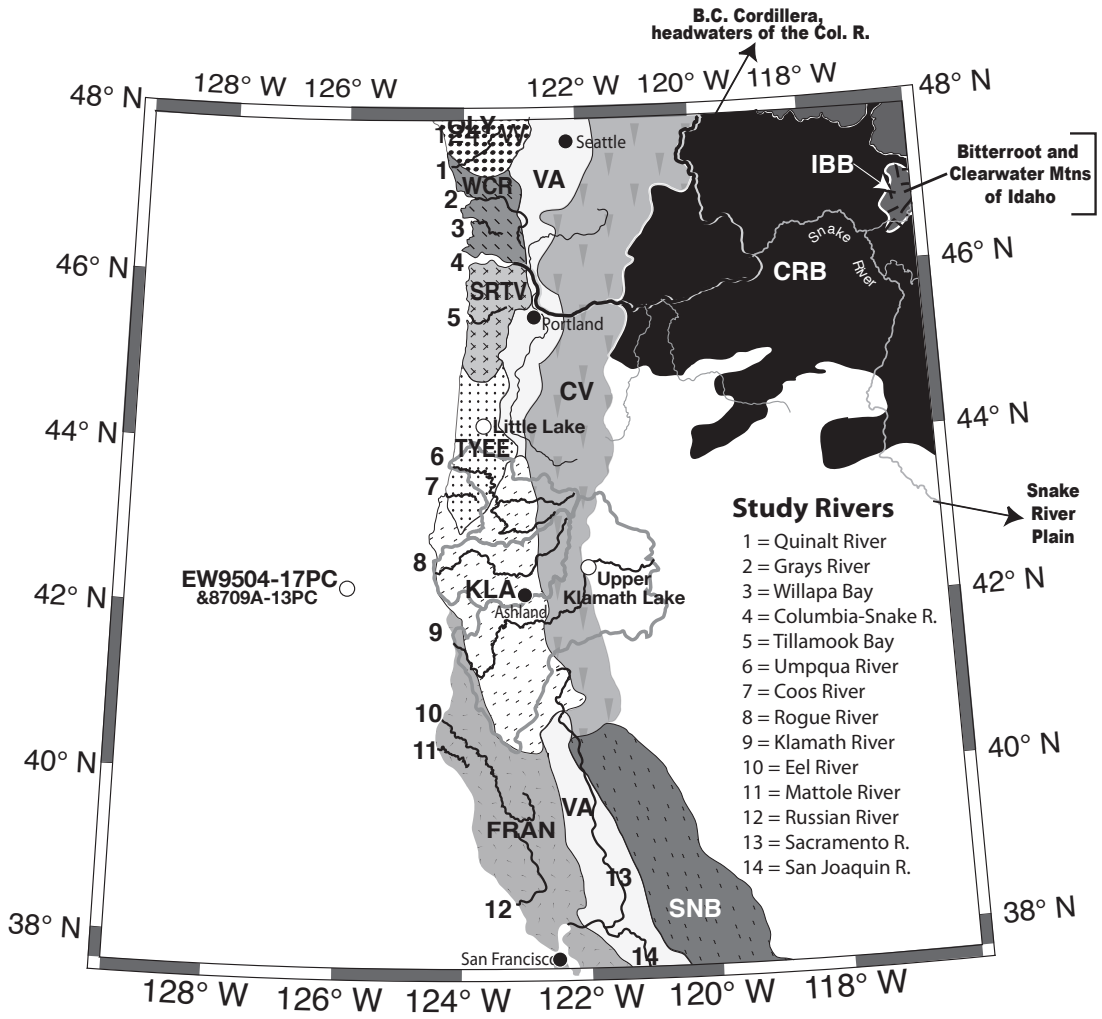

Figure 3.3 - Location map showing study rivers, core sites and bedrock geology of the western U.S. Heavy gray lines around the Umpqua, Rogue and Klamath Rivers denote the areal extent of their catchment basins. Major Columbia R. tributaries and British Columbia mountain belts are shown for reference. The far eastern portion of the Columbia River Basin is not shown. OLY = Olympic Mountain Accretionary Complex; WCR = Washington Coast Ranges; SRTV = Siletz River-Tillamook Volcanics; TYEE = Tyee Formation Turbidites; KLA = Klamath Mountain Accretionary Complex; FRAN = Franciscan Melange; VA = Valley Alluvium; SNB = Sierra Nevada Batholith; CV = Cascade Volcanics; CRB = Columbia River Basalts; WWC = Western Canadian Cordillera; IBB = Idaho-Bitterroot Batholith; VIR, CM and FP = Vancouver Island Ranges, Coast Mountains and Fraser Plateau (do not contribute to Columbia River.). See text for an explanation of lithologies.tion of lithologies.

of the basin area) and the Tertiary to Recent arc volcanic rocks of the Cascade Mountains (~8% of the Columbia River basin area). Even though all of these geologic provinces could be contributing to the sediment composition of the fluvial material traveling through the Columbia River out to sea, it has been shown previously that the present-day silt-sized Columbia River material is dominantly from the British Columbia Cordillera (VanLaningham et al., 2006).

Coastal sediment sources in central Oregon erode turbidite sequences and oceanic basalts with Eocene depositional ages. The largest rivers in southern Oregon and Northern California begin in Cenozoic basaltic and andesitic rocks of the central and southern Oregon Cascades and either traverse the turbidites of the Oregon Coast Ranges (Umpqua River) or the Mesozoic Klamath Mountains en route to the Pacific Ocean. The Klamath accretionary complex is composed of metasedimentary, meta-volcanic, granitic and gabbroic rocks and ophiolitic sequences.

The coastal range of northern and central California is dominated by the Franciscan Melange, a Cretaceous to lower Tertiary sequence of sandstones and mudstones, with large blocks (up to several kilometers in size) of serpentinite, blueschist, eclogite greenstone, chert and limestone (Blake and Jones, 1981; McLaughlin et al., 1994), although other less extensive volcanic lithologies are present in the region as well. The Eel River, western North America's largest present-day sediment producer, erodes these rocks, as do parts of the Russian River. Central Californian sediment sources (Sacramento and San Joaquin Rivers) drain the granitic rocks of the Mesozoic Sierra Nevada Mountains, Great Valley sediments and lesser contributions from the Klamath and Franciscan rocks.

3.4 Methods

3.4.1 Sampling and Preparation

Sediments at core site EW9504-17PC are made up of clay- to silt-sized particles. Hence, it is important to characterize similar size fractions from the river sediments that

contribute to margin sedimentation. Detailed descriptions of sampling and preparation procedures are provided in VanLaningham et al. (2006) and in an Oregon State University College of Oceanography reference manual (Robbins et al., 1984). Briefly, we sampled rivers near their mouths and usually above tidewater to obtain the most representative material that is transported out to sea. We treated the sieved 0-63 μm material with hydrogen peroxide to remove organic material while calcium carbonate was removed with buffered acetic acid. Oxyhydroxides were removed using 1.0N hydroxylamine hydrochloride buffered with sodium citrate. About 75-200 mg of silt-sized (20-63 μm) material was extracted from 100-200 g of bulk fluvial sediment by sieving and settling, while centrifugation was used to extract 2-20 and 0-2 μm size fractions.

In core EW9504-17PC, the terrigenous component dominates the sedimentology of the core (calcium carbonate content varies from 0-13% while organic carbon varies between 1-2%; Lyle et al., 2000). We collected 10 cm^3, sampled every 2 kyr from ~25 ka to Present and applied the same preparations to the core samples as with the river samples.

3.4.2 Nd Isotopic Procedures for river and downcore samples

We determined the Nd isotopic composition of bulk, silt-sized (20-63 μm) river and downcore samples. We first pulverized about 50-100 mg of sample and heated it in a furnace to 800° C to remove more refractory organic compounds not dissolved in the H_2O_2 step. Samples were digested in Teflon Savillex® beakers with 5 ml of concentrated HF and 1 ml of 8N HNO_3. The samples dissolved within 24-48 hours using a combination of sonication and heating (at ~110-140° C). We then converted solutions to chlorides by drying down in 6N HCl and then taking samples back up in 2.5N HCl for column chemistry. Each sample was first passed through a single cation exchange column of Dowex® AG50X8 to separate REEs from all other elements, using 2.5N HCl followed by collection of the REE in 6.0N HCl. A second chromatography column using ln-spec resin (Eichrom industries) was used to separate Nd from other REEs, using 0.25N HCl as the elutant.

Analyses were performed at the Oregon State University Keck Laboratory using a

Nu® multi-collector inductively coupled plasma mass spectrometer. Samples entered the instrument in dilute HNO_3 and were analyzed using a multi-dynamic analysis setup. Nd isotopic ratios in the samples and standard were mass fractionation corrected to $^{146}Nd/^{144}Nd = 0.7219$ (Wasserburg et al., 1981). A consistent offset of the J-Ndi standard was observed (around 0.8 ε_{Nd} units) relative to the accepted value of J-Ndi $^{143}Nd/^{144}Nd = 0.512115\pm7$ (Tanaka, 2000). The offset correction was applied to both samples and BCR-1 rock powders analyzed as unknowns. BCR-1 was processed using the same chemical procedures as samples. Reproducibility of the J-Ndi standard was 0.000024 (2σ, n=47). The mean value for BCR-1, adjusted using the J-Ndi standard was $^{143}Nd/^{144}Nd = 0.512632\pm23$ (2σ, n=10; See Appendix C). Each sample was bracketed by a J-Ndi or BCR-1 standard during the analytical campaign. Typical ion beam intensities attained for samples during runs were ~1.0 – 3.0 volts, while intensities of around 2.0 volts were consistently acquired for the 150 ppb J-Ndi standard. A small correction was applied for the isobaric interference of Sm on the ^{144}Nd peak by monitoring ^{147}Sm during analysis. This correction was typically less than the analytical uncertainty of the measured $^{143}Nd/^{144}Nd$.

3.4.3 ^{40}Ar-^{39}Ar Incremental Heating Procedures for Core Samples

We provide a full description of the procedures used here for ^{40}Ar-^{39}Ar analyses in a previous paper (VanLaningham et al., 2006). Briefly, samples were irradiated with the FCT-3 monitor standard (age = 28.03±0.18 Ma; Renne et al., 1994) in the 1MW TRIGA reactor at Oregon State University to induce the reaction ^{39}K (n, p) ^{39}Ar. The irradiated samples were analyzed using the MAP 215-50 mass spectrometer in the Ar geochronology laboratory at Oregon State University. They were heated incrementally with a defocused 10W CO_2 laser programmed to traverse the sample during each heating step (for approximately five minutes). Samples were degassed with 13 to 15 temperature steps, from 200-300°C to fusion at around 1400°C. Zr-Al getters removed active gases from the extracted Ar before measurement in the mass spectrometer. Isotopic masses for ^{40}Ar, ^{39}Ar, ^{38}Ar, ^{37}Ar and ^{36}Ar were measured so that appropriate corrections could be made for reactor-produced interferences (McDougall

and Harrison, 1999). The most important of these corrections is an atmospheric correction of ^{40}Ar via the $^{40}Ar/^{36}Ar$ ratio and reactor-induced ^{39}Ar and ^{36}Ar interferences from Ca that are corrected via ^{37}Ar.

The plateau and integrated (total fusion) ages were calculated from corrected $^{40}Ar/^{39}Ar$ ratios using ArArCalc (Koppers, 2002). A plateau age is a consecutive sequence of concordant heating step ages comprising more than 50% of its total ^{39}Ar released in the sample (Koppers, 2002; McDougall and Harrison, 1999). A mean square of weighted deviations (MSWD) calculation was made for every plateau age to assess the goodness of fit. When this value is much greater than 1.0, it suggests that geological factors such as alteration, multiple age populations in a given mineral phase (VanLaningham et al., 2006) or reactor effects such as Ar recoil, could be contributing to the measured ages and the weighted plateau ages might be underestimated (Koppers, 2002; McDougall and Harrison, 1999; Wendt and Carl, 1991). Potassium - calcium ratios (K/Ca) were also calculated from measured concentrations of ^{39}Ar derived from K and ^{37}Ar derived from Ca.

3.4.4 Other Methods

For the mixing model discussed later in this paper, we use Nd concentrations determined from separate sample dissolutions than those used for isotopic analyses and were measured using an EXCELL® ICP-MS in the College of Oceanic and Atmospheric Sciences at Oregon State University. Procedures used are summarized in Walczak (2006). $^{40}Ar^*$ (radiogenic ^{40}Ar) concentrations for each river sample used in the mixing model were estimated from the portion of the irradiated material (for which we have weights) used in the age determinations. Since the general trend in these estimates follow measurements of the K concentrations (using ICP-AES; VanLaningham et al., 2006), we are confident that the $^{40}Ar^*$ values are consistent, albeit crude estimates of the real concentrations.

We introduce clay mineralogic analyses made on the river and core samples using X-ray diffraction (XRD) in order to supplement the discussion of the influence (or lack thereof) of the Columbia River on the sedimentology of EW9504-17PC over the last glacial-

interglacial period. We incorporate standard clay mineral analyses (Moore and Reynolds, 1989) using a Scintag Pad V diffractometer on glycolated smear slides of the 0-2 μm material from 2°-34° 2θ using Cu radiation. The data were analyzed using MacDiff software (http://www.geologie.uni-frankfurt.de/Staff/Homepages/Petschick/ RainerE.html). Mineral abundances were calculated using an internal talc standard (10% by weight) following the procedures of Heath and Pisias (1979) so as to have a more quantitative assessment of smectite, illite and chlorite+kaolinite abundances. We calculate ratios of these abundances to further avoid any variations related to changes in sediment flux.

3.4.5 Age Model for Core Site EW9504-17PC

We improve the age model for EW9504-17PC over the last 25 kyr using the latest published reservoir-corrected ^{14}C dates (CALIB4) from foraminifera in nearby core W8709A-13PC (Mix et al., 1999), which is ~15 km away from EW9504-17PC. Similar features in the $CaCO_3$ records from each site were connected using tie points from the two cores (Table 3.2). A simple consistency test of the chosen tie points is done by comparing the thicknesses of sediment between each tie point in both cores and suggests that the control points are indeed reasonable choices since the thicknesses are comparable from each core over each interval (Table 3.2). The new age model adjusts depositional ages by 1-2.5 kyr relative to previous age models and has the largest impact around the LGM (Pisias et al., 2001; Lyle et al., 2000).

3.5 Results

3.5.1 Nd Isotopic Analyses of River Sediment Sources

Nd isotopic analyses of Pacific Northwest Rivers are presented in Table 3.3. The general features in this dataset are a range in ε_{Nd} from -10.8 to -0.1 (analytical errors are about 0.2 to 0.4 ε_{Nd} units). Triplicate analyses of KLA-2, each processed separately through column chemistry show a range of one ε_{Nd} unit (ε_{Nd} = -0.6±0.7). The river sources near the core site

Table 3.2 - Age control points for downcore age model. * = Based on reservoir corrected ^{14}C dates (using CAL-IB4.1) from Mix et al. (1999)

EW9504-17PC Depth (cm)	W8709A-13PC Equivalent Depth (cm)	EW9504-17PC Depth between CP's	W8709A-13PC Depth between CP's	Depositional Age (ka)*	Sedimentation Rate (cm/kyr)
0.0	----------	----------	----------	0.0	15.6
135.4	69.1	120.3	120.8	8.7	23.1
255.7	189.9	25.5	30.1	13.9	13.4
281.2	220.0	39.3	37.8	15.8	17.1
320.5	257.8	15.4	11.1	18.1	77.0
335.9	268.9	20.5	20.1	18.3	51.3
356.4	289.0	19.4	24.0	18.7	12.1
375.8	313.0	70.3	83.5	20.3	13.5
446.1	396.5	----------	----------	25.5	13.7

Table 3.3 - Nd isotopic results for Pacific Northwest Rivers. eNd = [$^{143}Nd/^{144}Nd$(sample)/ $^{143}Nd/^{144}Nd$(CHUR)-1]x10^4, where CHUR = present-day chondritic uniform reservoir value of $^{143}Nd/^{144}Nd$ = 0.512638. QUI = Quinalt River; COL = Columbia River; UMP = Umpqua River; COO = Coos River; ROG = Rogue River; KLA = Klamath River; EEL = Eel River; MAT = Mattole River; RUS = Russian River; SCN = Confluence of the Sacramento and San Joaquin Rivers.

Sample	**Lat. (°N)**	**Long. (°W)**	**size (microns)**	**total volts Nd**	**$^{143}Nd/^{144}Nd$**	**std. error 1s.e.**	**ε_{Nd}**	**std. error 1s.e.**
QUI-1	47.35	124.29	20-63	3.7	0.512282	4	-7.0	0.1
COL-3	46.25	123.49	20-63	2.9	0.512303	6	-6.5	0.1
COL-5	46.24	123.62	20-63	0.9	0.512192	13	-8.7	0.2
UMP-1A	43.70	124.07	20-63	1.3	0.512379	10	-5.0	0.2
UMP-1B	43.70	124.07	20-63	1.1	0.512425	12	-4.1	0.2
COO-1C	43.38	124.18	20-63	0.9	0.512084	13	-10.8	0.2
ROG-1	42.44	124.40	20-63	1.7	0.512605	7	-0.7	0.1
ROG-5	42.44	124.38	20-63	1.4	0.512538	11	-1.9	0.2
KLA-2	41.52	124.02	20-63	0.7	0.512631	20	-0.1	0.4
KLA-2.2			20-63	2.6	0.512569	6	-1.4	0.1
KLA-2.3			20-63	2.1	0.512578	7	-0.2	0.1
EEL-1A	40.64	124.28	20-63	1.6	0.512496	7	-2.8	0.1
EEL-2	40.63	124.28	20-63	1.1	0.512477	14	-3.2	0.3
MAT-1	40.31	124.28	20-63	2.3	0.512471	9	-3.3	0.2
RUS-2	38.43	123.10	20-63	1.5	0.512478	7	-3.1	0.1
SCN-1	38.07	121.86	20-63	1.5	0.512408	10	-4.5	0.2
COL-5			0-2	3.6	0.512430	4	-4.1	0.1
COL-5			2-20	3.4	0.512374	5	-5.1	0.1
UMP-1B			0-2	1.4	0.512561	16	-1.5	0.3
KLA-2			0-2	1.1	0.512553	13	-1.7	0.3
KLA-2			2-20	1.4	0.512553	12	-1.7	0.2
EEL-1B			0-2	1.6	0.512480	11	-3.1	0.2

showed a range of values between ε_{Nd} = -5.0 to -0.1. For the Umpqua River average ε_{Nd} = -5.0, whereas the Rogue River has ε_{Nd} = -1.3 and the Klamath River values are ε_{Nd} = -0.9. The largest sediment producer on the western margin of North America, the Eel River, has average ε_{Nd} = -3.0.

Different size fractions were also measured for a few samples (COL-5, UMP-1B, KLA-2 and EEL-1B). The Columbia River shows a notable shift to more radiogenic Nd isotopic values in the finer silt (2-20 μm) and clay (0-2 μm), as does the Umpqua River in the 0-2 μm fraction. The Eel and Klamath Rivers do not show any significant change in Nd isotopic values in different size fraction ranges.

Previous analyses of Columbia River Nd isotopic compositions are generally comparable (Goldstein et al., 1984; Goldstein and Jacobsen, 1988) although slightly different size fractions were analyzed. Their findings for bulk 0-63 μm sediment from the Columbia River were ε_{Nd} = -5.5 (Goldstein et al., 1984), whereas a measurement on mostly clay-sized suspended material was ε_{Nd} = -4.5 (Goldstein and Jacobsen, 1988). Our results from Columbia River were ε_{Nd} = -6.7 for 20-63 μm material, ε_{Nd} = -5.1 for 2-20 μm fine silt and ε_{Nd} = -4.1 for 0-2 μm clays, and generally consistent with these earlier studies. The trend to more radiogenic Nd values with finer material is consistent with the fact that fine-grained rocks such as basalts in the Columbia Basin are more radiogenic whereas the coarser grained granitic sources (British Columbia cordillera, for example) have a less radiogenic Nd signature (Ghosh, 1995).

3.5.2 Nd Isotopic Analyses of Downcore Sediments in EW9504-17PC

We analyzed fourteen samples from the core site for Nd isotopic composition (Table 3.4). Emphasis was placed on hemipelagic sediment samples from 25 ka to the Present. However, the only notable coarse interval (turbidite?) was also analyzed in hopes of determining if its source differed considerably from the hemipelagic material. Generally, the samples have a small range downcore (ε_{Nd} = -2.5 to -0.9). The largest difference in ε_{Nd} from present-day values occurs over the depth interval of 385-445 cm, at ~22-25 ka, while an obvious linear decrease in values occurs from 22 ka to 14 ka (Figure 3.4).

Table 3.4 – Downcore bulk Nd isotopic results. eNd = [$^{143}Nd/^{144}Nd$(sample)/$^{143}Nd/^{144}Nd$(CHUR)-1]x10^4, where CHUR = present-day chondritic uniform reservoir value of $^{143}Nd/^{144}Nd$ = 0.512638

	Core Site							
	EW9504-17PC	**Age**	**size**	**total volts**	**$^{143}Nd/^{144}Nd$**	**std. error**	**ε_{Nd}**	**std. error**
	Sample Depth (cm)	**(ka)**	**(microns)**	**Nd**		**1s**		**1s**
1	**4**	**0.3**	20-63	1.3	0.512511	10	-2.5	0.2
2	**32**	**2.1**	20-63	1.2	0.512531	10	-2.1	0.2
3	**50**	**3.2**	20-63	1.3	0.512534	7	-2.0	0.1
4	**75**	**4.8**	20-63	1.2	0.512529	9	-2.1	0.2
5	**110**	**7.1**	20-63	0.7	0.512545	12	-1.8	0.2
6	**140**	**8.9**	20-63	1.5	0.512544	9	-1.8	0.2
7	**180**	**10.6**	20-63	1.2	0.512550	11	-1.7	0.2
8	**225**	**12.6**	20-63	1.7	0.512545	10	-1.8	0.2
9	**260**	**14.2**	20-63	1.8	0.512513	9	-2.4	0.2
10	**316**	**17.8**	20-63	1.7	0.512540	8	-1.9	0.2
	360	**19.0**	20-63	-----	-----	-----	-----	-----
11	**385**	**21.0**	20-63	1.0	0.512577	13	-1.2	0.2
	403	**22.3**	20-63	-----	-----	-----	-----	-----
12	**420**	**23.6**	20-63	1.4	0.512594	10	-0.9	0.2
13	**445**	**25.4**	20-63	1.3	0.512541	10	-1.9	0.2
	313-Turbidite	**17.7**	20-63	1.8	0.512521	11	-2.3	0.2

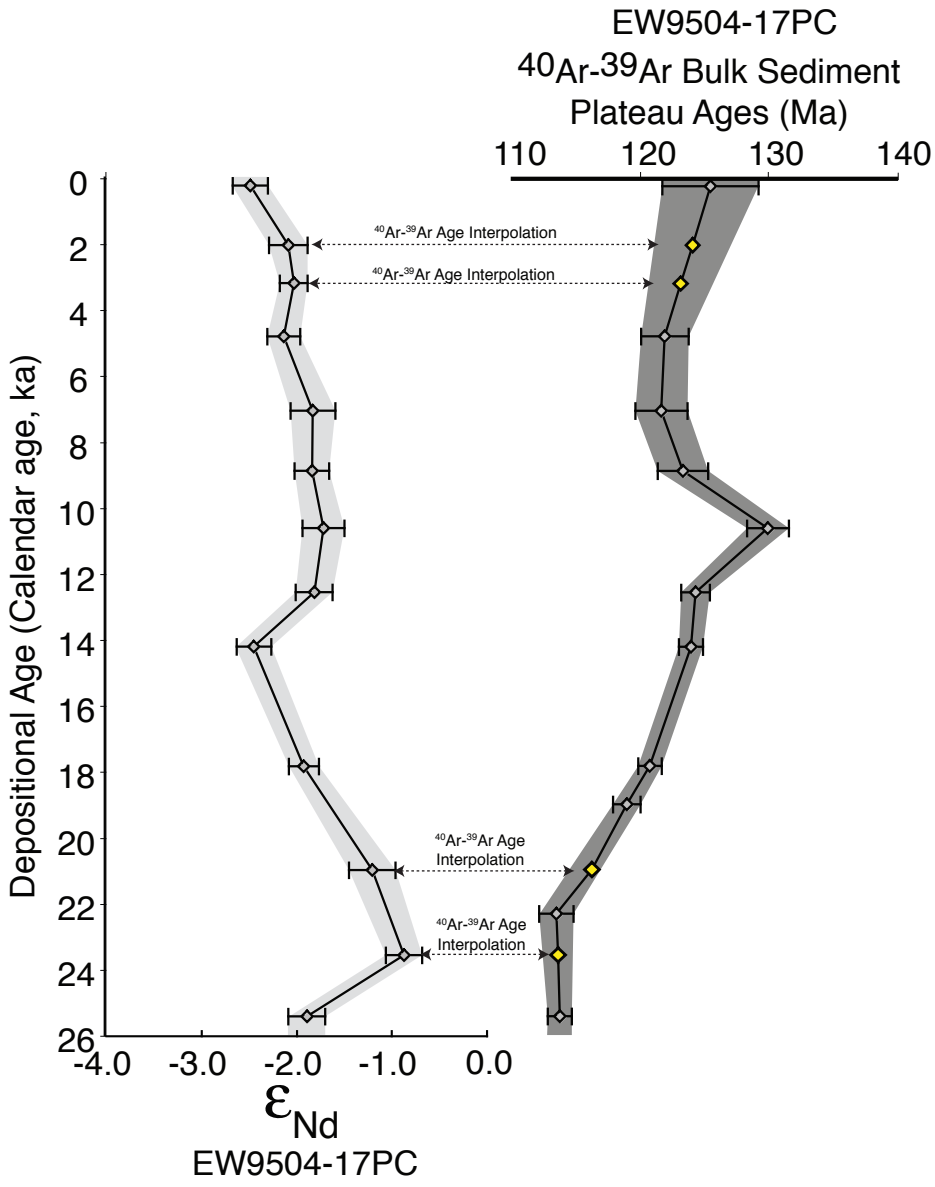

Figure 3.4 – Downcore ε_{Nd} and bulk sediment ^{40}Ar-^{39}Ar ages for core site EW9504-17PC. Yellow diamonds are interpolated bulk sediment ^{40}Ar-^{39}Ar ages, which are used in the mixing model discussion.

3.5.3 ^{40}Ar-^{39}Ar Plateau Ages and K/Ca of Downcore Sediments in EW9504-17PC

The bulk sediment ^{40}Ar-^{39}Ar and related K/Ca ratios are presented in Table 3.5. The downcore ^{40}Ar-^{39}Ar age spectra (Figure 3.5) consistently show plateaus ages and are comparable in their degassing pattern to the nearby river sources (see VanLaningham et al., 2006). The core samples have a range in plateau ages from 113.5 to 125.6 Ma (not including the turbidite) and standard errors of around 1.5 Ma (2σ). Similar to the downcore ε_{Nd} values, the ^{40}Ar-^{39}Ar ages show the largest change over a depth interval of 403-445 cm, 22-25 kyr ago. The K/Ca ratios, which are a crude indicator of mineralogy, have similar spectra from sample to sample. Generally K/Ca values are around 1.5-2.0 (most likely a mixture of kaolinite, K-feldspar and mica) at the lower ends of the spectra and decrease step-wise to values of around 0.1-0.3 (mostly plagioclase; see VanLaningham et al., 2006) at the highest degassing temperatures. The K/Ca values over age plateau-defining steps have a much smaller range of K/Ca = 0.2 – 0.5 (Table 3.5).

3.5.4 Clay Mineralogy

Talc-normalized clay mineral abundances are presented in Table 3.6 for both river and core samples. Focusing on the clay mineral ratios in the rivers, the Columbia, Umpqua and Coos Rivers north of the core site generally show high smectite/illite ratios (range = 2.28-3.06) while fluvial sediment sources at the same latitude and south of the core site such as the Rogue, Klamath and Eel Rivers have lower smectite/illite ratios ranging between 0.35-0.82. Kaolinite+chlorite/illite ratios are generally between 1.3-2.0 with the exception of the Columbia and Quinalt Rivers, which show distinctly lower kaolinite+chlorite/illite ratios (0.77 and 1.0, respectively).

3.6 Discussion

Now we discuss the possible sources of the terrigenous component of the marine

Table 3.5 - Downcore Bulk Sediment ^{40}Ar-^{39}Ar Ages

	Core Site EW9504-17PC Sample Depth (cm)	Age (ka)	size (microns)	^{40}Ar-^{39}Ar Age Fusion	^{40}Ar-^{39}Ar Age Plateau	std. error 2s	Steps	% Gas On Plateau	MSWD	K/Ca Plateau	$^{40}Ar_{(n)}/^{39}Ar_{(K)}$ Fusion	std. error 2s	$^{40}Ar_{(n)}/^{39}Ar_{(K)}$ Fusion	std. error 2s
1	**4**	**0.3**	20-63	114.8	125.6	3.8	4	41	0.2	0.4	34.4	1.0	31.4	0.7
2	**32**	**2.1**	20-63	-----	***124.2***	***Linear Interpolation***			-----	-----	-----	-----	-----	-----
3	**50**	**3.2**	20-63	-----	***123.2***	***Linear Interpolation***			-----	-----	-----	-----	-----	-----
4	**75**	**4.8**	20-63	118.8	122.0	1.9	8	79	1.5	0.3	39.5	0.6	38.5	0.4
5	**110**	**7.1**	20-63	116.1	121.7	2.0	7	64	0.1	0.4	39.7	0.6	37.8	0.5
6	**140**	**8.9**	20-63	118.3	123.4	2.0	7	63	1.5	0.3	34.2	0.5	32.7	0.4
7	**180**	**10.6**	20-63	126.6	130.1	1.7	6	67	0.4	0.4	36.2	0.4	35.2	0.4
8	**225**	**12.6**	20-63	120.5	124.4	1.1	5	57	1.9	0.5	40.2	0.3	38.9	0.1
9	**260**	**14.2**	20-63	120.9	124.0	1.0	4	58	0.5	0.4	39.4	0.2	38.3	0.1
10	**316**	**17.8**	20-63	118.6	120.8	0.9	8	77	0.3	0.3	38.0	0.2	37.3	0.2
	360	**19.0**	20-63	114.3	119.0	1.1	5	56	1.5	0.3	37.7	0.2	31.4	0.1
11	**385**	**21.0**	20-63	-----	***116.3***	***Linear Interpolation***			-----	-----	-----	-----	-----	-----
	403	**22.3**	20-63	109.8	113.5	1.3	5	55	6.5	0.2	36.3	0.4	35.0	0.1
12	**420**	**23.6**	20-63	-----	***113.6***	***Linear Interpolation***			-----	-----	-----	-----	-----	-----
13	**445**	**25.4**	20-63	110.0	113.8	0.9	7	70	2.6	0.3	36.2	0.2	35.0	0.1
	313-Turbidite	**17.7**	20-63	125.7	128.9	0.9	5	70	0.7	0.2	40.8	0.2	39.8	0.1

Figure 3.5 (next page) - ^{40}Ar-^{39}Ar incremental heating age and K/Ca spectra for silt-sized (20-63 micron) sediments from piston core site EW9504-17PC, offshore southern Oregon. Age spectra are black while the K/Ca spectra are medium gray. Analytical uncertainties (2-sigma) in age and K/Ca are depicted by the vertical scaling of each step-age box. The only coarse-grained unit (turbidite?) within the core was also analyzed. It is shown with a light gray background to distinguish it from the rest of the suite of samples deposited from hemipelagic sedimentation

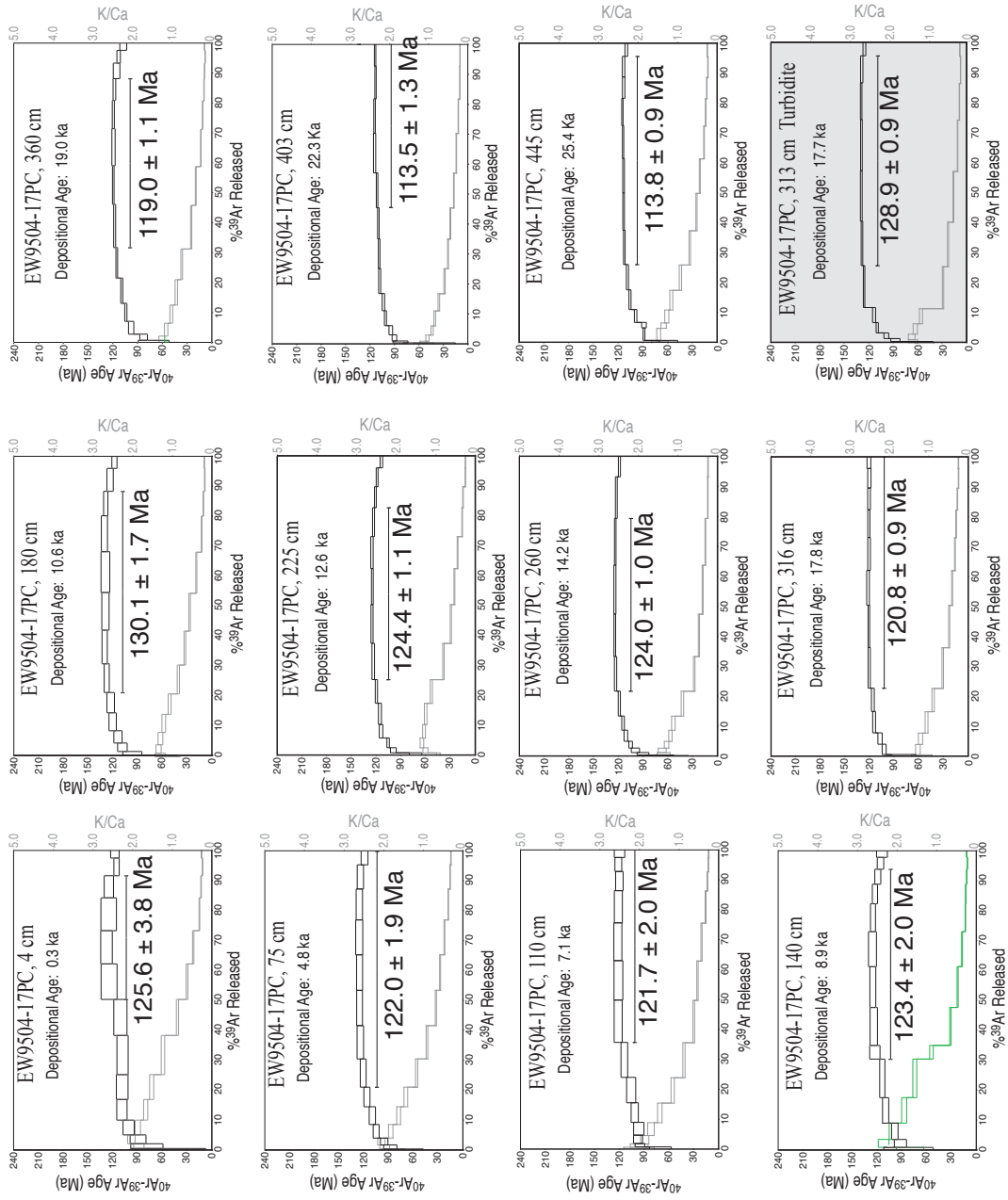
EW9504-17PC, 4 cm
Depositional Age: 0.3 ka
125.6 ± 3.8 Ma
EW9504-17PC, 75 cm
Depositional Age: 4.8 ka
122.0 ± 1.9 Ma
EW9504-17PC, 110 cm
Depositional Age: 7.1 ka
121.7 ± 2.0 Ma
EW9504-17PC, 140 cm
Depositional Age: 8.9 ka
123.4 ± 2.0 Ma
EW9504-17PC, 180 cm
Depositional Age: 10.6 ka
130.1 ± 1.7 Ma
EW9504-17PC, 225 cm
Depositional Age: 12.6 ka
124.4 ± 1.1 Ma
EW9504-17PC, 260 cm
Depositional Age: 14.2 ka
124.0 ± 1.0 Ma
EW9504-17PC, 316 cm
Depositional Age: 17.8 ka
120.8 ± 0.9 Ma
EW9504-17PC, 360 cm
Depositional Age: 19.0 ka
119.0 ± 1.1 Ma
EW9504-17PC, 403 cm
Depositional Age: 22.3 Ka
113.5 ± 1.3 Ma
EW9504-17PC, 445 cm
Depositional Age: 25.4 Ka
113.8 ± 0.9 Ma
EW9504-17PC, 313 cm Turbidite
Depositional Age: 17.7 ka
128.9 ± 0.9 Ma
K/Ca
40Ar-39Ar Age (Ma)
%39Ar Released

Table 3.6 - Talc-normalized clay mineral abundances for Rivers in the Pacific Northwest and Core Site EW9504-17PC

Rivers Name	Lat. (°N)	Long. (°W)	%sm	%ill	%k+chl	sm/ill	k+chl/ill	sm/k+chl
Quinalt River, n=2	47.35	124.29	2	35	35	0.06	1.00	0.06
Columbia River, n=5	46.25	123.49	19	9	7	2.28	0.77	2.78
Umpqua River, n=3	43.70	124.07	20	7	15	3.06	2.25	1.35
Coos River, n=3	42.44	124.40	19	7	13	2.97	1.92	1.59
Rogue River, n=3	42.44	124.38	14	18	32	0.82	1.82	0.44
Klamath River, n=4	41.52	124.02	6	20	35	0.33	1.73	0.18
Eel River, n=3	40.64	124.28	10	22	37	0.43	1.64	0.26
Mattole River, n=3	40.31	124.28	5	14	26	0.35	1.92	0.18
Russian River, n=2	38.43	123.10	20	16	22	1.30	1.33	0.95
Sacramento System, n=6	38.07	121.86	10	14	27	0.75	1.87	0.36

	Core Depth (cm)	Age (ka)							
1	4	0.3	----------	6	17	25	0.38	1.52	0.25
2	32	2.1	----------	7	15	22	0.44	1.51	0.29
3	50	3.2	----------	7	20	30	0.36	1.53	0.24
4	75	4.8	----------	4	13	20	0.33	1.54	0.22
5	110	7.1	----------	17	31	52	0.56	1.69	0.33
6	140	8.9	----------	5	16	34	0.32	2.07	0.15
7	180	10.6	----------	8	18	32	0.44	1.83	0.24
9	260	14.2	----------	8	15	30	0.54	1.93	0.28
10	316	17.8	----------	8	15	26	0.51	1.67	0.30
10b	360	19.0	----------	12	16	28	0.75	1.70	0.44
11	385	21.0	----------	15	18	26	0.82	1.47	0.56
11b	403	22.3	----------	14	16	22	0.88	1.38	0.64
12	420	23.6	----------	11	15	23	0.74	1.52	0.49
13	445	25.4	----------	13	18	27	0.71	1.52	0.47
	313-Turbidite	17.7	----------	8	12	22	0.61	1.77	0.34

sediment offshore southern Oregon and northern California, and cast the temporal trend of provenance changes in terms of the regional climate oscillations on glacial-interglacial to millennial timescales. Figure 3.6 shows the relationship between samples from core site EW9504-17PC relative to the fluvial sediment sources in ε_{Nd} - ^{40}Ar-^{39}Ar bulk sediment plateau age space. The majority of the core samples plot between the fields defined by the Eel, Rogue and Klamath Rivers, which are large coastal rivers (Table 3.1 and Figure 3.3) proximal to the core site. Three samples, however, suggest another source not depicted on Figure 3.6. We derive a mixing model using the Eel River (Franciscan Melange), Rogue and Klamath Rivers (the Klamath Accretionary Complex and Cascade Volcanic Arc) and the Umpqua River (which drains mostly the Eocene turbidites of the Tyee Formation and the Cascade Volcanic Arc) as end-members to examine whether mixtures of these fluvial sources can describe the downcore ε_{Nd} - ^{40}Ar-^{39}Ar compositional variations. These are the four largest rivers (by drainage area) within a 400 km band both north and south of the core site and, fortunately, drain distinctly different source rocks. In this way we can use the mixing model as a means to examine whether changes in sediment sources are due to changing influences of these nearby rivers. Since four samples that were analyzed for their Nd isotopic composition did not have ^{40}Ar-^{39}Ar age measurements made at the exact same depths, their ^{40}Ar-^{39}Ar bulk ages have been interpolated (Figure 3.4). This encourages a slight synthetic trend in those data, but since there are ^{40}Ar-^{39}Ar ages from nearby depths (Figure 3.4 and Table 3.5) that are consistent with the observed trends, we are more confident that these interpolations reflect natural processes.

3.6.1 The Mixing Model with Three Sediment Sources

We construct a ternary mixing model using the standard binary mixing equation from Langmuir et al. (1978; See Faure, 1986 for a summary) described by:

$$R_M = \frac{R_A X_A f + R_B X_B (1-f)}{X_A f + X_B (1-f)} \qquad (1)$$

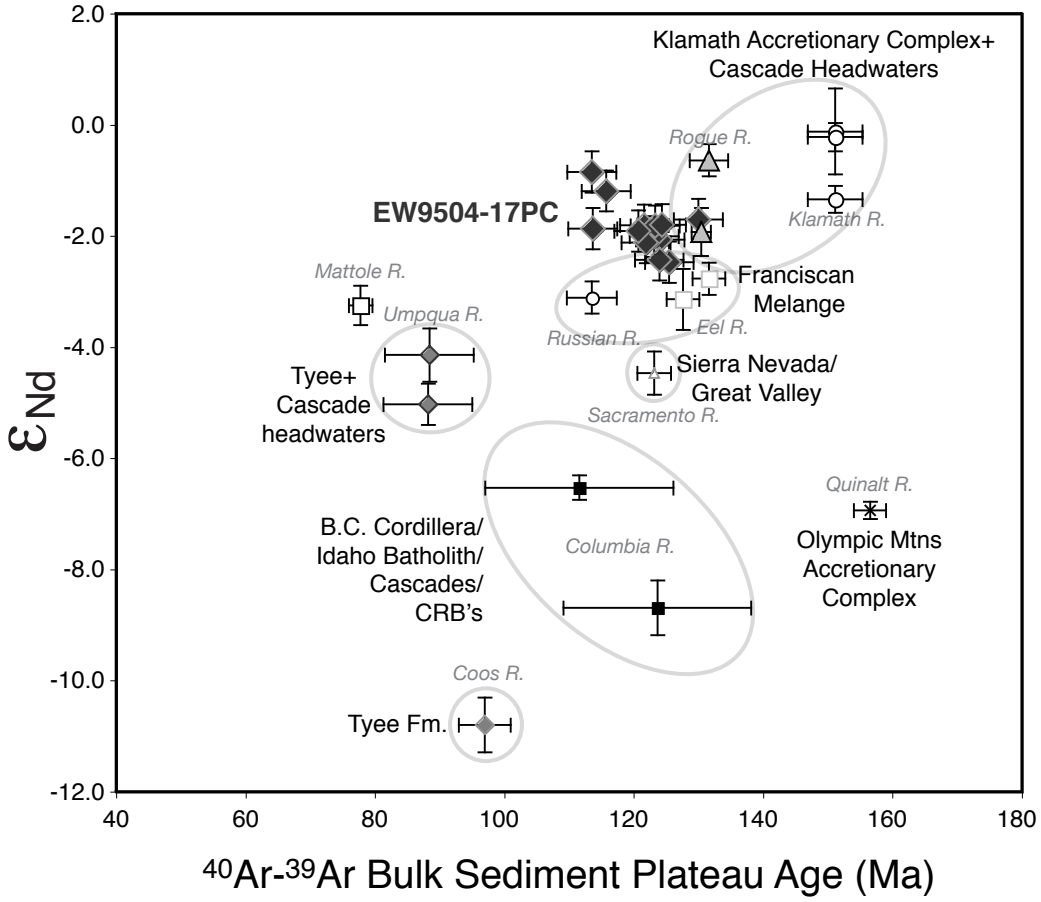

Figure 3.6 - River and core samples in epsilon Nd-^{40}Ar-^{39}Ar bulk sediment plateau age space. Samples are plotted with 2-sigma analytical uncertainties on the Ar plateau age weighted mean and ε_{Nd} mean (The Columbia River Ar-Ar ages are total fusion ages since consistent age plateaus did not develop in these samples). Samples with white-filled symbols denote rivers south of the core site while dark-filled symbols indicate rivers north of the core site. Ovals around groups of fluvial samples indicate sediment sources with similar source rock combinations. For example, the Klamath and Rogue Rivers both drain Klamath Accretionary Complex and Cascade Mountain lithologies, although in differing proportions. The core samples are also plotted (black diamonds) and their location on this diagram suggest that sediments at this core site derive from the proximal sources of the Eel, Klamath and Rogue Rivers, generally.

where R_M is the isotopic ratio of $^{40}Ar/^{39}Ar$ or ε_{Nd} in a mixture of two sources (A and B), X_A and X_B are the concentrations of $^{40}Ar^*$ or Nd in the end members A and B, while f is the proportion of end member A (f = A/A+B) and (1-f) is the proportion of end member B (following the nomeclature of Faure, 1986). We use the $^{40}Ar/^{39}Ar$ ratios (proportional to ^{40}Ar-^{39}Ar plateau ages) and normalize each sample to its unique J factor, which is a measure of how much K (through ^{39}K) has been converted to ^{39}Ar during irradiation. Since we usually discuss the ^{40}Ar-^{39}Ar provenance information in terms of age, we plot the ^{40}Ar-^{39}Ar ages along with the J-normalized $^{40}Ar/^{39}Ar$ ratios, recognizing that the ^{40}Ar-^{39}Ar ages are only approximate in this x-y mixing space. We use equation (1) to define a mixing field (through pseudo-binary mixing curves) with three distinct end-members, using the Eel River and the Klamath+Rogue Rivers for one component (upper line; Figure 3.7), the Eel River and the Umpqua River for the second component (lower line; Figure 3.7) and the Umpqua River and the Klamath+Rogue Rivers for the third component (right-side line; Figure 3.7). The mixing model parameters are shown in Table 3.7.

The mixing model in Figure 3.7 illustrates that indeed the majority of samples can be adequately described as a combination of the three major sediment sources proximal to the core site. The Klamath Mountain source contributed the most sediment to the site except in the youngest sample (~350 years ago) and at around 14 ka. At those times the Eel River contributed the most sediment to the mixture (Table 3.8). The near-surface sample is a mixture of 55% coastal California rivers, 34% Klamath Mountain rivers and 11% Umpqua River. Present-day sediment loads are inconsistent with these values (Wheatcroft et al., 2005; Karlin, 1980; Table 3.1). 78% of the total present-day sediment load is from coastal California (Eel, Mad, Redwood Cr., Trinity R.), 17% from rivers eroding the Klamath Mountains (Klamath, Rogue, Smith) and 6% from the Oregon Coast Range Rivers (Umpqua, Coos-Coquille-Sixes-Elk).

Three samples (two have interpolated ^{40}Ar-^{39}Ar ages and $^{40}Ar/^{39}Ar$ ratios) from around the last glacial interval do not fall within the ternary mixing field nor do they trend toward any fluvial source shown in Figure 3.6. The ^{40}Ar-^{39}Ar ages are younger but with ε_{Nd} values that are higher. The dominant geologic provinces along the margin that could contribute

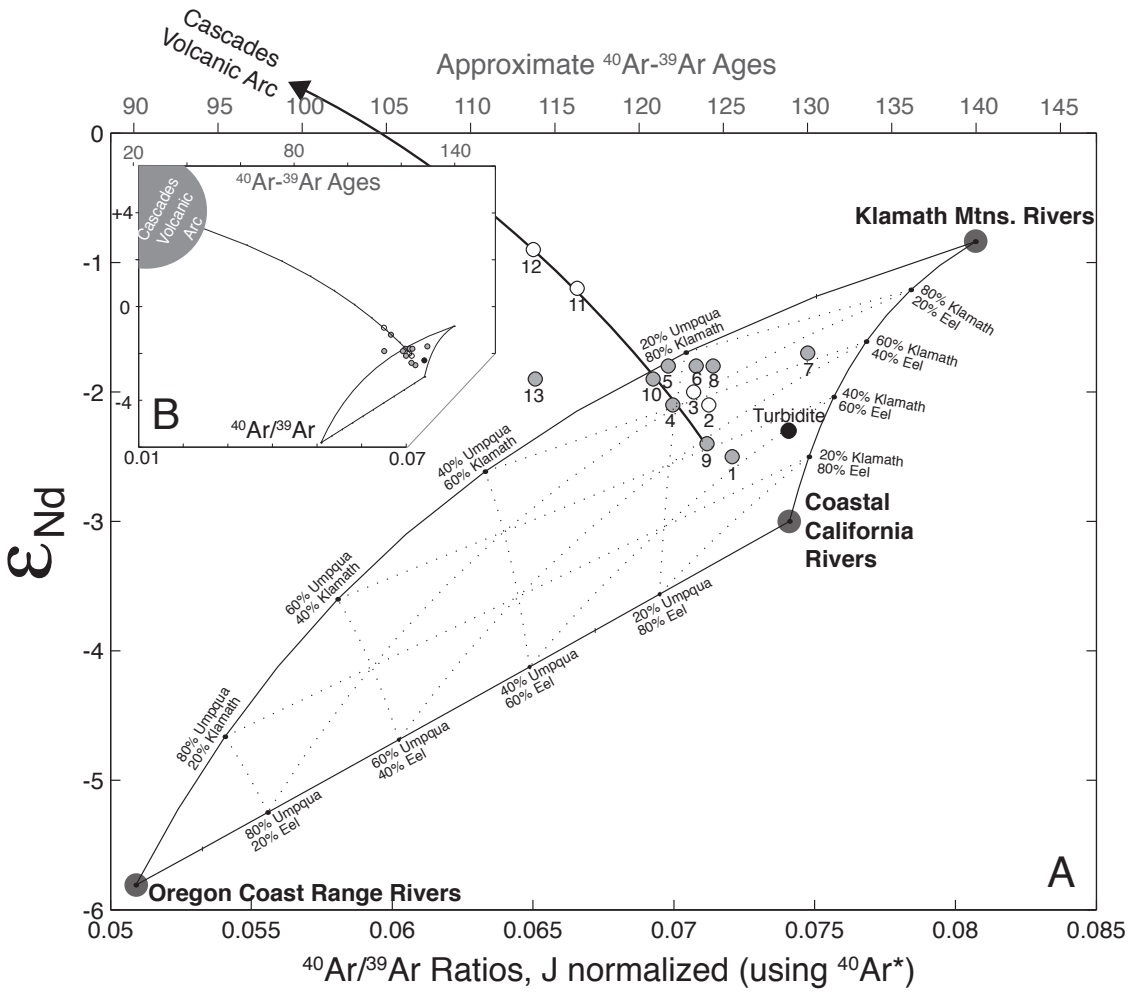

Figure 3.7 - Ternary, two-component mixing model (Langmuir et al., 1979) for terrigenous sediments offshore Oregon and California. Dotted lines represent 20% increments of end-member contributions assuming no differential erosion within basins from each end-member. A) Sediment source end members to the core site are defined in $^{40}Ar/^{39}Ar$ - epsilon Nd space. Corresponding ^{40}Ar- Ar ages are shown at the upper horizontal-axis. The end members are defined by: The Umpqua and Coos Rivers (”Oregon Coast Range Rivers”, north of the core site), the Klamath and Rogue Rivers (”Klamath Mtns. Rivers”, ~latitude of core site) and the Eel River (”Coastal California Rivers”, south of the core site). Core samples from EW9504-17PC are depicted as medium gray-filled circles. Core samples that are interpolated in their 40Ar/39Ar ratios are white-filled circles. The numbers correspond to increasing depth (or depositional age) with “1” being the shallowest (or youngest) and “13” being the deepest (oldest) in the core. A mixture of these three fluvial end members adequately describes the majority of core samples. However, samples 11, 12 and 13 are not easily described in terms of these fluvial sources only. A fourth component is needed (B) and a plausible source is the Cascade Mountains.

Table 3.7 - End Member compositions. (1) The $^{40}Ar/^{39}Ar$ ratios were multiplied by the J factor (in essense the dosimeter for irradiated material) for each sample. (2) The $^{40}Ar^*$ was estimated based on the observation that K concentrations are lower in the Cascdes relative to the other source rocks. (3) Assuming that the modeled Ar age in VanLaningham et al. (2006) is the pre-land use value.

End Members	**Concentrations**		**Isotope Ratios**	
Present-Day	$^{40}Ar^*$	Nd	$^{40}Ar/^{39}Ar_{(1)}$	Epsilon Nd
Umpqua River	9.3E-13	19.0	0.0502	-4.6
Rogue+Klamath	5.1E-13	24.5	0.0792	-0.9
Eel River	1.1E-12	19.0	0.0741	-3.2
LGM	$^{40}Ar^*$	Nd	$^{40}Ar/^{39}Ar_{(1)}$	Epsilon Nd
Cascades[(2)]	2.5E-13	15.0	0.0117	+4.1
Average of Non-LGM samples from 17PC	6.1E-13	19.0	0.0711	-2.0

Table 3.8 - Percent Contributions from River End-Members, Present-day Values. * = Interpolated $^{40}Ar/^{39}Ar$ ratio (see text).

	EW9504-17PC Sample Depth (cm)	Age (ka)	Eel River %	Klam+Rogue %	Umpqua %
1	4	0.3	55	34	11
2	32*	2.1	27	58	15
3	50*	3.2	19	63	18
4	75	4.8	20	60	20
5	110	7.1	5	73	22
6	140	8.9	10	72	18
7	180	10.6	30	65	5
8	225	12.6	14	71	15
9	260	14.2	43	42	15
10	316	17.8	7	69	24
13	445	25.4	0	67	33
	313-Turbidite	17.7	60	37	3

	LGM		% Increase in Cascade-Derived Sediment
11	385*	21.0	16
12	420*	23.6	22

younger, more radiogenic source rocks are the Columbia River Basalts and volcanic rocks in the Cascade Mountains. The Columbia River could be a considerable source of sediment derived from both of these geologic provinces, especially when the Late Pleistocene Missoula floods sculpted the Columbia Basin (Bretz, 1969; Benito and O'Connor, 2003) and sediment from these events was being transported across the northeast Pacific Ocean (Wolf et al., 1999; Zuffa et al., 2001). However, the Cordilleran rocks from the continental interior dominate the sediment signature of the Missoula floods (Kulm et al., 1973; Duncan et al., 1970; Knebel et al., 1968). Therefore, if Missoula flood-derived sediment was responsible for the change in provenance at EW9504-17PC around the time of the last glacial, the ^{40}Ar-^{39}Ar ages and ε_{Nd} values would be expected to trend towards older ages and less radiogenic Nd isotopic values, which is not the case.

Clay mineralogy is also not consistent with a Columbia River source. Previous work showed that smectite is indicative of volcanic source rocks such as those in the Cascades and Columbia River Basalts, while weathering of granitic rocks such as those in the upper portions of the Columbia watershed produce more illite (Knebel, 1968; Duncan et al., 1970) and metamorphic rocks such as those from the Klamath rocks contribute more chlorite (see Figure 3.2; Karlin, 1980). Smectite/illite and chlorite+kaolinite/illite ratios suggest that in the case of EW9504-17PC, volcanic rocks (from the southern Oregon Cascades?) were larger sediment contributors between 25-22 ka (points 11-13, Figure 3.8), while more chlorite+kaolinite-rich metamorphic rocks (from the Klamath Mountains?) became increasingly more important after 22 kyr ago and through deglaciation (points 6-10, Figure 3.8). Although the Columbia River may have contributed more illite (which would create the observed decrease in the smectite/illite ratio) during the Missoula floods, the Columbia River does not have a notable chlorite+kaolinite component. Thus, the southern Oregon Cascade Mountains are a more likely source since the Klamath, Rogue and Umpqua Rivers each erode Cascade volcanic rocks in their headwaters in varying proportions (Figure 3.3) and both the Klamath and Rogue Rivers drain considerable portions of the chlorite-rich Klamath Mountains.

We further examine the mixing of sediment sources by determining whether the samples trending away from the mixing field defined by the Eel, Klamath+Rogue and Umpqua

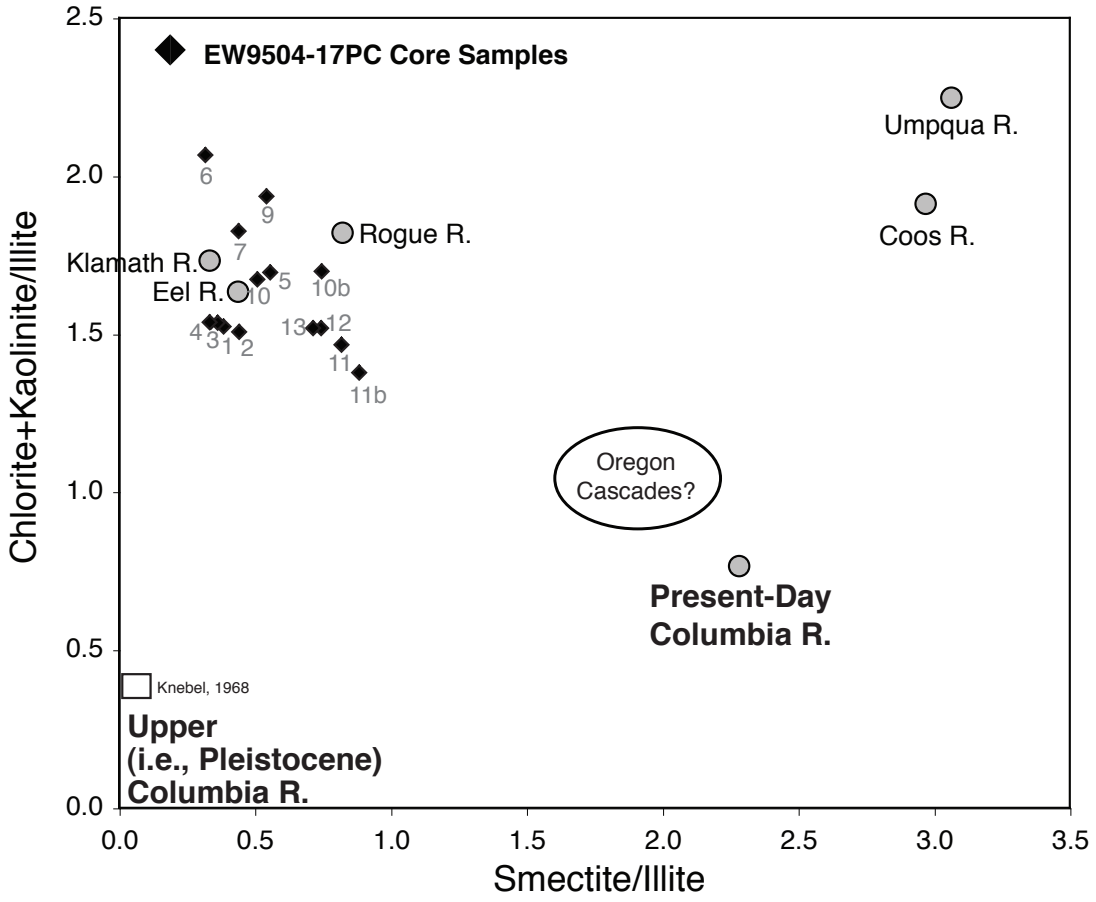

Figure 3.8 - Smectite/illite and chlorite+kaolinite/illite ratios from core site EW9504-17PC, the Columbia and other nearby rivers. Core site samples are plotted as black diamonds. Numbering increases with depth or depositional age in core with "1" being the shallowest or youngest and "13" being the deepest or oldest. Samples 10b and 11b (Table 3.5) were not analyzed for their Ar-Ar ages or Nd isotopic compositions and are labeled as such to keep consistency with numbers in Figure 3.6 and Table 3.4. Present-day river samples are plotted with gray-filled circles. The upper Columbia River clay ratios are plotted as a white square (Knebel, 1968). Duncan et al. (1970) postulate that the upper part of the Columbia basin contributed the majority of sediment during the Pleistocene Missoula Floods.

Rivers are consistent with mixing with the Cascade Arc ^{40}Ar-^{39}Ar ages and ε_{Nd} values. The non-Cascades lower end member is simply defined as the average of the core samples that are not from the last glacial (points 1-9; Figure 3.7). With reasonable ε_{Nd} and Nd concentration parameters assigned to the Cascades using the GEOROC database (http://georoc.mpch-mainz.gwdg.de/georoc/) and ^{40}Ar-^{39}Ar ages and $^{40}Ar^*$ estimates calculated from the weighted average of mapped units in the Umpqua Basin (VanLaningham et al., 2006), the 22 to 25 ka core samples fall directly on a mixing line towards the Cascade Mountains and suggest an increase in Cascades erosion relative to the coastal mountain ranges.

Although this is a reasonable result, the observation made previously (VanLaningham et al., 2006) that the present-day ^{40}Ar-^{39}Ar ages measured from sediments at the mouth of the Klamath River do not match the predicted bulk sediment ^{40}Ar-^{39}Ar age offers us another avenue to explore. Is the lack of present-day sediment contributions from the eastern Cascades portion of the Klamath River related to the low relief of the Upper Klamath Basin or is it a reflection of land-use practices in the Klamath Mountains? Coastal rivers in the region have experienced drastic changes in sedimentation as the result of land-use (Nolan and Janda, 1995). It has been suggested that gold mining and timber harvesting beginning in the 1800's drastically affected sediment production in the Klamath Mountains (Sommerfield and Wheatcroft, in review). Of all the rivers in the study area that might reflect an anthropogenic bias in its isotopic composition of sediments, the Klamath River is one of the best candidates because half of its basin lies east of the Cascades in a fairly low relief region while the other half is in the high relief, coastal Klamath Mountains. This is in contrast to the Rogue and Umpqua Rivers, for example, that erode topography that has more similar relief structures in the differing geologic provinces of the western Cascades and the coastal Klamath Mountains and Oregon Coast Ranges. Moreover, since the Eel River erodes Franciscan Melange along its entire length, erosion related to land-use might change its sediment flux but is unlikely to change its provenance signature. If recent land-use practices are the explanation, then the end members may not be properly defined.

With this in mind, we recast the ternary Ar-Nd isotopic mixing model by incorporating the ^{40}Ar-^{39}Ar model predicted age of 109 Ma (from VanLaningham et al., 2006), and derive

a new, drainage area-weighted average age for the Rogue+Klamath Rivers of 112 Ma. Even though the Nd isotopic signatures should also change by adding more Cascades material to the Klamath River pre-land use, we do not make an attempt to correct for this since we have not explored the change quantitatively and since the range of Nd isotopic variability is much smaller than the Ar ages and would have a more negligible impact on the mixing field. Figure 3.9 shows that the downcore samples are generally oscillating between the Eel and Rogue+Klamath Rivers through time. The samples numbered 11, 12, and 13, which previously plotted outside of the ternary mixing field are now contained within the new mixing field and yet remain consistent with the idea that there was an increase in Cascade-derived material (Figure 3.9B) since they are also on a mixing line between the Cascades and coastal California sediment sources. The mixing model predictions of 74%, 22% and 4% from the Coastal California, Klamath Mountain and Umpqua end-members, respectively in the near-surface sample are much more consistent (Table 3.9) with the present-day sediment load values (Wheatcroft et al., 2005) of 78% from coastal California (Eel, Mad, Redwood Cr., Trinity R.), 17% from rivers eroding the Klamath Mountains (Klamath, Rogue, Smith) and 6% from the Oregon Coast Range Rivers (Umpqua, Coos-Coquille-Sixes-Elk).

It could be that the change in sediment source to more Klamath Mountains-derived sediment may be due to a significant change in ocean circulation. If differential erosion is not the mechanism dictating the provenance change seen at the core site, a ~90% reduction in sediment from the Eel River (as the mixing model implies) and commensurate increase in the contribution from Klamath Mountain rivers around 22-25 ka requires either a complete shutdown of the Eel River, which is not feasible, a reversal in the sediment transport direction or some other extreme change in the dispersivity of sediment along the margin. If a change in sediment transport direction from present-day south-to-north transport, then we might expect a change to more negative ε_{Nd} values, because the Oregon Coast Ranges and Columbia River are much less radiogenic at ε_{Nd} = -7 to -11 (Figure 3.6) and all sources north of the core site are less than ε_{Nd} = -5. Since the downcore values trend in the opposite direction (ε_{Nd} = -1.0 at the LGM), the best explanation is an increase in more Cascades material through the Klamath and Rogue River systems. Differential erosion? A change in how sediment is dispersed along the

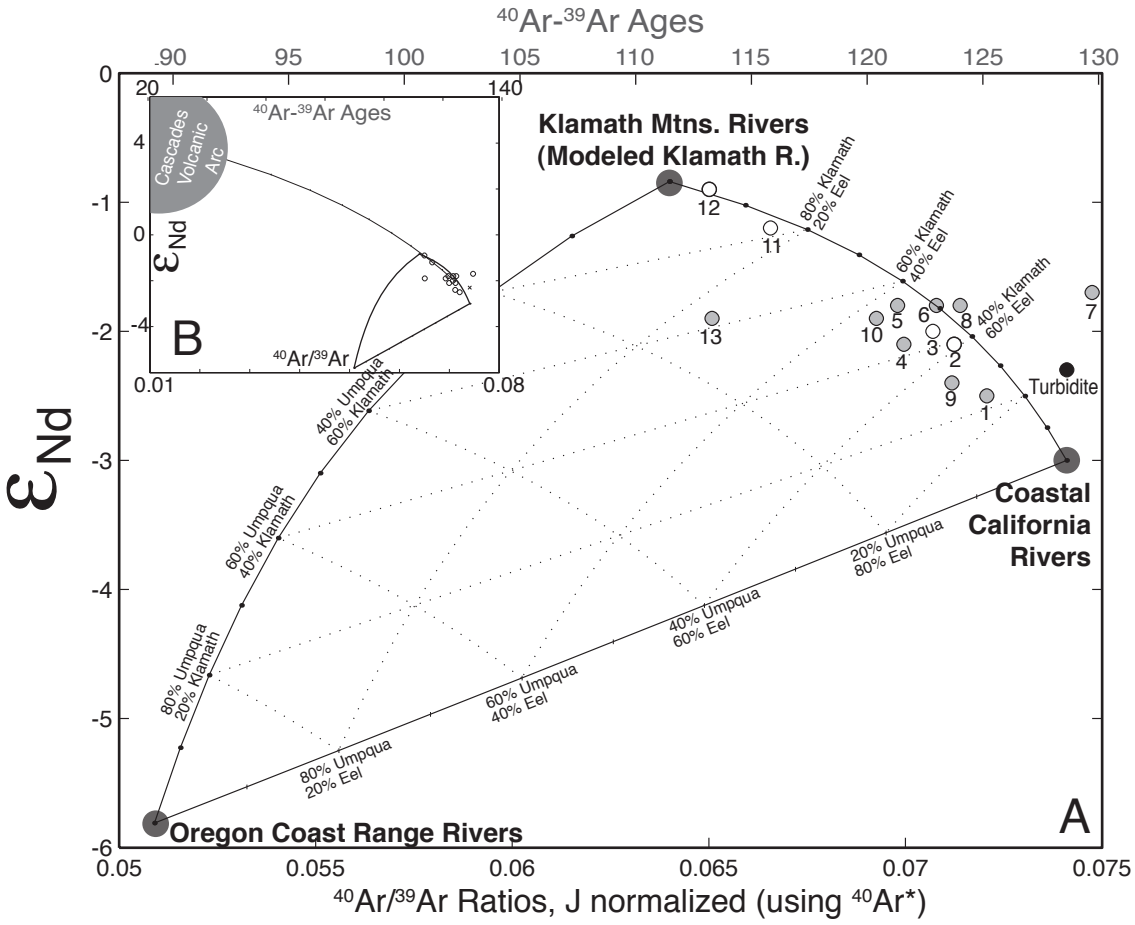

Figure 3.9 - Ternary, two-component mixing model as in Figure 3.6 except with a modeled ^{40}Ar-^{39}Ar age for the Klamath River, which we use as a pre-European settlement value. A) Sediment source end members to the core site are defined in ^{40}Ar/^{39}Ar - epsilon Nd space. Corresponding ^{40}Ar-^{39}Ar ages are shown at the upper horizontal-axis. The end members are defined by: The Umpqua and Coos Rivers (”Oregon Coast Range Rivers”, north of the core site), the Klamath and Rogue Rivers (”Klamath Mtns. Rivers”, ~latitude of core site) and the Eel River (”Coastal California Rivers”, south of the core site). Core samples from EW9504-17PC are depicted as medium gray-filled circles. Core samples that are interpolated in their 40Ar/39Ar ratios are white-filled circles. The numbers correspond to increasing depth (or depositional age) with “1” being the shallowest (or youngest) and “13” being the deepest (oldest) in the core. This illustrates that the downcore samples can be described as a mixture between rivers of the Klamath Mountains and those from coastal Califronia such as the Eel River. The fourth, Cascades component (B) is no longer needed to explain the samples from 22-25 ka. But most samples do lie on a mixing line the coastal California river signature, which remains consistent with a differential erosion component to the provenance evolution.

Table 3.9 - Percent contributions of river end-members, Modified Klamath Basin. * = Interpolated $^{40}Ar/^{39}Ar$ ratio (see text).

	EW9504-17PC Sample Depth (cm)	Age (ka)	Eel River %	Klam+Rogue %	Umpqua %
1	4	0.3	74	22	4
2	32*	2.1	59	39	2
3	50*	3.2	55	42	3
4	75	4.8	52	42	6
5	110	7.1	44	53	3
6	140	8.9	49	51	0
7	180	10.6	---	---	---
8	225	12.6	54	46	0
9	260	14.2	65	30	5
10	316	17.8	43	52	5
11	385*	21.0	17	81	2
12	420*	23.6	7	93	0
13	445	25.4	25	67	17
	313-Turbidite	17.7	---	---	---

margin under different sea level conditions? Since the Cascades were glaciated during MIS Stage 2, increased fluxes from glacial erosion is a plausible mechanism.

3.6.2 Provenance Linkages to Glacial Erosion

We now relate the downcore provenance records (^{40}Ar-^{39}Ar ages and ε_{Nd}) with other climate proxies in core EW9504-17PC and nearby marine and terrestrial records to investigate how the larger climate system might drive the provenance change. The results of the Ar-Nd mixing models from the previous section suggest that Cascades-derived material more heavily influenced the EW9504-17PC sediment signature just before the LGM and that a transition in provenance to more present-day type sediment occurred from 22 to 14 ka. A comparison of these findings with a record from Upper Klamath Lake supports our interpretation. This ^{14}C-dated record shows a large flux of glacial flour to Upper Klamath Lake, which lies at the base of the eastern flanks of the Oregon Cascades (Figure 3.3) and feeds into the Klamath River (Rosenbaum and Reynolds, 2004). This record suggests that the flux of Cascades-derived material increased by up to a factor of four relative to the pre-LGM values during glacial advance and retreat 22 to 14 ka (Figure 3.10). At the same time, core EW9504-17PC shows a notable linear change in both the ^{40}Ar-^{39}Ar ages, ε_{Nd}, and clay mineralogical provenance records. Moreover, there is a spike in sediment accumulation approximately three times above background values in EW9504-17PC, which is also coincident with the maximum glacial flour flux from Upper Klamath Lake, although a range of processes complicate interpretation of oceanic accumulation rates and age model errors affect sedimentation rates.

If a large flux of 10-20 Myr old (average ^{40}Ar-^{39}Ar eruption ages; see VanLaningham et al., 2006), radiogenic (higher ε_{Nd} values) Cascades-derived material was being delivered through the Klamath catchment at this time, then why do the ^{40}Ar-^{39}Ar ages increase in ^{40}Ar-^{39}Ar ages and the ε_{Nd} values decrease at the marine core site during the LGM and deglaciation? It is possible that, at the onset of glaciation in the Cascade Mountains (22 to 18 ka, Rosenbaum and Reynolds, 2004) there was a concurrent increase in glacial flour flux from the Trinity Alps and other high topographic regions in the Klamath Mountains. The oldest plutons (~400 Ma)

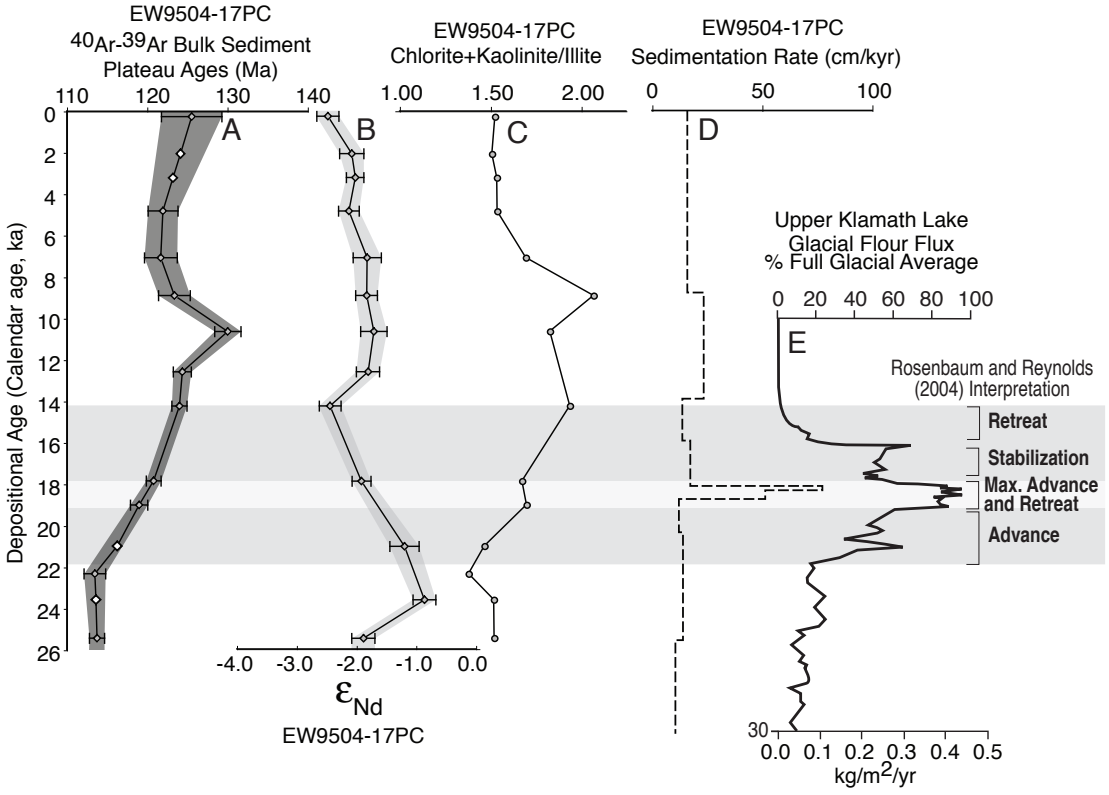

Figure 3.10 - Provenance and erosion records from the Pacific Northwest/northeast Pacific. A) Bulk sediment ^{40}Ar-^{39}Ar plateau ages. Medium gray-filled diamonds are plotted with 2-sigma analytical uncertainties (also defined by the dark gray band). White diamonds are interpolated points used in the mixing model section. B) Nd isotopic values. Medium gray-filled circles are plotted with 1-sigma error bars (also defined by the light gray band). A notable change occurs in ^{40}Ar-^{39}Ar plateau ages for samples deposited earlier than 22 ka. A more subtle change around the same time is seen in the epsilon Nd values. Although less diagnostic throughout the entire record, chlorite+kaolinite/illite ratios (C) show an increase over the same interval. A peak in sedimentation rate (D) from EW9504-17PC coincides precisely with the peak in glacial flour flux (E) from Upper Klamath Lake, which drains into the upper Klamath River and is carried down the river to the northeast Pacific margin at 41.5° N. The transparent gray horizontal bar indicates the time spanning initation of large fluxes of glacial flour and its cessation (22-14 ka). This is also coincident with the linear change from a glacial regime to interglacial conditions for both the ^{40}Ar-^{39}Ar plateau ages, ε_{Nd} values and chlorite+kaolinite/illite.

in the Klamath Mountains are exposed in the Trinity Alps (Irwin and Wooden, 1999) but they cover only a small percentage of the total basin area (<5%). The surrounding glaciated rocks have an average ^{40}Ar-^{39}Ar age of around 150 Ma (VanLaningham et al., 2006). A large influx of this older material into the Klamath River could compensate for the young ages contributed by the Cascades and serve to offset any trend toward younger bulk sediment ages.

Records of Klamath Mountain glaciation are sparse and timing is not well constrained (Sharp, 1960; Woods, 1976; Porter et al., 1983; Bevis, 1995). However, cirque-based equilibrium line altitude (ELA) estimates suggest that glaciers were at ~1500 m, while estimates for the southern Oregon Cascades are ~2000 m (Porter et al., 1983). This would have likely led to a major increase in sediments derived from the older source rocks and led to the temporal trend observed downcore in the bulk sediment ^{40}Ar-^{39}Ar ages and ε_{Nd}. Moreover, downcore chlorite+kaolinite/illite ratios from the marine site increase linearly from 22-14 ka and are also consistent with an increase in sediments from the chlorite-rich Klamath Mountains in that period (Figure 3.10C).

Several other mechanisms are also possible that would change the type and amount of material from the terrestrial source region. The Ar-Nd mixing model suggests an increase in Eel River material at younger downcore bulk ^{40}Ar-^{39}Ar ages (Table 3.8), which would lead to an increase in those ages and a decrease in ε_{Nd} upcore. Because the Eel River is the dominant sediment producer presently, and because precipitation was enhanced around the Eel River region during the last glacial (Adam and West, 1983), it is quite possible that the provenance change between 22-14 ka is also related to an increase in Eel River sediment to the margin, adding complexity to our above interpretation about a significant influence being from glacial erosion. A model is being developed to test the competing influences of different sediment sources to the Oregon-California margin over this time interval (VanLaningham, N.G. Pisias, S. Hostetler, R.A. Duncan, *Exploring climate-driven erosion through a ^{40}Ar-^{39}Ar detrital mixture model: A sensitivity test of Pacific Northwest rivers to glacial-interglacial hydrologic changes,* in preparation).

Secondary processes that could have also led to such a change in the downcore ^{40}Ar-^{39}Ar ages and ε_{Nd} include storage of material eroded previously from the Klamath Accretionary

Complex, and remobilization of that material during the period of high glacial flour flux (and water?) from the Cascades. Alternatively, it is possible that the higher concentration of suspended Cascades material enhanced erosion in the higher gradient bed of the lower stretches of the Klamath River through an improved ability to abrade the river channel (Sklar and Dietrich, 1998)?

We emphasize that the relative changes between the Eel, Rogue+Klamath and Umpqua basins presented in Tables 3.8 and 3.9 are only useful in a general way because the change in provenance may be largely due to differential contributions from different parts of the onshore drainage basins. The Ar-Nd isotopic mixing model does not quantitatively address this potential for differential erosion since it only accounts for changes in the proportions of the three major sources.

3.6.3 A Provenance Change at 10 ka: Changing Ocean Circulation or Sediment Flux?

In the downcore record of ^{40}Ar-^{39}Ar plateau ages, a notable shift also occurs at 10.6 ka (Figure 3.10A) in addition to the change during the time of the last glacial. Although only one sample has a significantly older ^{40}Ar-^{39}Ar bulk sediment age than its neighbors, there is a trend toward older ages on each side of the sample at 10.6 ka, suggesting that a real provenance change may have occurred. The Ar-Nd isotopic data suggest an increase in the incorporation of present-day Klamath+Rogue River (Figure 3.7) or Rogue (Figure 3.9) material at this time. A variety of processes, both in the terrestrial and marine realms could have led to this provenance change.

In the terrestrial environment, one explanation might relate to the aggradational event recorded in river terraces of the Oregon Coast Ranges. Several coastal Oregon river floodplains archive anywhere from 2-11 meters of sediment above a strath terrace (Personius et al., 1993). The strath-forming event has been dated at approximately 10.4 ka (average of nine calendar-calibrated radiocarbon ages from four rivers in Personius et al., 1993), contemporaneous with the 10.6 ka peak in ^{40}Ar-^{39}Ar plateau ages. Because this increase in sediment production was regional and spanned at least the central and southern Oregon Coast

Ranges, it is thought that the mechanism was climate driven (Personius et al., 1993). It has been speculated that an increase in precipitation may have led to enhanced denudation of the coastal mountain landscape (Personius et al., 1993). Alternatively, drying, which could have led to extreme events like forest fires would also encourage denudation of the coastal mountain landscape by reducing the amount of hillslope-stabilizing vegetation.

There is support for drying around the time interval of 12-9 ka in the terrestrial pollen records of Little Lake, Oregon (Worona and Whitlock, 1995), in Upper Klamath Lake and in nearby Tulelake (Hakala et al., 2004), supporting the hypothesis that drier conditions resulted in a sudden landscape denudation response. Alder pollen, which is an indicator of a disturbance (Pisias et al., 2001) shows a subdued maximum in both the downcore EW9504-17PC abundance record as well as in the Little Lake pollen history (Worona and Whitlock, 1995). This may also be reflective of extreme denudation, although this highly speculative.

A shift in ocean circulation, wherein less southerly water was being advected to the north during the time sediment is transported along the margin could also produce the observed change in Ar-Nd isotopic data at 10.6 ka. It would have led to an increased proportion of more Klamath and Rogue River sediment relative to the Eel River sediments. Radiolaria species (Pisias et al., 2001) do not show any notable changes in ocean conditions around 10 ka but a five-fold increase in the abundances of subarctic diatom species has been documented (Lopes, 2006). Is this advection of northern waters, which would have resulted in a reduction in the influence of the Eel River and an increase in more Klamath-derived sediment? This, however, might lead to less evaporation of ocean waters (reduced air-sea temperature gradient), which in turn might reduce or produce little change in precipitation.

Although denser sampling at the core site around this time interval is needed to resolve whether the marine realm was perturbed by, and/or captures the terrestrial record of a 10 ka “event”, the tentative relationships between terrestrial and oceanic systems seen here suggest that a climatically driven pulse of precipitation (or extreme drought?), erosion and possibly advection of northerly waters related to a larger aberration in the climate system may have occurred around the Pleistocene-Holocene transition in the Pacific Northwest-northeast Pacific region.

3.6 4 Provenance and the Pollen Record

Lastly, we discuss the downcore pollen records in EW9504-17PC as they relate to the ^{40}Ar-^{39}Ar ages and ε_{Nd} sediment provenance signatures. The provenance records indicate that rivers transported a greater proportion of material from the Cascades volcanic arc to core site EW9504-17PC during the time of the last glaciation compared with today. The record of glacial flour flux suggests that from 25-22 ka, sediment was making its way out of the Cascades to the core site and was contributing more material than today. Then, from 22-14 ka, glaciers advanced and retreated, leading to a large influx of eroded Cascades material as well as increased flux of Klamath Mountain material, judging from the simultaneous increase in ^{40}Ar-^{39}Ar ages and decrease in ε_{Nd} values. Figure 3.11 shows that the spruce pollen abundances from core site EW9504-17PC generally follow the glacial flour flux patterns from the terrestrial Upper Klamath Lake record as does the peak in sedimentation rate observed at the marine site. This alone might indicate that the spruce pollen at the marine site records the flux of sediment and pollen from the Cascade Mountains. However, comparison of the EW9504-17PC spruce pollen record with that from the Upper Klamath Lake suggests that another source of spruce pollen is needed to balance the record captured at the marine site.

The spruce pollen abundances in Upper Klamath Lake (Figure 3.11F; Hakala et al., 2004) are generally low (0-5%) and have a broad increase without much in the way of a "peak" in the record. The marine pollen record has a more notable increase at ~23 ka to greater than 10% spruce and a reduction to a low level (0-5%) by 14 ka. A lacustrine record from the central Oregon Coast Ranges, ~250 km north of both EW9504-17PC and the Upper Klamath Lake (Figure 3.1), suggests that significant spruce growth occurred in the coastal mountains of Oregon around the time of the LGM (Figure 3.11G; Worona and Whitlock, 1995). It is feasible that the spruce pollen increases over the interval of the LGM, 22-18 ka at the core site are therefore related to the introduction of more coastal spruce pollen from the Klamath Mountains during this time interval either from the differential erosion and/or the succession of spruce into the Klamath Mountains during that time.

Figure 3.11 (next page) - Bulk sediment ^{40}Ar-^{39}Ar plateau ages, ε_{Nd}, sedimentation rate and spruce pollen from core site EW9504-17PC (Pisias et al., 2001) compared with glacial flour flux (Rosenbaum and Reynolds, 2004) and spruce pollen (Hakala et al., 2004) from Upper Klamath Lake in the southern Oregon Cascades and Little Lake in the Oregon Coast Ranges (Worona and Whitlock, 1995). Variation in spruce pollen abundances from EW9504-17PC (E; gray circles), Upper Klamath Lake (F, Hakala et al., 2004) and Little Lake (G, Worona and Whitlock, 1995) suggest that the core site reflects a complex combination of climate change as well as discharge and sediment flux changes from the continent. Gray band as in Figure 3.9.

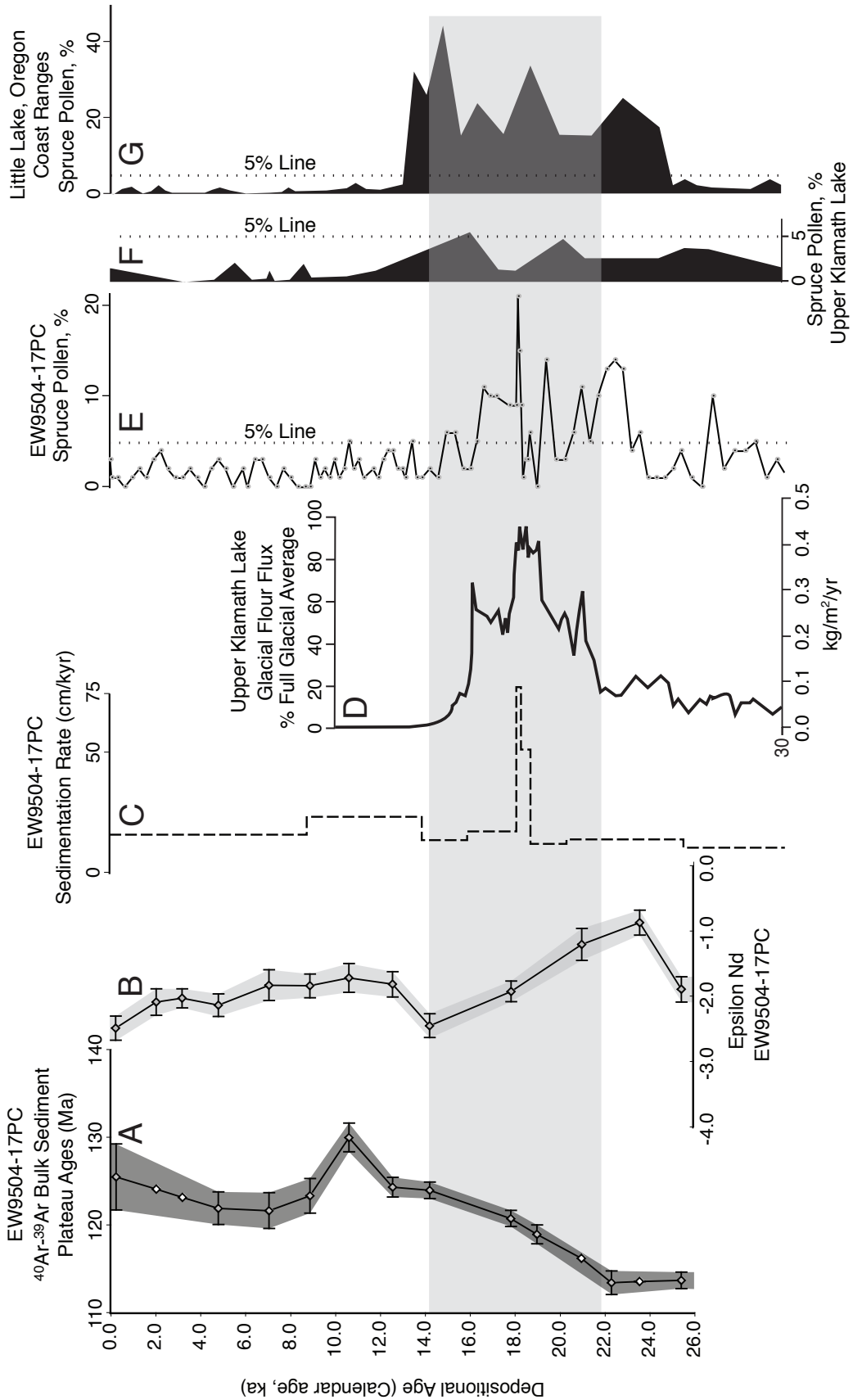
Depositional Age (Calendar age, ka)
EW9504-17PC
40Ar-39Ar Bulk Sediment
Plateau Ages (Ma)
A
B
Epsilon Nd
EW9504-17PC
EW9504-17PC
Sedimentation Rate (cm/kyr)
C
Upper Klamath Lake
Glacial Flour Flux
% Full Glacial Average
D
kg/m2/yr
EW9504-17PC
Spruce Pollen, %
E
5% Line
F
Spruce Pollen, %
Upper Klamath Lake
Little Lake, Oregon
Coast Ranges
Spruce Pollen, %
G
5% Line

3.7 Conclusions

We have invoked a combination of ^{40}Ar-^{39}Ar plateau ages and Nd isotopic compositions to characterize the bulk, silt-sized fluvial and marine sediment in the Pacific Northwest of North America. This has been done to investigate sediment transport changes related to differential erosion and ocean circulation and what this means in terms of terrestrial-ocean climate linkages. Bulk sediment ^{40}Ar-^{39}Ar ages and ε_{Nd} from rivers in the Pacific Northwest have resolvably different characteristics. Future provenance studies in the region will be able to further unravel how the land, ocean and atmosphere respond collectively to climate change. The coupled Ar-Nd isotopic technique provides robust information about the terrestrial source of marine sediments on the continental margin and provides a multi-tracer fingerprinting technique that is resistant to alteration processes.

Sediment from EW9504-17PC can be described as a mixture from the Klamath and Rogue Rivers (same latitude as the core site), the Eel River (south of the core site) and the Umpqua River (north of the core site). Land use affects in the Klamath River Basin appear to have amplified the potential for problems in defining fluvial fingerprints from present-day river samples in that river system. Specifically, this amplification of land-use relates to changes in sediment production from the high-relief Klamath Mountains relative to the low-relief eastern Cascades/high desert part of the Klamath River. With this in mind, we conclude that the downcore sediments represent an oscillating mixture between the Klamath+Rogue Rivers and the Eel River, and that the Umpqua and other coastal rivers north of 42 °N have had little influence on sedimentation at the core site over the last 25 kyr. There is also no evidence that any significant amount of Columbia River material was deposited at the core either, based on the Ar-Nd isotopic compositions as well as clay mineralogy.

Cascades-derived material from the headwaters of the proximal rivers was more significant at the core site before 22 ka relative to today, implying reduced precipitation in the coastal mountains relative to present or an increased ability of Cascade Mountain glaciers to erode the landscape. During the LGM and subsequent deglaciation (22-14 ka) a

commensurate increase in glacial erosion in the Klamath Mountains and Cascades introduced more material from the Klamath Accretionary Complex, leading to a net increase in bulk sediment ^{40}Ar-^{39}Ar ages, although increases in other sediment sources such as the Eel River could also contribute to older bulk sediment ages observed at the core site. The comparison of pollen records, in light of the information offered by the provenance data, suggests that more spruce pollen may have been introduced to the core site as the result of an increase in material from the Klamath Mountains. Thus, spruce pollen abundances in this core site reflect the integrated signal of terrestrial vegetation succession (which responds to precipitation+tem perature) as well as variations in erosional flux (which also responds to precipitation). Since other pollen species are similarly affected, downcore pollen abundances reflect a complex integration of precipitation-related processes.

Future studies can exploit the fact that the rivers in this region carry information related to erosion in the interior Cascades volcanic arc as well as the coastal mountains. Since the Cascades were glaciated during Marine Isotope Stages (MIS) 2, 4 and 6 and the Klamath Mountains were only glaciated during MIS 2 and 6 (Bevis, 1995), future studies can assess the landscape response to thresholds in the climate system, glacial erosion, pollen succession, sediment transport and oceanic changes. Furthermore, future studies linking provenance and pollen records in a suite of core sites to the north and south will yield a more complete understanding of terrestrial, ocean and atmospheric changes where the North Pacific and Alaskan Gyres intersect along western North America.

3.8 References

Adam, D. P., and West, G. J., 1983, Temperature and precipitation estimates through the last glacial cycle from Clear Lake, California, Pollen Data: Science, v. 219, p. 168-171.

Alley, R. B., Clark, P. U., Keigwin, L. D., and Webb, R. S., 1999, Making Sense of Millennial-Scale Climate Change, *in* Clark, P. U., Webb, R. S., and Keigwin, L. D., eds., Mechanisms of Global Climate Change at Millennial Time Scales: Washington, D.C., American Geophysical Union, p. 394p.

Benito, G., and O'Conner, J. E., 2003, Number and size of last-glacial Missoula floods in the Columbia River valley between the Pasco Basin, Washington, and Portland, Oregon

Geological Society of America Bulletin, v. 115, no. 5, p. 624-638.

Bevis, K. A., 1995, Reconstruction of Late Pleistocene paleoclimatic characteristics in the Great Basin and adjacent areas [Ph.D. thesis]: Oregon State University, 277 p.

Biscaye, P. E., 1965, Mineralogy and sedimentation of recent deep-sea clays in the Atlantic Ocean and adjacent seas and oceans: Geological Society of America Bulletin, v. 76, p. 803-832.

Blake, M. C., and Jones, D. L., 1981, The Franciscan melange in northern California: A reinterpretation, *in* W.G., E., ed., The geotectonic evolution of California: Englewood Cliffs, NJ, Prentice Hall, p. 306-328.

Bond, G. C., Showers, W., Cheseby, M., Lotti, R., Almasi, P., deMenocal, P., Cullen, H., Hajdas, I., and Bonani, G., 1997, A pervasive millennial-scale cycle in North Atlantic Holocene and glacial climates: Science, v. 278, p. 1257-1266.

Brandon, M. T., and Vance, J. A., 1992, Tectonic evolution of the Cenozoic Olympic subduction complex, Washington state, as deduced from fission track ages for detrital zircons: American Journal of Science, v. v. 292, p. p. 565-636.

Bretz, J. H., 1969, The Lake Missoula floods and the Channeled Scabland: Journal of Geology, v. 77, p. 505–543.

Clark, P. U., Keigwin, L. D., and Webb, R. S., 1999, Making Sense of Millennial-Scale Climate Change, Mechanisms of Global Climate Change at Millennial Time Scales: Washington, D.C., American Geophysical Union, 394p.

Clift, P. D., 2006, Controls on the erosion of Cenozoic Asia and the flux of clastic sediment to the ocean: Earth and Planetary Science Letters, v. 241, p. 571-580.

Clift, P. D., and Blusztajn, J., 2005, Reorganization of the western Himalaya river system after five million years ago: Nature, v. 438, no. doi:10.1038, p. 1001-1003.

Duncan, J. R., Kulm, L. D., and Griggs, G. B., 1970, Clay mineral composition of the Late Pleistocene and Holocene sediments of the Cascadia basin, northeastern Pacific Ocean: Journal of Geology, v. 78, p. 213-221.

Faure, G., 1986, Principles of isotope geology: New York, John Wiley and Sons, 589 p.

Ghosh, D., 1995, Nd-Sr isotopic constraints on the interactions of the intermontane Superterrane with the western edge of North America in the southern Canadian Cordillera: Can. Jour. Earth Sci., v. 32, p. 1740-1758.

Goldstein, S. J., and Jacobsen, S. B., 1988, Nd and Sr isotopic systematics of river water suspended material: Implications for crustal evolution: Earth and Planetary Science Letters, v. 87, p. 249-265.

Goldstein, S. L., O'Nions, R. K., and Hamilton, P. J., 1984, A Sm-Nd isotopic study of

atmospheric dusts and particulates from major river systems: Earth and Planetary Science Letters, v. 70, p. 221-236.

Hakala, K. J., and Adam, D. P., 2004, Late Pleistocene vegetation and climate in the southern Cascade Range and the Modoc Plateau region: Journal of Paleolimnology, no. 31.

Haugerud, R. A., 1999, Digital elevation model (DEM) of Cascadia, latitude 39N-53N, longitude 116W-133W.

Heath, G. R., and Pisias, N. G., 1979, A method for the quantitative estimation of clay minerals in North Pacific deep-sea sediments: Clays and Clay Minerals, v. 27, no. 3, p. 175-184.

Heusser, L., 1998, Direct correlation of millenial-scale changes in western North American vegetation and climate with changes in the California Current system over the past 60 kyrs: Paleoceanography, v. 13, no. 3, p. 252-262.

Hickey, B. M., 1979, The California current system—Hypotheses and facts: Progress in Oceanography, v. 8, p. 191–279.

Hickey, B. M., and Banas, N. S., 2003, Oceanography of the U.S. Pacific Northwest Coastal Ocean and Estuaries with Application to Coastal Ecology: Estuaries, v. 26, no. 4B, p. 1010-1031.

Hickey, B. M., and Royer, T., 2001, California and Alaskan Currents, *in* Steele, J. H., Thorpe, S. A., and Turekian, K. A., eds., Encyclopedia of Ocean Sciences: San Diego, California, Academic Press, p. 368–379.

Hostetler, S., Pisias, N., and Mix, A., 2006, Senstivity of the Last Glacial Maximum climate to uncertainties in the tropical and subtropical ocean temperatures: Quaternary Science Reviews, v. 25, p. 1168-1185.

Hostetler, S. W., Clark, P. U., Bartlein, P. J., Mix, A. C., and Pisias, N. G., 1999, Atmospheric transmission of North Atlantic Heinrich events: Journal of Geophysical Research, v. 104, p. 3947-3952.

Irwin, W. P., and Wooden, J. L., 1999, Plutons and accretionary episodes of the Klamath mountains, California and Oregon.

Karlin, R., 1980, Sediment Sources and Clay Mineral Distributions Off the Oregon Coast: JSP, v. 50, no. 2, p. 543-560.

Knebel, H. J., Kelly, J. C., and Whetten, J. T., 1968, Clay minerals of the Columbia River: A qualitative, quantitative, and statistical evaluation: Journal of Sedimentary Petrology, v. 38, no. 2, p. 600-611.

Koppers, A. P., 2002, ArArCalc - software for $^{40}Ar/^{39}Ar$ age calculations: Computers & Geosciences, v. 28, p. 605-619.

Kulm, L. D., Prince, R. A., and Snavely, P. D., Jr., 1973, Site Survey of the northern Oregon continental margin and Astoria Fan: Init. Rep. Deep Sea Dril. Proj., v. v. XVIII, no. Appendix I, Part A, p. p. 979-987.

Lamy, F., Hebbeln, D., Rohl, U., and Wefer, G., 2001, Holocene rainfall variability in southern Chile: A marine record of latitudinal shifts fo the Southern Westerlies: Earth and Planetary Science Letters, v. 185, p. 369-382.

Langmuir, C. H., Vocke, R. D., Hanson, G. N., and Hart, S. R., 1978, A general mixing equation with applications to Icelandic basalts: Earth and Planetary Science Letters, v. 37, p. 380-382.

Lyle, M., Mix, A. M., Ravelo, C., Andreasen, D., Heusser, L., and Olivarez, A., 2000, Millennial-scale CaCO3 and corg events along the northern and central California margins: stratigraphy and origins, *in* Lyle, M., Koizumi, I., Richter, C., and Moore, T. C., Jr., eds., Proceedings of the Ocean Drilling Program, Scientific Results: College Station, TX.

McDougall, I., and Harrison, T. M., 1999, Geochronology and thermochronology by the $^{40}Ar/^{39}Ar$ method: New York, Oxford University Press, 269 p.

McLaughlin, R. J., Sliter, W. V., Fredriksen, N. O., Harbert, W. P., and McCulloch, D. S., 1994, Plate motions recorded in tectonostratigraphic terranes of the Franciscan Complex and evolution of the Mendocino Triple Junction, Northwestern California.

Merritts, D., and Vincent, K. R., 1989, Geomorphic response of coastal streams to low, intermediate, and high rates of uplift, Mendocino triple junction region, California: Geological Society of America Bulletin, v. 101, no. 11, p. 1373-1388.

Mix, A. C., Lund, D. C., Pisias, N., Boden, P., Bornmalm, L., Lyle, M., and Pike, J., 1999, Rapic climate oscillations in the northeast Pacific during the last deglaciation reflect northern and southern hemisphere sources, *in* Clark, P. U., Webb, R. S., and Keigwin, L. D., eds., Mechanisms of Global Climate Change at Millennial Time Scales: Washington D.C., American Geophysical Union.

Monger, J. W., Price, R. A., and Templeman-Kluit, D. J., 1982, Tectonic accretion and the origin of the two major metamorphic and plutonic belts in the Canadian Cordillera: Geology, v. 10, p. 70-75.

Moore, D. M., and Reynolds, R. C., 1989, X-ray diffraction and the identification and analysis of clay minerals: New York, Oxford University Press, 332 p.

Nolan, K. M., and Janda, R. J., 1995, Impacts of logging on stream sediment discharge in the Redwood Creek Basin: US Geological Survey Professional Paper, v. 1454.

Personius, S., Kelsey, H. M., and Grabau, P. C., 1993, Evidence for regional stream aggradation in the central Oregon Coast Range during the Pleistocene-Holocene

transition: Quaternary Research, v. 40, p. 297-308.

Pisias, N., Sancetta, C., and Dauphin, P., 1973, Spectral analysis of late Pleistocene-Holocene sediments: Quaternary Research, v. 3, p. 3-9.

Pisias, N. G., Mix, A. C., and Heusser, L., 2001, Millennial scale climate variability of the northeast Pacific Ocean and northwest North America based on radiolaria and pollen: Quaternary Science Reviews, v. 20, p. 1561-1576.

Porter, S. C., Pierce, K. L., and Hamilton, T. D., 1983, Late Wisconsin glaciation in the Western United States, *in* Porter, S. C., ed., Late-Quaternary environments of the United States: Minneapolis, Univ. of Minnesota Press, p. 71-111.

Renne, P. R., Deino, A. L., Walter, R. C., Turrin, B. D., Swisher, C. C., Becker, T. A., Curtis, G. H., Sharp, W. D., and Jaouni, A.-R., 1994, Intercalibration of astronomical and radioisotopic time: Geology, v. 22, p. 783-786.

Rosenbaum, J. G., and Reynolds, R. L., 2004, Record of Late Pleistocene glaciation and deglaciation in the southern Cascade Range. II. Flux of glacial flour in a sediment core from Upper Klamath Lake, Oregon: Journal of Paleolimnology, v. 31, p. 235-252.

Sharp, R. P., 1960, Pleistocene glaciation in the Trinity Alps of northern California: American Journal of Science, v. 258, p. 305-340.

Sherwood, C. R., Jay, D. A., Harvey, R. B., Hamilton, P., and Simenstad, C. A., 1990, Historical changes in the Columbia River estuary: Progress in Oceanography, v. 25, p. 299-352.

Sklar, L. S., and Dietrich, W. E., 1998, River longitudinal profiles and bedrock incision models: Stream power and the influence of sediment supply, *in* Tinkler, K. J., and Wohl, E. E., eds., Rivers Over Rock: Fluvial Processes in Bedrock Channels: Washington, American Geophysical Union, p. 237-259.

Snyder, N. P., Whipple, K. X., Tucker, G. E., and Merritts, D. J., 2000, Landscape response to tectonic forcing: Digital elevation model analysis of stream profiles in the Mendocino triple junction region, northern California: GSA Bulletin, v. 112, no. 8, p. 1250-1263.

Strub, P. T., Allen, J. S., Huyer, A., and Smith, R. L., 1987, Large-scale structure of the spring transition in the coastal ocean off western North America: Journal of Geophysical Research, v. 92, p. 1527–1544.

Syvitski, J. P. M., Vorosmarty, C. J., Kettner, A. J., and Green, P., 2005, Impact of Humans on the Flux of Terrestrial Sediment to the Global Coastal Ocean Science, v. 308, p. 376-380.

Tanaka, T., Shigeko Togashib, Hikari Kamiokab, Hiroshi Amakawac, Hiroo Kagamid, Takuji Hamamotod, Masaki Yuharad, Yuji Orihashie, Shigekazu Yonedaf, Hiroshi Shimizug, Takanori Kunimarug, Kazuya Takahashih, Takeru Yanagii, Takanori Nakanoj,

Hirokazu Fujimakik, Ryuichi Shinjol, Yoshihiro Asaharaa, Tanimizua, M., and Dragusanua, C., 2000, JNdi-1: a neodymium isotopic reference in consistency with LaJolla neodymium: Chemical Geology v. 168, no. 3-4, p. 279-281.

VanLaningham, S., Duncan, R. A., and Pisias, N. G., 2006, Erosion by rivers and transport pathways in the ocean: A provenance tool using ^{40}Ar-^{39}Ar incremental heating on fine-grained sediment: Journal of Geophysical Research, v. 111, no. F04014, p. doi:10.1029/2006JF000583.

Vorosmarty, C. J., Meybeck, M., Fekete, B., Sharma, K., Green, P., and Syvitski, J. M., 2003, Anthropogenic sediment retention: major global impact from registered river impoundments: Global and Planetary Change, v. 39, no. 169-190.

Walczak, P. S., 2006, Submarine plateau volcanism and Cretaceous Ocean Anoxic Event 1a : geochemical evidence from Aptian sedimentary sections: Oregon State University, 172 p.

Walker, G. W., and MacLeod, N. S., 1991, Geologic Map of Oregon: U.S. Geological Survey, scale 1:500,000.

Wasserburg, G. J., Jacobsen, S. B., DePaolo, D. J., McCulloch, M. T., and Wen, T., 1981, Precise determinations of Sm/Nd ratios, Sm and Nd isotopic abundances in standarc solutions: Geochim. Cosmochim. Acta, v. 45, p. 2311-2323.

Wendt, I., and Carl, C., 1991, The statistical distribution of the mean standard weighted deviation: Chemical Geology (Isot. Geosci. Sect.), v. 86, p. 275-285.

Werner, F., and Hickey, B. M., 1983, The role of an alongshore pressure gradient in Pacific Northwest coastal dynamics: Journal of Physical Oceanography, v. 13, p. 395–410.

Wheatcroft, R. A., and Sommerfield, C. K., 2005, River sediment and shelf sediment accumulation rates on the Pacific Northwest margin: Continental Shelf Research, v. 25, p. 311-332.

Wolf, S. C., Nelson, H., Hamer, M. R., Dunhill, G., and Phillips, R. L., 1999, The Washington and Oregon mid-shelf silt deposit and its relation to the late Holocene Columbia River sediment budget.

Woods, M. C., 1976, Pleistocene Glaciation in the Canyon Creek area, Trinity Alps, California: California Geology, p. 109-113.

Worona, M. A., and Whitlock, C., 1995, Late Quaternary vegetation and climate history near Little Lake, central Coast Range, Oregon: GSA Bulletin, v. 107, no. 7, p. 867-876.

Zuffa, G. G., de Rosa, R., and Normark, W. R., 1997, Shifting sources and transport paths for the later Quaternary Escanaba Trough sediment fill (northeast Pacific): Giornale di Geologia, v. 59, no. 1/2, p. 35-53.

Chapter 4

Exploring climate-driven erosion through a ^{40}Ar-^{39}Ar detrital mixture model: A sensitivity test of Pacific Northwest rivers to glacial-interglacial hydrologic changes

Sam VanLaningham[1], Nicklas G. Pisias[1], Steven W. Hostetler[2], Robert A. Duncan[1]

[1]College of Oceanic and Atmospheric Sciences
Oregon State University, Corvallis Oregon 97331

[2]U.S. Geological Survey
Oregon State University, Corvallis Oregon 97331

4.1 Abstract

We develop a methodology to explore the variable response of the terrestrial landscape along the western North American margin to changing hydrologic conditions on glacial-interglacial timescales. Specifically, we set out to determine how changes in patterns of precipitation between 22-14 ka and today could affect the ^{40}Ar-^{39}Ar bulk sediment provenance offshore southern Oregon, at core site EW9504-17PC (2671 m water depth). This core site lies in an excellent position to test this new modeling approach because it captures the combined sediment fluxes from the coastal Klamath Mountains and the interior Cascade Volcanic Ranges, which have drastically different ^{40}Ar-^{39}Ar crystallization-cooling ages (147 ma versus 21 Ma on average, respectively) and different climate responses occurring on glacial-interglacial timescales. We examine downcore provenance changes by developing a model that balances basin-averaged ^{40}Ar-^{39}Ar ages (detrital mixtures) of the contributing fluvial basins and predicts the bulk sediment value at the core site. In conjunction, we expect that the total range of model-predicted erosion rates over a glacial-interglacial cycle should crudely track the total range in sedimentation rates ($CaCO_3$ and C_{org} free) at the marine site. The model is used freely (sensitivity test) to reproduce the total range of variability observed in downcore, bulk ^{40}Ar-^{39}Ar sediment ages and to investigate which rivers exert a dominant control on the ^{40}Ar-^{39}Ar provenance signature and sediment fluxes. We find that the Upper Klamath Basin (which contained pluvial Lake Modoc during Marine Isotope Stage 2) is the most influential source area that can contribute to younger bulk sediment ^{40}Ar-^{39}Ar ages at the core site, relative to present day values. In terms of erosion/sedimentation rates, however, the Eel River (presently the largest sediment producer along the west coast) is the only sediment source in the vicinity of the core site that has any notable influence on changes in margin sedimentation rates from terrigenous sources. Combinations of increases in the sediment fluxes out of these two basins can describe the combined ^{40}Ar-^{39}Ar provenance evolution/ sedimentation rate peak observed at the core site over the 22-14 ka time period. If this model has captured the dominant controls on sediment delivery to the core site, a plausible climate scenario requires a band of moisture deflecting around the southern Klamath Mountains,

preferentially passing over the Eel River basin, and then channeling through lower topography south of Mount Shasta to eastern Oregon and the Great Basin. Interpretations about the jet stream position from Lake Lahontan lake levels as the Laurentide Ice Sheet grew and contracted are generally consistent with this, although further constraints on precipitation from regional climate models as well as better chronology on pluvial Lake Modoc will help determine the validity of these proposed climate mechanisms.

4.2 Introduction and Motivation

Sedimentary material transported through mountainous landscapes to the deep ocean records a history of surface erosion controlled by processes related to climate and tectonics. Motivation to understand the role of each on the topographic landscape is at the forefront of surface process studies (Willett et al., 2006). Quantitative information about how the landscape is exhumed related to tectonically driven mountain building are being acquired through erosion modeling (Beaumont et al., 1992; Whipple and Tucker, 1999; Willett, 1999) and thermochronometric methods (Brandon and Vance, 1992; Kirby et al., 2002; Burbank, 2002; Carter and Bristow, 2003; Carrapa et al., 2004; Reiners, 2005; Shuster and Farley, 2005; Hodges et al., 2005). Beyond orographic effects, the explicit relationship of climate with erosion is now beginning to be quantified through thermochronology in the terrestrial landscape (Kirchner et al., 2001; Reiners et al., 2003; Burbank et al., 2003; Dadsen et al., 2003; Shuster et al., 2005; Anders et al., 2006).

These leaps in our understanding of erosion have been substantial and yet, it remains difficult to quantify erosion rates through detrital material in marine settings over climatic timescales for a variety of reasons such as the fact that mineral cooling trajectories (Reiners et al., 2005) are difficult to resolve on glacial-interglacial to millennial timescales (Molnar, 2003). Presently, more traditional sedimentological/provenance methods are still the most useful for resolving trends in erosion through marine records (Clift, 2006; Hebbeln et al., 2007). But the continental margin hosts a tantalizing, continuous record of earth surface processes and holds promise for unraveling landscape evolution at very high temporal and

spatial resolutions. To quantify erosion rates through geochemistry in the marine record, the major hurdles of small grain/sample sizes and the fact that sedimentation at a given location is an integration of marine and terrestrial processes need to be overcome.

In this paper we use bulk sediment geochemistry in conjunction with digital geology, geomorphology and present-day sediment loads to develop a model that investigates the temporal evolution of downcore sediment provenance over a glacial-interglacial cycle. The over-arching question is how do glacial-interglacial precipitation changes occurring in this diverse geologic region affect the composition (erosional regime) of river-borne sediment along the Oregon continental margin?

This study focuses on predicting downcore ^{40}Ar-^{39}Ar bulk sediment plateau ages offshore southern Oregon (Figure 4.1), which suggest a simple change in provenance from more Cascades Mountains-dominated material to increasingly Klamath Mountains-like sediment over the last glacial interval (Figure 4.2). Our larger goal is to evaluate precipitation-driven erosional changes by perturbing this model with regional hydrologic outputs from REGCM2 (Hostetler et al., 2006) style climate simulations, once the topographic resolution of these types of models incorporate the coastal (Oregon Coast Ranges and Klamath Mountains) and Cascades Mountains. For this paper, we develop the model, test the sensitivity and then apply reasonable perturbations to reproduce a best fit of the observed downcore data to better understand the likely controls on terrigenous sedimentation along the southern Oregon–northern California margin.

4.3 Study Area

The study area occupies the rivers between ~40-44° N and core site EW9504-17PC (42.24° N, 125.89° W) situated 100 km offshore (Figure 4.1). The major sediment sources to this part of the northeast Pacific Ocean margin are the Eel, Klamath, Rogue and Umpqua River basins, whereas the Columbia River is too far north to have any significant impact on terrigenous sedimentation on the Gorda Rise either presently (Wolf et al., 1999) or during the last glacial (See Chapter 3; VanLaningham et al., in preparation). Although the dominant

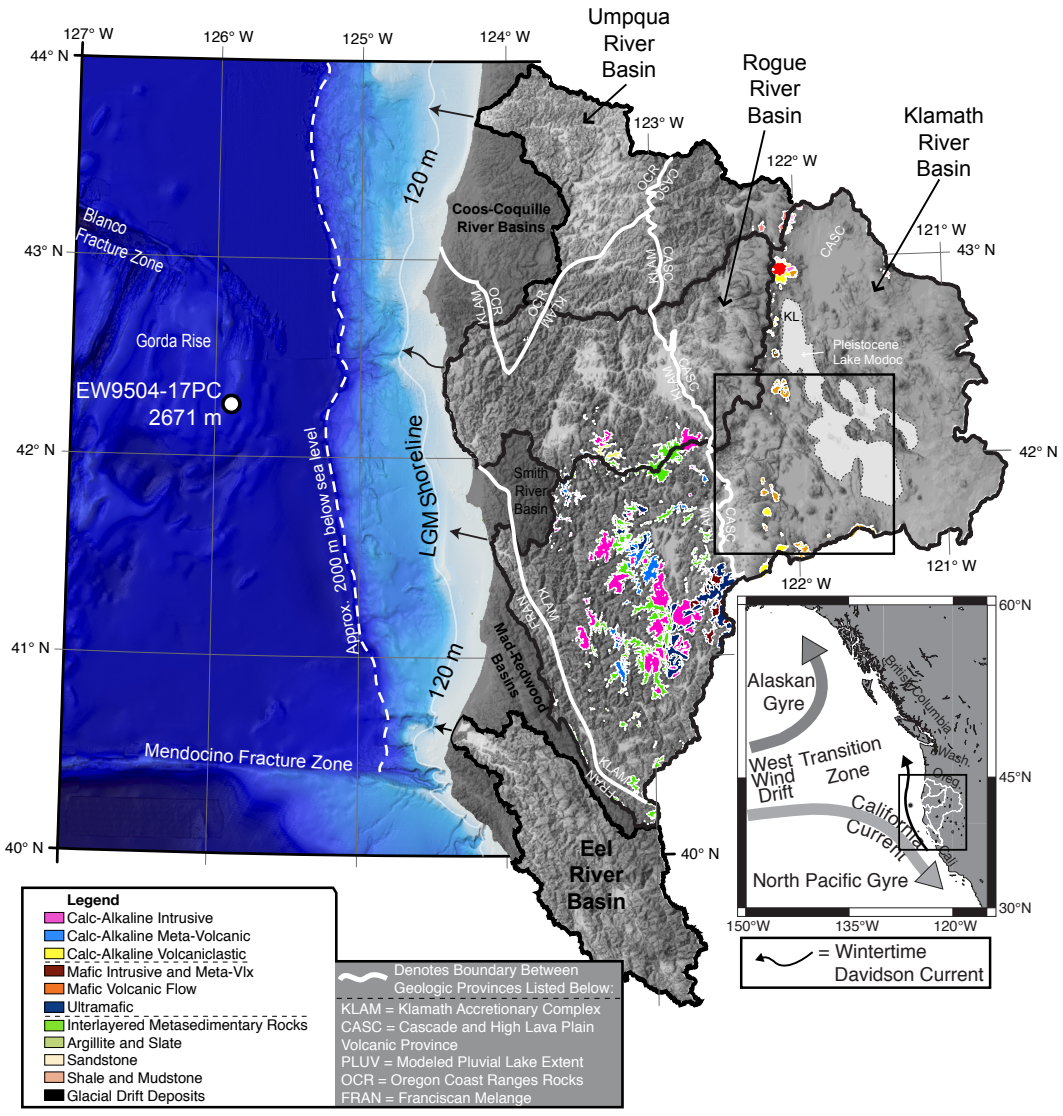

Figure 4.1 - Location map of study area. Inset shows major components of surface ocean circulation and regional geography. Main figure shows major river basins, the core site, topographic/bathymetric features, geology exposed to glaciation and boundaries between major geologic provinces. The colored geologic units relate to those rocks above the last glacial ELA (equilibrium line altitude) and exposed to glacial erosion. In the Klamath Accretionary Complex (KLAM), the ELA was at 1500 m, while in the Cascade volcanic province (CASC) the ELA is estimated at 2000 m based on cirque floor elevations (Porter et al., 1983). See Tables 4.2, 4.3 and 4.4 for age and areal attributes of lithologies.

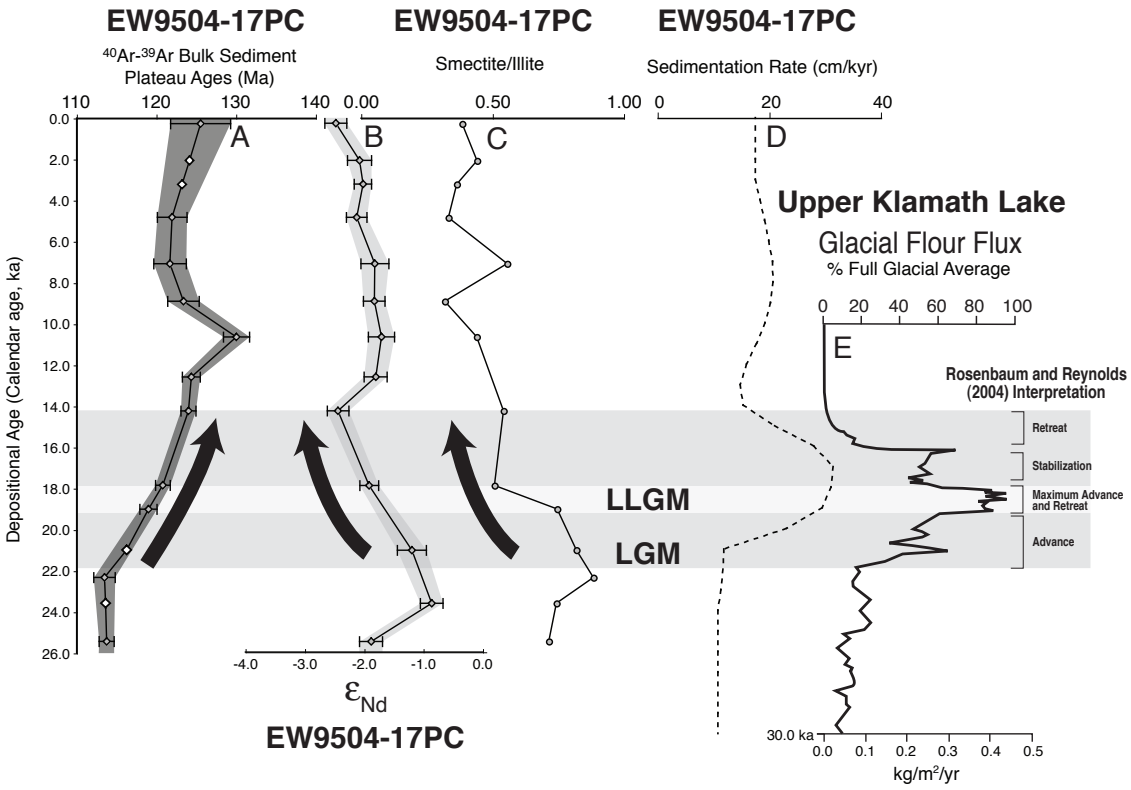

Figure 4.2 - Downcore records of the provenance change seen at marine core site EW9504-17PC and a corresponding record of glacial flour flux from Upper Klamath Lake. The linear trend during the last glaciation (denoted by the horizontal gray band and emphasized with heavy black arrows) is consistent in bulk sediment ^{40}Ar-^{39}Ar ages (A), Nd isotopic analyses (B) and clay mineral ratios (C). Each isotopic/mineralogical record of change is consistent with a transition from Cascade-derived material before the LGM to more coastal-derived sediments (from the Klamath Mountains) after the deglaciation at 14 ka. Across this transition, there is also a large spike in sedimentation rate (D) at the core site. Glacial flour fluxes from the Cascades (E; Rosenbaum and Reynolds, 2004) also suggest a climate response between 22-14 ka in the region.

oceanographic feature along this margin is the southward flowing California Current, sediment dispersal occurs predominantly during the winter months when offshore shelf and slope transport are south to north via the Davidson Current (Inset, Figure 4.1 - Karlin, 1980; Strub, 1987; Hickey and Banas, 2003). From the combined Ar-Nd isotopic data from Pacific Northwest rivers and from the terrigenous sediment at EW9504-17PC, it is likely that changes in ocean circulation are at most subtle, and the downcore provenance change is driven more by differential erosion (see Chapter 3; VanLaningham, et al., in preparation), which has motivated this study.

4.3.1 River Discharge and Sediment Loads

River discharge and sediment loads from rivers in the study area are presented in Table 4.1 (Karlin, 1980; Wheatcroft and Sommerfield, 2005). The Rogue River releases the most freshwater to the study area (12.4 km^3/yr), while the Klamath River discharges slightly less (12.0 km^3/yr). In terms of total sediment loads, however, the Eel River delivers the most sediment presently at about $18x10^9$ kg of sediment per year whereas the Trinity River (Klamath River tributary) contributes $6.7x10^9$ kg and the Klamath River adds $3.4x10^9$ kg of sediment to the ocean annually. The other rivers in the study area each contribute less than $3x10^9$ kg/year of sediment.

Sediment yields (a drainage area-normalized measure of sediment flux) are extremely high in the central and northern California coastal rivers such as the Eel, Trinity, Mad Rivers, and Redwood Creek. This is related to the combined effects of erodable Franciscan Melange rocks (McLaughlin et al., 1994) and their degree of shearing related to high deformation rates along the San Andreas Fault system (Merritts and Vincent, 1989; Snyder et al., 2000).

4.3.2 Geology of source terranes

The largest rivers in southern Oregon and Northern California begin in Cenozoic basaltic and andesitic rocks of the central and southern Oregon Cascades and High Lava Plains

Table 4.1 - Sediment yields from basins with letter subscripts were estimated based on the measured yields from adjacent basins, $_{a}$Umpqua, $_{c}$Smith. The Rogue (b) is a composite of the Klamath and Smith Rivers. Refer to Wheatcroft et al. (2005) for details.

River	Basin size (km^2)	Avg. discharge (km^3/yr)	Avg. annual load ($\times 10^9$ kg)	Sed. yield ($\times 10^3$ kg/km^2/yr)
Umpqua	9,534	6.7	1.4	147
Coos$_a$	*1,567*	*2.7*	*0.2*	*150*
Coquille$_a$	*1,960*	*2.2*	*0.3*	*150*
Millicoma$_a$, Sixes$_a$, Elk$_a$	*1,277*	*0.9*	*0.6*	*150*
Rogue$_b$	*13,394*	*12.4*	*2.3*	*170*
Chetco$_c$	*702*	*2.3*	*0.2*	*250*
Smith	1,590	3.3	0.4	252
Klamath	21,950	7.3	3.3	150
-Trinity(Klamath Trib.)	7,390	4.7	6.8	920
---Klamath total	29,340	12.0	10.1	344
Redwood Creek	720	0.9	1.3	1805
Mad	1,256	1.3	2.6	2070
Eel	8.063	6.6	18.0	2232

and either traverse the turbidites of the Oregon Coast Ranges (Umpqua River) or the Mesozoic Klamath Mountains (Klamath and Rogue Rivers) en route to the Pacific Ocean. Lithologies in the Klamath Mountains are composed of metasedimentary, meta-volcanic, granitic and gabbroic rocks and ophiolitic sequences in the Klamath Accretionary Complex.

The coastal range of northern and central California is dominated by the Franciscan Melange, a Cretaceous to lower Tertiary sequence of sandstones and mudstones, with large blocks (up to several kilometers in size) of serpentinite, blueschist, eclogite greenstone, chert and limestone (Blake and Jones, 1981; McLaughlin et al., 1994), although other less extensive volcanic lithologies are present in the region as well. The Eel River, Trinity River, Mad River, and Redwood Creek erode these rocks.

4.4 Model Setup

Our modeling strategy is based on previous work detailing bulk sediment ^{40}Ar-^{39}Ar ages of modern river sediments from the Pacific Northwest (VanLaningham et al., 2006). This work showed that the bulk ^{40}Ar-^{39}Ar ages of river mouth sediments can be predicted from areal averaging of the geologic units in the contributing drainage areas of river basins. Here we apply this strategy downcore to address the ^{40}Ar-^{39}Ar bulk sediment provenance evolution of fine-grained detritus at the core site because we observe a notable change in three independent provenance indicators spanning the time interval 22-14 ka (Figure 4.2). Bulk sediment ages increase, Nd isotopes become less radiogenic, and smectite/illite decreases. These three observations suggest that sediment changes along this margin from a source that is Cascades dominated to a more Klamath Mountains- or Eel River-dominated source over this time interval.

Our model incorporates an isotopic/geochemical component (^{40}Ar-^{39}Ar ages and K concentrations), a sediment delivery component (present-day sediment loads), drainage areas of contributing rock types (which are further subdivided into associated physiographic / climatic zones), as well as parameters that allow sub-basin sediment loads (defined by climate/ geology /drainage basin extents) to be perturbed.

We noted previously that the upper part of the Klamath River is not likely contributing to the bulk ^{40}Ar-^{39}Ar age signature captured at the mouth presently (VanLaningham et al., 2006), and that sediment derived from the Klamath Mountains dominates the composition. We postulated that low relief alone accounted for this. However, we now think it is possible that the Cascades contributed sediment in the geologic past. The lack of sediment from the Upper Klamath Basin presently could be due more to a combination of heavy land-use practices in the lower Klamath watershed from gold exploration and logging (Sommerfield and Wheatcroft, in review, Late Holocene sediment accumulation on the northern California shelf: Oceanic, fluvial and anthropogenic influences) as well as damming that has considerably reduced the flow of material out of the upper part of the Klamath watershed. The topography of the basin (Figure 4.1) is ideally suited to amplify any affects from land-use because the upper basin is characterized by low relief, is more arid and is composed of young volcanic rocks while the lower basin has high relief, is heavily vegetated and is composed of older metamorphic and granitic lithologies. We have demonstrated that the downcore terrigenous sediments are better described by considering land-use effects (Chapter 3) and so, for the model, we assume that in the geologic past the Upper Klamath Basin contributed sediment to the riverine material cast out to sea even though it does not appear to be doing so presently.

4.4.1 The Erosion Component: Sub-basin Perturbations

We evaluate the provenance change over time by parsing each geologic/climatic zone into sub-basins. These sub-basins are characterized by: the Oregon Coast Ranges, the Klamath Accretionary Complex, the Cascade Mountains and the coastal California region (Figure 4.1). A further subdivision is made for basins that experienced glaciation (higher elevations of the Cascades and Klamath Mountains) and the Upper Klamath Basin where pluvial Lake Modoc existed (Smith and Street-Perrod, 1983). For the glacial terrain we use published values of equilibrium line altitudes (ELA) based on average cirque floor elevations (Porter et al., 1983) to establish the topographic area and lithologies exposed to glacial erosion

during the LLGM. Erosion rates can be enhanced in glacial parts of mountain belts (Shuster et al., 2005; Burbank, 2002) and would respond differently than the fluvial system to erosion in the region. The ELA is estimated to be 1500 m in the Klamath Mountains and 2000 m in the southern Oregon Cascade Mountains (Porter et al., 1983).

Pluvial Lake Modoc in Upper Klamath Basin grew to 2800 km^2 at its maximum extent during the Late Pleistocene (Smith and Street-Perrod, 1983). Lake level fluctuations in the Great Basin are considered to have resulted from pluvial inflow rates ranging between 2.4-6 times present-day values (Weide, 1976; Smith and Street-Perrod, 1983), although it has been argued that pluvial lakes may not need to receive large quantities of precipitation if they freeze in winter (Negrini, 2002). We investigate the effects of increased outflow from this region because it could play an important role in sedimentation along the margin.

Sediment loads (Wheatcroft et al., 2005) are assigned to each of these sub-basins (calculated by areally averaging the sediment loads estimated for the mouths of each river). They are perturbed in the model and their changes are meant to simulate changes in precipitation and, therefore, water discharge. We assume that these perturbations (i.e., changes in discharge) correspond to erosion rate with a power law relation because this is the present-day observation between sediment load and discharge in many fluvial systems of the Pacific Northwest (Figure 4.3). This relationship is commonly cited in the literature (see review by Whipple, 2004), although intriguing recent work postulates that a shift to more arid conditions (less precipitation) might actually increase sediment loads with a power law relation (Molnar et al., 2006). We focus on applying increases in erosion with increased perturbation values (i.e., increased precipitation) because this is the more established paradigm and because none of our contributing river basins likely ever exhibit truly arid conditions.

We recognize that orographic precipitation might have an impact on our results but do not take it into account. We also do not directly take into account rock resistance or the other physical characteristics in rivers that relate to physical erosion of hillslopes and the glacio-fluvial network (see review by Whipple, 2004; Burbank, 2002), although rock resistance is indirectly accounted for by driving our model by present-day sediment loads and the two power-law scalings in different geologic provinces.

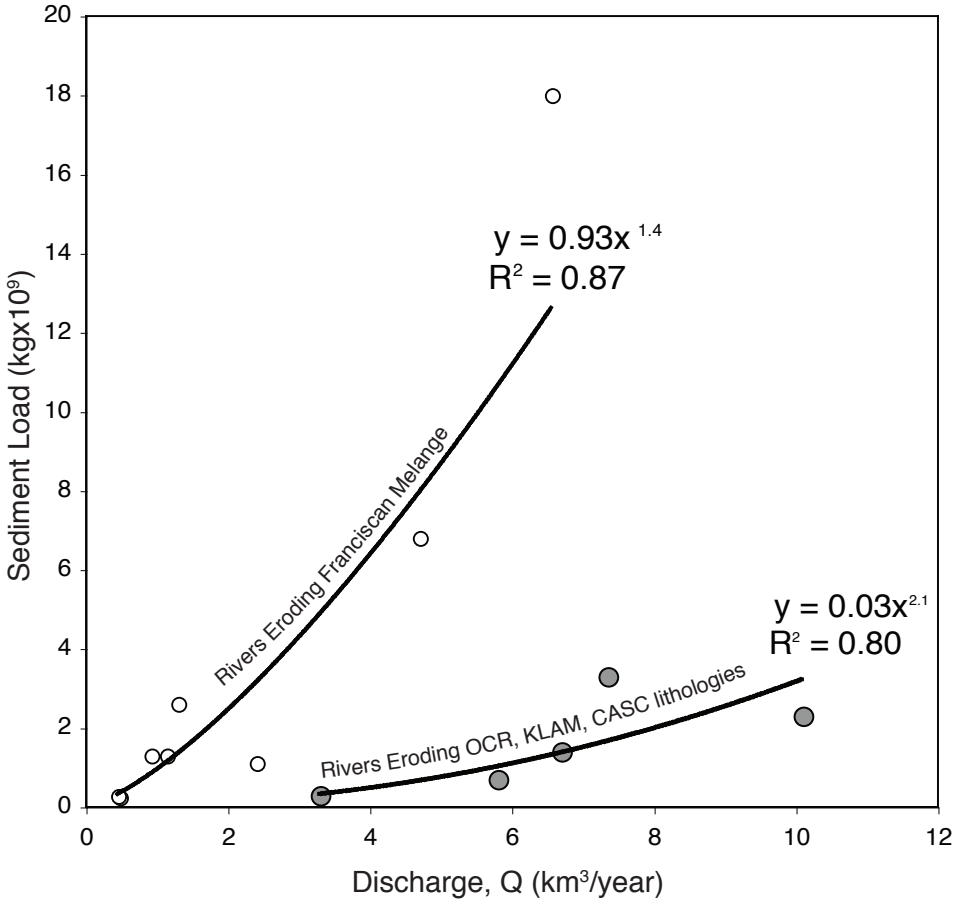

Figure 4.3 - Discharge-sediment load relationships in Pacific Northwest rivers eroding the weak, sheared sedimentary Franciscan Melange rocks (open circles) and the more resistant Tyee sandstone in the Oregon Coast Ranges (OCR), the Klamath Mountains metamorphosed and plutonic rocks (KLAM) and the volcanic litholiges in the Cascades Mountains (CASC) which are denoted by gray-filled circles. These relationships are used to scale erosion in the study area rivers by the power law relations shown here. Discharge and load data from Wheatcroft and Sommerfield (2005).

4.4.2 The Ar-Ar and K Component

To establish ^{40}Ar-^{39}Ar ages and K concentrations in the sub-basins, the 1:500,000 digital geologic map of Oregon (Walker and MacLeod, 1991) and the digital geologic map of the Pacific Northwest (Open-File Report 95-680, Johnson and Raines, 1995) were "clipped" by the bounding areas of each sub-basin polygon (illustrated in Figure 4.1; data shown in Tables 4.3, 4.4 and 4.5) using ARCGIS® and Matlab® algorithms. This leaves behind only the areal extents of rock units within each of the sub-basins. Then, ^{40}Ar-^{39}Ar ages were assigned to each mapped rock unit greater than 10 km^2. Mapped units under the same rock unit designation smaller than 10 km^2 were summed and assigned the average age of the larger units with the same mapped name (listed under the subheading of "undivided" in Tables 4.2, 4.3 and 4.4). These smaller units represent only a small proportion of the total area of geologic units.

Assigning ages was relatively straightforward for mapped geologic units in the Cascades and eastern Oregon; ages were taken from the sources in the geologic map of Oregon (Walker and MacLeod, 1991). However, many of the plutons and metamorphosed units in the Klamath Mountains either do not have radiometric age control or are dated by U-Pb techniques, which can be significantly older than those attained from the K-Ar system because of their different closure temperatures. However, where there are both ^{40}Ar-^{39}Ar and U-Pb ages in this region, they are in good agreement and thus we assume that all units have ^{40}Ar-^{39}Ar ages of the nearest pluton for which any type of radiometric ages are available (Irwin and Wooden, 1999). This is reasonable if emplacement of the plutons occurred fairly rapidly. As for the Oregon Coast Range sedimentary units (e.g., the Tyee Formation), estimates of an average ^{40}Ar-^{39}Ar age were based on the published estimated mixtures of paleo-Idaho Batholith-Klamath Mountain lithologies (Ryu and Niem, 1999; also see VanLaningham et al., 2006 for a more detailed discussion) because these geologic provinces were the original sources to the Tyee Formation (Heller et al., 1985).

Potassium concentrations were assigned to the feldspar component of each rock type whether they are basalt, basaltic andesite, andesite, dacite, rhyolite, granitic, diorite, gabbro,

Table 4.2 (next page) – Lithologies above the Klamath and Cascades Mountains ELA during MIS 2. iv = intermediate volcanics; um = ultramafic; ss = sandstone; ms-p&s = metasediment-phyliite and schist; mi = mafic intrusion; ims = interlayered metasedimentary rocks; ca-mv = calc-alkaline meta-volcanics; cai = calc-alkaline intrusives; sh&mud = shale and mudstone; mmv = mafic leta-colcanics. *Undivided = These units are a sum of all units lells than 10 km2 of a listed rock type. ** = If the total weighted average age for the glaciated Klamaths is adjusted to take into account that the youngest, not the nearest pluton, sets the average age, then the new weighted average = 170 Ma. Notes describe if a given unit's age was estimated from an adjacent unit since no direct age control was available, while those units that did have age. information available have notes denoting the mineral that the age was measured from: Z = zircon, U=Pb age; Hb = Hornblende, ^{40}Ar-^{39}Ar age, B = biotite, ^{40}Ar-^{39}Ar age.

Area(km^2)	LITHOLOGY	K ppm	Age (Ma)	Unit name	NOTES
278	um	1,000	404	trinity	nearest intrusive? If youngest, then 136 ma**
63	um	1,000	136	trinity	youngest intrusion and seems appropriate
55	um	1,000	136	trinity	youngest intrusion and seems appropriate
51	um	1,000	431	trinity	nearest intrusion
39	um	1,000	160	rattlesnake creek terrane	youngest nearby intrusions; I used 129 ma for 2006 paper
29	um	1,000	136	trinity	near craggy peak
19	um	1,000	142	rattlesnake creek terrane	near buckskin Peak
17	um	1,000	162	rattlesnake creek terrane	near sunkard(sp?)
13	um	1,000	162	rattlesnake creek terrane	near wooley creek
10	um	1,000	136	trinity	near craggy peak
18	ss	6,000	147	rattlesnake creek terrane	near glen creek
71	ms-p&s	6,000	162	condrey mtn terrane	youngest intrusion
54	ms-p&s	6,000	143	central metamorphic terrane	youngest intrusion
36	ms-p&s	6,000	143	central metamorphic terrane	youngest intrusion
22	ms-p&s	6,000	149	central metamorphic terrane	near china creek
21	ms-p&s	6,000	136	central metamorphic terrane	near craggy peak
16	ms-p&s	6,000	138	central metamorphic terrane	near Caribou Mtn
13	ms-p&s	6,000	149	central metamorphic terrane	near east fork
26	mi	4,000	415	china mtn	Z
24	mi	4,000	431	bonanza king	Z
22	mi	4,000	404	porcupine creek	Z
16	mi	4,000	418	CP Gabbro	HB
11	mi	4,000	415	china mtn	Z
9	mi	4,000	431	trinity	Near Bonanza King
59	ims	6,000	143	fort jones terrane	youngest intrusion
41	ims	6,000	162	north fork terrane	next to english peak
37	ims	6,000	160	rattlesnake creek terrane	youngest nearby intrusions; I used 129 ma for 2006 paper
36	ims	6,000	138	fort jones terrane	near Caribou Mtn
33	ims	6,000	162	rattlesnake creek terrane	near wooley creek
31	ims	6,000	147	rattlesnake creek terrane	near glen creek
30	ims	6,000	160	e. hayfork	near youngs peak; youngest pluton is eanglish peak
29	ims	6,000	160	rattlesnake creek terrane	youngest nearby intrusions; I used 129 ma for 2006 paper
26	ims	6,000	193	yreka	age of fort jones (van2006)
26	ims	6,000	160	rattlesnake creek terrane	youngest nearby intrusions; I used 129 ma for 2006 paper

CONTINUED

Area(km	LITHOLOGY	K ppm	Age (Ma)	Unit name	NOTES
22	ims	6,000	165	fort jones terrane	near vesa bluffs
18	ims	6,000	149	north fork terrane	near east fork
17	ims	6,000	169	e. hayfork	near wildwood
16	ims	6,000	162	rattlesnake creek terrane	near sunkard(sp?)
15	ims	6,000	141	fort jones terrane	near deadman peak
15	ims	6,000	147	rattlesnake creek terrane	near glen creek
15	ims	6,000	167	rattlesnake creek terrane	near heather lake
15	ims	6,000	168	e. hayfork	Near Denny Complex
14	ims	6,000	159	fort jones terrane	near russian peak
11	ims	6,000	193	yreka	age of fort jones (van2006)
11	ims	6,000	138	central metamorphic terrane	near Caribou Mtn
11	ims	6,000	189	unmaned	near saddle gulch
10	ims	6,000	162	rattlesnake creek terrane	near wooley creek
75	ca-mv	6,000	159	north fork terrane	next to russian peak
46	ca-mv	6,000	167	north fork terrane	next to heather lake intrusion
33	ca-mv	6,000	149	north fork terrane	near east fork
16	ca-mv	6,000	142	rattlesnake creek terrane	near coon mtn complex
11	ca-mv	6,000	160	north fork terrane	near english peak
10	ca-mv	6,000	160	north fork terrane	near youngs peak; youngest pluton is eanglish peak
9	ca-mv	6,000	141	north fork terrane	near canyon cr.
118	cai	11,000	136	craggy peak	biotite
113	cai	11,000	159	russian peak	Z
101	cai	11,000	162	wooley creek	Z
73	cai	11,000	143	canyon creek	Z141-145, z160-170
72	cai	11,000	162	english peak	Z
70	cai	11,000	143	deadman pk	Z
49	cai	11,000	170	ironside mtn	Z
42	cai	11,000	137	sugar pine	Hb
31	cai	11,000	161	Ashland Pluton	Z
26	cai	11,000	160	e. hayfork	near youngs peak; youngest pluton is eanglish peak
18	cai	11,000	138	caribou Mtn	Hb
14	cai	11,000	431	Unnamed	Near Bonanza King
12	cai	11,000	167	Heather Lake	Z
11	cai	11,000	149	monument peak	near east fork
10	cai	11,000	141	rattlesnake creek terrane	near coon mtn complex

CONTINUED

Area(km^2)	LITHOLOGY	K ppm	Age (Ma)	Unit name	NOTES
Klamath, undivided*					
88	um	1,000	201		
4	sh&mud	4,000	147		
19	ss	6,000	147		
26	ms-p&s	6,000	146		
7	mmv	6,000	419		
50	mi	4,000	419		
202	ims	6,000	161		
131	ca-mv	6,000	154		
115	cai	11,000	152		
3071			174 Ma		
Rogue Basin					
60	cai	11,000	161	Ashland Pluton	Z
49	ims	6,000	161	Rattlesnake Creek Terrane	Near Ashland Pluton
42	ms-p&s	6,000	161	Condrey Mtn Terrane	Near Ashland Pluton
31	cai	11,000	160	Greyback Pluton	Z
27	ims	6,000	160	Rattlesnake Creek Terrane	Near Greyback Pluton
18	a&s	4,000	160	Rattlesnake Creek Terrane	Near Greyback Pluton
17	a&s	4,000	160	Rattlesnake Creek Terrane	Near Greyback Pluton
Rogue, undivided*					
11	um	1,000	201		
1	ss	6,000	161		
6	ms-p&s	6,000	161		
7	mi	4,000	161		
10	ims	6,000	161		
20	ca-mv	6,000	161		
7	cai	11,000	161		
0	a&s	4,000	161		
10	a&s	4,000	161		
317			161 Ma		
Klamath, undivided					
509	iv	4,000	21		Weighted Average from Umpqua Basin
Rogue, undivided					
58	iv	4,000	21		Weighted Average from Umpqua Basin
Umpqua,, undivided					
43	iv	4,000	21		Weighted Average from Umpqua Basin

Table 4.3 (next page) - Upper Klamath Basin Lithologies (from High Desert). *Sum of Areas Under Same Mapped Unit Name. (1) Nomenclature from Walker and Macleod, 1991. ** Units are partly coeval with Saddle Mountains Basalt.

area (km^2)	Lithology	K (ppm)	Age (Ma)	Unit Name(1)	Notes
50	Silicic Vents	11,000	5.0	Tvs	Based on Walker and MacLeod (1991) isochrons
47	Silicic Vents	11,000	5.0	Tvs	Based on Walker and MacLeod (1991) isochrons
34	Silicic Vents	11,000	5.0	Tvs	Based on Walker and MacLeod (1991) isochrons
29	Silicic Vents	11,000	5.0	Tvs	Based on Walker and MacLeod (1991) isochrons
23	Silicic Vents	11,000	5.0	Tvs	Based on Walker and MacLeod (1991) isochrons
20	Silicic Vents	11,000	5.0	Tvs	Based on Walker and MacLeod (1991) isochrons
156	Andesite-Rhyolite Vents	8,000	30.0	Tvm	K. Scarberry, unpublished data ^{40}Ar-^{39}Ar ages
82	Andesite-Rhyolite Vents	8,000	30.0	Tvm	K. Scarberry, unpublished data ^{40}Ar-^{39}Ar ages
82	Andesite-Rhyolite Vents	8,000	30.0	Tvm	K. Scarberry, unpublished data ^{40}Ar-^{39}Ar ages
18	Andesite-Rhyolite Vents	8,000	30.0	Tvm	K. Scarberry, unpublished data ^{40}Ar-^{39}Ar ages
11	Andesite-Rhyolite Vents	8,000	30.0	Tvm	K. Scarberry, unpublished data ^{40}Ar-^{39}Ar ages
109	Basaltic lava flows	4,000	21.0	Tub	No ages mentioned, assume Cascades Average
33	Basaltic lava flows	4,000	21.0	Tub	No ages mentioned, assume Cascades Average
13	Basaltic lava flows	4,000	21.0	Tub	No ages mentioned, assume Cascades Average
24	undifferentiated intermediate seds.	6,000	27.0	Tu	Average of radiometric ages on ash flow interbeds
65	Rhyolite tuff and tuffaceous seds.	14,000	28.0	Tsf	K-Ar age range of 36-20 Ma
26	Rhyolite tuff and tuffaceous seds.	14,000	28.0	Tsf	K-Ar age range of 36-20 Ma
125	Tuffaceous seds. And tuff	6,000	6.6	Ts	K-Ar age on ash-flow tuff
120	Tuffaceous seds. And tuff	6,000	6.6	Ts	K-Ar age on ash-flow tuff
82	Tuffaceous seds. And tuff	6,000	6.6	Ts	K-Ar age on ash-flow tuff
57	Tuffaceous seds. And tuff	6,000	6.6	Ts	K-Ar age on ash-flow tuff
49	Tuffaceous seds. And tuff	6,000	6.6	Ts	K-Ar age on ash-flow tuff
44	Tuffaceous seds. And tuff	6,000	6.6	Ts	K-Ar age on ash-flow tuff
39	Tuffaceous seds. And tuff	6,000	6.6	Ts	K-Ar age on ash-flow tuff
35	Tuffaceous seds. And tuff	6,000	6.6	Ts	K-Ar age on ash-flow tuff
35	Tuffaceous seds. And tuff	6,000	6.6	Ts	K-Ar age on ash-flow tuff
32	Tuffaceous seds. And tuff	6,000	6.6	Ts	K-Ar age on ash-flow tuff
23	Tuffaceous seds. And tuff	6,000	6.6	Ts	K-Ar age on ash-flow tuff
21	Tuffaceous seds. And tuff	6,000	6.6	Ts	K-Ar age on ash-flow tuff

CONTINUED

area (km^2)	Lithology	K (ppm)	Age (Ma)	Unit Name(1)	Notes
15	Tuffaceous seds. And tuff	6,000	6.6	Ts	K-Ar age on ash-flow tuff
14	Tuffaceous seds. And tuff	6,000	6.6	Ts	K-Ar age on ash-flow tuff
13	Tuffaceous seds. And tuff	6,000	6.6	Ts	K-Ar age on ash-flow tuff
13	Tuffaceous seds. And tuff	6,000	6.6	Ts	K-Ar age on ash-flow tuff
12	Tuffaceous seds. And tuff	6,000	6.6	Ts	K-Ar age on ash-flow tuff
19	Rhyolite and Dacite	11,000	14.5	Trh	K-Ar range = 13-16 Ma
16	Rhyolite and Dacite	11,000	14.5	Trh	K-Ar range = 13-16 Ma
16	Rhyolite and Dacite	11,000	14.5	Trh	K-Ar range = 13-16 Ma
848	basalt to basaltic andesite	5,000	6.5	Trb	4 to 8 or 9 Ma (K-Ar)
55	basalt to basaltic andesite	5,000	6.5	Trb	4 to 8 or 9 Ma (K-Ar)
1,198	Olivine Basalt	4,500	5.5	Tob	between 4-7 Ma (K-Ar ages)
1,084	Olivine Basalt	4,500	5.5	Tob	between 4-7 Ma (K-Ar ages)
349	Olivine Basalt	4,500	5.5	Tob	between 4-7 Ma (K-Ar ages)
136	Olivine Basalt	4,500	5.5	Tob	between 4-7 Ma (K-Ar ages)
105	Olivine Basalt	4,500	5.5	Tob	between 4-7 Ma (K-Ar ages)
84	Olivine Basalt	4,500	5.5	Tob	between 4-7 Ma (K-Ar ages)
48	Olivine Basalt	4,500	5.5	Tob	between 4-7 Ma (K-Ar ages)
24	Olivine Basalt	4,500	5.5	Tob	between 4-7 Ma (K-Ar ages)
22	Olivine Basalt	4,500	5.5	Tob	between 4-7 Ma (K-Ar ages)
16	Olivine Basalt	4,500	5.5	Tob	between 4-7 Ma (K-Ar ages)
15	Olivine Basalt	4,500	5.5	Tob	between 4-7 Ma (K-Ar ages)
15	Olivine Basalt	4,500	5.5	Tob	between 4-7 Ma (K-Ar ages)
14	Olivine Basalt	4,500	5.5	Tob	between 4-7 Ma (K-Ar ages)
13	Olivine Basalt	4,500	5.5	Tob	between 4-7 Ma (K-Ar ages)
12	Olivine Basalt	4,500	5.5	Tob	between 4-7 Ma (K-Ar ages)
11	Olivine Basalt	4,500	5.5	Tob	between 4-7 Ma (K-Ar ages)
10	Olivine Basalt	4,500	5.5	Tob	between 4-7 Ma (K-Ar ages)
356	Basalt	4,000	14.0	Tb	Steens, Picture Gorge, Owyhee*
197	Basalt	4,000	14.0	Tb	Steens, Picture Gorge, Owyhee*
70	Basalt	4,000	14.0	Tb	Steens, Picture Gorge, Owyhee*
46	Basalt	4,000	14.0	Tb	Steens, Picture Gorge, Owyhee*
45	Basalt	4,000	14.0	Tb	Steens, Picture Gorge, Owyhee*
45	Basalt	4,000	14.0	Tb	Steens, Picture Gorge, Owyhee*
34	Basalt	4,000	14.0	Tb	Steens, Picture Gorge, Owyhee*

CONTINUED

area (km^2)	Lithology	K (ppm)	Age (Ma)	Unit Name(1)	Notes
33	Basalt	4,000	14.0	Tb	Steens, Picture Gorge, Owyhee*
32	Basalt	4,000	14.0	Tb	Steens, Picture Gorge, Owyhee*
30	Basalt	4,000	14.0	Tb	Steens, Picture Gorge, Owyhee*
30	Basalt	4,000	14.0	Tb	Steens, Picture Gorge, Owyhee*
18	Basalt	4,000	14.0	Tb	Steens, Picture Gorge, Owyhee*
18	Basalt	4,000	14.0	Tb	Steens, Picture Gorge, Owyhee*
15	Basalt	4,000	14.0	Tb	Steens, Picture Gorge, Owyhee*
11	Silicic Ash flow tuff	11,000	7.5	Tat	K-Ar 6-9 Ma
68	Basalt and Basaltic Andesite	5,000	2.6	QTba	K-Ar 1.2-3.9 Ma
23	Basalt and Basaltic Andesite	5,000	2.6	QTba	K-Ar 1.2-3.9 Ma
20	Basalt and Basaltic Andesite	5,000	2.6	QTba	K-Ar 1.2-3.9 Ma
15	Basalt and Basaltic Andesite	5,000	2.6	QTba	K-Ar 1.2-3.9 Ma
15	Basalt and Basaltic Andesite	5,000	2.6	QTba	K-Ar 1.2-3.9 Ma
14	Basalt and Basaltic Andesite	5,000	2.6	QTba	K-Ar 1.2-3.9 Ma
13	Basalt and Basaltic Andesite	5,000	2.6	QTba	K-Ar 1.2-3.9 Ma
11	Basalt and Basaltic Andesite	5,000	2.6	QTba	K-Ar 1.2-3.9 Ma
Unidivided*					
68	Andesite-Rhyolite Vents	11,000	30.0	Tvm	K. Scarberry, unpublished data ^{40}Ar-^{39}Ar ages
16	Rhyolite tuff and tuffaceous seds.	14,000	28.0	Tsf	K-Ar age range of 36-20 Ma
10	Basaltic lava flows	4,000	21.0	Tub	No ages mentioned
3	Mafic to intermediate intrusive rocks	5,000	15.0	Tim	Pliocene to Miocene
2	Mafic to intermediate intrusive rocks	5,000	15.0	Tib	Pliocene to Miocene
23	Rhyolite and Dacite	11,000	14.5	Trh	K-Ar 13-16 Ma
0	Hornblende diorite	5,000	14.0	Thi	K-Ar 8-22 Ma
47	Basalt	4,000	14.0	Tb	Steens, Picture Gorge, Owyhee*
13	Silicic Ash flow tuff	11,000	7.5	Tat	K-Ar 6-9 Ma
109	Tuffaceous seds. And tuff	6,000	6.6	Ts	K-Ar age on ash-flow tuff
6	basalt to basaltic andesite	5,000	6.5	Trb	4 to 8 or 9 Ma (K-Ar)
144	Olivine Basalt	4,500	5.5	Tob	between 4-7 Ma (K-Ar ages)
43	Silicic Vents	11,000	5.0	Tvs	Based on Wlaker and MacLeod isochrons
29	Basalt and Basaltic Andesite	5,000	2.6	QTba	K-Ar 1.2-3.9 Ma
	WEIGHTED AVERAGE AGE----->		10 Ma		

Table 4.4 - Study Area Subbasin Statistics. *= includes Pistol and Chetco Rivers. ** = Based on a sediment density of 2.6 g/cm^3. OCR = Oregon Coast Ranges.

	Area (km^2)	LOAD kgx10^9/year	Erosion Rate** mm/year	K (ppm)	Weighted Average Age (Ma)
Upmqua River	9,534				
-Upper, Cascades	3,757	**0.6**	**0.1**	4,000	21
-Lower Basin (OCR)	5,734	**0.8**	**0.1**	11,000	106
-glaciated Cascades	43	**0.01**	**0.06**	4,000	21
Rogue River *	13,394				
-Upper basin (Cascades)	3,916	**0.7**	**0.1**	4,000	21
-Lower Basin (Klam. Mtns.)	9,103	**1.7**	**0.1**	11,000	147
-glaciated Cascades	58	**0.01**	**0.07**	4,000	21
-glaciated Klam. Mtns.	317	**0.1**	**0.1**	11,000	161
Klamath River	29,340				
-Upper basin (Cascades&E. Oregon)	13,493	**2.4**	**0.1**	4,000	15
-Lower Basin (Klam. Mtns.)	9,467	**1.4**	**0.1**	11,000	147
-glaciated Cascades	509	**0.1**	**0.1**	4,000	21
-glaciated Klam. Mtns.	3,071	**0.5**	**0.1**	11,000	174
	2,800				
Trinity River		**6.8**	**0.4**		
Eel River	8,063	**18.0**	**0.9**	7,000	129
Coos-Coquille-Sixes-Elk	4,804	**0.7**	**0.1**	8,500	109
Smith River	1,590	**0.3**	**0.1**	9,500	147
Mad-Redwood Cr.	1,976	**3.9**	**0.8**	7,000	129

ultramafic and metasediments derived from these rock types. We use K concentrations of feldspars because it was shown (VanLaningham et al., 2006) that bulk sediment ^{40}Ar-^{39}Ar plateau ages are driven by the most abundant K-bearing phase (in the case of this study area, plagioclase). Wide ranges in K concentrations within minerals from each rock type are observed worldwide (GEOROC database, http://georoc.mpch-mainz.gwdg.de/georoc/), from which we assign average values. Hence, the relationships between these rock units and feldspar K concentrations are appropriate.

From the ^{40}Ar-^{39}Ar ages, K concentrations and areal extents of each mapped geologic unit, a weighted average age is calculated using:

$$T_{kat} = \sum_{i=1}^{n} K_i a_i t_i \div \sum_{i=1}^{n} K_i a_i \quad (1)$$

Where n is the number of mapped lithologies, K_i is the concentration of potassium in feldspars from each rock type (in ppm), a_i is outcrop area of each rock type (in km^2), and t_i is the age of the feldspars in each mapped lithology (in years).

This equation is used to calculate the weighted average age of the glaciated Klamath Mountains above 1500 m in the Rogue and Klamath River basins (Table 4.2) and the Upper Klamath Basin in Oregon not characterized by the glaciated high Cascades (Table 4.3). This equation was also used previously to make estimates of the non-glaciated Cascades and Coast Ranges components of the Umpqua, Rogue and Klamath River basins (VanLaningham et al., 2006; Table 4.2 and 4.4). The weighted average age of 21 Ma calculated for the Cascade units in the Umpqua Basin (VanLaningham et al., 2006) is applied to the unglaciated and glaciated Cascade portion of the Rogue River. A more simple weighted average is made for the smaller Coos-Coquille-Elk-Sixes region by assuming an Oregon Coast Range component of 97 Ma (bulk sediment age of the Coos River samples; VanLaningham et al., 2006) comprising 76% of the total area, and a Klamath Mountains component of 147 Ma (weighted average age of the entire Klamath Mountains; VanLaningham et al., 2006) comprising the other 24% of the basin area. For the Smith River (California) we use the weighted average age for the entire Klamath Mountains (147 Ma), while Trinity River, Mad River and Redwood Creek are assigned the

same bulk sediment ^{40}Ar-^{39}Ar plateau age as the Eel River (129 Ma) because they all erode the Franciscan Melange.

4.4.3 The Downcore Modeling Approach

We set up the model to examine three key periods of the climate transition as expressed through sediments in Core EW9504-17PC: 1) the time interval between 25-22 ka (just prior to the global LGM), 2) the peak of the Local Last Glacial Maximum in the region (LLGM; 18.5 ka; Rosenbaum and Reynolds, 2004) and 3) coming out of the glaciation (~14 ka).

We perturb present-day sediment loads in each sub-basin to explore their sensitivity to precipitation and the resulting erosional changes. We construct a best fitting ^{40}Ar-^{39}Ar curve to offer insight about the changes in precipitation needed to describe the provenance evolution at the core site. The largest change in bulk sediment ages occurs aournd the onset of the LGM (25-21 ka). At this time, perturbations are made only in the fluvial and pluvial sub-basins. Then, at 18.5 ka (LLGM), we increase the sediment fluxes out of glaciated regions by four times present-day values, consistent with the observed increase of glacial flour delivered out of the southern Oregon Cascades Mountains at this time (Rosenbaum and Reynolds, 2004) and investigate the model response in the fluvial/pluvial components. At 14 ka, we assume that conditions are similar to the present and thus use the present-day sediment loads unperturbed (i.e., the control run).

Equation 1 is modified for downcore purposes because sediment loads are used instead of contributing areas of rock types. This is done because the amount of sediment delivered to the ocean is more important than the contributing basin area in controlling provenance along the continental margin. Additionally, the equation is modified to incorporate a perturbation parameter to increase or decrease sediment loads (to mimic changes in precipitation). To attain the downcore weighted average model ages, equation 1 becomes:

$$T_{kpt} = \sum_{i=1}^{n} K_i (p_i \times {x_f}^m) t_i \div \sum_{i=1}^{n} K_i (p_i \times {x_f}^m) \qquad (2)$$

where p_i is the present-day sediment loads for a given sub-basin, x_f is a parameter that increases or decreases p_i by factor changes (in essence, percent changes in precipitation) and m is the power scaling value (1.4 for the rivers eroding Franciscan Melange rocks and 2.1 for all other rivers; Figure 4.3). The perturbation parameters, x_f, are the Oregon Coast Ranges factor, the unglaciated Klamath Mountains factor, the coastal California factor, the glaciated Klamath Mountains factor and the glaciated Cascades factor (glaciated sub-basins have linear increases in erosion applied to them because this is the observed relation in the southern Oregon Cascades; Rosenbaum and Reynolds, 2004). There is also the Upper Klamath Basin factor, which incorporates pluvial Lake Modoc. We do not parse Lake Modoc into its 2800 km^2 glacial extent (Smith and Street-Perrod, 1983) because the contributing area to the lake was the entire upper basin. The sub-basins that these parameters affect are summarized in Table 4.5. Each are used in essence as sediment flux factors, where a value of 1 equals present-day conditions and increases of the parameters equate to more enhanced precipitation/ erosion and decreases equate to decreased precipitation/erosion.

4.5 Experiment Runs

A control run is first carried out using the present-day sediment loads unperturbed to test the consistency of the model with the observed near-surface ^{40}Ar-^{39}Ar bulk sediment sample age (125.6 Ma). We then show results of the sensitivity of each sub-basin to perturbations ranging from 25% of the present-day sediment loads to 200% above today's values. The glaciated Cascades and Klamath Mountains are perturbed linearly from no increase in erosion (no glaciers) to an increase ten times today's values. After the sensitivity examination, a best fitting experimental run is carried out to track the ^{40}Ar-^{39}Ar bulk sediment trend from core site EW9504-17PC. This helps elucidate the major controls on the provenance changes over the last 22-14 ka.

We also calculate an erosion rate for each sub-basin and over the total drainage area covered by rivers in this study. This is done as a further consistency test to interpret the sedimentation rate at the core site over the modeled interval of 25-14 ka that shows an increase

Table 4.5 - Sub-basin Factors

	Parts of Basins that Parameter Affects……
Oreg. Coast Ranges	Lower Umpqua and Coos-Coquille-Sixes-Elk
Klamath Mtns, precip only	Lower Rogue, Smith, Lower Klamath
Cascade Mtns, precip only	Unglaciated (I.e., topography < 2000 m) Upper Umpqua, Upper Rogue, and Upper Klamath
Coastal California	Eel, Trinity, Mad, Redwood Cr.
Glacial Cascades	Umpqua, Rogue and Klamath basins ABOVE 2000 meters
Glacial Klamaths	Rogue and Klamath basins ABOVE 1500 meters
Upper Klamath Basin	Upper Klamath Basin and pluvial Lake Modoc

over this time interval that is three to four times higher than the background values (Figure 4.2D). It also provides a boundary condition: The overall trend and magnitude of increase in erosion rate should be similar to the terrigenous sedimentation rate offshore because the core site is dominated by inputs from riverine material along this margin. The absolute values of erosion rate, however, need not match the sedimentation rate values at the core site.

The erosion rate is calculated by assuming a density of erodable rocks that is 2.6 g/cm^3. We then convert sediment load (Wheatcroft and Sommerfield, 2005; Table 4.1) to a landscape lowering rate (Table 4.5). This calculation incorporates erosion related to land-use as well as natural erosion. Because these erosion rates are within the range of incision rates estimated in Oregon coastal rivers since the Holocene (0.1 – 1.0 mm/yr; Personius et al., 1993; Personius, 1995) and other estimates of erosion rates determined in the study area (Heimsath et al., 2001; Ferrier et al., 2005), the conversion of sediment load to erosion rate is a reasonable first-order approach.

4.6 Results

The control run results in a modeled ^{40}Ar-^{39}Ar age of 125.1 Ma. This is within error of the downcore ^{40}Ar-^{39}Ar near-surface age of 125.6 Ma. It is also within error of the samples at 12.6 ka and 14.2 ka (124.4 and 124.0 Ma, respectively), which we postulate might be similar to present-day (pre-European settlement) conditions (VanLaningham et al., in preparation; Chapter 3).

The Upper Klamath Basin stands out as the single most influential sub-basin to the bulk sediment ^{40}Ar-^{39}Ar ages (Figure 4.4) after perturbing each by the 25% to 200% (fluvial) and 0 to 10x (glacial) changes. Sediment fluxes out of the Upper Klamath Basin can lead to downcore provenance changes that span the total range of observed downcore bulk ages. The glaciated and unglaciated Klamath Mountains are also influential to margin sedimentation, but only have significant controls on the ^{40}Ar-^{39}Ar ages near the older end of the observed downcore range. The Cascades have a nominal impact on bulk sediment ages. Changing the erosivity in the coastal California rivers can also have a notable influence on bulk sediment

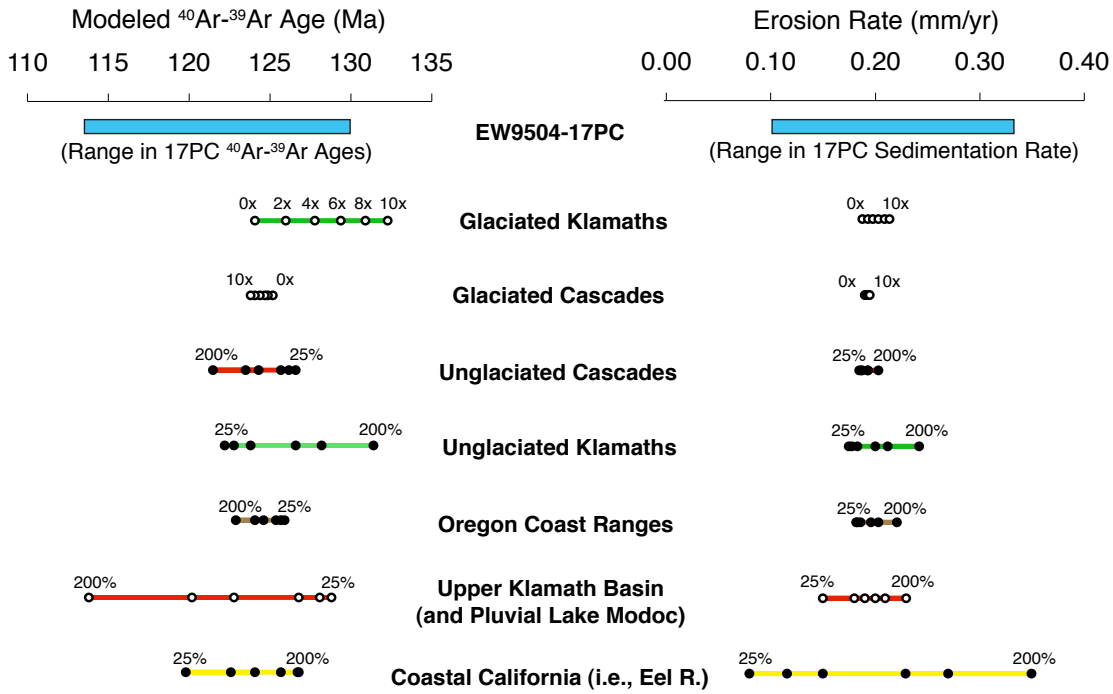

Figure 4.4 - Model sensitivity of sub-basins to 25%, 50%, 75%, 150%, 200% changes (non-glacial parameters and 0x, 2x, 4x, 6x, 8x, and 10x changes. The observed changes seen at core site EW9504-17PC also shown (blue rectangles).

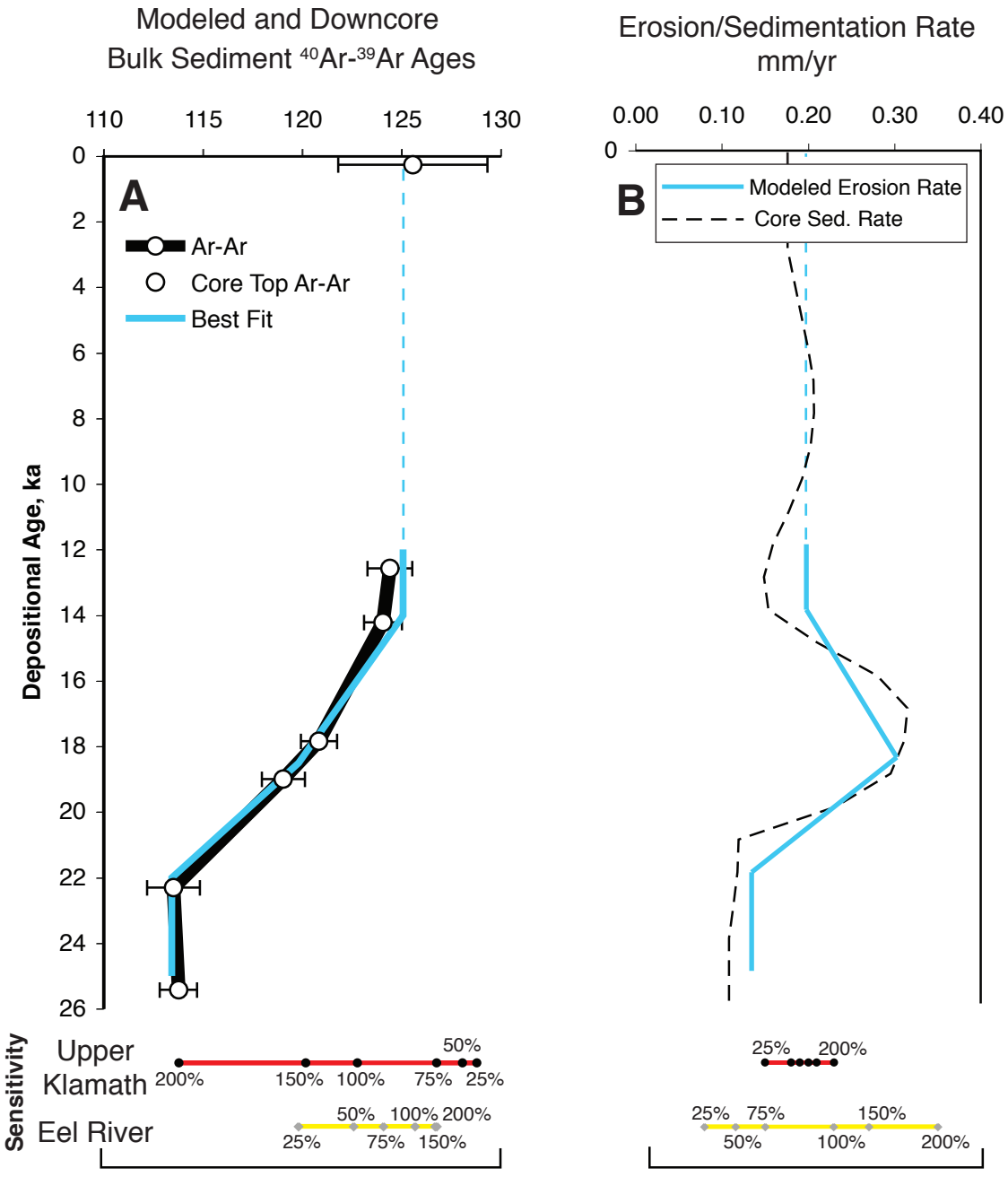

Figure 4.5 - Model and observed bulk sediment ^{40}Ar-^{39}Ar ages, erosion/sedimentation rates and model sensitivity of most important sub-basins. A) Bulk sediment ^{40}Ar-^{39}Ar ages. The best-fitting curve requires up to a 1.8x increase in erosional fluxes from the Upper Klamath Basin. Errors on EW9504-17PC measurements are ±2-sigma. B) Modeled erosion rate through time overlayed on the core site terrigenous sedimentation rate. The lower part of each figure illustrates the model sensitivity to changes in the Upper Klamath and coastal California (Eel) parameters. The ^{0}Ar-^{39}Ar ages are very sensitive to the Upper Klamath Basin while the erosion rate is more sensitive to changes in the Eel River.

Table 4.6 – Sub-basin Changes (Perturbation Factors)

Model Basins	Control	22 ka	18.5 ka	
Upper Klamath Basin	1	1.4	1.8	
Oregon Coast Ranges	1	0.7	0.7	
Klamath Mtns.	1	0.53	0.53	
Unglaciated Cascades Mtns.	1	0.84	0.84	
Coastal California	1	0.6	1.6	
Glaciated Cascades Mtns.	1	2	3.36	
Glaciated Klamath Mtns.	1	0.53	2.1	
Age	**125.1**	**113.4**	**119.8**	Ma

ages but cannot alone lead to the younger downcore bulk ages observed at the core site ~25-21 ka, even when the Eel and other coastal California rivers are, in essence, shut off (25% of present-day values).

When assessing sediment fluxes to the margin through the modeled landscape-scale lowering rate, the coastal California rivers exert the dominant control on margin sedimentation. Sediment delivery from the Upper Klamath Basin and all other sub-basins is considerably less influential (Figure 4.5). Glacial fluxes from the Klamath Mountains have a small impact on modeled sediment fluxes while the glaciated Cascades have essentially no effect.

To reproduce the young ^{40}Ar-^{39}Ar bulk sediment ages observed between 25-21 ka, the model requires a 1.4x increase in the Upper Klamath Basin factor in conjunction with decreases in the other sub-basins (~30-40% decreases; Table 4.6). Fourfold increases above their pre-LGM values in both the Cascades (Rosenbaum and Reynolds, 2004) and Klamath glacial erosion parameters at 18.5 ka cannot reproduce the ~5 Myr increase in bulk ages between 22 – 18.5 ka and require the coastal California parameter to increase from a 30% decrease (compared to present-day) at 22 ka to 60% above present-day at 18.5 ka (Table 4.6), if all other parameters are kept the same as the 22 ka calculation. This is also necessary to produce erosion rates that track the magnitude of change in the sedimentation rate curve (Figure 4.5B).

4.7 Discussion

The simplest way to reproduce the downcore trend in ^{40}Ar-^{39}Ar ages using the detrital mixture model requires increases in both the Upper Klamath Basin and Eel River region (coastal California) as well as decreases in sediment output from all other basins. The model sub-basins could be perturbed with other combinations of parameter adjustments to arrive at the observed downcore provenance trend, but not without invoking even more drastic changes than those assigned to the Upper Klamath and coastal California Basins and not without deviating from the trend observed in the sedimentation rate curve. Thus, our first-

order conclusion is that the dominant regions contributing to margin sedimentation are the pluvial lake region from Upper Klamath Basin and the Eel River region of coastal California, assuming that we have accounted for all of the major controls on continental margin sedimentation.

Are the changes invoked in this model consistent with other paleoclimate datasets from the region? Pluvial lake histories and pollen records in the study area are probably the best proxies to estimate past precipitation changes (the driver of erosion) over the last glacial. We will discuss these records in light of what we have learned from our erosion model in an attempt to elucidate the significance of erosional changes as a function of regional climate.

4.7.1 The Role of Pluvial Lake Modoc

This detrital mixture model incorporates the effects of erosion and outwashing from pluvial Lake Modoc indirectly (Figure 4.1) by perturbations of the bulk sediment ^{40}Ar-^{39}Ar fluxes from the Upper Klamath Basin. Of any of the sub-basins parsed out in the erosion model, the Upper Klamath Basin has the largest impact on the bulk ^{40}Ar-^{39}Ar ages (Figure 4.4). Lake Modoc occupied about 20% of the total Upper Klamath Basin at its maximum extent (Smith and Street-Perrod, 1983), although in terms of contributing area, the entire upper part of the basin accumulated water and channeled it to the pluvial lake. The timing of outbursts of freshwater from Lake Modoc may have been intermittent (and difficult to constrain in the model) because its outflow must have been blocked for it to grow to its Pleistocene areal extent (Smith and Street-Perrod, 1983).

Nevertheless, there is evidence that during the time of the younger downcore ^{40}Ar-^{39}Ar ages (22-25 ka) pluvial lake levels increased across much of the Great Basin. There are no constraints on the precise timing of lake levels at Lake Modoc (Negrini, 2002) but good temporal characterization has been achieved at nearby Lake Lahontan (100 km south of Lake Modoc). Lake level records there show a large increase from before 24 ka to 22 ka and lake level stabilization until ~18 ka (Benson et al., 1995) when another pulse of precipitation may have occurred. This is also generally consistent with lake level histories

east of Upper Klamath Basin at Fort Rock and Chewaucan Lakes (Negrini, 2002). Thus, the timing of increases in pluvial lake levels in the Great Basin before 22 ka – most likely caused by increasing precipitation considering the rapid changes in lake levels - occurs at the same time the downcore ^{40}Ar-^{39}Ar age record suggests a larger than normal contribution of younger source rocks (average ^{40}Ar-^{39}Ar age of lithologies in the Upper Klamath Basin are around 10 Ma). Estimates of increases in runoff into the Great Basin pluvial lakes during MIS 2 vary from 2.4-3.0 times above present-day values in Warner Valley (Weide, 1976) to 5-6 times greater than today in the Bonneville and Lahontan lake systems (Smith and Street-Perrod, 1983). Thus, increasing runoff by 2-6 times present-day values can easily produce modeled bulk sediment ages that simulate the younger bulk sediment ^{40}Ar-^{39}Ar ages observed at the core site. However, an unconstrained variable is how much sediment is stored in these lakes? For now, we cannot speculate on this.

If our assertions above are correct, which suggest that the Upper Klamath Basin/ Lake Modoc region contributed additional material to the continental margin 22-25 ka, it would suggest that there was no significant impoundment to block flow out of this region as suggested by Smith and Street-Perrod (1983). The combined effects of low relief and higher pre-LGM inflow rates in the Upper Klamath Basin may have encouraged lake filling because there was not enough slope in the region to keep pace with outflow through the Klamath River. If so, then offshore records such as EW9504-17PC and ODP Site 1019 likely capture a long history (several glacial-interglacial cycles) of pluvial lake changes in the western Great Basin through the Lake Modoc system. A field investigation to resolve whether natural phenomena (landslides, volcanic eruptions) blocked flow of Upper Klamath Basin water and sediment to the lower drainage system would determine the viability of examining this idea further through marine records.

4.7.2 Precipitation Changes in the Eel River Region

The erosion model illustrates the importance of rivers eroding the Franciscan Melange on the flux of sediment to the core site (Figure 4.4). To increase both bulk sediment ages

and erosion rates at 18.5 ka requires a 60% increase above present-day sediment loads from the coastal California region. This suggests a large increase in precipitation in the Eel River region at the LLGM. Pollen records from Clear Lake, California just south of the Eel River headwaters show that throughout the last glacial, conditions were much wetter (Adam and West, 1983) and by 14-17 ka precipitation began to rapidly decline (Adam et al., 1981). Adam and West (1983) predict from pollen transfer functions that precipitation may have decreased from ~325 cm/year between 30-17 ka to present-day rates of 125 cm. The flat response of pollen in the Clear Lake core during full glacials and interglacials suggests that the basin vegetation may not be sensitive to subtler precipitation/climate oscillations that may have led to the provenance change seen at the core site over the relatively short time interval of 25-14 ka, which thwarts further interpretation. Regardless, the pollen records from Clear Lake supports a higher erosion rate in response to increased precipitation from the Eel River region during the last glacial, which we require in our model.

A numerical model incorporating a vast array of components such as physical basin attributes, temperature and precipitation in the basin, snow and glacial attributes, vegetative effects on erosion and more was used to investigate the response of the Eel River to conditions around the LLGM (HYDROTREND model; Syvitski and Morehead, 1999). Using past temperature and precipitation boundary conditions from a variety of paleo-indicators (Precipitation minus evaporation from regional climate models from Hostetler et al., 1994, floral indices from Forester et al., 1996, and a Mono Lake oxygen isotope record that estimates precipitation from Benson et al., 1997). HYDROTREND predicts a 25% increase in annual sediment delivered to the margin in response to 45% increase in precipitation. They use a lower nival sediment-discharge rating curve that leads to a lower sediment yield from the regions covered by snow during the last glacial, which might explain the difference between the percent changes in sediment load and precipitation. Although it is difficult to assess whether a ~60% or 25% increase occurs in the Eel River region, combining our geochemical approach with a more physically-based model such as HYDROTREND may offer a new and powerful way of unraveling landscape erosion through marine sedimentary records.

4.7.3 The Larger Climate Mechanism

The continental margin ^{40}Ar-^{39}Ar detrital mixture model requires fairly sizable, localized increases in precipitation in the Eel River region and the Upper Klamath Basin, and similar decreases in precipitation in the coastal Oregon and Klamath Mountains to reproduce the observed downcore trend. If our model is representative of how the fluvial system responded in the geologic past, then the larger climate mechanism may be related to a change in the position of the locus of storms as they track the deflection of the Jet Stream in response to expansion and contraction of the Laurentide Ice Sheet (LIS) between 25-14 ka (Kutzbach, 1987). There is considerable uncertainty about whether this led to more precipitation (Smith and Street-Perrod, 1983; Benson et al., 1995) or less (Kutzbach, 1987). We can only postulate that the pluvial lakes persisted in the Upper Klamath Basin and that material from this region likely contributed significantly (nearly twice present-day amounts) to the sediments on the Oregon marine margin. The fact that our model requires enhanced precipitation over both the Eel River and Upper Klamath Basin might also suggest that bands of moisture are focused in this region. Recent work from the Russian River region, which lies just south of the Eel River basin, suggests that all major flooding on this river is due to "atmospheric rivers" (Ralph et al., 2006). These atmospheric rivers are a phenomena just beginning to be recognized as a major source of focused meriodonal water vapor transport (up to 90%; Ralph et al., 2006). It is possible that these focused bands of moisture are responsible for the complex precipitation patterns needed to describe the downcore ^{40}Ar-^{39}Ar provenance record at core site EW9504-17PC.

It is also possible that the entire region was drier and that the pluvial lakes in the Upper Klamath Basin represent "stored" water from a previously cold, wet period (before 25 ka) with low evaporation (Negrini, 2002). If so, Lake Modoc may have continued to drain during this dry period, bringing more High Lava Plains/Cascades material relative to present, while the rest of the southern Oregon-northern California region contributed substantially less sediment. Although REGCM2 model outputs of precipitation minus evaporation from LGM-present runs (Hostetler et al., 2006) cannot reproduce the total range seen in the core site ^{40}Ar-

^{39}Ar ages (model runs not shown), the REGCM2 model does predict precipitation decreases in the Oregon Coast Ranges, the Klamath Mountains and the Cascades as well as increases around the Eel River region, consistent with what drives our best-fitting model result. The REGCM2 model does not yet take into account the coastal and Cascades mountain topography so when the topographic resolution improves, we will imbed the hydrologic balance from the climate model into our detrital mixture modeling approach.

4.7.4 Other Considerations

The continental shelf stores sediment and can change sediment transport pathways. Approximately 20-30% of the Eel River sediment is stored on the shelf during interglacials (Wheatcroft and Sommerfield, 2005). Would this demonstrably affect sedimentation rate and the sources of sediment to a point source on the margin on glacial-interglacial timescales? Bypassing the shelf, all else being equal, would have led to increases in sedimentation rate along the continental slope environs. We see this at core site EW9504-17PC. But if this were the only major change, sedimentation rates would follow a step change from higher rates during glacials to lower rates during interglacials. We observe low sedimentation rates before the LGM, when sea level was at or below the shelf depth of 120 m (Lambeck et al., 2002) and thus rivers were still depositing their sediment load directly to the deep ocean. At 22 ka an increase in terrigenous sediment occurs at the core site, followed by a decrease as sea level rises. The peak in terrigenous sedimentation rate suggests that processes beyond sea-level change were dictating accumulation.

There is also potential for sea-level changes to affect sediment provenance by changing the dispersivity of sediment. This is not well understood at this core site but we speculate that during sea level lowstands, the provenance would likely not change significantly compared to today because all rivers would bypass the shelf. Moreover, the sensitivity test showed that reducing output (or transport) of coastal California rivers to 25% of today's values still could not reproduce the total range in provenance change we observe at the core site, so even a major re-routing of Eel River sediment during the last glacial would not explain the

provenance change we observe downcore. A way to improve our understanding of changes in dispersivity along the margin would involve examining provenance along a transect of core sites across the continental slope out to the deeper ocean. For now, we postulate that the effects of sea level on sedimentation rate and provenance are small relative to precipitation-related erosion occurring in the terrestrial landscape.

A variety of other factors within the bulk sediment ^{40}Ar-^{39}Ar model, such as constraints on K concentrations, rock resistance, orographic effects and the physical processes that drive erosion in the glacio-fluvial landscape (Burbank, 2002; Whipple, 2004) all may have significant impacts on the system. In the future, we will improve the constraints placed on K concentrations by acquiring specific K values from lithologic units that have radiometric ages rather than assigning average values. An orographic component will also be necessary for using this approach on tectonic timescales and we will incorporate more physically based strategies to investigate what the two approaches (geochemical/isotopic mass balancing versus physical erosion models) can offer together.

4.8 Conclusions

A linear increase in bulk sediment ^{40}Ar-^{39}Ar ages at a core site offshore Oregon suggests differential erosion over a glacial-interglacial cycle, alternating between the interior Cascades and the coastal northern California and southern Oregon mountains. We investigate and quantify the relationship of the provenance change recorded at the core by evaluating the sensitivity of the fluvial system to changes in precipitation (or erosion). We develop a ^{40}Ar-^{39}Ar bulk sediment detrital mixture model to examine the downcore change. We assume that physical erosion does not vary with rock type, and make no allowance for orographic precipitation, nival runoff, or other physical controls. We simply assume a power law relation between sediment load and discharge and find that the most sensitive regions to changes in precipitation and erosion are the Upper Klamath Basin and the Eel River region.

To track the downcore provenance evolution over the time interval between 22 to 14 ka, the ^{40}Ar-^{39}Ar bulk sediment model requires a sizable, but not unrealistic increase in the

contribution of Upper Klamath Basin sediments before the LGM. Although we parse out the glacial regions in the study area and incorporate them into the erosion model, we find that a fourfold increase in glacial sediment fluxes does not significantly impact the bulk ^{40}Ar-^{39}Ar ages or predicted erosion rates at ~18.5 ka downcore. A 60% increase in sediment load out of the coastal California rivers is the simplest way to achieve the needed increases in bulk sediment ages and sedimentation rate observed at the core site at the LLGM.

A mechanism to describe the increased fluxes from the Upper Klamath Basin involves pluvial Lake Modoc. Records of other pluvial lakes in the Great Basin suggest much higher P-E values between 25-22 ka, lending support to our interpretation. Pollen records in coastal California are also consistent with increased precipitation during the last glacial and lend support to our proposed increase in coastal California river input at 18.5 ka.

This approach invoking isotope geochemistry and mixture modeling to address erosion on glacial-interglacial timescales should work well in any marine setting that shows discernible variations in ^{40}Ar-^{39}Ar cooling-crystallization ages. It will be effective in resolving changes in erosion at resolutions of most climate cycles, for very little sample is needed from sediment cores. An added advantage is that there exists a huge ^{40}Ar-^{39}Ar source age database. This technique should also be powerful in unraveling tectonic records of erosion captured in fine-grained deep-sea sediment cores. Future studies will address physical erosion and orographic effects more directly, as well as look to provide better constraints on the radiometric ages and geochemistry of the source rocks in river basins to better evaluate the utility of the technique. Expanding these types of studies to other cores in the region and further back in time will unravel the pluvial lake history in Oregon as well as resolve the erosional response of the Eel River to glacial-interglacial climate change. It would also help determine the degree of change in bulk sediment ages and sedimentation rate offshore that is induced by sea level changes.

4.9 References

Adam, D. P., Sims, J. D., and Throckmorton, C. K., 1981, 130,000-yr continuous pollen record from Clear Lake, Lake County, California: Geology, v. 9, p. 373-377.

Adam, D. P., and West, G. J., 1983, Temperature and precipitation estimates through the last glacial cycle from Clear Lake, California, Pollen Data: Science, v. 219, p. 168-171.

Allegre, C. J., Dupre, B., Negrel, P., and Gaillardet, J., 1996, Sr-Nd-Pb isotopic systematics in Amazon and Congo River systems: Constraints about erosion processes: Chemical Geology, v. 131, p. 93-112.

Anders, A. M., Roe, G. H., Hallet, B., Montgomery, D. R., Finnegan, N. J., and Putkonen, J., 2006, Spatial patterns of precipitation and topography in the Himalaya, *in* Willett, S., Hovius, N., Brandon, M. T., and Fisher, D. M., eds., Tectonics, Climate, and Landscape Evolution: Boulder, CO, The Geological Society of America.

Beaumont, C., Fullsack, P., and Hamilton, J., 1992, Erosional control of active compressional systems, *in* McClay, K. R., ed., Thrust Tectonics: New York, Chapman Hall, p. 1-18.

Benson, L. V., Kashgarian, M., and Rubin, M., 1995, Carbonate deposition, Pyramid Lake sub-basin, Nevada; 2: Lake levels and polar jet stream positions reconstructed from radiocarbon ages and elevations of carbonates (tufas) deposited in the Lahontan Basin: Palaeogeog., Palaeoclim., Palaeoecol., v. 117, p. 1-30.

Blake, M. C., and Jones, D. L., 1981, The Franciscan melange in northern California: A reinterpretation, *in* W.G., E., ed., The geotectonic evolution of California: Englewood Cliffs, NJ, Prentice Hall, p. 306-328.

Brandon, M. T., and Vance, J. A., 1992, Tectonic evolution of the Cenozoic Olympic subduction complex, Washington state, as deduced from fission track ages for detrital zircons: American Journal of Science, v. v. 292, p. p. 565-636.

Burbank, D. W., 2002, Rates of erosion and their implications for exhumation: Mineralogical Magazine, v. 66, no. 1, p. 25-52.

Burbank, D. W., Blythe, A. E., Putkonen, J., Pratt-Sitaula, B., Gabet, E., Oskin, M., Barros, A. P., and Ojha, T. P., 2003, Decoupling of erosion and precipitation in the Himalayas: Nature, v. 426, no. 11 December 2003, p. 652-655.

Carrapa, B., Wijbrams, J., and Bertolli, G., 2004, Detecting provenance variations and cooling patterns within the western Alpine orogen through $^{40}Ar/^{39}Ar$ geochronology on detrital sediments: The Tertiary Piedmont Basin, northwest Italy, *in* Bernet, M., and Spiegel, C., eds., Detrital Thermochronology - Provenance analysis, exhumation, and landscape evolution of mountain belts: Boulder, Colorado, The Geological Society of America, p. 67-103.

Carter, A., and Bristow, C. S., 2003, Linking hinterland evolution and continental basin sedimentation by using detrital zircon thermochronology; a study of the Khorat

Plateau basin, eastern Thailand: Basin Research, v. 15, no. 2, p. 271-285.

Clift, P., Carter, A., Campbell, I. H., Pringle, M. S., Van Lap, N., Allen, C. M., Hodges, K. V., and Tan, M. T., 2006, Thermochronology of mineral grains in the Red and Mekong Rivers, Vietnam: Provenance and exhumation implications for Southeast Asia: Geochemistry, Geophysics, Geosystems, v. 7, no. 10, p. doi:10.1029/2006GC001336.

Clift, P. D., 2006, Controls on the erosion of Cenozoic Asia and the flux of clastic sediment to the ocean: Earth and Planetary Science Letters, v. 241, p. 571-580.

CLIMAP, M., 1981, *in* MC-3, M. a. C. S., ed., Geological Society of America.

Dadson, S. J., Hovius, N., Chen, H., Dade, B. W., Hsieh, M., Willett, S. D., Hu, J., Horng, M., Chen, M., Stark, C. P., and Lin, J., 2003, Links between erosion, runoff variability and seismicity in the Taiwan orogen: Nature, v. 426, p. 648-651.

Ferrier, K. L., Kirchner, J. W., and Finkel, R., 2005, Erosion rates over millennial and decadel timescales at Caspar Creek ad Redwood Creek, Northern California Coast Ranges: Earth Surface Processes and Landforms, v. 30, p. 1025-1038.

Gaillardet, J., Dupre, B., Allegre, C. J., and Negrel, P., 1997, Chemical and physical denudation in the Amazon River Basin: Chemical Geology, v. 142, p. 141-173.

Hebbeln, D., Lamy, F., Mohtadi, M., and Echtler, H., 2007, Tracing the impact of glacial-interglacial climate variability on erosion of the southern Andes Geology, v. 35, no. 2, p. 131-134.

Heimsath, A. M., Dietrich, W. E., Nishiizumi, K., and Finkel, R. C., 2001, Stochastic processes of soil production and transport: Erosion rates, topographic variation and cosmogenic nuclides in the Oregon Coast Range: Earth Surface Processes and Landforms, v. 26, p. 531-552.

Heller, P. L., Peterman, Z. E., O'Neil, J. R., and Shafiqullah, M., 1985, Isotopic provenance of sandstones from the Eocene Tyee Formation, Oregon Coast Range: GSA Bulletin, v. 96, p. 770-780.

Hickey, B. M., and Banas, N. S., 2003, Oceanography of the U.S. Pacific Northwest Coastal Ocean and Estuaries with Application to Coastal Ecology: Estuaries, v. 26, no. 4B, p. 1010-1031.

Hodges, K. V., Ruhl, K. W., Wobus, C. W., and Pringle, M. S., 2005, $^{40}Ar/^{39}Ar$ thermochronology of detrital minerals, *in* Reiners, P. W., and Ehlers, T. A., eds., Low-Temperature Thermochronology: Techniques, Interpretations, and Applications: Reviews in mineraology and geochemistry.

Hostetler, S. W., Clark, P. U., Bartlein, P. J., Mix, A. C., and Pisias, N. G., 1999, Atmospheric transmission of North Atlantic Heinrich events: Journal of Geophysical Research, v. 104, p. 3947-3952.

Hostetler, S.W., Giorgi, F., Bates, G.T., Bartlein, P.J., 1994. Lake–atmosphere feedbacks associated with paleolakes Bonneville and Lahontan. Science 263, 665–668.

Huntington, K. W., and Hodges, K. V., 2006, A comparative study of detrital mineral and bedrock age-elevation methods for estimating erosion rates: Journal of Geophysical Research, v. 111, no. F03011, p. doi:10.1029/2005JF000454

Irwin, W. P., and Wooden, J. L., 1999, Plutons and accretionary episodes of the Klamath mountains, California and Oregon.

Johnson, B. R., and Raines, G. L., 1995, Digital map of major bedrock lithologic units for the Pacific Northwest: a contribution to the Interior Columbia Basin Ecosystem Management Project.

Karlin, R., 1980, Sediment Sources and Clay Mineral Distributions Off the Oregon Coast: JSP, v. 50, no. 2, p. 543-560.

Kirby, E., Reiners, P. W., Krol, M. A., Whipple, K. X., Hodges, K. V., Farley, K. A., Tang, W., and Chen, Z., 2002, Late Cenozoic evolution of the eastern margin of the Tibetan Plateau: Inferences from $^{40}Ar/^{39}Ar$ and (U-Th)/He thermochonology: Tectonics, v. 21, no. 1, p. doi:10.1029/2000TC001246.

Lambeck, K., Yokoyama, Y., and Purcell, T., 2002, Into and out of the Last Glacial Maximum: sea-level change during Oxygen Isotope Stages 3 and 2: Quaternary Science Reviews, v. 21, p. 343-360.

Lyle, M., Mix, A. M., Ravelo, C., Andreasen, D., Heusser, L., and Olivarez, A., 2000, Millennial-scale CaCO3 and corg events along the northern and central California margins: stratigraphy and origins, *in* Lyle, M., Koizumi, I., Richter, C., and Moore, T. C., Jr., eds., Proceedings of the Ocean Drilling Program, Scientific Results: College Station, TX.

McLaughlin, R. J., Sliter, W. V., Fredriksen, N. O., Harbert, W. P., and McCulloch, D. S., 1994, Plate motions recorded in tectonostratigraphic terranes of the Franciscan Complex and evolution of the Mendocino Triple Junction, Northwestern California.

Merritts, D., and Vincent, K. R., 1989, Geomorphic response of coastal streams to low, intermediate, and high rates of uplift, Mendocino triple junction region, California: Geological Society of America Bulletin, v. 101, no. 11, p. 1373-1388.

Molnar, P., 2003, Nature, Nurture and landscape: Nature, v. 426, p. 612-614.

Molnar, P., Anderson, R. S., Kier, G., and Rose, J., 2006, Relationships among probability distributions of stream discharges in floods, climate, bed load transport, and river incision: Journal of Geophysical Research, v. 111, no. F02001, p. 10.1029/2005JF000310.

Negrini, R. M., 2002, Pluvial lake sizes in the northwestern Great Basin throughout the Quaternary period, *in* Hershler, R., Madsen, D. B., and Currey, D. R., eds., Great

Basin aquatic systems history: Washington, D.C., Smithsonian Institution, p. 11-52.

Peucker-Ehrenbrink, B., and Miller, M. W., 2002, Quantitative bedrock geology of the conterminous United States of America: Geochemistry, Geophysics, Geosystems, v. 3, no. 10, p. doi:10.1029/2002GC000366.

Porter, S. C., Pierce, K. L., and Hamilton, T. D., 1983, Late Wisconsin glaciation in the Western United States, *in* Porter, S. C., ed., Late-Quaternary environments of the United States: Minneapolis, Univ. of Minnesota Press, p. 71-111.

Ralph, F.M., Neiman, P. J., Wick, G. A., Gutman, S. I., Dettinger, M. D., Cayan, D. R., and White, A. B., 2006, Flooding on California's Russian River: Role of atmospheric rivers: Geophysical Research Letters, v. 33, no. L13801, p. 2006GL026689.

Reiners, P. W., 2005, Zircon (U-Th)/He Thermochronometry, *in* Reiners, P. W., and Ehlers, T. A., eds., Low-Temperature Thermochronology: Techniques, Interpretations, and Applications, p. 151-179.

Reiners, P. W., Campbell, I. H., Nicolescu, S., Allen, C. M., Hourigan, J. K., Garver, J. I., Mattinson, J. M., and Cowan, D. S., 2005, (U-Th)/(He-Pb) Double Dating Of Detrital Zircons: American Journal of Science, v. 305, p. 259-311.

Reneau, S. L., and Dietrich, W. E., 1991, Erosion rates in the southern Oregon Coast Ranges: evidence for an equilibrium between hillslope erosion and sediment yield: Earth Surface Processes and Landforms, v. 16, p. 307-322.

Rosenbaum, J. G., and Reynolds, R. L., 2004, Record of Late Pleistocene glaciation and deglaciation in the southern Cascade Range. II. Flux of glacial flour in a sediment core from Upper Klamath Lake, Oregon: Journal of Paleolimnology, v. 31, p. 235-252.

Ryu, I., and Niem, A. R., 1999, Sandstone diagenesis, reservoir potential and sequence stratigraphy of the Eocene Tyee Basin, Oregon: Journal of Sedimentary Research, v. 69, no. 2, p. 384-393.

Shuster, D. L., Ehlers, T. A., Rusmore, M. E., and Farley, K. A., 2005, Rapid Glacial Erosion at 1.8 Ma Revealed by $^{4}He/^{3}He$ Thermochronometry: Science, v. 310, p. 1668-1670.

Shuster, D. L., and Farley, K. A., 2005, $^{4}He/^{3}He$ Thermochronometry: Theory, Practice, and Potential Complications, *in* Reiners, P. W., and Ehlers, T. A., eds., Low-Temperature Thermochronology: Techniques, Interpretations, and Applications, p. 181-203.

Smith, G. I., and Street-Perrott, F. A., 1983, Pluvial lakes of the western United States, The late Pleistocene: Minneapolis, University of Minnesota Press, 190-210 p.

Snyder, N. P., Whipple, K. X., Tucker, G. E., and Merritts, D. J., 2000, Landscape response to tectonic forcing: Digital elevation model analysis of stream profiles in the Mendocino triple junction region, northern California: GSA Bulletin, v. 112, no. 8, p. 1250-1263.

Strub, P. T., Allen, J. S., Huyer, A., and Smith, R. L., 1987, Large-scale structure of the spring transition in the coastal ocean off western North America: Journal of Geophysical Research, v. 92, p. 1527–1544.

Syvitski, J.P., M.D. Morehead, 1999, Estimating river-sediment discharge to the ocean: Application to the Eel Margin, northern California. Marine Geology, 154, 13-28.

Syvitski, J.P.M., Morehead, M., Nicholson, M., 1998. HYDROTREND: a climate-driven hydrologic-transport model for predicting discharge and sediment load to lakes or oceans. Comput. Geosci. 24, 51–68.

Turcotte, D. L., and Greene, L., 1993, A scale-invariant approach to flood-frequency analysis: Stochastic Environmental Research and Risk Assessment, v. 7, no. 10.1007/BF01581565, p. 33-40.

VanLaningham, S., Duncan, R. A., and Pisias, N. G., 2006, Erosion by rivers and transport pathways in the ocean: A provenance tool using ^{40}Ar-^{39}Ar incremental heating on fine-grained sediment: Journal of Geophysical Research, v. 111, no. F04014, p. doi:10.1029/2006JF000583.

Walker, G. W., and MacLeod, N. S., 1991, Geologic Map of Oregon: U.S. Geological Survey, scale 1:500,000.

Weide, D. L., 1976, The Warner Valley: A test of pluvial climatic conditions, *in* Fourth Biennial Conference, Abstracts, Arizona State University.

Wheatcroft, R. A., and Sommerfield, C. K., 2005, River sediment and shelf sediment accumulation rates on the Pacific Northwest margin: Continental Shelf Research, v. 25, p. 311-332.

Whipple, K. X., 2004, Bedrock rivers and the geomorphology of active orogens: Annual Reviews Earth and Planetary Science, v. 32, no. 151–185.

Whipple, K. X., and Tucker, G. E., 1999, Dynamics of the stream-power river incision model: Implications for height limits of mountain ranges, landscape response timescales, and research needs: Journal of Geophysical Research, v. 104, p. 17661-17674.

Willett, S., 1999, Orogeny and orography: The effects of erosion on the structure of mountain belts: Journal of Geophysical Research, v. 104, no. B12, p. 28,957-28,981.

Willett, S., Hovius, N., Brandon, M. T., and Fisher, D. M., 2006, Introduction, *in* Willett, S., Hovius, N., Brandon, M. T., and Fisher, D. M., eds., Tectonics, Climate, and Landscape Evolution: Boulder, CO, The Geological Society of America.

Willett, S. D., Fisher, D., Fuller, C., En-Chao, Y., and Lu, C.-Y., 2003, Erosion rates and orogenic-wedge kinematics in Taiwan inferred from fission-track thermochronometry: Geology, v. 31, no. 11, p. 945-948.

Wolf, S. C., Nelson, H., Hamer, M. R., Dunhill, G., and Phillips, R. L., 1999, The Washington

and Oregon mid-shelf silt deposit and its relation to the late Holocene Columbia River sediment budget.

Chapter 5

Conclusions

A major goal of this dissertation has been to unravel terrestrial-ocean climate linkages through the analysis of fluvial sediments, pollen assemblages and climate data from the marine record. We documented a new method to characterize bulk sediment for provenance studies using the ^{40}Ar-^{39}Ar incremental heating technique. We analyzed the 20-63 μm size fraction of bulk river sediments from the mouths of 14 Pacific Northwest rivers and a marine core site offshore southern Oregon-northern California. We focused our efforts on the silt-sized material since this component contains mostly rock-forming minerals and yet it is small enough to be transported to continental margin sediment sites via ocean currents.

Reproducible age spectra provide robust "fingerprints" for many individual rivers in the Pacific Northwest, both by the shape of the age spectra and by the bulk sediment ^{40}Ar-^{39}Ar plateau ages. A K/Ca degassing model is developed to test, in light of bulk mineralogy and diffusion of silicates, whether measured K/Ca spectra (determined from ^{39}Ar and ^{37}Ar) are reasonable indicators of contributing minerals, given typical K- and Ca-compositions. The model shows that the bulk mineralogy is reflected in the outgassing K/Ca spectra and that plagioclase is likely to be the dominant mineral producing the age plateaus, followed by K-feldspar.

A basin-scale detrital mixture model that weights areal extent of rock type, K concentration and ^{40}Ar-^{39}Ar ages was developed to test the consistency of measured bulk sediment plateau ages with known source rock age and compositions. Tests were conducted for the Umpqua, Rogue and Klamath River basins. The Umpqua basin model prediction is 90 Ma, very similar to the average bulk sediment ^{40}Ar-^{39}Ar age (92 Ma). The model predicted

128 Ma for the Rogue River is virtually identical to the average bulk sediment age of 129 Ma calculated from four ^{40}Ar-^{39}Ar analyses. The modeled age for the Klamath River is 109 Ma, considerably younger than the average bulk sediment age of 151 Ma. However, if we include the effect of increased erosion and/or land-use effects occurring in the high-relief Klamath Mountains relative to the low-relief Cascades, a model age of 147 Ma is predicted.

Nd isotopic analyses of the river silts showed a range in ε_{Nd} of around ten units. Near the core site, however, river sediment showed a smaller spread ranging from ε_{Nd} = -5.0 in the Umpqua River to around ε_{Nd} = -1.0 in the Rogue and Klamath Rivers. Values in the Eel River were ε_{Nd} = -3.0. In the core sediments, ^{40}Ar-^{39}Ar ages ranged from 113 to 130 Ma, while ε_{Nd} values varied between -2.5 to -0.9. When combined, the ^{40}Ar-^{39}Ar plateau ages and Nd isotopic compositions from river sediments show resolvably different end-member compositions.

In terms of how the downcore provenance records from the ^{40}Ar-^{39}Ar ages and Nd isotopic compositions relate to the regional climate system, we show that the sediment from EW9504-17PC can be described as a mixture dominated by the Klamath+Rogue Rivers (equi-latitudinal with the core site) and the Eel River (south of the core site). The Umpqua and other rivers north of the core site appear to have little contribution either during interglacials or glacial times. There is no evidence that any significant amount of Columbia River material was deposited at the core, both from the Ar-Nd isotopic compositions as well as clay mineralogy, even though the Missoula Floods had significant affects on sedimentation elsewhere along the margin around the Last Glacial Maximum (LGM).

We see evidence that Cascades-derived material from the headwaters of the proximal rivers was a more important sediment contributor to the core site before 22 ka relative to today, implying reduced precipitation in the coastal mountains relative to present or an increased sediment flux from the Cascades Mountains and High Lava Plains region in Upper Klamath basin. During the LGM and subsequent deglaciation a commensurate increase in glacial erosion in the Klamath Mountains and Cascades between 22-18 ka introduced more material derived from rock units in the Klamath Accretionary Complex, leading to a net increase in bulk sediment ^{40}Ar-^{39}Ar ages. Increases in sediment from the Eel River may have

contributed to the change as well.

The comparison of pollen records, in light of the information offered by the geochemical tracers of provenance, suggests that more spruce pollen may have been introduced to the core site as the result of an increase in river-borne material from the Klamath Mountains. Thus, spruce pollen abundances in this core site reflect the integrated signal of terrestrial vegetation succession due to changes in precipitation+temperature as well as variations in erosional flux, which also responds to precipitation. Since other pollen species are similarly affected, downcore pollen abundances reflect a complex integration of precipitation-related processes.

This research culminates in an exploration of regional climate model outputs of precipitation minus evaporation and ^{40}Ar-^{39}Ar bulk sediment age balances from river basins. The range in P-E variation at the LGM cannot adequately explain the total range of variability indicated by the provenance change and could be related to the low resolution of the topography in the climate model or changes in frozen ground, which can have effects on runoff.

The ^{40}Ar-^{39}Ar bulk detrital mixture model requires a sizable, but not unrealistic increase in the contribution of Upper Klamath Basin sediments before the LGM. After ~21 ka, an increase above REGCM2-derived precipitation values is needed in the Eel River region to fully track the ^{40}Ar-^{39}Ar provenance evolution between 22-14 ka and remain consistent with increased sedimentation rates observed along the margin. Although we parse out the glacial regions in the study area and incorporate them into the detrital mixture/erosion model, we find that a fourfold increase in glacial sediment fluxes does not significantly impact the bulk ^{40}Ar-^{39}Ar ages or predicted erosion rates. The Eel River and Upper Klamath regions have the most notable effects on the model.

A mechanism to describe the increased fluxes from the Upper Klamath Basin involves pluvial Lake Modoc. Records of lakes in the Great Basin suggest much higher P-E values between 25-22 ka, lending support to our interpretation. Pollen records in coastal California are also consistent with notably increased precipitation during the last glacial and lend support to our postulation of increased coastal California river input at 18.5 ka.

Future studies in this region should yield interesting results about draining of pluvial lakes and possibly the degree of glaciation in the Cascades and Klamath Mountains during Marine Isotope Stages 4 and 6, which the terrestrial environs record less faithfully due to glacial successions erasing previous glacial features and deposits. The diversity seen in river Ar-Nd isotopic values in Pacific Northwest coastal rivers bodes well for future provenance studies that will further unravel how the land, ocean and the atmosphere respond to climate change.

The larger implications of this work concern the utility of the technique in other regions and for other purposes. The coupled Ar-Nd isotopic technique will improve the ability to interpret how the landscape responds to natural processes through fine-grained provenance studies by offering a multi-tracer fingerprinting technique that is resistant to alteration processes. Regions that include a variety of geologic provinces in diverse climate zones that experience different rates of precipitation will show the most promise. The detrital mixture modeling approach combined with quantitative constraints on erosion rates may yield insightful information about the rates of climatically driven landscape evolution preserved in marine sedimentary settings. It will be effective in resolving changes in erosion at resolutions of most climate cycles because very little sample is needed from core sites, coupled with the large database of ^{40}Ar-^{39}Ar ages from potential source terranes. This technique should also prove to be useful in unraveling longer, tectonic records of exhumation captured in fine-grained deep-sea sediment cores.

Bibliography

Adam, D. P., Sims, J. D., and Throckmorton, C. K., 1981, 130,000-yr continuous pollen record from Clear Lake, Lake County, California: Geology, v. 9, p. 373-377.

Adam, D. P., and West, G. J., 1983, Temperature and precipitation estimates through the last glacial cycle from Clear Lake, California, Pollen Data: Science, v. 219, p. 168-171.

Ahnert, F., 1970, A comparison of theoretical slope models with slopes in the field: Zeitschrift Fur Geomorphologie Supplementband, v. 9, p. 88-101.

Allegre, C. J., Dupre, B., Negrel, P., and Gaillardet, J., 1996, Sr-Nd-Pb isotopic systematics in Amazon and Congo River systems: Constraints about erosion processes: Chemical Geology, v. 131, p. 93-112.

Allen, C. M., Barnes, C. G., and Campbell, I. H., 2002, U-Th-U ages from Klamath River detrital zircons using LA-ICP-MS: Geological Society of America-Abstracts with Programs, v. 34, no. 6, p. 434.

Alley, R. B., Clark, P. U., Keigwin, L. D., and Webb, R. S., 1999, Making Sense of Millennial-Scale Climate Change, *in* Clark, P. U., Webb, R. S., and Keigwin, L. D., eds., Mechanisms of Global Climate Change at Millennial Time Scales: Washington, D.C., American Geophysical Union, p. 394p.

Anders, A. M., Roe, G. H., Hallet, B., Montgomery, D. R., Finnegan, N. J., and Putkonen, J., 2006, Spatial patterns of precipitation and topography in the Himalaya, *in* Willett, S., Hovius, N., Brandon, M. T., and Fisher, D. M., eds., Tectonics, Climate, and Landscape Evolution: Boulder, CO, The Geological Society of America.

Barnes, C. G., 1987, Mineralogy of the Wooley Creek batholith, Slinkard pluton and related dikes, Klamath Mountains, northern California: American Mineralogist, v. 72, p. 879-901.

Barnes, C. G., Barnes, M. A., and Kistler, R. W., 1992, Petrology of the Caribou Mountain Pluton, Klamath Mountains, California: Journal of Petrology, v. 33, no. 1, p. 95-124.

Barnes, C. G., Rice, J. M., and Gribble, R. F., 1986, Tilted plutons in the Klamath Mountains of California and Oregon: Journal of Geophysical Research, v. 91, no. B6, p. 6059-6071.

Beaumont, C., Fullsack, P., and Hamilton, J., 1992, Erosional control of active compressional systems, *in* McClay, K. R., ed., Thrust Tectonics: New York, Chapman Hall, p. 1-18.

Benito, G., and O'Conner, J. E., 2003, Number and size of last-glacial Missoula floods in the Columbia River valley between the Pasco Basin, Washington, and Portland, Oregon Geological Society of America Bulletin, v. 115, no. 5, p. 624-638.

Benson, L. V., Kashgarian, M., and Rubin, M., 1995, Carbonate deposition, Pyramid Lake

subbasin, Nevada; 2: Lake levels and polar jet stream positions reconstructed from radiocarbon ages and elevations of carbonates (tufas) deposited in the Lahontan Basin: Palaeogeog., Palaeoclim., Palaeoecol., v. 117, p. 1-30.

Bernet, M., Brandon, M. T., Garver, J. I., and Molitor, B., 2004, Fundamentals of detrital zircon fission-track analysis for provenance and exhumation studies with examples from the European Alps, *in* Bernet, M., and Spiegel, C., eds., Detrital Thermochronology - Provenance analysis, exhumation and landscape evolution of mountain belts: Boulder, Colorado, Geological Society of America Special Paper 378, p. 25-36.

Bevis, K. A., 1995, Reconstruction of Late Pleistocene paleoclimatic characteristics in the Great Basin and adjacent areas [Ph.D. thesis]: Oregon State University, 277 p.

Biscaye, P. E., 1965, Mineralogy and sedimentation of recent deep-sea clays in the Atlantic Ocean and adjacent seas and oceans: Geological Society of America Bulletin, v. 76, p. 803-832.

Blake, M. C., and Jones, D. L., 1981, The Franciscan melange in northern California: A reinterpretation, *in* W.G., E., ed., The geotectonic evolution of California: Englewood Cliffs, NJ, Prentice Hall, p. 306-328.

Bond, G. C., Showers, W., Cheseby, M., Lotti, R., Almasi, P., deMenocal, P., Cullen, H., Hajdas, I., and Bonani, G., 1997, A pervasive millennial-scale cycle in North Atlantic Holocene and glacial climates: Science, v. 278, p. 1257-1266.

Brady, J. B., 1995, Diffusion data for silicate minerals, glasses and liquids, *in* Ahrens, T. J., ed., A handbook of physical constants: Mineral physics and crystallography (Vol.2): Washington D.C., American Geophysical Union, p. 269-290.

Brandon, M. T., and Vance, J. A., 1992, Tectonic evolution of the Cenozoic Olympic subduction complex, Washington state, as deduced from fission track ages for detrital zircons: American Journal of Science, v. v. 292, p. p. 565-636.

Bretz, J. H., 1969, The Lake Missoula floods and the Channeled Scabland: Journal of Geology, v. 77, p. 505–543.

Burbank, D. W., 2002, Rates of erosion and their implications for exhumation: Mineralogical Magazine, v. 66, no. 1, p. 25-52.

Burbank, D. W., Blythe, A. E., Putkonen, J., Pratt-Sitaula, B., Gabet, E., Oskin, M., Barros, A. P., and Ojha, T. P., 2003, Decoupling of erosion and precipitation in the Himalayas: Nature, v. 426, no. 11 December 2003, p. 652-655.

Carrapa, B., Wijbrams, J., and Bertolli, G., 2004, Detecting provenance variations and cooling patterns within the western Alpine orogen through $^{40}Ar/^{39}Ar$ geochronology on detrital sediments: The Tertiary Piedmont Basin, northwest Italy, *in* Bernet, M., and Spiegel, C., eds., Detrital Thermochronology - Provenance analysis, exhumation, and

landscape evolution of mountain belts: Boulder, Colorado, The Geological Society of America, p. 67-103.

Carter, A., 1999, Present status and future avenues of source region discrimination and characterization using fission track analyses: Sedimentary Geology, v. 124, p. 31-45.

Carter, A., and Bristow, C. S., 2003, Linking hinterland evolution and continental basin sedimentation by using detrital zircon thermochronology; a study of the Khorat Plateau basin, eastern Thailand: Basin Research, v. 15, no. 2, p. 271-285.

Clark, P. U., Keigwin, L. D., and Webb, R. S., 1999, Making Sense of Millennial-Scale Climate Change, Mechanisms of Global Climate Change at Millennial Time Scales: Washington, D.C., American Geophysical Union, 394p.

Clift, P., Carter, A., Campbell, I. H., Pringle, M. S., Van Lap, N., Allen, C. M., Hodges, K. V., and Tan, M. T., 2006, Thermochronology of mineral grains in the Red and Mekong Rivers, Vietnam: Provenance and exhumation implications for Southeast Asia: Geochemistry, Geophysics, Geosystems, v. 7, no. 10, p. doi:10.1029/2006GC001336.

Clift, P. D., 2006, Controls on the erosion of Cenozoic Asia and the flux of clastic sediment to the ocean: Earth and Planetary Science Letters, v. 241, p. 571-580.

Clift, P. D., and Blusztajn, J., 2005, Reorganization of the western Himalaya river system after five million years ago: Nature, v. 438, no. doi:10.1038, p. 1001-1003.

Clift, P. D., Campbell, I. H., Zhang, X., Carter, A., Hodges, K. V. K., A.A., and Allen, C. M., 2004, Thermochronology of the modern Indus River bedload: New insight into the controls on the marine stratigraphic record: Tectonics, v. 23, no. 5.

Clift, P. D., Lee, J. I., Hildebrand, P., Shimizu, N., Layne, G. D., Blum, J. D., Garzanti, E., and Khan, A. A., 2002, Nd and Pb isotope variability in the Indus River system: Implications for crustal heterogeneity in the Western Himalaya: Earth and Planetary Science Letters, v. 200, p. 91-106.

Clift, P. D., Shimizu, N., Layne, G. D., and Blusztajn, J., 2001, Tracing patterns of erosion and drainage in the Paleogene Himalaya through ion probe Pb isotope analysis of detrital K-feldspars in the Indus Molasse, India: Earth and Planetary Science Letters, v. 188, no. 3-4, p. 475-491.

CLIMAP, M., 1981, *in* MC-3, M. a. C. S., ed., Geological Society of America.

Copeland, P., Harrison, M., and Heizler, M. T., 1990, $^{40}Ar/^{39}Ar$ single-crystal dating of detrital muscovite and K-feldspar from Leg 116, southern Bengal Fan: Implications for uplift and erosion of the Himalayas, *in* Cochran, J. R., Stow, D. A. V., and et al., eds., Proceedings of the Ocean Drilling Program: Scientific Results: College Station, TX, Ocean Drilling Program, p. 93-114.

Dadson, S. J., Hovius, N., Chen, H., Dade, B. W., Hsieh, M., Willett, S. D., Hu, J., Horng, M., Chen, M., Stark, C. P., and Lin, J., 2003, Links between erosion, runoff variability and

seismicity in the Taiwan orogen: Nature, v. 426, p. 648-651.

Dalrymple, G. B., Alexander, E. C., Jr., Lanphere, M. A., and Kraker, G. P., 1981, Irradiation of samples for $^{40}Ar/^{39}Ar$ dating using the Geological Survey TRIGA reactor: U. S. Geological Survey Professional Paper.

Dalrymple, G. B., and Lanphere, M. A., 1969, Potassium-argon dating: Principles, techniques and applications to geochronology: San Francisco, W.H. Freeman and Co., 258 p.

Darby, D. A., 2003, Sources of sediment found in sea ice from the western Arctic Ocean, new insights into processes of entrainment and drift patterns: Journal of Geophysical Research, v. 108, no. C8, p. 3257.

Deer, W. A., Howie, R. A., and Zussman, J., 1992, An introduction to rock-forming minerals: New York, John Wiley and Sons, Inc, 696 p.

Dong, H., Hall, C. M., Peacor, D. R., and Halliday, A. N., 1995, Mechanisms of argon retention in clays revealed by laser ^{40}Ar-^{39}Ar dating: Science, v. 267, p. 355-359.

Drever, J. I., and Clow, D. W., 1995, Weathering rates in catchments, *in* White, A. F., and Brantley, S. L., eds., Chemical weathering rates in silicate minerals: Washington, D.C., Mineralogical Society of America, p. 463-481.

Duncan, J. R., Kulm, L. D., and Griggs, G. B., 1970, Clay mineral composition of the Late Pleistocene and Holocene sediments of the Cascadia basin, northeastern Pacific Ocean: Journal of Geology, v. 78, p. 213-221.

Fagel, N., Hillaire-Marcel, C., Humblet, M., Brasseur, R., Wieis, D., and Stevenson, R., 2004, Nd and Pb isotope signatures of the clay-size fraction of Labrador Sea sediments during the Holocene: Implications for the inception of the modern deep circulation pattern Paleoceangraphy, v. 19, p. doi:10.1029/2003PA000993.

Fagel, N., Innocent, C., Gariepy, C., and Hillaire-Marcel, C., 2002, Sources of Labrador Sea sediments since the last glacial maximum inferred from Nd-Pb isotopes: Geochimica et Cosmochimica Acta, v. 66, no. 14, p. 2569-2581.

Fagel, N., Innocent, C., Stevenson, R., Gariepy, C., and Hillaire-Marcel, C., 1996, A high resolution Nd and Pb isotopic study of Labrador Sea clays at the 2/1 transition; implications for sedimentary supplies and deep circulation changes: Enriched: AGU 1996 fall meeting Eos, Transactions, American Geophysical Union, v. 77, no. 46, p. 324.

Faure, G., 1986, Principles of isotope geology: New York, John Wiley and Sons, 589 p.

Fechtig, H., and Kalbitzer, S., 1966, The diffusion of argon in potassium-bearing solids, *in* Schaeffer, O. E., and Zahringer, J., eds., Potassium Argon Dating: Berlin-Heidelberg, Springer-Verlag, p. 68-107.

Ferrier, K. L., Kirchner, J. W., and Finkel, R., 2005, Erosion rates over millennial and decadal timescales at Caspar Creek ad Redwood Creek, Northern California Coast Ranges: Earth Surface Processes and Landforms, v. 30, p. 1025-1038.

Fleck, R. J., 1990, Neodymium, strontium and trace-element evidence of crustal anatexis and magma mixing in the Idaho Batholith, *in* Anderson, J. L., ed., The nature and origin of Cordilleran magmatism: Boulder, CO, The Geological Society of America, p. 359-374.

Gaillardet, J., Dupre, B., Allegre, C. J., and Negrel, P., 1997, Chemical and physical denudation in the Amazon River Basin: Chemical Geology, v. 142, p. 141-173.

Garzanti, E., Critelli, S., and Ingersoll, R. V., 1996, Paleogeographic and paleotectonic evolution of the Himalayan Range as reflected by detrital modes of Tertiary sandstones and modern sands (Indus transect, India and Pakistan): Geological Society of America Bulletin, v. 108, no. 6, p. 631-642.

Garzanti, E., Vezzoli, G., Andò, S., Paparella, P., and Clift, P. D., 2005, Petrology and mineralogy of Indus River sands: A key to interpret erosion history of the Western Himalayan Syntaxis: Earth and Planetary Science Letters, v. 229, p. 287–302.

Ghosh, D., 1995, Nd-Sr isotopic constraints on the interactions of the intermontane Superterrane with the western edge of North America in the southern Canadian Cordillera: Can. Jour. Earth Sci., v. 32, p. 1740-1758.

Gillespie, A. R., Huneke, J. C., and Wasserburg, G. J., 1982, An assessment of ^{40}Ar-^{39}Ar dating of incompletely degassed xenoliths: Journal of Geophysical Research, v. 87, no. B11, p. 9247-9257.

Goldstein, S. L., and Jacobsen, S. B., 1988, Nd and Sr isotopic systematics of river water suspended material: Implications for crustal evolution: Earth and Planetary Science Letters, v. 87, p. 249-265.

Goldstein, S. L., O'Nions, R. K., and Hamilton, P. J., 1984, A Sm-Nd isotopic study of atmospheric dusts and particulates from major river systems: Earth and Planetary Science Letters, v. 70, p. 221-236.

Hakala, K. J., and Adam, D. P., 2004, Late Pleistocene vegetation and climate in the southern Cascade Range and the Modoc Plateau region: Journal of Paleolimnology, no. 31.

Harrison, T. M., Duncan, I., and McDougall, I., 1985, Diffusion of ^{40}Ar in biotite: Temperature, pressure and compositional effects: Geochimica et Cosmochimica Acta, v. 49, p. 2461-2468.

Haugerud, R. A., 1999, Digital elevation model (DEM) of Cascadia, latitude 39N-53N, longitude 116W-133W.

Heath, G. R., and Pisias, N. G., 1979, A method for the quantitative estimation of clay

minerals in North Pacific deep-sea sediments: Clays and Clay Minerals, v. 27, no. 3, p. 175-184.

Hebbeln, D., Lamy, F., Mohtadi, M., and Echtler, H., 2007, Tracing the impact of glacial-interglacial climate variability on erosion of the southern Andes Geology, v. 35, no. 2, p. 131-134.

Heimsath, A. M., Dietrich, W. E., Nishiizumi, K., and Finkel, R. C., 2001, Stochastic processes of soil production and transport: Erosion rates, topographic variation and cosmogenic nuclides in the Oregon Coast Range: Earth Surface Processes and Landforms, v. 26, p. 531-552.

Heller, P. L., Peterman, Z. E., O'Neil, J. R., and Shafiqullah, M., 1985, Isotopic provenance of sandstones from the Eocene Tyee Formation, Oregon Coast Range: GSA Bulletin, v. 96, p. 770-780.

Heller, P. L., Renne, P. R., and O'Neil, J. R., 1992, River mixing rate, residence time, and subsidence rates from isotopic indicators: Eocene snadstones from the U.S. Pacific Northwest: Geology, v. 20, p. 1095-1098.

Hemming, S. R., Broecker, W. S., Sharp, W. D., Bond, G. C., Gwiazda, R. H., McManus, J. F., Klas, M., and Hajdas, I., 1998, Provenance of Heinrich layers in core V28-82, northeastern Atlantic: $^{40}Ar/^{39}Ar$ ages of ice-rafted hornblende, Pb isotopes in feldpar grains, and Nd-Sr-Pb isotopes in the fine sediment fraction: Earth and Planetary Science Letters, v. 164, p. 317-333.

Hemming, S. R., Hall, C. M., Biscaye, S. M., Higgins, S., Bond, G. C., McManus, J. F., Barber, D. C., Andrew, J. T., and Broecker, W. S., 2002, $^{40}Ar/^{39}Ar$ ages and $^{40}Ar^*$ concentrations of fine-grained sediment fractions from North Atlantic Heinrich layers: Chemical Geology, v. 182, p. 583-603.

Heusser, L., 1998, Direct correlation of millenial-scale changes in western North American vegetation and climate with changes in the California Current system over the past 60 kyrs: Paleoceanography, v. 13, no. 3, p. 252-262.

Hickey, B. M., 1979, The California current system—Hypotheses and facts: Progress in Oceanography, v. 8, p. 191–279.

Hickey, B. M., and Banas, N. S., 2003, Oceanography of the U.S. Pacific Northwest Coastal Ocean and Estuaries with Application to Coastal Ecology: Estuaries, v. 26, no. 4B, p. 1010-1031.

Hickey, B. M., and Royer, T., 2001, California and Alaskan Currents, *in* Steele, J. H., Thorpe, S. A., and Turekian, K. A., eds., Encyclopedia of Ocean Sciences: San Diego, California, Academic Press, p. 368–379.

Hodges, K. V., Ruhl, K. W., Wobus, C. W., and Pringle, M. S., 2005, $^{40}Ar/^{39}Ar$ thermochronology of detrital minerals, *in* Reiners, P. W., and Ehlers, T. A., eds.,

Low-Temperature Thermochronology: Techniques, Interpretations, and Applications: Reviews in mineraology and geochemistry.

Hostetler, S., Pisias, N., and Mix, A., 2006, Senstivity of the Last Glacial Maximum climate to uncertainties in the tropical and subtropical ocean temperatures: Quaternary Science Reviews, v. 25, p. 1168-1185.

Hostetler, S. W., Clark, P. U., Bartlein, P. J., Mix, A. C., and Pisias, N. G., 1999, Atmospheric transmission of North Atlantic Heinrich events: Journal of Geophysical Research, v. 104, p. 3947-3952.

Hostetler, S.W., Giorgi, F., Bates, G.T., Bartlein, P.J., 1994. Lake–atmosphere feedbacks associated with paleolakes Bonneville and Lahontan. Science, 263, 665–668.

Howard, A. D., 1994, A detachment-limited model of drainage basin evolution: Water Resources research, v. 30, p. 2261-2285.

-, 1998, Long profile development of bedrock channels: Interaction of weathering, mass wasting, bed erosion and sediment transport, *in* Tinkler, K. J., and Wohl, E. E., eds., Rivers over rock: Fluvial processes in bedrock channels: Washington, American Geophysical Union, p. 323.

Huntington, K. W., and Hodges, K. V., 2006, A comparative study of detrital mineral and bedrock age-elevation methods for estimating erosion rates: Journal of Geophysical Research, v. 111, no. F03011, p. doi:10.1029/2005JF000454

Irwin, W. P., 1997, Preliminary map of selected post-Nevadan geologic features of the Klamath Mountains and adjacent areas, California and Oregon: U.S. Geological Survey Open-File Report, v. 97-465, p. 29p.

Irwin, W. P., and Wooden, J. L., 1999, Plutons and accretionary episodes of the Klamath mountains, California and Oregon.

Jantschik, R., and Huon, S., 1992, Detritial silicates in northeast Atlantic deep-sea sediments during the Late Quaternary: Mineralogical and K-Ar isotopic data: Eclogae geol. Helv., v. 85, no. 1, p. 195-212.

Johnson, B. R., and Raines, G. L., 1995, Digital map of major bedrock lithologic units for the Pacific Northwest: a contribution to the Interior Columbia Basin Ecosystem Management Project.

Karlin, R., 1980, Sediment Sources and Clay Mineral Distributions Off the Oregon Coast: JSP, v. 50, no. 2, p. 543-560.

Kirby, E., Reiners, P. W., Krol, M. A., Whipple, K. X., Hodges, K. V., Farley, K. A., Tang, W., and Chen, Z., 2002, Late Cenozoic evolution of the eastern margin of the Tibetan Plateau: Inferences from $^{40}Ar/^{39}Ar$ and (U-Th)/He thermochonology: Tectonics, v. 21, no. 1, p. doi:10.1029/2000TC001246.

Kirchner, J. W., Finkel, R., Riebe, C. S., Granger, D. E., Clayton, J. L., King, J. G., and Megahan, W. F., 2001, Mountain erosion over 10 yr, 10 k.y., and 10 m.y. time scales: Geology, v. 29, no. 7, p. 591-594.

Knebel, H. J., Kelly, J. C., and Whetten, J. T., 1968, Clay minerals of the Columbia River: A qualitative, quantitative, and statistical evaluation: Journal of Sedimentary Petrology, v. 38, no. 2, p. 600-611.

Koppers, A. P., 2002, ArArCalc - software for $^{40}Ar/^{39}Ar$ age calculations: Computers & Geosciences, v. 28, p. 605-619.

Kowalewski, M., and Rimstidt, J. D., 2003, Average lifetime and age spectra of detrital grains: Toward a unifying theory of sedimentary particles: Journal of Geology, v. 111, p. 427-439.

Kuhlemann, J., Frisch, W., Dunkl, I., Kazmer, M., and Schmiedl, 2004, Miocene siliciclastic deposits of Naxos Island: Geodynamic and environmental implications for the evolution of the southern Aegean Sea (Greece), *in* Bernet, M., and Spiegel, C., eds., Detrital Thermochronology - Provenance analysis, exhumation, and landscape evolution of mountain belts: Boulder, Colorado, The Geological Society of America, p. 51-65.

Kulm, L. D., Prince, R. A., and Snavely, P. D., Jr., 1973, Site Survey of the northern Oregon continental margin and Astoria Fan: Init. Rep. Deep Sea Dril. Proj., v. v. XVIII, no. Appendix I, Part A, p. p. 979-987.

Lambeck, K., Yokoyama, Y., and Purcell, T., 2002, Into and out of the Last Glacial Maximum: sea-level change during Oxygen Isotope Stages 3 and 2: Quaternary Science Reviews, v. 21, p. 343-360.

Lamy, F., Hebbeln, D., Rohl, U., and Wefer, G., 2001, Holocene rainfall variability in southern Chile: A marine record of latitudinal shifts of the Southern Westerlies: Earth and Planetary Science Letters, v. 185, p. 369-382.

Lamy, F., Hebbeln, D., and Wefer, G., 1998a, Late Quaternary precessional cycles of terrigenous sediment input off the Norte Chico (27.5°S) and paleoclimatic implications: Paleogeography, Paleoclimate, Paleoecology, v. 141, p. 233-251.

-, 1998b, Late Quaternary precessional cycles of terrigenous sediment input off the Norte Chico, Chile (27.5 °S) and palaeoclimatic implications: Palaeogeography, Palaeoclimatology, Palaeoecology, v. 141, p. 233-251.

-, 1999, High resolution marine record of climatic change in mid-latitude Chile during the last 28 ka based on terrigenous sediment parameters: Quaternary Research, v. 51, p. 83-93.

Langmuir, C. H., Vocke, R. D., Hanson, G. N., and Hart, S. R., 1978, A general mixing equation with applications to Icelandic basalts: Earth and Planetary Science Letters, v. 37, p. 380-382.

Lisitzin, A. P., 1996, Oceanic sedimentation: Lithology and geochemistry: Washington D.C., American Geophysical Union, 399 p.

Liu, Z., Colin, C., Trentesaux, A., Blamart, D., Bassinot, F., Siani, G., and Sicre, M.-A., 2004, Erosional history of the eastern Tibetan Plateau since 190 kyr ago; clay mineralogical and geochemical investigations from the southwestern South China Sea: Marine Geology, v. 209, no. 1-4, p. 1-18.

Logan, J. M., 2002, Intrusion related mineral occurrences of the Cretaceous Bayonne Magmatic Belt, southeast British Columbia.

Lovera, O. M., Grove, M., Harrison, T. M., and Mahon, K. I., 1997, Systematic analysis of K-feldspar $^{40}Ar/^{39}Ar$ step heating results: I. Significance of activation energy determinations: Geochimica et Cosmochimica Acta, v. 61, no. 15, p. 3171-3192.

Lyle, M., Mix, A. M., Ravelo, C., Andreasen, D., Heusser, L., and Olivarez, A., 2000, Millennial-scale $CaCO_3$ and C_{org} events along the northern and central California margins: stratigraphy and origins, *in* Lyle, M., Koizumi, I., Richter, C., and Moore, T. C., Jr., eds., Proceedings of the Ocean Drilling Program, Scientific Results: College Station, TX.

McDougall, I., and Harrison, T. M., 1999, Geochronology and thermochronology by the $^{40}Ar/^{39}Ar$ method: New York, Oxford University Press, 269 p.

McLaughlin, R. J., Sliter, W. V., Fredriksen, N. O., Harbert, W. P., and McCulloch, D. S., 1994, Plate motions recorded in tectonostratigraphic terranes of the Franciscan Complex and evolution of the Mendocino Triple Junction, Northwestern California.

Merritts, D., and Vincent, K. R., 1989, Geomorphic response of coastal streams to low, intermediate, and high rates of uplift, Mendocino triple junction region, California: Geological Society of America Bulletin, v. 101, no. 11, p. 1373-1388.

Mix, A. C., Lund, D. C., Pisias, N., Boden, P., Bornmalm, L., Lyle, M., and Pike, J., 1999, Rapic climate oscillations in the northeast Pacific during the last deglaciation reflect northern and southern hemisphere sources, *in* Clark, P. U., Webb, R. S., and Keigwin, L. D., eds., Mechanisms of Global Climate Change at Millennial Time Scales: Washington D.C., American Geophysical Union.

Molnar, P., 2003, Nature, Nurture and landscape: Nature, v. 426, p. 612-614.

Molnar, P., Anderson, R. S., Kier, G., and Rose, J., 2006, Relationships among probability distributions of stream discharges in floods, climate, bed load transport, and river incision: Journal of Geophysical Research, v. 111, no. F02001 p. 10.1029/2005JF000310.

Monger, J. W., Price, R. A., and Templeman-Kluit, D. J., 1982, Tectonic accretion and the origin of the two major metamorphic and plutonic belts in the Canadian Cordillera: Geology, v. 10, p. 70-75.

Montgomery, D. R., and Dietrich, W. E., 1994, A physically-based model for the topographic control on shallow landsliding: Water Resources Research, v. 30, p. 1153-1171.

Moore, D. M., and Reynolds, R. C., 1989, X-ray diffraction and the identification and analysis of clay minerals: New York, Oxford University Press, 332 p.

Mueller, P. A., Shuster, R. D., D'Arcy, K. A., Heatherington, A. L., Nutman, A. P., and Williams, I. S., 1995, Source of the northeastern Idaho Batholith: Isotopic evidence for a Paleoproterozoic terrane in the northwestern U.S.: Journal of Geology, v. 103, p. 63-72.

Najman, Y., Carter, A., Oliver, G., and Garzanti, E., 2005, Provenance of Eocene foreland basin sediments, Nepal; constraints to the timing and diachroneity of early Himalayan orogenesis: Geology Boulder, v. 33, no. 4, p. 309-312.

Negrini, R. M., 2002, Pluvial lake sizes in the northwestern Great Basin throughout the Quaternary period, *in* Hershler, R., Madsen, D. B., and Currey, D. R., eds., Great Basin aquatic systems history: Washington, D.C., Smithsonian Institution, p. 11-52.

Nolan, K. M., and Janda, R. J., 1995, Impacts of logging on stream sediment discharge in the Redwood Creek Basin: US Geological Survey Professional Paper, v. 1454.

Personius, S., Kelsey, H. M., and Grabau, P. C., 1993, Evidence for regional stream aggradation in the central Oregon Coast Range during the Pleistocene-Holocene transition: Quaternary Research, v. 40, p. 297-308.

Peterson, C., Scheidegger, K. F., and Komar, P., 1982, Sand-dispersal patterns in an active-margin estuary of the northwestern United States as indicated by sand composition, texture and bedforms: Marine Geology, v. 50, no. 1-2, p. 77-96.

Peterson, C., Scheidegger, K. F., P, K., and Niem, W., 1984, Sediment composition and hydrography in six high-gradient estuaries of the northwestern United States: Jour. Sed. Petrology, v. 54, no. 1, p. 86-97.

Pettke, T., Halliday, A. N., Hall, C. M., and Rea, D. K., 2000, Dust production and deposition in Asia and the north Pacific Ocean over the past 12 Myr: Earth and Planetary Science Letters, v. 178, p. 397-413.

Peucker-Ehrenbrink, B., and Miller, M. W., 2002, Quantitative bedrock geology of the conterminous United States of America: Geochemistry, Geophysics, Geosystems, v. 3, no. 10, p. doi:10.1029/2002GC000366.

Pisias, N., Sancetta, C., and Dauphin, P., 1973, Spectral analysis of late Pleistocene-Holocene sediments: Quaternary Research, v. 3, p. 3-9.

Pisias, N. G., Mix, A. C., and Heusser, L., 2001, Millennial scale climate variability of the northeast Pacific Ocean and northwest North America based on radiolaria and pollen: Quaternary Science Reviews, v. 20, p. 1561-1576.

Porter, S. C., Pierce, K. L., and Hamilton, T. D., 1983, Late Wisconsin glaciation in the Western United States, *in* Porter, S. C., ed., Late-Quaternary environments of the United States: Minneapolis, Univ. of Minnesota Press, p. 71-111.

Reiners, P. W., 2005, Zircon (U-Th)/He Thermochronometry, *in* Reiners, P. W., and Ehlers, T. A., eds., Low-Temperature Thermochronology: Techniques, Interpretations, and Applications, p. 151-179.

Reiners, P. W., Campbell, I. H., Nicolescu, S., Allen, C. M., Hourigan, J. K., Garver, J. I., Mattinson, J. M., and Cowan, D. S., 2005a, (U-Th)/(He-Pb) Double Dating Of Detrital Zircons: American Journal of Science, v. 305, p. 259-311.

Reiners, P. W., Ehlers, T. A., and Zeitler, P. K., 2005b, Past, present, and future of thermochronology, *in* Reiners, P. W., and Ehlers, T. A., eds., Low-Temperature Thermochronology: Techniques, Interpretations, and Applications, p. 1-18.

Reiners, P. W., Ehlers, T. A., Mitchell, S. G., and Montgomery, D. W., 2003, Coupled spatial variations in precipitation and long-term erosion rates across the Washington Cascades: Nature, v. 426, p. 645-647.

Reneau, S. L., and Dietrich, W. E., 1991, Erosion rates in the southern Oregon Coast Ranges: evidence for an equilibrium between hillslope erosion and sediment yield: Earth Surface Processes and Landforms, v. 16, p. 307-322.

Renne, P. R., Deino, A. L., Walter, R. C., Turrin, B. D., Swisher, C. C., Becker, T. A., Curtis, G. H., Sharp, W. D., and Jaouni, A.-R., 1994, Intercalibration of astronomical and radioisotopic time: Geology, v. 22, p. 783-786.

Rosenbaum, J. G., and Reynolds, R. L., 2004, Record of Late Pleistocene glaciation and deglaciation in the southern Cascade Range. II. Flux of glacial flour in a sediment core from Upper Klamath Lake, Oregon: Journal of Paleolimnology, v. 31, p. 235-252.

Roy, M., Clark, P. U., Duncan, R. A., and Hemming, S. R., 2005, Constraints on a long-lived Keewatin ice dome from $^{40}Ar/^{39}Ar$ dating of mineral grains from midcontinent glacial deposits.

Ryu, I., and Niem, A. R., 1999, Sandstone diagenesis, reservoir potential and sequence stratigraphy of the Eocene Tyee Basin, Oregon: Journal of Sedimentary Research, v. 69, no. 2, p. 384-393.

Sharp, R. P., 1960, Pleistocene glaciation in the Trinity Alps of northern California: American Journal of Science, v. 258, p. 305-340.

Sherwood, C. R., Jay, D. A., Harvey, R. B., Hamilton, P., and Simenstad, C. A., 1990, Historical changes in the Columbia River estuary: Progress in Oceanography, v. 25, p. 299-352.

Shuster, D. L., Ehlers, T. A., Rusmore, M. E., and Farley, K. A., 2005, Rapid Glacial Erosion

at 1.8 Ma Revealed by $^{4}He/^{3}He$ Thermochronometry: Science, v. 310, p. 1668-1670.

Shuster, D. L., and Farley, K. A., 2005, $^{4}He/^{3}He$ Thermochronometry: Theory, Practice, and Potential Complications, *in* Reiners, P. W., and Ehlers, T. A., eds., Low-Temperature Thermochronology: Techniques, Interpretations, and Applications, p. 181-203.

Sklar, L. S., and Dietrich, W. E., 1998, River longitudinal profiles and bedrock incision models: Stream power and the influence of sediment supply, *in* Tinkler, K. J., and Wohl, E. E., eds., Rivers Over Rock: Fluvial Processes in Bedrock Channels: Washington, American Geophysical Union, p. 237-259.

Smith, G. I., and Street-Perrott, F. A., 1983, Pluvial lakes of the western United States, The late Pleistocene: Minneapolis, University of Minnesota Press, 190-210 p.

Snyder, N. P., Whipple, K. X., Tucker, G. E., and Merritts, D. J., 2000, Landscape response to tectonic forcing: Digital elevation model analysis of stream profiles in the Mendocino triple junction region, northern California: GSA Bulletin, v. 112, no. 8, p. 1250-1263.

Spiegel, C., Siebel, W., Kuhlemann, J., and Frisch, W., 2004, Toward a comprehensive provenance analysis: A multi-method approach and its implications for the evolution of the Central Alps, *in* Bernet, M., and Spiegel, C., eds., Detrital Thermochronology - Provenance analysis, exhumation, and landscape evolution of mountain belts: Boulder, Colorado, The Geological Society of America, p. 37-50.

Strub, P. T., Allen, J. S., Huyer, A., and Smith, R. L., 1987, Large-scale structure of the spring transition in the coastal ocean off western North America: Journal of Geophysical Research, v. 92, p. 1527–1544.

Stuiver, M., and Grootes, P. M., 2000, GISP2 oxygen isotope ratios: Quaternary Research, v. 53, p. 277-284.

Syvitski, J.P.M., Morehead, M., Nicholson, M., 1998. HYDROTREND: a climate-driven hydrologic-transport model for predicting discharge and sediment load to lakes or oceans. Comput. Geosci. 24, 51–68.

Syvitski, J. P. M., and Morehead, M. D., 1999, Estimating river-sediment discharge to the ocean: application to the Eel margin, northern California: Marine Geology, v. 154, p. 13-28.

Syvitski, J. P. M., Vorosmarty, C. J., Kettner, A. J., and Green, P., 2005, Impact of Humans on the Flux of Terrestrial Sediment to the Global Coastal Ocean Science, v. 308, p. 376-380.

Tanaka, T., Shigeko Togashib, Hikari Kamiokab, Hiroshi Amakawac, Hiroo Kagamid, Takuji Hamamotod, Masaki Yuharad, Yuji Orihashie, Shigekazu Yonedaf, Hiroshi Shimizug, Takanori Kunimarug, Kazuya Takahashih, Takeru Yanagii, Takanori Nakanoj, Hirokazu Fujimakik, Ryuichi Shinjol, Yoshihiro Asaharaa, Tanimizua, M., and Dragusanua, C., 2000, JNdi-1: a neodymium isotopic reference in consistency with

LaJolla neodymium: Chemical Geology v. 168, no. 3-4, p. 279-281.

Turcotte, D. L., and Greene, L., 1993, A scale-invariant approach to flood-frequency analysis: Stochastic Environmental Research and Risk Assessment, v. 7, no. 10.1007/BF01581565, p. 33-40.

Turner, G., and Cadogan, P. H., 1974, Possible effects of ^{39}Ar recoil in ^{40}Ar-^{39}Ar dating: Geochimica et Cosmochimica Acta, v. 5, no. 2, p. 1601-1615.

VanLaningham, S., Duncan, R. A., and Pisias, N. G., 2006, Erosion by rivers and transport pathways in the ocean: A provenance tool using ^{40}Ar-^{39}Ar incremental heating on fine-grained sediment: Journal of Geophysical Research, v. 111, no. F04014, p. doi:10.1029/2006JF000583.

Verplanck, E. P., and Duncan, R. A., 1987, Temporal variations in plate convergence and eruption rates in the Western Cascades, Oregon: Tectonics, v. 6, p. 197-209.

Vorosmarty, C. J., Meybeck, M., Fekete, B., Sharma, K., Green, P., and Syvitski, J. M., 2003, Anthropogenic sediment retention: major global impact from registered river impoundments: Global and Planetary Change, v. 39, no. 169-190.

Walczak, P. W., 2006, Submarine plateau volcanism and Cretaceous Ocean Anoxic Event 1a : geochemical evidence from Aptian sedimentary sections: Oregon State University, 172 p.

Walker, G. W., and MacLeod, N. S., 1991, Geologic Map of Oregon: U.S. Geological Survey, scale 1:500,000.

Walter, H. J., Hegner, E., Diekmann, B., Kuhn, G., and Rutgers van der loeff, M. M., 2000, Provenance and transport of terrigenous sediment in the South Atlantic Ocean and their relations to glacial and interglacial cycles: Nd and Sr isotopic evidence: Geochimica et Cosmochimica Acta, v. 64, no. 22, p. 3813-3827.

Wang, S., McDougall, I., Tetley, N., and Harrison, T. M., 1980, ^{40}Ar/^{39}Ar age and thermal history of the Kirin Chondrite: Earth and Planetary Science Letters, v. 49, p. 117-131.

Wasserburg, G. J., Jacobsen, S. B., DePaolo, D. J., McCulloch, M. T., and Wen, T., 1981, Precise determinations of Sm/Nd ratios, Sm and Nd isotopic abundances in standarc solutions: Geochim. Cosmochim. Acta, v. 45, p. 2311-2323.

Weide, D. L., 1976, The Warner Valley: A test of pluvial climatic conditions, *in* Fourth Biennial Conference, Abstracts, Arizona State University.

Wells, R. E., Jayko, A. S., Niem, A. R., Black, G., Wiley, T., Baldwin, E., Molenaar, K. M., Wheeler, K. L., DuRoss, C. B., and Givler, R. W., 2000, Geologic map and database of the Roseburg 30 X 60 quadrangle, Douglas and Coos counties, Oregon.

Wendt, I., and Carl, C., 1991, The statistical distribution of the mean standard weighted

deviation: Chemical Geology (Isot. Geosci. Sect.), v. 86, p. 275-285.

Werner, F., and Hickey, B. M., 1983, The role of an alongshore pressure gradient in Pacific Northwest coastal dynamics: Journal of Physical Oceanography, v. 13, p. 395–410.

Wheatcroft, R. A., and Sommerfield, C. K., 2005, River sediment and shelf sediment accumulation rates on the Pacific Northwest margin: Continental Shelf Research, v. 25, p. 311-332.

Whipple, K. X., 2004, Bedrock rivers and the geomorphology of active orogens: Annual Reviews Earth and Planetary Science, v. 32, no. 151–185.

Whipple, K. X., Kirby, E., and Brocklehurst, S. H., 1999, Geomorphic limits to climate-induced increases in topographic relief: Nature, v. 401, p. 39-43.

Whipple, K. X., and Tucker, G. E., 1999, Dynamics of the stream-power river incision model: Implications for height limits of mountain ranges, landscape response timescales, and research needs: Journal of Geophysical Research, v. 104, p. 17661-17674.

Willett, S., 1999, Orogeny and orography: The effects of erosion on the structure of mountain belts: Journal of Geophysical Research, v. 104, no. B12, p. 28,957-28,981.

Willett, S., Hovius, N., Brandon, M. T., and Fisher, D. M., 2006, Introduction, *in* Willett, S., Hovius, N., Brandon, M. T., and Fisher, D. M., eds., Tectonics, Climate, and Landscape Evolution: Boulder, CO, The Geological Society of America.

Willett, S. D., Fisher, D., Fuller, C., En-Chao, Y., and Lu, C.-Y., 2003, Erosion rates and orogenic-wedge kinematics in Taiwan inferred from fission-track thermochronometry: Geology, v. 31, no. 11, p. 945-948.

Wobus, C. W., Hodges, K. V., and Whipple, K. X., 2003, Has focused denudation sustained active thrusting at the Himalayan topographic front?: Geology, v. 31, no. 10, p. 861-864.

Wobus, C. W., Whipple, K. X., Kirby, E., Snyder, N. P., Johnson, J., Spyropolou, K., Crosby, B. T., and Sheehan, D., 2006, Tectonics from topography: Procedures, promise and pitfalls, *in* Willett, S. D., Hovius, N., Brandon, M. T., and Fisher, D., eds., Tectonics, Climate and Landscape Evolution: Geological Society of America Special Paper 398: Boulder, CO, Geological Society of America, p. 55-74.

Wolf, S. C., Nelson, H., Hamer, M. R., Dunhill, G., and Phillips, R. L., 1999, The Washington and Oregon mid-shelf silt deposit and its relation to the late Holocene Columbia River sediment budget.

Woods, M. C., 1976, Pleistocene Glaciation in the Canyon Creek area, Trinity Alps, California: California Geology, p. 109-113.

Worona, M. A., and Whitlock, C., 1995, Late Quaternary vegetation and climate history near

Little Lake, central Coast Range, Oregon: GSA Bulletin, v. 107, no. 7, p. 867-876.

Zhang, G., Germaine, J. T., Martin, R. T., and Whittle, A. J., 2003, A simple sample-mounting method for random powder X-ray diffraction: Clays and Clay Minerals, v. 51, no. 2, p. 218-225.

Zuffa, G. G., de Rosa, R., and Normark, W. R., 1997, Shifting sources and transport paths for the later Quaternary Escanaba Trough sediment fill (northeast Pacific): Giornale di Geologia, v. 59, no. 1/2, p. 35-53.

Appendices

Appendix A

Clay Mineralogy of Pacific Northwest River and Core EW9504-17PC Sediments

Clay Mineral Analyses

River and core sediment samples were analyzed for their clay mineral content. Focus was placed on the major clays smectite, illite and kaolinite+chlorite. Samples were prepared using the following procedure. About 100-300 g of bulk sample was washed with DI water through a 63 μm sieve into a 1000 ml beaker. Sample in beaker is then poured into one to four 250 ml bottles. 250 ml bottles are centrifuged at 7500 rpm for 5 minutes and decanted to remove most DI water. Samples in centrifuged 250 ml bottles are washed with DI water into a 1000 ml beaker. 50 ml of H_2O_2 is added to beaker and stirred occasionally under a hood. Once samples seemed relatively stable, they were poured into 250 ml bottles. Another 30-50 ml H_2O_2 was added and samples were shaken in 250 ml bottles on a shaker table for 60-72 hours. Then, samples were centrifuged to remove excess H_2O_2. Specifically, samples were run in a centrifuge for 5 minutes at 7500 rpm three times to wash the sample.

To remove carbonate, buffered acetic acid was used. 125 ml of glacial acetic acid was mixed with 410g of Na Acetate. Samples in 250 ml bottles were filled to about 3/4 full with the buffered solution and put on shaker table for 24-48 hrs. Size separation of 20-63, 2-20, 0-2 μm was then carried out. Settling times were used for separating 20-63 μm from the 0-20 μm sediment. Specifically, samples were placed in a 250 ml bottle and filled with DI water to 8-10 cm height. The sample were shaken vigorously and then allowed to sit for 3 minutes, 25 seconds. The 0-20 μm material was carefully decanted into a 1000 ml beaker, being careful not to pour off any of the coarse 20-63 μm. This was repeated until supernatant was relatively clear. Then to separate the 0-2 μm from the 2-20 μm material, samples were vigorously suspended and then centrifuged at 600 for six minutes. The supernatant (0-2 μm) was poured off. This process was repeated repeat until supernatant was clear.

Samples were analyzed for their clay mineral abundances on a Scintag Pad-V X-ray diffractometer (XRD). An internal talc standard was added (10% by weight) to make semi-quantitative calculations of the mineral abundances. Samples were smeared onto slides placed in a glycolthing at ~80°C for ~8 hours. Samples were scanned from 2°-34° 2θ using Cu radiation. The following data table shows the clay mineral abundances and ratios for the main rivers draining into the northeast Pacific Ocean between latitudes 38° N to 48° N. Tributary

samples from the Klamath and Eel River systems were also analyzed as were Quaternary fluvial deposits that may have derived from these river systems in the past. The Gold Bluffs samples are from a paleo-Klamath River while the Hookton, Scotia Bluffs and Carlotta Formations samples are from a paleo-Eel River source. Clay from core EW9504-17PC are also analyzed and shown in the data table.

Talc-normalized clay mineralogy for rivers, selected tributaries, Quaternary fluvial deposits and core sediments in the Pacific Northwest

River	Sample Name	Latitude	Longitude	%sm	%ill	%k+chl	sm/ill	k+chl/ill	sm/k+chl
Quinalt River, WA	QUI-1	47.35	-124.29	2.1	33.4	32.1	0.06	1.0	0.07
	QUI-2	47.35	-124.29	1.7	35.7	37.3	0.05	1.0	0.04
Grays Harbor, WA	GRA-2	46.97	-123.80	33.1	5.6	9.2	5.93	1.6	3.60
	GRA-3	46.97	-123.80	32.5	4.9	12.0	6.63	2.5	2.70
	GRA-1	46.97	-123.90	34.1	7.3	11.8	4.67	1.6	2.90
Willapa Bay	WIL-2	46.72	-123.93	37.3	6.2	10.4	6.01	1.7	3.59
	WIL-1	46.72	-123.92	30.8	7.9	7.3	3.91	0.9	4.22
	WIL-4	46.68	-123.75	57.8	7.5	9.8	7.73	1.3	5.89
	WIL-3	46.68	-123.76	30.0	4.8	4.8	6.25	1.0	6.29
Columbia River	COL-1	46.26	-123.49	23.4	10.7	7.8	2.20	0.7	2.99
	COL-2	46.26	-123.49	18.9	5.0	6.2	3.75	1.2	3.02
	COL-3	46.25	-123.49	17.8	10.3	6.6	1.73	0.6	2.67
	COL-4	46.25	-123.63	15.6	8.4	5.9	1.86	0.7	2.63
	COL-5	46.24	-123.62	19.1	10.2	7.4	1.86	0.7	2.58
Nehalem River	NEH-1	45.72	-123.89	49.4	4.6	6.9	10.82	1.5	7.18
	NEH-2	45.71	-123.89	38.8	4.6	5.5	8.50	1.2	7.01
Tillamook Bay	TIL-3	45.55	-123.92	38.0	3.9	5.4	9.67	1.4	7.02
	TIL-5	45.53	-123.90	23.7	2.0	2.1	11.93	1.0	11.44
	TIL-4	45.53	-123.89	46.1	4.6	5.4	9.93	1.2	8.53
	TIL-1	45.48	-123.90	65.0	4.5	6.8	14.55	1.5	9.56
	TIL-2	45.47	-123.89	42.0	3.8	5.0	11.18	1.3	8.33
Siletz River	SIL-1	44.89	-123.99	39.2	5.2	7.5	7.56	1.4	5.24
	SIL-2	44.78	-123.92	32.1	5.3	7.8	6.11	1.5	4.13
Siuslaw River	SIU-1C	43.97	-124.08	11.4	3.6	6.5	3.13	1.8	1.74
	SIU-1A	43.97	-124.08	10.3	3.8	6.9	2.67	1.8	1.50
	SIU-2A	43.97	-124.07	18.5	5.5	15.6	3.35	2.8	1.18
	SIU-1B	43.97	-124.08	9.3	3.9	6.7	2.39	1.7	1.39
	SIU-2B	43.97	-124.07	11.6	3.6	6.6	3.23	1.9	1.74
Umpqua River	UMP-1A	43.70	-124.07	21.3	8.1	18.6	2.63	2.3	1.14
	UMP-1C	43.70	-124.07	19.5	6.4	12.1	3.02	1.9	1.60
	UMP-1B	43.69	-124.06	18.2	5.2	14.0	3.53	2.7	1.30
Coquille River	COQ-1A	43.13	-124.40	26.1	12.8	23.0	2.04	1.8	1.13
	COQ-2	43.16	-124.36	27.3	11.2	18.6	2.45	1.7	1.47
Coos River	COO-1B	43.37	-124.20	17.5	4.7	7.8	3.69	1.7	2.23
	COO-1C	43.37	-124.19	16.9	7.8	18.1	2.17	2.3	0.93
	COO-1A	43.13	-124.40	21.8	7.2	13.5	3.04	1.9	1.61
Rogue River	ROG-1	42.44	-124.40	18.3	17.6	33.3	1.04	1.9	0.55
	ROG-1(DUPLICATE)	42.44	-124.40	18.1	16.8	32.2	1.08	1.9	0.56
Chetco River	CHE-1	42.07	-124.26	0.8	22.1	41.5	0.03	1.9	0.02
	CHE-2	42.07	-124.26	0.0	14.4	23.0	0.00	1.6	0.00
	CHE-3A	42.07	-124.26	0.5	34.5	43.6	0.01	1.3	0.01
	CHE-3B	42.07	-124.26	0.3	37.5	54.2	0.01	1.4	0.01
Smith River, CA	SMI-2	41.90	-124.16	2.5	18.0	41.6	0.14	2.3	0.06
	SMI-1	41.89	-124.15	2.9	17.8	43.6	0.16	2.4	0.07
Klamath River, CA	KLA-3B	41.52	-124.01	6.1	20.7	36.3	0.29	1.8	0.17
	KLA-2	41.52	-124.02	6.7	19.5	36.4	0.34	1.9	0.18
	KLA-1	41.52	-124.00	4.4	27.9	38.8	0.16	1.4	0.11
	KLA-4	41.52	-124.00	7.0	13.5	28.0	0.52	2.1	0.25
Redwood Creek, CA	RED-1A	41.29	-124.06	0.2	29.6	35.4	0.01	1.2	0.01
	RED-1B	41.29	-124.06	0.3	32.8	36.6	0.01	1.1	0.01
	RED-2A	41.29	-124.06	1.5	19.3	40.4	0.08	2.1	0.04
Mad River, CA	MAD-1	40.91	-124.07	5.0	10.6	19.6	0.47	1.8	0.26
	MAD-2	40.91	-124.07	6.8	23.8	35.4	0.29	1.5	0.19
Eel River, CA	EEL-1A	40.64	-124.28	11.5	21.6	39.4	0.53	1.8	0.29
	EEL-1B	40.64	-124.28	9.8	22.9	37.6	0.43	1.6	0.26

River	Sample Name	Latitude	Longitude	%sm	%ill	%k+chl	sm/ill	k+chl/ill	sm/k+chl
	EEL-2	40.63	-124.28	7.7	22.5	33.3	0.34	1.5	0.23
Mattole River, CA	MAT-2	40.31	-124.28	2.3	10.6	22.0	0.21	2.1	0.10
	MAT-1B	40.31	-124.28	4.8	11.1	23.0	0.43	2.1	0.21
	MAT-1A	40.31	-124.28	7.8	19.8	33.3	0.39	1.7	0.23
Russian River, CA	RUS-1	38.43	-123.10	12.6	18.5	23.1	0.68	1.3	0.54
	RUS-2	38.43	-123.10	27.3	14.2	20.1	1.92	1.4	1.35
Sacramento River	SAC-1	38.06	-121.79	13.8	17.2	37.4	0.80	2.2	0.37
	SAC-2	38.07	-121.79	7.8	12.1	32.9	0.64	2.7	0.24
San Joaquin River	SAN-1	38.03	-121.86	13.5	11.5	23.8	1.17	2.1	0.57
Confluence of..	SCN-1	38.07	-121.86	20.0	11.8	23.2	1.69	2.0	0.86
	SCN-2A	38.06	-121.86	0.8	16.8	28.7	0.05	1.7	0.03
	SCN-2B	38.06	-121.86	1.7	12.3	15.1	0.14	1.2	0.11
Tributary Samples									
Klamath River									
Shasta River	SHA-1	41.82	-122.59	24.3	10.4	8.1	2.34	0.8	3.01
Scott River	SCO-1	41.77	-123.02	11.1	8.4	11.4	1.31	1.3	0.97
Salmon River	SAL-1	41.38	-123.97	12.9	16.3	41.4	0.79	2.5	0.31
Trinity River	TRI-1	41.18	-123.71	1.9	27.1	34.5	0.07	1.3	0.06
Eel River									
Eel-VanDuzen	EEL-3	40.35	-123.91	1.5	18.1	30.7	0.08	1.7	0.05
South Fork Eel	SFEEL-1	40.34	-123.94	4.3	10.9	20.5	0.39	1.9	0.21
North Fork Eel	NFEEL-1	39.94	-123.35	0.6	22.5	30.3	0.03	1.3	0.02
Middle Fork Eel	MFEEL-1	39.71	-123.34	3.2	28.8	47.1	0.11	1.6	0.07
Eel, Near Dos Rios	EEL-6	39.64	-123.34	2.2	17.8	23.8	0.12	1.3	0.09
Eel, Above Pillsbury Res.	EEL-5	39.47	-122.84	2.1	42.1	55.8	0.05	1.3	0.04
Eel, Trout Cr.	EEL-4	39.37	-122.06	10.2	32.4	38.5	0.31	1.2	0.26
Quaternary Fluvial Samples									
Paleo-Klamath River									
Gold Bluffs (Qt)	GB-1	41.36	-124.07	6.4	5.6	5.9	1.15	1.1	1.09
Gold Bluffs (Qt)	GB-2	41.36	-124.07	13.2	1.6	26.0	8.27	16.4	0.51
Gold Bluffs (Qt)	GB-3	41.36	-124.07	7.2	4.9	7.5	1.45	1.5	0.96
Paleo-Eel River									
Hookton Fm.	QHTB-2	40.70	-124.27	2.0	8.5	10.0	0.23	1.2	0.20
Hookton Fm.	QHTB-3	40.70	-124.27	3.5	13.2	14.8	0.27	1.1	0.24
Hookton Fm.	QHTB-1	40.70	-124.27	3.7	19.4	23.4	0.19	1.2	0.16
Hookton Fm.	QH-1	40.58	-124.15	10.1	17.9	27.9	0.57	1.6	0.36
Hookton Fm.	QH-2	40.56	-124.14	0.0	5.9	16.5	0.00	2.8	0.00
Carlotta Fm.	QC-1	40.56	-124.27	7.4	16.1	19.7	0.46	1.2	0.37
Carlotta Fm.	QC-2	40.56	-124.27	9.6	13.4	10.4	0.71	0.8	0.92
Scotia Bluffs	QSB-1	40.57	-124.35	18.5	18.5	7.6	1.00	0.4	2.43
Scotia Bluffs	QSB-2	40.56	-124.35	0.3	1.4	5.2	0.18	3.6	0.05
Scotia Bluffs	QSB-3	40.56	-124.35	0.0	1.7	9.7	0.00	5.5	0.00
Core Sediments									
EW9504-17PC	4	42.3	125.9	6.4	16.5	25.1	0.38	1.5	0.25
EW9504-17PC	32	42.3	125.9	6.6	14.8	22.4	0.44	1.5	0.29
EW9504-17PC	50	42.3	125.9	7.1	19.6	30.0	0.36	1.5	0.24
EW9504-17PC	75	42.3	125.9	4.3	12.8	19.6	0.33	1.5	0.22
EW9504-17PC	110	42.3	125.9	17.1	30.8	52.1	0.56	1.7	0.33
EW9504-17PC	140	42.3	125.9	5.2	16.4	33.9	0.32	2.1	0.15
EW9504-17PC	180	42.3	125.9	7.8	17.6	32.2	0.44	1.8	0.24
EW9504-17PC	260	42.3	125.9	8.4	15.4	29.8	0.54	1.9	0.28
EW9504-17PC	313	42.3	125.9	7.6	12.5	22.1	0.61	1.8	0.34
EW9504-17PC	316	42.3	125.9	7.9	15.5	25.9	0.51	1.7	0.30
EW9504-17PC	360	42.3	125.9	12.1	16.2	27.6	0.75	1.7	0.44
EW9504-17PC	385	42.3	125.9	14.7	17.9	26.3	0.82	1.5	0.56
EW9504-17PC	403	42.3	125.9	14.2	16.0	22.1	0.88	1.4	0.64
EW9504-17PC	420	42.3	125.9	11.3	15.2	23.1	0.74	1.5	0.49
EW9504-17PC	443	42.3	125.9	12.6	17.6	26.7	0.71	1.5	0.47

sm = smectite; ill = illite; k+chl = kaolinite+chlorite; Qt = Quaternary

eg = ethylene glycol, meaning samples were glycolated

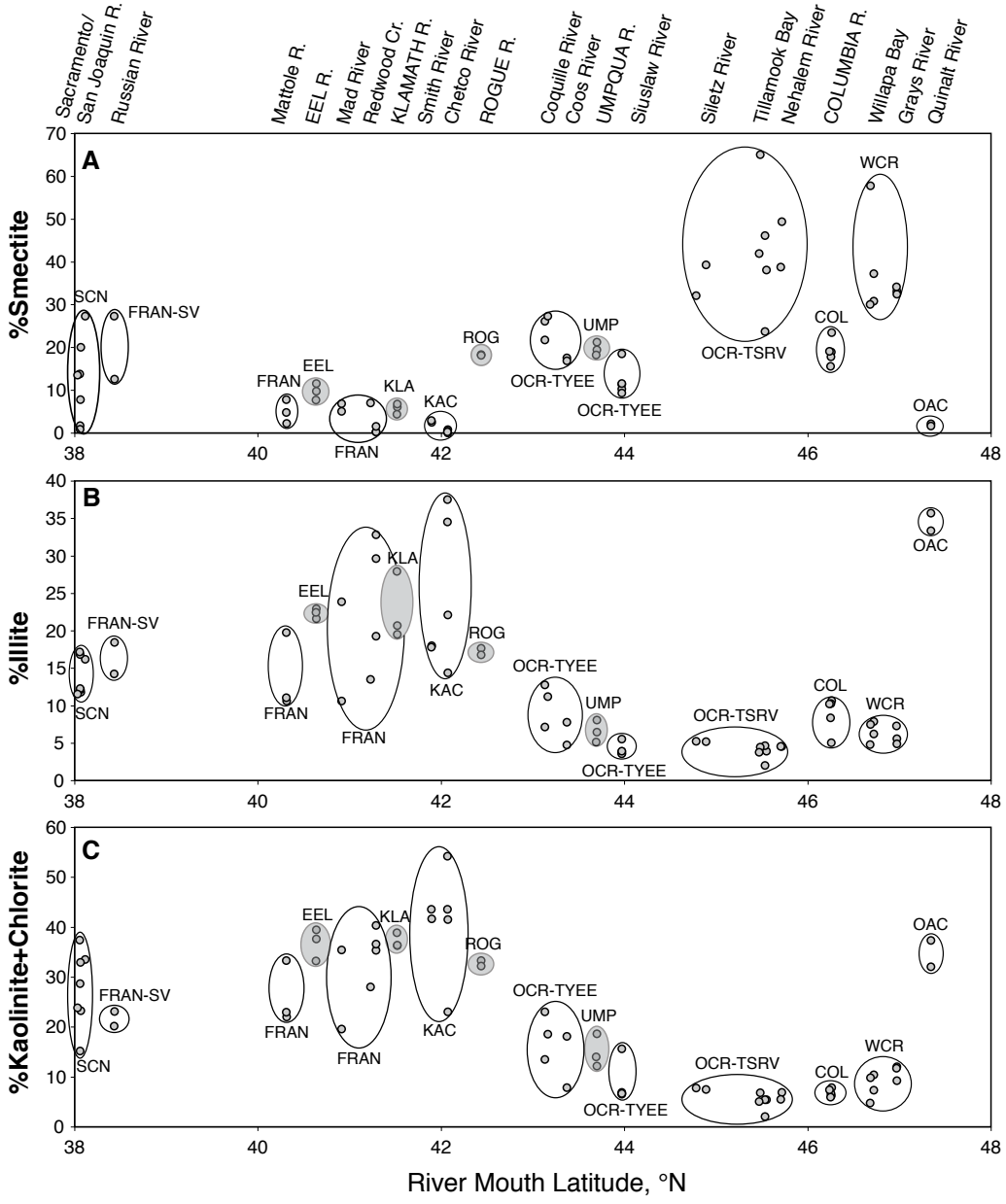

Figure A.1 - Talc-normalized smectite (A), illite (B) and kaolinite+chlorite (C) clay mineral abundances for Pacific Northwest Rivers. River names are plotted on the upper part of figure. Black-outlined ovals depict different geologic provinces. OAC = Olympic Accretionary Complex; WCR = Washington Coast Ranges; OCR-TSRV = Oregon Coast Ranges - Tillamook and Siletz River Volcanics; OCR-TYEE = Oregon Coast Ranges - Tyee Formation; KAC = Klamath Accretionary Complex; FRAN = Franciscan Melange; FRAN-SV = Franciscan Melange and Sonoma Volcanics; SCN = Sacramento-San Joaquin Rivers, which drain the Sierra Nevadas, Cascades, Great Valley sediments among other geologic provinces. The gray ovals depict the major river sediment sources to the region of the core site EW9504-17PC.

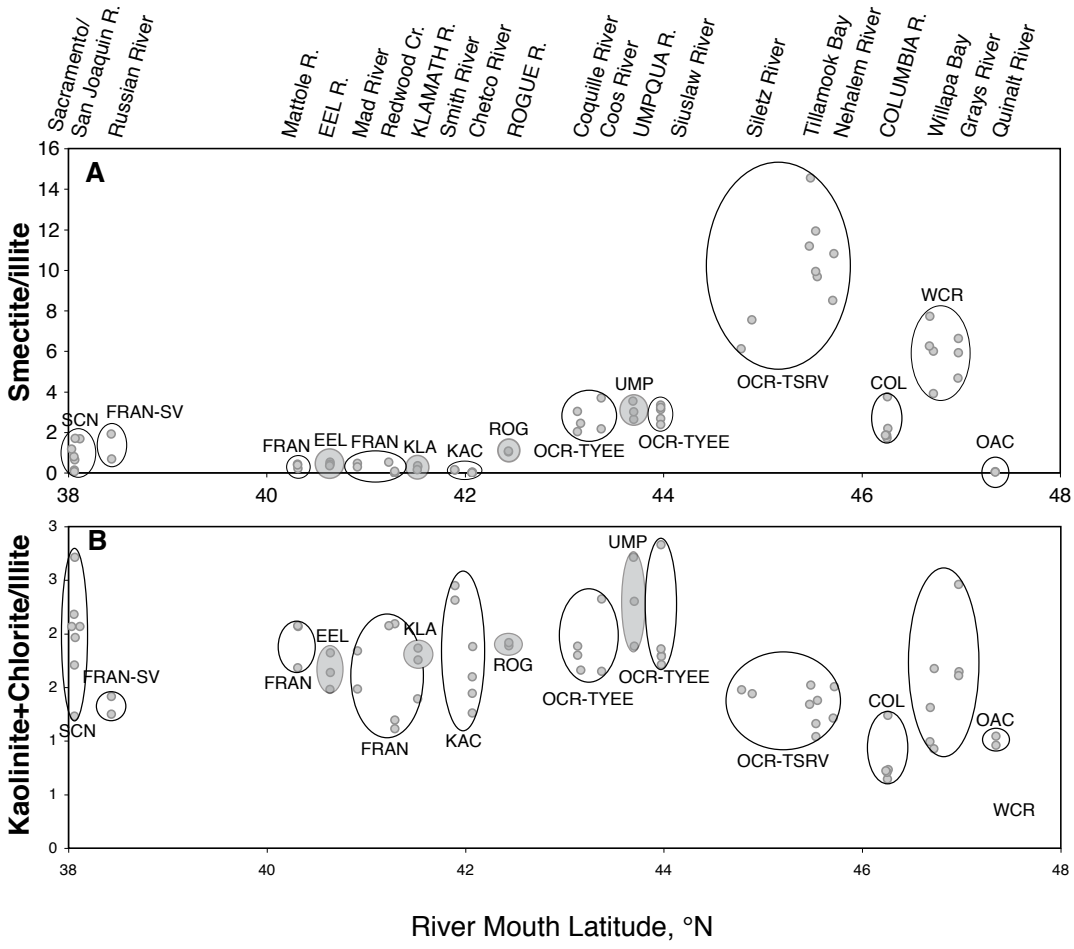

Figure A.2 - Talc-normalized smectite/illite (A) and kaolinite+chlorite/illite (B) clay mineral ratios for Pacific Northwest Rivers. River names are plotted on the upper part of figure. Black-outlined ovals depict different geologic provinces. OAC = Olympic Accretionary Complex; WCR = Washington Coast Ranges; OCR-TSRV = Oregon Coast Ranges - Tillamook and Siletz River Volcanics; OCR-TYEE = Oregon Coast Ranges - Tyee Formation; KAC = Klamath Accretionary Complex; FRAN = Franciscan Melange; FRAN-SV = Franciscan Melange and Sonoma Volcanics; SCN = Sacramento-San Joaquin Rivers, which drain the Sierra Nevadas, Cascades, Great Valley sediments among other geologic provinces. The gray ovals depict the major river sediment sources to the region of the core site EW9504-17PC.

Appendix B

Major and Trace Element Geochemistry of Pacific Northwest River and core site EW9504-17PC Sediments

Major and Trace Element Analyses

River and core sediment samples were analyzed for their major and trace element geochemical signature. Trace element analyses were performed on an EXCELL® ICP-MS in the College of Oceanic and Atmospheric Sciences at Oregon State University. Major element analyses were done on the ICP-OES and AES instruments in COAS. Both clay and silt-sized sediment samples were analyzed after organics and carbonate was removed, following the preparation procedures in Appendix A.

Eight standards were used to calibrate instrument-derived intensities of masses to elemental concentrations. The standards used were SCO-1, SGR-1, AGV-1, MAG-1, BCR-3, G-2, GSP-1 and SDO-1. The concentrations for these standards were taken from *Geochemical Reference Material Compositions* (Potts, Tindle, Webb, 2000).

Major Element Concentrations for Pacific Northwest River clay (0-2 micron)

Sample Name	Lat., °N	Long., °W	Al2O3	K2O	Ba	Ca	Fe	Mg	Mn	Na	P	Sr	Ti
			wt %	wt %	ppm	ppm	ppm	ppm	ppm	ppm	ppm	ppm	ppm
0-2 micron river samples													
QUI-1	47.3	-124.3	8.1	2.3	576	2,961	56,622	11,724	464	12,776	1,482	100	7,128
GRA-2	47.0	-123.8	14.5	1.2	219	4,639	68,391	15,876	321	12,059	2,210	77	9,655
WIL-4	46.7	-123.7	10.4	1.0	161	3,545	66,703	12,237	297	9,410	1,508	54	7,984
COL-2	46.3	-123.5	12.5	1.0	306	8,412	75,631	7,089	600	12,406	2,203	110	8,046
COL-3	46.3	-123.5	10.9	1.9	518	7,239	75,357	14,382	531	7,311	1,752	130	7,436
COL-4	46.2	-123.6	12.4	1.9	576	5,853	82,203	15,258	418	7,164	1,603	122	8,341
COL-5	46.2	-123.6	10.4	1.5	446	10,085	67,763	9,667	626	14,075	1,418	150	8,481
NEH-2	45.7	-123.9	11.7	4.8	448	14,814	66,494	24,855	1,019	39,768	910	187	5,951
TIL-4	45.5	-123.9	14.2	1.1	202	7,249	87,138	25,775	478	4,587	2,266	86	11,481
TIL-1	45.5	-123.9	13.2	1.0	220	3,264	81,288	16,039	272	9,559	2,172	52	9,202
SIL-2	44.8	-123.9	11.7	1.5	360	2,972	77,467	20,976	720	3,830	2,439	62	9,647
SIU-2B	44.0	-124.1	9.7	1.1	244	1,209	62,691	13,428	245	4,943	2,574	37	4,912
UMP-1C	43.7	-124.1	11.6	1.3	313	2,760	76,516	17,701	445	10,459	1,670	59	7,203
UMP-1B	43.7	-124.1	16.3	1.1	190	2,025	98,402	12,978	325	21,720	1,859	37	6,521
COO-1C	43.4	-124.2	9.2	1.8	383	1,655	60,896	14,045	281	8,264	1,606	52	6,707
COQ-2	43.2	-124.4	9.4	1.8	409	2,586	65,767	30,684	500	9,957	1,487	48	5,542
CHE-3A	42.1	-124.3	13.0	2.7	858	3,350	79,908	24,193	1,105	6,453	1,075	47	4,315
SMI-1	41.9	-124.2	18.3	2.4	779	14,261	110,226	80,512	911	7,790	2,016	85	7,508
KLA-2	41.5	-124.0	7.2	1.0	345	30,119	48,278	36,040	822	18,774	1,146	173	5,942
RED-2B	41.3	-124.1	11.1	2.1	432	1,345	67,056	9,396	906	7,260	867	33	6,669
EEL-1B	40.6	-124.3	12.0	2.8	728	5,574	76,524	42,486	1,202	9,662	1,131	53	5,672
EEL-1A	40.6	-124.3	12.3	2.7	741	9,574	77,896	46,853	1,085	7,221	985	70	5,718
MAT-1	40.3	-124.3	10.8	1.5	247	7,246	91,389	16,606	533	11,871	2,008	90	9,540
RUS-1	38.4	-123.1	12.4	3.1	624	7,328	80,143	62,616	903	7,913	948	57	6,974
RUS-2	38.4	-123.1	11.0	2.5	686	8,413	70,208	41,552	846	8,636	1,045	76	7,604
SCN-1	38.1	-121.9	11.5	1.5	592	3,967	74,830	22,520	519	8,244	1,195	55	6,149
SAC-2	38.1	-121.8	5.8	0.9	380	2,763	43,546	9,130	326	9,516	632	26	6,731
SAN-1	38.0	-121.9	10.1	1.4	510	3,238	68,051	16,924	423	8,293	1,093	41	6,695

See Appendix A for naming convention

Trace Element Analyses of 0-2 micron (clay) Pacific Northwest River Sediments

Sample Name	Lat., °N	Long., °W	Sc	V	Cr	Co	Ni	Cu	Zn	Rb	Sr	Y	Zr	Nb	Mo	Cd	Sn	Sb	Cs	Ba
Main Rivers			ppm																	
QUI-1	47.3	-124.3	11	188	91	12	41	44	123	12	93	7	173	19	2	0	13	0	3	420
GRA-2	47.0	-123.8	15	264	93	20	52	86	149	9	78	16	238	19	3	0	13	1	2	184
WIL-4	46.7	-123.7	11	179	83	13	43	53	152	7	40	11	259	20	2	1	8	1	3	50
COL-2	46.3	-123.5	7	161	63	20	45	72	211	6	106	11	274	19	2	0	14	2	3	271
COL-3	46.3	-123.5	23	179	77	17	50	96	256	108	137	40	254	20	2	0	23	3	8	517
COL-4	46.2	-123.6	21	177	86	17	51	87	272	25	113	29	274	20	3	0	27	5	6	488
COL-5	46.2	-123.6	6	157	68	21	52	58	344	8	137	12	235	20	2	1	12	6	4	345
NEH-1	45.7	-123.9	22	261	65	25	49	78	149	18	87	22	344	34	3	0	17	1	3	222
TIL-4	45.5	-123.9	24	199	87	28	92	100	146	55	92	35	307	33	2	0	10	1	4	207
TIL-1	45.5	-123.9	18	214	99	19	67	68	148	6	36	19	290	28	3	1	13	1	2	165
SIL-2	44.8	-123.9	21	254	116	24	93	128	156	35	62	25	229	26	2	0	15	1	6	329
SIU-2B	44.0	-124.1	17	107	86	11	56	39	123	21	31	16	179	17	3	0	214	1	4	235
UMP-1C	43.7	-124.1	28	184	137	23	120	80	171	20	58	11	188	16	2	0	45	1	5	297
UMP-1B	43.7	-124.1	16	212	122	16	97	53	126	7	32	11	176	14	3	0	39	1	3	97
COO-1C	43.4	-124.2	15	152	118	14	71	42	152	14	28	12	218	26	3	0	12	1	5	322
COQ-2	43.2	-124.4	20	249	218	24	226	50	146	104	52	16	137	12	3	0	14	1	7	397
CHE-3B	42.1	-124.3	12	255	154	28	171	110	198	7	25	8	126	9	1	0	13	1	2	351
SMI-1	41.9	-124.2	35	319	639	81	1064	139	205	101	91	35	164	14	3	0	22	2	8	741
KLA-2	41.5	-124.0	24	179	506	23	195	30	88	31	185	30	155	10	1	2	1	0	1	357
RED-2B	41.3	-124.1	4	331	239	41	139	134	195	5	23	5	237	14	2	0	14	2	2	55
EEL-1B	40.6	-124.3	23	237	275	37	313	88	177	113	56	28	167	12	1	0	8	1	10	696
EEL-1A	40.6	-124.3	23	231	294	38	348	84	175	44	72	26	155	12	1	0	4	1	7	647
MAT-1	40.3	-124.3	20	218	261	38	308	96	172	42	51	22	127	10	2	0	21	2	6	583
RUS-1	38.4	-123.1	27	220	437	49	609	72	177	112	59	33	182	16	2	1	5	1	9	594
RUS-2	38.4	-123.1	25	208	327	34	376	57	159	114	81	41	186	18	2	0	3	1	7	661
SCN-1	38.1	-121.9	21	278	215	29	206	97	221	14	35	18	170	11	2	1	12	1	4	413
SAC-2	38.1	-121.8	4	197	171	14	125	54	157	3	15	3	185	12	2	0	7	2	2	63
SAN-1	38.0	-121.9	14	206	185	17	148	78	236	8	28	11	183	12	2	0	15	1	3	321

See appendix A for naming convention

Trace Element Analyses of 0-2 micron (clay) Pacific Northwest River Sediments (continued)

Sample Name	La	Ce	Pr	Nd	Sm	Eu	Gd	Tb	Dy	Ho	Er	Tm	Yb	Lu	Hf	Ta	W	Tl	Pb	Bi	Th	U
Main Rivers																						
QUI-1	3	0	1	8	2	1	1	0	2	0	1	0	1	0	4	1	1	1	25	0	3	3
GRA-2	10	19	3	17	3	1	3	1	3	1	2	0	2	0	6	1	1	0	28	0	4	3
WIL-4	6	35	2	11	2	1	2	0	2	0	1	0	2	0	7	1	1	0	21	0	3	3
COL-2	4	14	1	9	2	1	2	0	2	0	1	0	1	0	7	1	2	1	50	1	2	3
COL-3	37	70	10	39	7	2	7	1	6	1	4	1	3	1	6	1	3	1	86	1	14	2
COL-4	23	43	7	29	6	1	6	1	5	1	3	0	3	0	7	1	3	1	90	1	10	2
COL-5	7	12	2	10	2	0	2	0	2	0	1	0	2	0	6	1	5	1	70	1	3	3
NEH-1	19	49	7	28	5	1	5	1	4	1	3	0	3	0	9	2	1	0	15	0	7	3
TIL-4	31	74	9	36	7	2	7	1	6	1	3	1	3	0	7	2	1	0	21	0	8	2
TIL-1	15	45	5	22	4	1	4	1	4	1	2	0	2	0	7	2	1	0	20	1	8	2
SIL-2	23	48	6	25	5	1	5	1	4	1	3	0	2	0	6	2	2	0	27	0	9	3
SIU-2B	24	55	7	27	5	1	4	1	3	1	2	0	2	0	5	1	1	0	106	1	15	4
UMP-1C	9	17	3	15	3	1	3	0	3	1	2	0	2	0	5	1	1	1	128	1	7	4
UMP-1B	6	18	2	10	2	1	2	0	2	0	1	0	2	0	5	1	1	0	78	1	5	3
COO-1C	14	34	4	18	3	1	3	0	3	1	2	0	2	0	6	2	2	1	50	1	13	4
COQ-2	17	28	4	18	3	1	3	0	3	1	2	0	2	0	4	1	1	1	22	0	8	2
CHE-3B	3	4	1	7	1	0	1	0	1	0	1	0	1	0	3	1	1	1	24	1	2	3
SMI-1	21	41	6	26	5	2	5	1	5	1	4	1	4	1	4	1	1	1	57	1	10	3
KLA-2	21	41	6	25	5	1	5	1	5	1	3	0	3	0	4	1	1	0	3	0	4	1
RED-2B	2	4	1	6	1	0	1	0	1	0	1	0	1	0	6	1	2	1	29	1	1	3
EEL-1B	21	44	6	25	5	1	5	1	4	1	3	0	3	0	4	1	1	1	48	1	9	3
EEL-1A	17	38	5	20	4	1	4	1	4	1	3	0	3	0	4	1	1	1	33	1	7	3
MAT-1	15	35	4	19	4	1	3	1	3	1	2	0	2	0	3	1	1	1	54	1	6	2
RUS-1	22	50	6	25	5	1	5	1	5	1	3	1	3	1	5	1	1	1	25	0	10	3
RUS-2	30	59	9	35	7	2	7	1	6	1	4	1	4	1	5	1	1	1	24	0	10	3
SCN-1	10	25	3	16	3	1	3	1	3	1	2	0	2	0	4	1	2	1	30	1	6	3
SAC-2	2	0	0	4	1	0	0	0	1	0	0	0	1	0	5	1	2	1	40	0	1	2
SAN-1	7	13	2	12	2	1	2	0	2	0	1	0	2	0	5	1	2	1	32	0	6	3

See appendix A for naming convention

Pacific Northwest River and core site EW9504-17PC
silt-sized (20-63 micron) major element sediment analyses

Sample Name	Lat., °N	Long., °W	Al_2O_3	K_2O	Ba	Ca	Fe	Mg	Mn	Na	P	Sr	Ti
			wt%	wt%	ppm	ppm	ppm	ppm	ppm	ppm	ppm	ppm	ppm
QUI-1	47.3	-124.3	10.4	1.1	326	9,446	20,017	7,972	242	20,645	652	182	4,454
GRA-2	47.0	-123.8	13.6	1.6	458	30,559	34,949	14,749	548	20,846	608	332	7,000
WIL-4	46.7	-123.7	14.4	1.9	530	25,431	32,776	12,596	441	20,775	585	342	6,646
COL-1	46.3	-123.5	14.1	1.6	642	29,680	48,264	14,442	639	21,687	1,146	376	8,054
COL-1	46.3	-123.5	14.7	1.7	649	30,852	49,203	15,157	642	21,713	749	369	8,034
COL-3	46.3	-123.5	15.2	1.6	556	30,249	39,493	12,438	569	24,452	923	420	6,250
COL-4	46.2	-123.6	14.1	1.9	677	26,883	31,759	11,220	480	22,200	761	384	6,502
TIL-4	45.5	-123.9	13.9	1.1	348	44,711	75,993	27,745	1,000	17,523	1,014	303	19,403
TIL-1	45.5	-123.9	13.1	1.6	459	30,572	46,171	17,934	647	19,263	779	299	11,067
TIL-2	45.5	-123.9	14.6	1.3	351	45,310	64,739	27,001	927	20,499	986	326	15,711
SIL-2	44.8	-123.9	14.2	1.8	577	25,903	55,838	20,088	694	15,473	1,120	250	10,728
UMP-1A	43.7	-124.1	13.3	1.5	483	19,801	29,262	13,397	422	20,705	514	292	4,780
UMP-1B	43.7	-124.1	12.4	1.3	429	20,636	30,853	14,063	464	21,442	493	271	5,075
COO-1A	43.4	-124.2	13.9	2.5	745	12,297	19,567	9,703	235	21,522	478	316	3,861
COO-1C	43.4	-124.2	14.4	2.6	784	12,333	20,560	9,315	214	21,813	385	338	3,693
ROG-5	42.4	-124.4	13.1	1.2	361	20,300	45,787	32,502	675	18,076	919	162	4,784
KLA-1	41.5	-124.0	12.0	1.1	347	25,288	44,393	34,455	742	18,350	1,026	163	5,004
KLA-3B	41.5	-124.0	12.8	1.3	450	26,506	43,491	28,959	803	18,485	825	181	5,213
EEL-1A	40.6	-124.3	11.8	1.3	498	11,441	27,170	17,389	455	22,137	733	147	3,937
RUS-2	38.4	-123.1	10.1	1.2	391	11,975	24,932	17,691	392	18,412	535	137	3,916
SAN-1	38.0	-121.9	12.4	1.3	475	20,764	26,358	13,666	441	18,415	502	249	4,245
Tributary Samples, 20-63 micron													
SCO-1	41.8	-123.0	7.9	0.9	266	38,714	56,081	64,989	914	19,667	829	196	6,530
TRI-1	41.2	-123.7	7.5	1.4	470	22,399	52,283	37,384	746	19,143	749	143	5,522
EEL-4	39.4	-122.1	6.6	1.6	571	10,389	45,247	19,934	580	23,797	798	146	5,055
EEL-3	40.3	-123.9	8.1	2.5	600	7,427	58,664	34,631	833	7,456	548	54	4,555
EEL-3	40.3	-123.9	4.8	1.4	548	10,005	34,441	18,978	497	23,669	886	108	4,704
Core Samples													
17PC-110 cm	42.3	-125.9	12.7	1.3	609	18,965	32,513	20,986	504	21,843	735	217	4,375
17PC-225 cm	42.3	-125.9	12.3	1.2	544	20,468	31,119	21,979	506	20,595	840	213	3,947
17PC-260 cm	42.3	-125.9	12.8	1.3	547	22,745	34,199	23,399	566	21,450	941	236	4,044
17PC-313 cm	42.3	-125.9	13.1	1.2	454	27,105	38,289	25,653	675	20,910	796	259	4,787
17PC-316 cm	42.3	-125.9	14.0	1.4	558	25,596	36,794	23,962	626	22,238	756	289	4,670
17PC-403 cm	42.3	-125.9	14.0	1.3	538	29,890	36,642	24,291	650	22,538	757	339	4,510
17PC-443 cm	42.3	-125.9	13.3	1.3	452	24,581	35,399	23,137	596	21,976	787	279	4,183

River and core site EW9504-17PC silt-sized (20-63 micron) sediment trace element analyses

Sample Name	Lat., °N	Long., °W	Sc	V	Cr	Co	Ni	Cu	Zn	Rb	Sr	Y	Zr	Nb	Mo	Cd	Sn	Sb	Cs	Ba
Main Rivers			ppm																	
QUI-1	47.3	-124.3	17	63	53	4	14	13	37	35	175	32	165	12	0	0	3	0	1	311
GRA-2	47.0	-123.8	39	126	109	12	20	29	59	40	319	31	176	13	1	0	2	0	1	433
WIL-4	46.7	-123.7	31	103	78	9	17	25	64	49	330	26	176	14	1	0	2	0	2	505
COL-1	46.3	-123.5	18	177	91	17	32	36	104	55	393	28	164	16	1	0	3	1	2	639
COL-1	46.3	-123.5	19	174	87	17	32	36	103	56	400	30	148	17	1	0	3	1	2	628
COL-3	46.3	-123.5	14	128	57	13	24	27	90	53	448	24	141	13	1	0	2	1	2	547
COL-4	46.2	-123.6	15	117	72	10	21	23	86	63	405	25	142	16	1	0	2	1	3	670
TIL-4	45.5	-123.9	32	302	244	31	69	57	129	33	315	29	232	38	1	0	2	0	1	345
TIL-1	45.5	-123.9	53	200	170	20	29	41	106	44	346	30	239	27	1	0	2	0	1	525
TIL-2	45.5	-123.9	67	228	180	24	38	49	113	28	309	28	213	36	1	0	2	0	1	335
SIL-2	44.8	-123.9	24	198	216	20	67	65	102	65	262	28	161	23	1	0	3	0	3	570
UMP-1A	43.7	-124.1	26	97	163	9	28	20	55	45	280	20	106	9	0	0	2	0	2	460
UMP-1B	43.7	-124.1	29	107	216	9	26	20	59	40	257	22	107	8	1	0	3	0	2	407
COO-1A	43.4	-124.2	15	60	137	5	17	10	186	72	304	28	146	13	1	0	2	0	3	699
COO-1C	43.4	-124.2	14	57	106	5	17	12	46	77	326	28	151	12	0	0	2	0	3	754
ROG-5	42.4	-124.4	40	138	697	18	110	31	73	38	156	33	201	7	1	0	2	0	2	348
KLA-1	41.5	-124.0	48	144	422	19	96	39	81	39	173	34	143	9	1	0	3	1	2	426
KLA-3B	41.5	-124.0	21	153	422	21	200	36	74	31	170	25	113	8	1	0	1	0	1	340
EEL-1A	40.6	-124.3	19	82	222	11	55	23	56	37	142	21	91	8	0	0	1	0	1	471
RUS-2	38.4	-123.1	18	79	386	11	71	17	47	34	132	19	112	8	0	0	1	0	1	375
SAN-1	38.0	-121.9	27	96	188	8	33	19	54	36	239	20	99	7	0	0	2	0	2	454
Tributary Samples																				
SCO-1	41.8	-123.0	24	190	891	34	483	40	76	24	203	27	79	10	1	0	6	0	1	270
TRI-1	41.2	-123.7	28	173	368	21	203	46	96	43	153	21	102	9	1	0	8	1	2	468
EEL-3	40.3	-123.9	14	114	225	11	115	29	69	51	113	22	117	10	1	0	4	1	2	535
EEL-4	39.4	-122.1	18	148	215	16	124	52	97	66	152	22	119	9	1	0	2	1	4	546
Core Samples																				
17PC-110 cm	42.3	-125.9	26	96	247	9	51	31	68	37	205	24	113	7	0	0	1	0	2	580
17PC-225 cm	42.3	-125.9	26	95	236	9	51	22	59	36	198	22	100	7	0	0	1	1	2	507
17PC-260 cm	42.3	-125.9	30	104	245	11	57	24	63	36	222	23	97	7	0	0	1	0	2	517
17PC-316 cm	42.3	-125.9	31	114	239	12	58	25	64	39	269	24	121	7	0	0	1	0	2	526
17PC-403 cm	42.3	-125.9	33	115	236	13	55	23	60	33	314	24	103	7	0	0	1	0	1	506
17PC-443 cm	42.3	-125.9	31	109	235	12	57	23	59	34	265	21	113	7	1	0	1	0	1	437

See Appencix A for sample naming convention

River and core site EW9504-17PC silt-sized (20-63 micron) sediment trace element analyses **continued**

Sample Name	La	Ce	Pr	Nd	Sm	Eu	Gd	Tb	Dy	Ho	Er	Tm	Yb	Lu	Hf	Ta	W	Tl	Pb	Bi	Th	U
Main Rivers																						
QUI-1	37	71	8	31	6	1	4	1	6	1	3	1	3	0	5	1	1	0	9	0	8	2
GRA-2	28	53	6	24	5	1	4	1	5	1	3	1	3	0	5	1	1	0	12	0	7	2
WIL-4	27	53	6	24	5	1	4	1	5	1	2	0	2	0	5	1	1	0	13	0	7	2
COL-1	32	67	9	31	6	2	5	1	4	1	3	0	2	0	4	1	1	0	25	0	8	2
COL-1	38	81	10	37	7	2	6	1	5	1	3	0	3	0	4	1	1	0	24	0	12	2
COL-3	29	60	8	29	5	1	5	1	4	1	2	0	2	0	4	1	1	0	21	0	7	2
COL-4	33	69	9	32	6	1	5	1	4	1	2	0	2	0	4	1	1	0	25	0	9	2
TIL-4	26	57	8	30	6	2	6	1	5	1	3	0	2	0	6	2	1	0	13	0	6	2
TIL-1	27	55	6	24	5	2	4	1	5	1	3	1	3	0	6	2	1	0	13	0	6	2
TIL-2	25	51	6	24	5	2	4	1	6	1	3	1	2	0	5	3	1	0	15	0	5	1
SIL-2	28	57	8	29	6	2	6	1	5	1	3	0	2	0	4	2	1	0	17	0	6	2
UMP-1A	18	35	4	16	3	1	2	0	3	1	2	0	2	0	3	1	1	0	16	0	6	2
UMP-1B	19	35	4	17	3	1	3	0	4	1	2	0	2	0	3	0	1	0	17	0	6	2
COO-1A	33	62	7	26	5	1	3	1	5	1	3	1	3	0	4	1	1	0	17	0	10	3
COO-1C	35	64	7	27	5	1	4	1	5	1	3	1	3	0	4	1	1	0	16	0	11	3
ROG-5	27	51	7	27	6	1	4	1	6	1	3	1	3	0	5	0	1	0	19	0	6	2
KLA-1	22	42	5	22	5	1	4	1	6	1	3	1	3	0	4	1	1	0	11	0	5	2
KLA-3B	18	32	5	22	4	1	4	1	4	1	2	0	2	0	3	1	1	0	3	0	4	1
EEL-1A	20	38	5	19	4	1	3	1	4	1	2	0	2	0	3	1	1	0	8	0	5	2
RUS-2	17	33	4	16	3	1	2	0	3	1	2	0	2	0	3	1	1	0	8	0	5	1
SAN-1	17	33	4	17	3	1	3	0	3	1	2	0	2	0	3	0	1	0	12	0	5	2
Tributary Samples																						
SCO-1	10	18	3	17	4	1	4	1	4	1	3	0	2	0	2	1	1	0	7	0	2	1
TRI-1	7	14	2	13	3	1	3	1	3	1	2	0	2	0	3	1	1	0	9	0	2	1
EEL-3	21	43	6	22	4	1	4	1	3	1	2	0	2	0	3	1	1	0	7	0	7	2
EEL-4	16	32	4	18	4	1	4	1	3	1	2	0	2	0	3	1	2	0	13	0	6	2
Core Samples																						
17PC-110 cm	19	38	5	19	4	1	3	1	4	1	2	0	2	0	3	0	1	0	10	0	5	2
17PC-225 cm	19	36	5	19	4	1	3	1	4	1	2	0	2	0	3	0	1	0	9	0	5	2
17PC-260 cm	18	36	4	18	4	1	3	1	4	1	2	0	2	0	3	0	1	0	10	0	5	2
17PC-316 cm	20	40	5	20	4	1	3	1	4	1	2	0	2	0	4	0	1	0	10	0	5	2
17PC-403 cm	19	38	5	20	4	1	3	1	4	1	2	0	2	0	3	0	1	0	10	0	5	2
17PC-443 cm	18	36	4	18	4	1	3	1	4	1	2	0	2	0	3	0	1	0	10	0	4	2

See Appencix A for sample naming convention

Appendix C

Nd Isotopic Analyses of Standards

J-Ndi and BCR-1 Standard Runs

A Nu multi-collector ICP-MS was used to analyze river and sediment samples for their Nd isotopic compositions (Chapter 3). Each sample was bracketed by either a J-Ndi or BCR-1 standard. The $^{143}Nd/^{144}Nd$ value of 0.512074±0.000012 (2-sigma) or ε_{Nd} = 10.99±0.23 was attained from 47 analyses of the J-Ndi standard using the Nu. Whereas the accepted value is $^{143}Nd/^{144}Nd$ = 0.512115±0.000007 (Tanaka et al., 2000) or ε_{Nd} = 10.20±0.13. BCR-1, which went through the same chemistry as samples, were run as unknowns. Since values BCR-1 were offset from its known value (ε_{Nd} ~0) the same amount as J-Ndi, a linear correction was made to all samples and BCR-1 standard analyses.

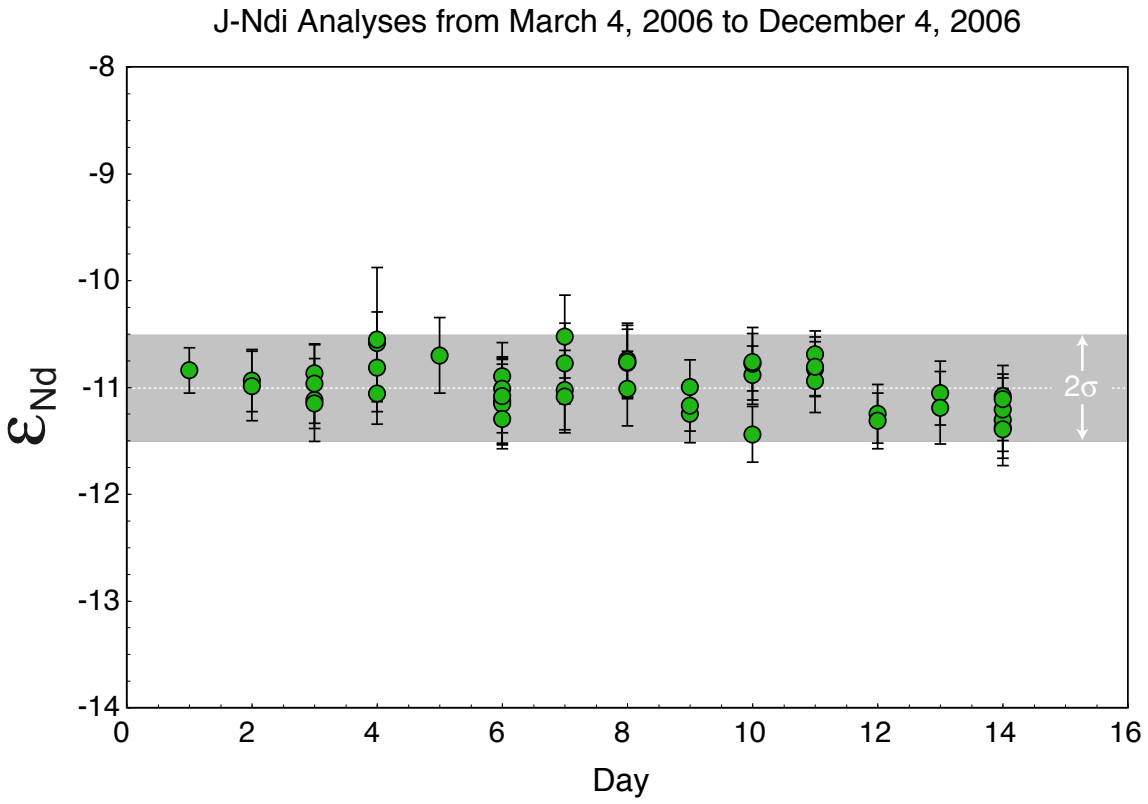

Figure C.1 - Nd isotopic values (ε_{Nd}) for the J-Ndi standard (Tanaka et al., 2000). Gray band denotes the 2-sigma uncertainty on the mean (ε_{Nd} = -10.99±0.46; n = 47). The published Nd isotopic values is ε_{Nd} = 10.20 (Tanaka et al., 2000).

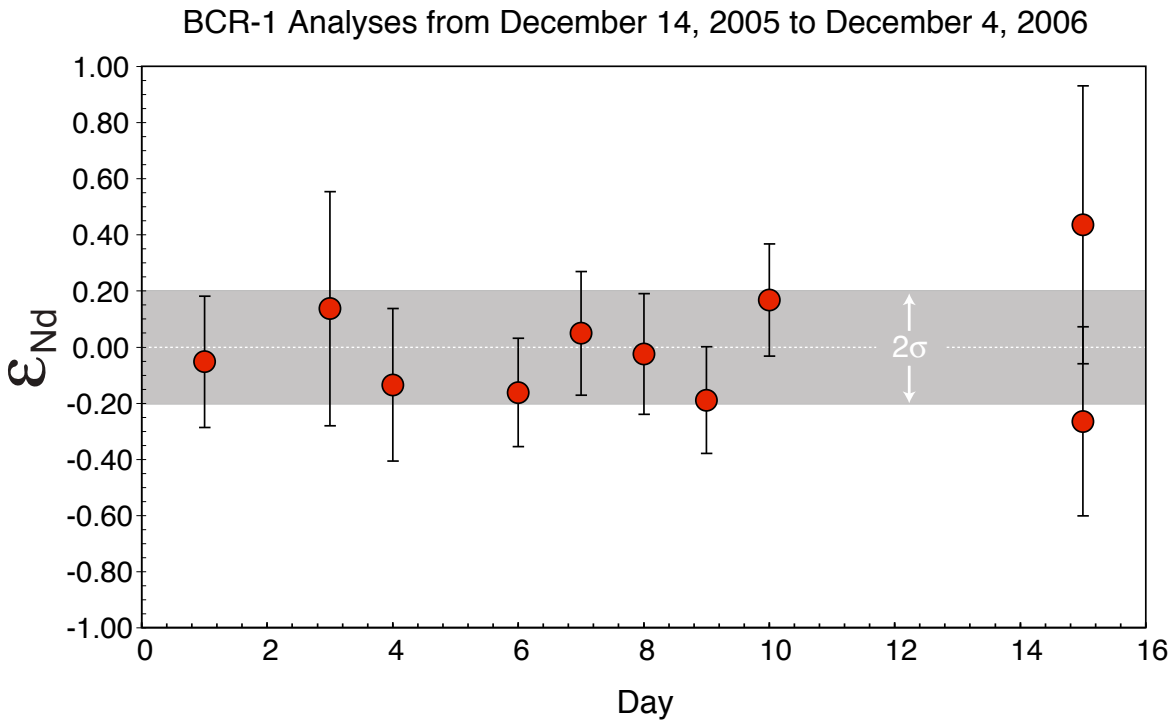

Figure C.2 - Nd isotopic values (ε_{Nd}) for BCR-1 and corrected using the J-Ndi offset of $\varepsilon_{Nd} = 0.79$. Gray band denotes the 2-sigma uncertainty on the mean ($\varepsilon_{Nd} = 0.0 \pm 0.21$). The published Nd isotopic value for J-Ndi is $\varepsilon_{Nd} = 10.20$ (Tanaka et al., 2000).